



Drug Discovery based on Oxidative Stress and HDAC6 for Treatment of Neurodegenerative Diseases

*Arzneimittelforschung basierend auf oxidativem Stress und HDAC6
zur Behandlung neurodegenerativer Erkrankungen*

Doctoral thesis for a doctoral degree
at the Graduate School of Life Sciences,
Julius-Maximilians-Universität Würzburg,
Section Neuroscience

submitted by

Feng He

from

Jiangxi, China

Würzburg **2021**



The presented work has been carried out under the supervision of Professor Dr. Michael Decker at the Chair of Pharmaceutical and Medicinal Chemistry at the Institute of Pharmacy and Food Chemistry of the Julius Maximilian University Würzburg between September 2018 and August 2021. This thesis was funded by China Scholarship Council and was supported by the Graduate School of Life Sciences.



Graduate School
Life Sciences

Affidavit

I hereby confirm that my thesis entitled *Drug Discovery based on Oxidative Stress and HDAC6 for Treatment of Neurodegenerative Diseases* is the result of my own work. I did not receive any help or support from commercial consultants. All sources and/or materials applied are listed and specified in the thesis.

Furthermore, I confirm that this thesis has not yet been submitted as part of another examination process neither in identical nor in similar form.

Place, Date

Signature

Eidesstattliche Erklärung

Hiermit erkläre ich an Eides statt, die Dissertation *Arzneimittelforschung basierend auf oxidativem Stress und HDAC6 zur Behandlung neurodegenerativer Erkrankungen* eigenständig, d.h. insbesondere selbständig und ohne Hilfe eines kommerziellen Promotionsberaters, angefertigt und keine anderen als die von mir angegebenen Quellen und Hilfsmittel verwendet zu haben.

Ich erkläre außerdem, dass die Dissertation weder in gleicher noch in ähnlicher Form bereits in einem anderen Prüfungsverfahren vorgelegen hat.

Ort, Datum

Unterschrift

Submitted on:

Office stamp

Members of the Thesis Committee

Chairperson: Prof. Dr. Keram Pfeiffer

Primary Supervisor: Prof. Dr. Michael Decker

Supervisor (Second): Prof. Dr. Christoph Sotriffer

Supervisor (Third): Prof. Dr. Tessa Lühmann

Date of Public Defence:

Date of Receipt of Certificates:

Table of Contents

Table of Contents	I
List of Publications.....	III
Other Scientific Contributions.....	IV
Copyrights	V
Declaration of Authorship	VI
Acknowledgments	VII
1. Introduction.....	1
1.1. Alzheimer’s Disease.....	1
1.2. HDACs and AD	2
1.3. Oxidative Stress and Neuroprotectants	3
1.3.1. Neuroprotectants against Oxytosis/Ferroptosis	4
1.3.2. Neuroprotectants based on the Nrf2 Pathway	6
1.4. Photopharmacology.....	8
2. Scope and Objective	11
3. Published Article: Melatonin- and Ferulic Acid-Based HDAC6 Selective Inhibitors Exhibit Pronounced Immunomodulatory Effects <i>In Vitro</i> and Neuroprotective Effects in a Pharmacological Alzheimer’s Disease Mouse Model.....	13
3.1. Introduction	14
3.2. Synthesis.....	15
3.3. Biological Evaluation.....	16
3.4. Conclusions	22
4. Unpublished Work.....	24
4.1. Design, Synthesis and Bio-Evaluation of Hybrid Neuroprotectants based on Vitamin K Derivatives for Treatment of Neurodegenerative Disorders	24
4.1.1. Introduction	24
4.1.2. Results and Discussion.....	25
4.1.3. Conclusions	34
4.1.4. Experimental Section.....	34
4.2. Structure-Activity Relationship (SAR) Study of Quinones as Free Radical Scavengers and Neuroprotectants	41
4.2.1. Introduction	41
4.2.2. Results and Discussion.....	44
4.2.3. Conclusions	47
4.2.4. Experimental Section.....	47

4.3. Design, Synthesis, Photophysicochemical Characterization and Bio-Evaluation of Photoswitchable HDAC6 Inhibitors.....	54
4.3.1. Introduction	54
4.3.2. Results and Discussion	56
4.3.3. Conclusions	62
4.3.4. Experimental section	62
5. Summary	77
6. Zusammenfassung	80
7. Abbreviations	83
8. References	85
9. Appendix	95

List of Publications

1. **He, F.**; Chou, C. J.; Scheiner, M.; Poeta, E.; Yuan Chen, N.; Gunesch, S.; Hoffmann, M.; Sotriffer, C.; Monti, B.; Maurice, T.; Decker, M. Melatonin- and ferulic acid-based HDAC6 selective inhibitors exhibit pronounced immunomodulatory effects in vitro and neuroprotective effects in a pharmacological Alzheimer's disease mouse model. *J. Med. Chem.* **2021**, *64* (7), 3794-3812.
2. Scheiner, M.; Hoffmann, M.; **He, F.**; Poeta, E.; Chatonnet, A.; Monti, B.; Maurice, T.; Decker, M. Selective pseudo-irreversible butyrylcholinesterase inhibitors transferring antioxidant moieties to the enzyme show pronounced neuroprotective efficacy in vitro and in vivo in an Alzheimer's disease mouse model. *J. Med. Chem.* **2021**, *64* (13), 9302-9320.

Other Scientific Contributions

1. **He, F.**, Design, synthesis and bio-evaluation of HDAC inhibitors incorporating antioxidants melatonin and ferulic acid for treatment of neurodegenerative disorders, Poster, Eureka! 14th International GSLS Students Symposium, Würzburg (Germany), October 9th – 10th, **2019**.
2. **He, F.**, Development of “cis-on” photochromic histone deacetylase 6 (HDAC6) inhibitors, Poster, Eureka! 15th International GSLS Students Symposium, Virtual Event, October 7th – 8th, **2020**.
3. **He, F.**, Design, synthesis and bio-evaluation of hybrid neuroprotectants based on vitamin K derivatives for treatment of neurodegenerative disorders, Poster, 56th International Conference on Medicinal Chemistry (RICT 2021), Virtual Event, July 7th – 9th, **2021**.

Copyrights

Parts of this work have been published previously and are reproduced, adapted and/or modified with the permission of:

He, F.; Chou, C. J.; Scheiner, M.; Poeta, E.; Yuan Chen, N.; Gunesch, S.; Hoffmann, M.; Sotriffer, C.; Monti, B.; Maurice, T.; Decker, M. Melatonin- and ferulic acid-based HDAC6 selective inhibitors exhibit pronounced immunomodulatory effects in vitro and neuroprotective effects in a pharmacological Alzheimer's disease mouse model. *J. Med. Chem.* **2021**, *64* (7), 3794-3812.

Copyright (2021) American Chemical Society.

<https://pubs.acs.org/doi/10.1021/acs.jmedchem.0c01940>

Declaration of Authorship

Publication (complete reference): He, F. ; Chou, C. J.; Scheiner, M.; Poeta, E.; Yuan Chen, N.; Gunesch, S.; Hoffmann, M.; Sottriffer, C.; Monti, B.; Maurice, T.; Decker, M. Melatonin- and ferulic acid-based HDAC6 selective inhibitors exhibit pronounced immunomodulatory effects in vitro and neuroprotective effects in a pharmacological Alzheimer's disease mouse model. <i>J. Med. Chem.</i> 2021 , <i>64</i> (7), 3794-3812.			
Participated in	Author Initials , Responsibility decreasing from left to right		
Design of target compounds	F.H./M.D.		
Synthesis and Characterization	F.H.		
Enzyme-based and cellular HDAC inhibition assays	C.J.C.		
DPPH, ORAC, Metal Chelation Assays	F.H.		
Docking Study	N.Y.C.	C.S.	
Neurotoxicity and Neuroprotection Assays	S.G.		
Immunomodulatory Studies	E.P.	B.M.	
<i>In Vivo</i> Studies	M.S./T.M.	M.H.	
Manuscript Writing	F.H.	M.D.	C.J.C/M.S./E.P./N.Y.C/C.S./B.M./T.M.

Explanations (if applicable): exclusive first authorship

Acknowledgments

I would like to thank my supervisor Professor Michael Decker first. He offered me this precious chance to study in the University of Würzburg in Germany for my PhD, and I have spent a great three years here. Thanks to his strict supervision, I have been trained to be a more competent and qualified researcher and have gained pronounced achievements. Decker group is one of the best research groups I ever know and Professor Michael Decker is a role model as mentor.

Also, I feel really appreciated for the great help from my additional supervisors Professor Christoph Sotriffer and Professor Tessa Lühmann. Thanks to Professor Sotriffer for providing the chance to work with his group and I have learnt a lot about the standard way of docking studies. Many thanks to Professor Sotriffer and Professor Lühmann for all helpful scientific instructions.

Furthermore, I would like to thank all my colleagues in the University of Würzburg: Dr. Xinyu Chen, Dr. Luca Agnetta, Dr. Sandra Gunesch, Dr. Matthias Hoffmann, Matthias Scheiner, Julian Hofmann, Christian Gentsch, Sophie Steinmüller, Anna Tutov, Diego Alejandro Rodriguez Soacha, Alexandra Sink, Thomas Zimmermann, Hubert Gerwe, and Philipp Spatz from Decker group, Erik Endres and Natalia Yuan Chen from Sotriffer group, Mohamed Marzouk from Holzgrabe group, and my practical student Benedikt Schäd. I have learnt a lot from them, and they all offered me great help in my research work and personal life in Germany. Special thanks to Julian, who contributed essentially to vitamin K projects for neuroprotection assays and all helpful support.

I want to thank all of my collaboration partners, without whose substantial supports, this work would not be so successful.

Professor C. James Chou is a very reliable partner, who has helped me for HDAC inhibition assay since my master's study. His contribution is one of the main pillars of my doctoral projects, including our ongoing vitamin K project. Thank you so much!

Dr. Tangui Maurice from the University of Montpellier, my colleagues Dr. Matthias Hoffmann and Matthias Scheiner contributed to the very important *in vivo* studies, which greatly improved the quality and profundity of my doctoral studies.

Professor Barbara Monti and Eleonora Poeta's work on immunomodulatory studies of my HDAC inhibitors and ongoing vitamin K derivatives contributed substantially to my projects.

Great thanks to Professor Christoph Sotriffer and Natalia Yuan Chen from the Institute of Pharmacy and Food Chemistry at the University of Würzburg for their docking studies on HDAC inhibitors.

Professor Christophe Stove and Eline Pottie are working on the β -arrestin 2 recruitment assay to monitor 5-HT_{2A}R activation for my photoswitchable 5-HT ligands, which is the key link to keep this additional project going. Also, great thanks to Hubert for continuing this unfinished project.

Special acknowledgments to China Scholarship Council for funding my PhD studies in Germany. I also want to express gratitude to GSLS (Graduate School of Life Sciences) office for holding colorful and useful transferable courses, which greatly enriched my life and improved my English.

Surely, any of my success cannot leave from the support of my families, and their support is the main

motivation to push me go further. Finally, I want to thank my girlfriend Huiying, whose love gives me the confidence and strength to overcome all the difficulties. I am looking forward to grow together with her in the rest of life.

1. Introduction

1.1. Alzheimer's Disease

With the increasing number of aging population worldwide, the age-related neurodegenerative disorders like dementia is expected to reach 152 million patients by 2050.¹ Although the Food and Drug Administration (FDA) has approved cholinesterase inhibitors (donepezil, rivastigmine, and galantamine) and an *N*-methyl-D-aspartate receptor (NMDAR) antagonist (memantine) for the treatment of Alzheimer's disease (AD), the most common cause of dementia, none of them could prevent the progressive neurodegeneration of AD patients.²

Multiple factors, such as low levels of acetylcholine, β -amyloid ($A\beta$) deposits, and tau-protein aggregation, have been suggested to contribute to the progression of AD.³ As one of the major pathological hallmarks, $A\beta$ peptides deposition was previously thought to be the main cause of AD. However, the high failure rate of clinical trials targeting $A\beta$ indicates that there is no direct correlation between the formation of senile plaques in brains and the progression of AD.⁴ Recently, two controversial drugs, GV-971 and aducanumab, respectively, have been approved by China FDA (CFDA) and FDA for the treatment of AD, but their effectiveness still needs to be further evaluated by postmarketing clinical trials.^{5,6}

Therefore, new targets and drug design strategies are still necessary to develop more effective drugs for the treatment of AD. Recent years, some other targets like oxidative stress,⁷⁻⁹ neuroinflammation,¹⁰ histone deacetylase (HDAC),¹¹ and biometals chelation¹² have aroused researchers' attention (**Figure 1.1**). Besides, the multi-target-directed ligands (MTDL) strategy based on "one molecule, multiple target" paradigm has been developed by acting on multi-target synergistically for the efficient treatment of the multifactorial disease like AD and cancer.¹³ Multiple drug candidates have been developed based on new targets and MTDL strategy possessing promising potential for treatment of AD.¹⁴⁻¹⁶ Herein, HDACs and oxidative stress are of the most interests to us, and the relationships between HDACs and AD, oxidative stress and AD, which will be reviewed in following text.

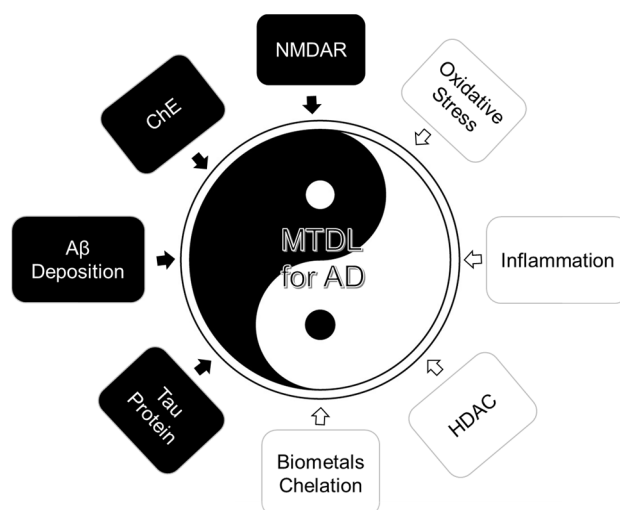


Figure 1.1. Some of the representative biological targets involved in AD pathology.

1.2. HDACs and AD

HDACs are a family consisting of 18 isoforms with different specific locations and distinct functions, which are grouped into four classes based on their phylogenetic features. Class I (HDAC1, 2, 3, 8), class IIa (HDAC4, 5, 7, 9), class IIb (HDAC6, 10) and class IV (HDAC11) are unique Zn^{2+} dependent HDACs. The sirtuins (SIRT1–7) constitute the class III HDACs and utilize NAD^+ as a cofactor instead of zinc. HDACs deacetylate lysine residues in histones and multiple non-histone substrates, leading to the relaxation of chromatin structure and triggering transcriptional activation. HDACs are essential enzymes in epigenetic regulation, which regulate the genetic expression without affecting the sequence of DNA.¹⁷

HDAC inhibitors generally comprise a zinc binding group (ZBG), a cap group binding to the surface of the enzyme, and a hydrophobic linker group connecting the ZBG and the cap group. Based on the structural differences, especially various ZBGs, most of the HDAC inhibitors can be classified as hydroxamates, cyclic peptides, short chain fatty acid, and benzamides (**Figure 1.2**).¹⁸ Structures in **Figure 1.2** have been approved for treatment of cancer, meanwhile, it has been reported that multiple HDAC subtypes are associated with the progression of AD. HDAC2 controls multiple memory-related genes, and is increased in the nuclei of hippocampal CA1 and entorhinal cortex neurons in AD compared with non-cognitively impaired aged controls.¹⁹⁻²¹ Kim *et al.* reported that the absence of HDAC4 results in impairments in hippocampal-dependent learning and memory and long-term synaptic plasticity, while HDAC5's absence does not. The spatial and associative memory functions were restored in a mouse model for AD when HDAC6 was knocked out, while no severe effects under basal conditions.²² HDAC6 modulates the hyperphosphorylation of tau protein, which is correlated to the formation of neurofibrillary tangles (NFTs), an essential hallmark of AD.²³⁻²⁵ HDAC6 also regulates mitochondrial transport in hippocampal neurons, and its activity is closely linked with glycogen synthase kinase 3 β (GSK3 β) inhibition.²⁶

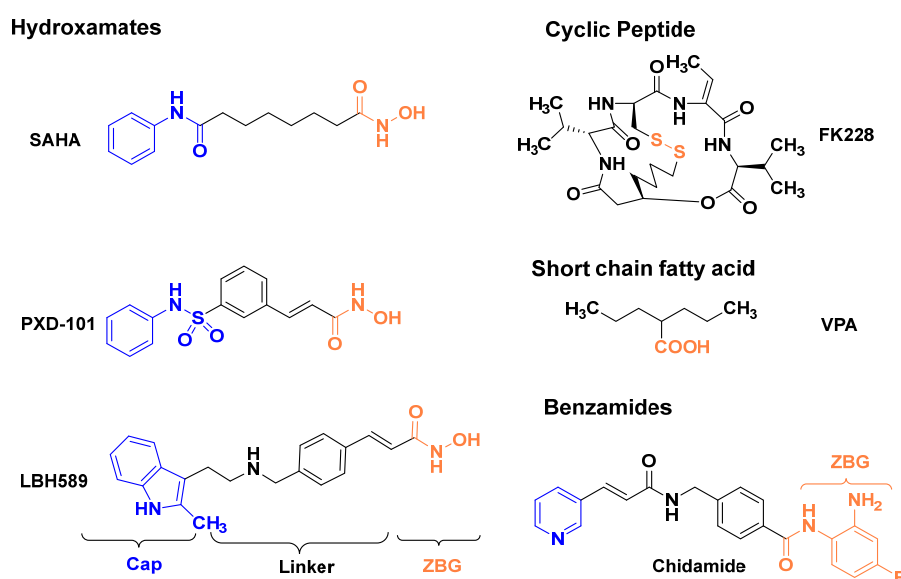


Figure 1.2. Structures of marketed HDAC inhibitors and their classification.

Inspired by the promising therapeutic potential of HDACs for treatment of AD, numerous of HDAC inhibitors have been designed into multi-target compounds and show potential disease-modifying effects for AD. The cap groups of HDAC inhibitors possessing high compatibility are normally diverse aromatic groups, which can be replaced by different pharmacophores addressing a second target (**Figure 1.3**). Based on the close connection between GSK3 β and HDAC, the first-in-class GSK3 β -HDAC dual inhibitor (**1**) possessing balanced inhibition towards GSK3 β and HDAC6, together with neurogenesis promotion and immunomodulatory effects have been designed, indicating disease-modifying effects *in vitro* for AD.²⁷ Oyarzabal's group reported compound **2** exhibiting balanced inhibition against HDAC6 and phosphodiesterase 5 (PDE5), which can rescue the impaired long-term potentiation from APP/PS1 mice and reverse cognitive deficits in Tg2576 mice.²⁸ Compound **3** and **4** were designed by merging the pharmacophore groups of AChE inhibitor tacrine and NMDAR antagonist memantine into HDAC inhibitors, and both of them show highly potent activity toward dual-target, and are promising drug candidates for treatment of AD.^{29, 30} Meanwhile, Tseng *et al.* designed another series of HDAC-AChE multi-target inhibitors based on tacrine and screened compound **6**, which not only possesses potent inhibition against HDAC6 and AChE, but also enhances the neurite outgrowth and shows significant anti-A β -aggregation.³¹ Our group designed a series of hybrid HDAC inhibitors incorporating with melatonin and ferulic acid, and compound **5** was identified as potent selective HDAC6 inhibitor with pronounced antioxidant capacity, *in vitro* immunomodulatory effects, and *in vivo* neuroprotection in an A β ₁₋₄₂ induced mouse model.³² Transglutaminase 2 (TG2) catalyzes the formation of covalent bonds highly resistant to proteolysis and contributes to the formation of toxic aggregates in the AD brain.³³ Thus, a new class of TG2-HDAC dual inhibitors have been designed and HDAC6 selective inhibitor **7** shows protective effects against glutamate impairment in mouse primary cortical neurons.³³ Compound **8** is an HDAC inhibitor showing pronounced antioxidant capacity and protective effects against toxic stimuli induced by H₂O₂ in PC3 cell lines, which was designed by incorporating a selenium-containing multifunctional antioxidant ebselen.³⁴

All in all, HDAC inhibitors have been widely investigated through MTDL strategy to discover novel drug candidates for treatment of AD. However, the successful drug discovery for AD treatment remains several challenging tasks and still suffers limitations. AD pathophysiology and the relationship with HDAC needs to be further revealed and more effective animal models need to be established. Only few of AD drug candidates targeting HDACs have been studied *in vivo*, therefore, the multi-target drug candidates needs to be thoroughly studied and the design needs to keep up with the latest discoveries in AD pathophysiology and reflect on results of AD clinical trials.

1.3. Oxidative Stress and Neuroprotectants

Oxidative stress is a major common hallmark of AD and many other neurodegenerative disorders such as Parkinson's disease (PD), amyotrophic lateral sclerosis (ALS), and stroke. The dysregulation of the redox state induces a regulated cell-death pathway named as oxytosis/ferroptosis, and also activates multiple cell signaling pathways which provide neuroprotective effects against oxidative stress.

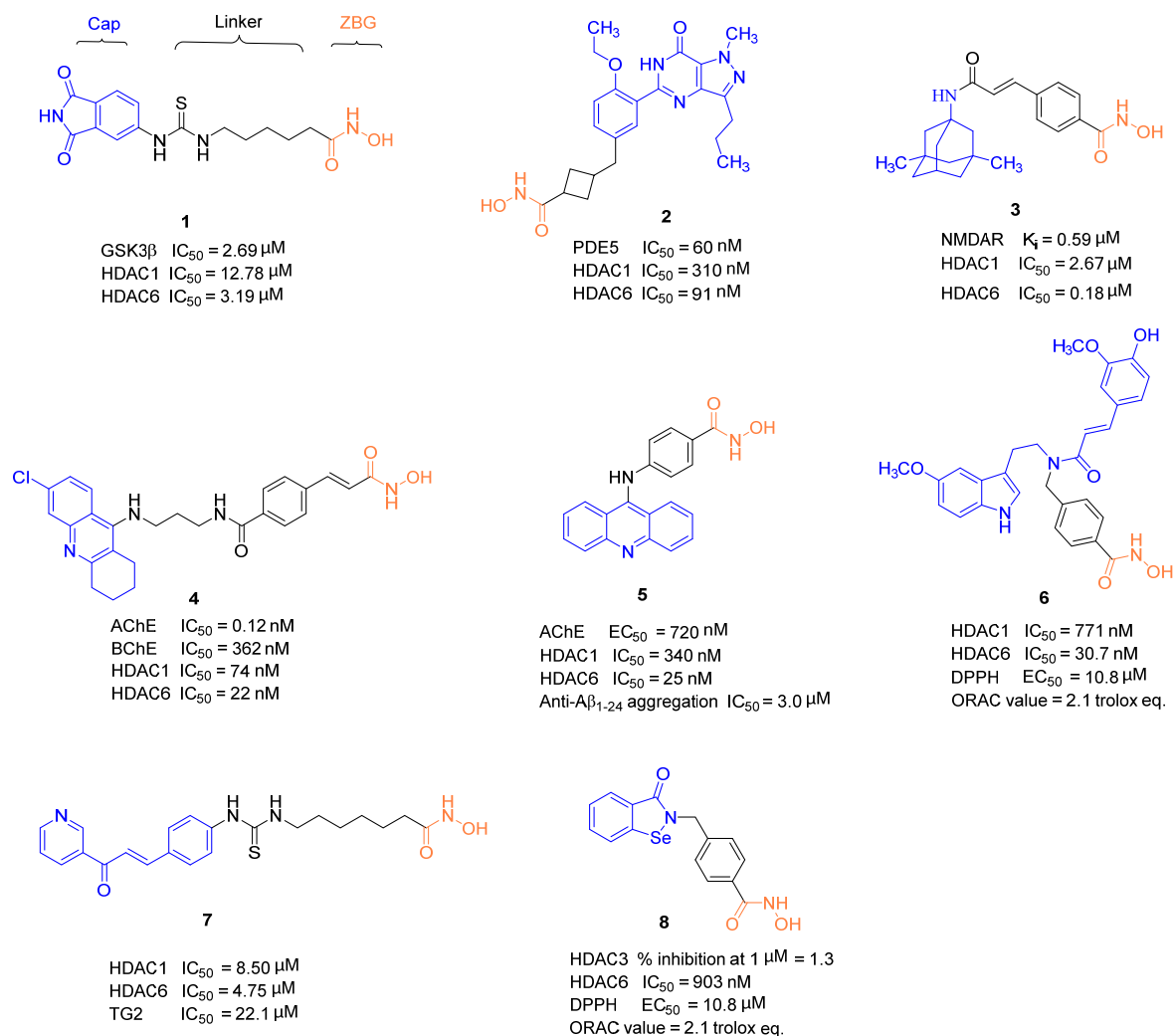


Figure 1.3. A selection of multi-target HDAC inhibitors related to Alzheimer's disease.

Multiple drug candidates have been developed based on oxytosis/ferroptosis and Keap-Nrf2-ARE pathways showing pronounced neuroprotective effects and promising potential for treatment of AD,^{35, 36} which will be discussed in following paragraphs.

1.3.1. Neuroprotectants against Oxytosis/Ferroptosis

Oxytosis and ferroptosis pathways were initially named by a lab of the Salk Institute for Biological Studies³⁷ and Stockwell's lab,³⁸ respectively, and were renamed as oxytosis/ferroptosis subsequently since numerous pieces of evidence indicates that these are the same cell-death pathways.³⁵ As described in **Figure 1.4**, the initial step is the inhibition of cysteine uptake into the cells induced by system X_c⁻ inhibitors glutamate or erastin, which leads to intracellular glutathione (GSH) depletion. Following with GSH depletion is the production of ROS and GPx4 inhibition, which causes the lipid peroxidation and cell death directly. RSL3 is an inhibitor of glutathione peroxidase 4 (GPX4), also the initiator of ferroptosis pathway. Both GPx4 inhibition and GSH depletion lead to the activation of 12/15-lipoxygenase (12/15LOX) together with increasing of cGMP levels. Calcium influx is the downstream of ROS and immediately leads to cell death.³⁵

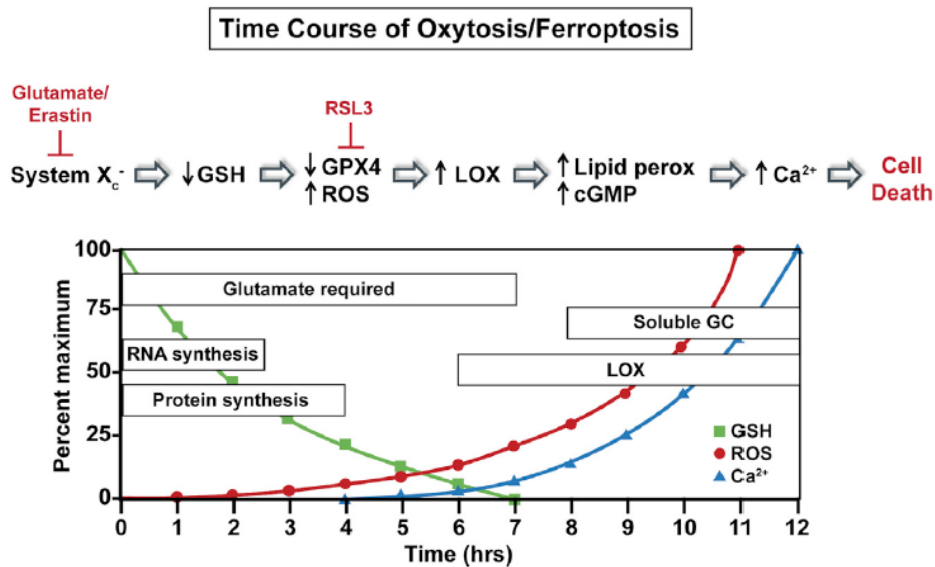


Figure 1.4. Time course of major pathophysiological changes that occur during oxytosis/ferroptosis. Adapt from Maher *et al.*³⁵

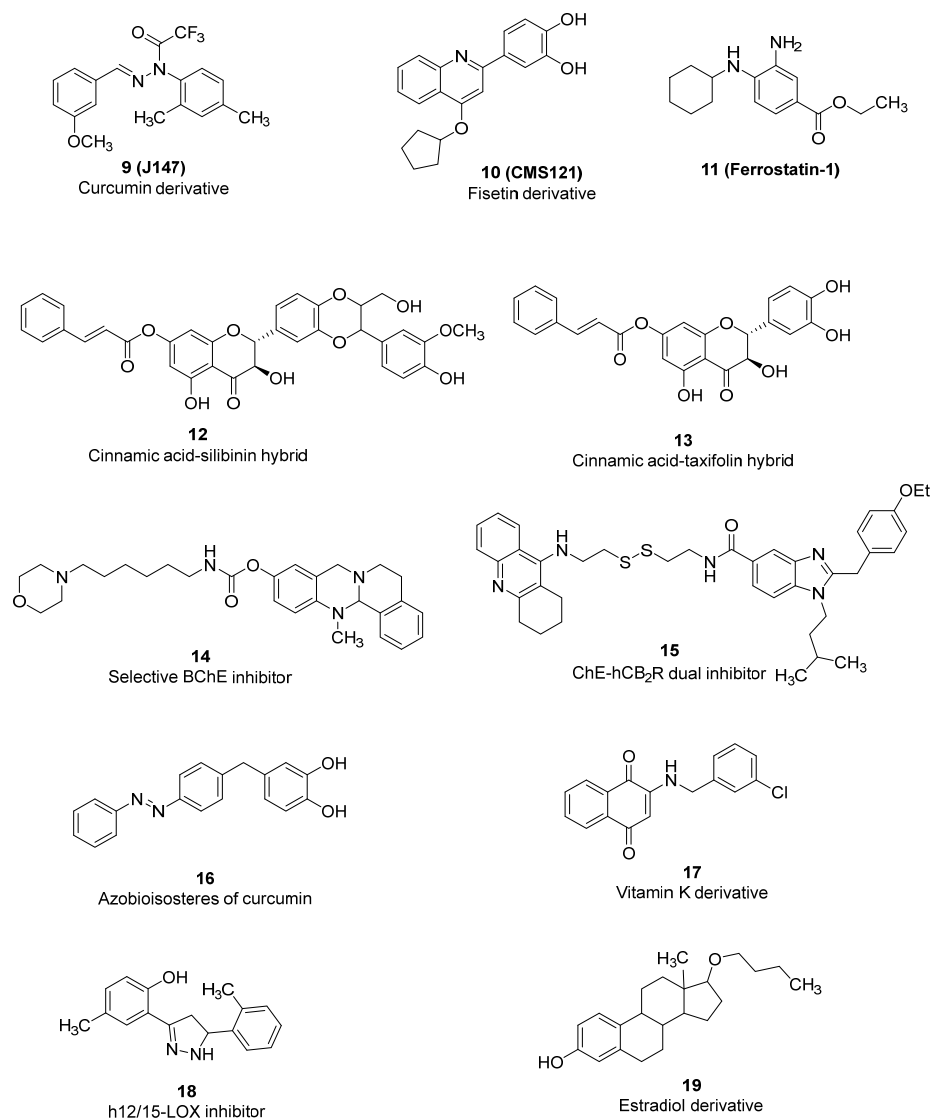


Figure 1.5. Neuroprotectants based on the oxytosis/ferroptosis pathway.

In **Figure 1.5**, a selection of neuroprotectants based on the oxytosis/ferroptosis pathway is shown. Compound **9** (J147) was developed based on the natural product curcumin and is currently in phase I clinical trials (NCT03838185) for treatment of AD, which was initially screened in an oxytosis/ferroptosis assay with low nanomolar EC_{50} .^{35,39} By using the same drug-discovery platform, compound **10** (CMS121) was developed from the flavonoid fisetin with greatly enhanced neuroprotective effects against oxytosis/ferroptosis and improved drugable properties.⁴⁰ Compound **10** also exhibited cognitive benefits *in vivo* in both rapidly aging SAMP8 mice and APP^{swe}/PS1 Δ E9 transgenic mouse models of AD and is currently in the investigational new drug (IND) process.^{40,41} The Stockwell lab firstly described the ferroptosis pathway and identified compound **11** (Ferrostatin 1) as a potent neuroprotectant against ferroptosis with EC_{50} of 60 nM.³⁸

Compounds **12** and **13** were developed by our group based on the hybridization of cinnamic acid with silibinin and taxifolin, respectively.^{42,43} Both compounds **12** and **13** already showed highly potent neuroprotection at 5 μ M in oxytosis/ferroptosis assay, while the parent compounds cinnamic acid, silibinin and taxifolin, respectively, were not able to protect cells from oxytosis/ferroptosis at 1 - 25 μ M. Compounds **14-16** are selective butyrylcholinesterase (BChE) inhibitor, ChE-hCB₂R dual inhibitor, and azobioisosteres of curcumin, respectively, also developed by our group, and screened as potent neuroprotectants in oxytosis/ferroptosis assay.⁴⁴⁻⁴⁶

Vitamin K has been reported as neuroprotectant in preventing oxidative injury to develop oligodendrocytes and neurons,⁴⁷ therefore the structure-activity relationship of vitamin K were studied and compound **17** was identified as the most potent neuroprotectant against oxytosis/ferroptosis.⁴⁸ Besides, compound **17** showed prevention against oxidative stress induced dysfunction of mitochondria, which probably worked as an enhanced or alternative electron carriers. Compound **18** was identified as a selective human reticulocyte 12/15-lipoxygenase (h12/15-LOX) inhibitor with EC_{50} of 3.4 μ M. As mentioned above, LOX is involved in the oxytosis/ferroptosis pathway and compound **18** indeed protect HT22 cells from glutamate induced oxytosis/ferroptosis with EC_{50} of 10 μ M.⁴⁹ The antioxidant capacity and neuroprotective activities of 17 β -estradiol has been widely studied, and its derivative **19** showed more potent protection (< 1 μ M) against oxytosis/ferroptosis compared with 17 β -estradiol.⁵⁰

1.3.2. Neuroprotectants based on the Nrf2 Pathway

Oxidative stress activates multiple cell signaling pathways including Nrf2 (nuclear factor erythroid 2-related factor),³⁶ HIF-1 α (hypoxia inducible factor),⁵¹ ATF4 (activating transcription factor 4)⁵² and others, which provide neuroprotection against oxidative damages. Nrf2 is a major regulator of cellular stress response, which is accumulated and translocated to the nucleus after oxidants and electrophiles interacting with Keap1 (Kelch-like ECH-associated protein 1). Nrf2 binds to the antioxidant response element (ARE) in the nucleus and induces transcription and upregulation of antioxidant enzymes, including NAD(P)H quinone oxidoreductase-1 (NQO1), glutathione S-transferase (GST), heme oxygenase-1 (HO-1), *etc.* (**Figure 1.6**).³⁶

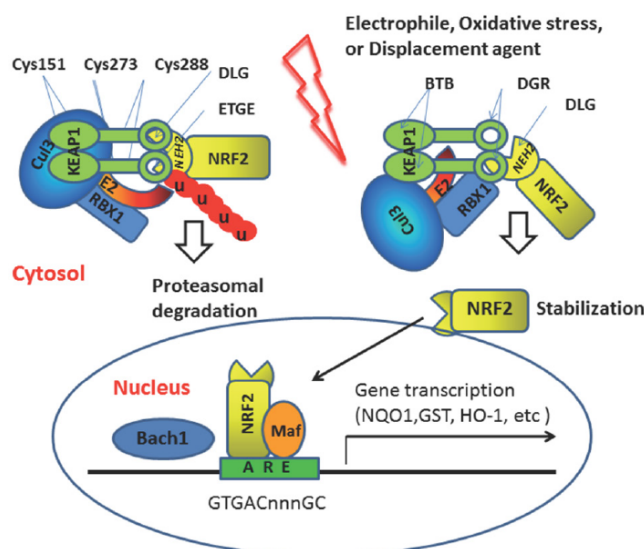


Figure 1.6. Keap-Nrf2-ARE pathway activation response to oxidative stress. DGR: Double glycine repeat; Bach1: BTB domain and CNC homolog 1. Adapt from Thomas *et al.*³⁶

The Nrf2-based drug discovery represents a promising approach to neuroprotection in the treatment of neurodegenerative diseases including Parkinson's and Alzheimer's diseases. Most of the pharmacological Nrf2 activators are electrophilic molecules that covalently modify cysteine residues present in the KEAP1 protein by oxidation or alkylation, which have been comprehensively reviewed in several recent papers.^{36, 53} Electrophilics including sulforaphane (**20**),⁵⁴ resveratrol (**21**),⁵⁵ *tert*-butylhydroquinone (TBHQ, **22**),⁵⁶ nordihydroguaiaretic acid (**23**),⁵⁷ and dimethylfumarate (**24**)⁵⁸ have been widely studied as Nrf2 activators and are now in different phases of clinical trials for neurodegenerative treatment. More specifically, dimethylfumarate (**24**, BG-12 or Tecfidera, from Biogen) has been approved in 2013 by FDA for relapsing-remitting multiple sclerosis (MS). However, electrophiles can non-specifically and covalently modify nucleophilic groups in proteins such as cysteine residues and produce severe side-effects.

Therefore, Nrf2-based activators which are non-electrophilic and non-toxic are in urgent need to avoid the severe side-effects for treatment of chronic neurodegenerative diseases. Compound **25** is a selective HDAC6 inhibitor exhibiting highly potent neuroprotective effects in four independent *in vitro* models of neurodegeneration through activation of Nrf2 and HIF1 α pathways, while class I HDAC inhibitors were not active, indicating that HDAC6 inhibition might be a new mechanism to activate the Nrf2 pathway.⁵⁹ Moreover, several protein-protein interaction (PPI) inhibitors can interfere with the binding of Nrf2 to Keap1 and provide higher selectivity than electrophilic molecules. Compound **26** is a PPI inhibitor blocking the Nrf2 peptide binding site and inducing Nrf2 stability in a cell-reporter assay through a mechanism other than electrophilic addition.⁶⁰ Besides, GSK-3-inhibitor tideglusib (**27**) was reported to have regulatory effects on the Nrf2 pathway in MPP⁺-induced cell damage, indicating a new strategy to design selective neuroprotectants based on the Nrf2 pathway.⁶¹

As shown above, multiple targets are involved in each single signaling pathway in response to oxidative stress, and these targets are correlated to each other. In this case, the MTDL strategy holds a bright future

to develop novel neuroprotectants to insure sufficient safety and high efficiency for treatment of neurodegenerative diseases.

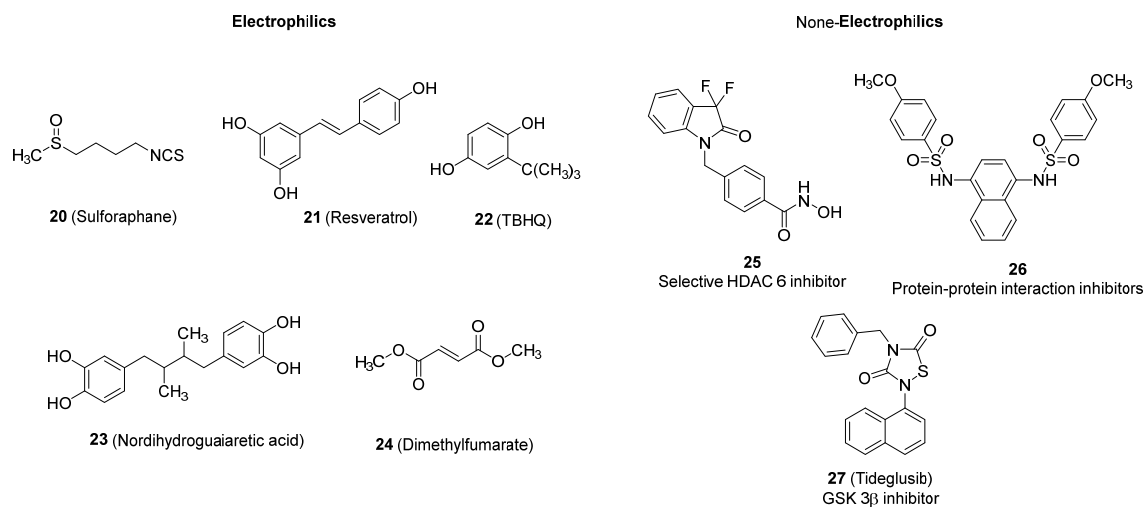


Figure 1.7. Neuroprotectants based on the Nrf2 pathway.

1.4. Photopharmacology

Light is a fascinating tool in its ability to control biological system with advantages of high spatial and temporal resolution, noninvasive, remote action, as well as reversibility. Generally, administering a photoactive drug in a state with low toxicity and efficacy to a patient, followed by irradiation to convert it into a state with high biological activity in a defined region is the core principle to develop photo-dependent molecular tools or drug candidates.

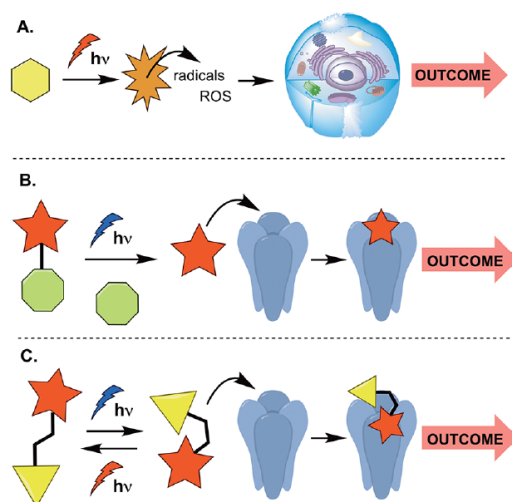


Figure 1.8. Photopharmacological approaches: (A) photodynamic therapy; (B) irreversible photopharmacology (photodecaging); (C) reversible photopharmacology (photoswitching). Adapt from Fuchter, M. J. *et al.*⁶²

Main photopharmacological approaches have been described in **Figure 1.8**, including photodynamic therapy (PDT), irreversible photopharmacology (photodecaging), and reversible photopharmacology (photoswitching) approaches.⁶² Cancer patients under photodynamic therapy were administered with photosensitizing dye molecule, followed by light dosing and inducing reactive oxygen species (ROS) formation to kill cancer cells (**Figure 8A**).⁶³ Photodecaging is an irreversible approach by adding a

photoactive protecting group to a biological ligand and block its target-based activity, which can release substance of interest under the action of light (**Figure 8B**).^{64, 65} Photoswitchable compounds are reversible photopharmacological agents possessing two different structural states, which can be switched to another state under the irradiation with corresponding wavelengths of lights.^{62, 66, 67}

Since the development of photopharmacology has been thoroughly reviewed in several recent papers,^{62, 68-70} the following part mainly focused on the application of photopharmacology in HDACs, which is the target of our interests.

Generally, the predominant way to design photoswitchable compounds is to take an established ligand for a desired biological target and to synthetically modify it by incorporating photoswitchable groups, such as azobenzene,⁷¹ dithienylethene,⁷² fulgimide,⁷³ and azopyrazole.⁷⁴ Several HDAC inhibitors, including romidepsin, Vorinostat (SAHA), Panobinostat and Belinostat, have been approved by FDA as chemotherapeutic agents for the treatment of hematologic malignancies. However, despite significant efforts, side-effects caused by off-site toxicity cannot be avoid. Thus, successful photoswitchable HDAC inhibitors showing high activity in the thermodynamically unstable state and low cytotoxicity in the stable state would be potential photocontrolled chemotherapeutic agents for improved, safer cancer therapy with less severe side effects. A selection of reported photopharmacological HDAC inhibitors shows in **Figure 1.9**.

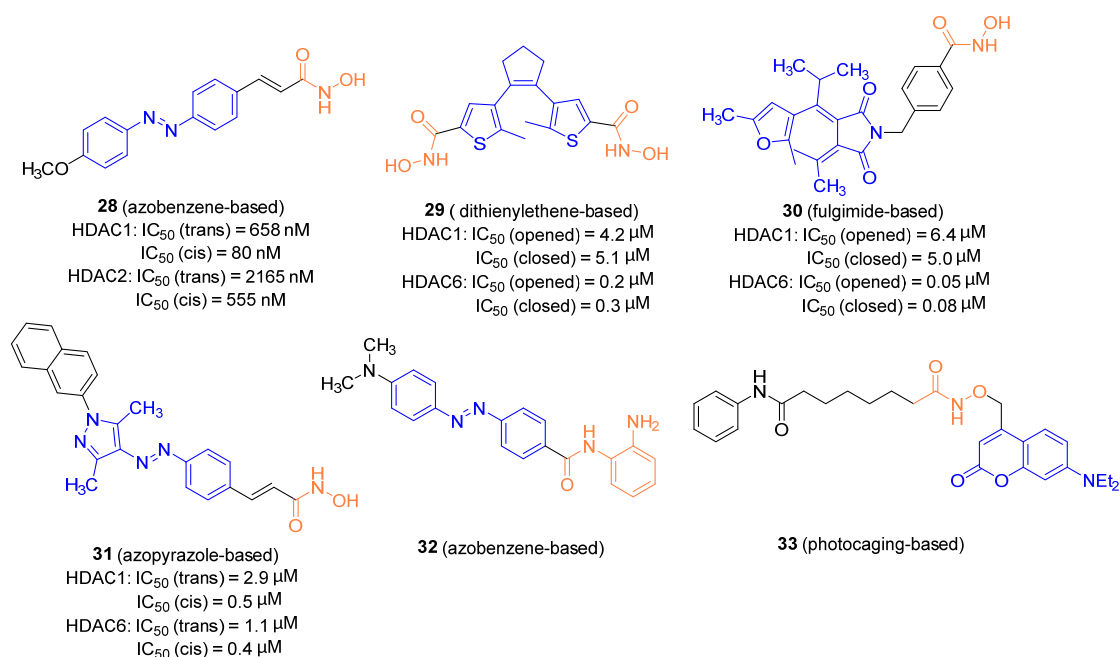


Figure 1.9. Structures and biological activities of a selection of photopharmacological HDAC inhibitors.

Szymanski *et al.* have designed the first-in-class of photoswitchable HDAC inhibitors based on azobenzene, and compound **28** was screened and showed high potency and high difference in activity between *trans*- and *cis*-isomers. Moreover, the *cis*-isomer of compound **28** is more potent than its *trans*-isomer for class I HDACs inhibition (39-fold for HDAC2), indicating that it has a “*cis*-on” effect and can be developed as a promising photocontrolled chemotherapeutic agent.⁷⁵ Compounds **29** and **30** were designed by merging two photoswitches dithienylethene and fulgimide, respectively, into the cap groups

of HDAC inhibitors. However, only small difference in activity could be observed between corresponding opened- and closed-isomers, which indicated that dithienylethene and fulgimide as cap groups were not optimal strategy to design photoswitchable HDAC inhibitors.⁷³ Azopyrazole is an excellent photoswitch with quantitative *trans* to *cis* conversion and high thermal stability of the *cis*-isomer.⁷⁴ Compound **31** was designed based on azopyrazole achieving good inhibitory activities and its *cis*-isomer exhibited more potent inhibition towards HDAC1 and HDAC6.⁷⁶ Compound **32** is an *ortho*-aminoanilide-based class I selective inhibitor with highly potent inhibition towards HDAC1-3 and high difference between *trans*- and *cis*-isomers (*cis*-on). More importantly, the enriched *cis*-isomer could be obtained by the irradiation of 470 nm blue light, indicating less toxicity and high penetrability to biological tissues.⁷⁷ The zinc binding groups of HDAC inhibitors are core structures contributing to HDAC inhibition, thus, Ieda *et al.* designed compound **33** by esterification the hydroxamate group with a photocage to produce a photocontrolled HDAC inhibitor.⁷⁸

Although significant progress has been achieved, further *in vivo* studies of photopharmacological HDAC inhibitors are extremely in need. For this purpose, photocontrolled chemotherapeutic agents possessing the ability of visible light conversion are necessary, and the selective inhibition of photoswitchable HDAC inhibitors is essential to avoid the off-target toxicity.

2. Scope and Objective

As described in the introduction part, age related diseases, especially AD, are facing a great challenge since the high failure rate of clinical trials. To continue the efforts have been invested in the drug discovery for AD treatment, this thesis mainly focuses on oxidative stress hypothesis by using MTDL strategy to develop novel hybrid compounds, seeking for a cure for AD patients. This goal was addressed by an approach: design, synthesis, *in vitro* and *in vivo* evaluation of hybrid compounds with antioxidant capacity.

Besides, the pathogenesis of AD and other neurodegenerative diseases remains unclear, and many proposed pathogenic mechanisms remain to be elucidated. To develop novel molecular tools to uncover the mechanism of AD related targets, another approach used in this thesis is the design, synthesis, photophysical characterization, and bio-evaluation of photoswitchable compounds.

For the first purpose, HDAC6 inhibitors and oxidative stress targeted antioxidants related to AD pathogenesis have been merged into one entity to design novel hybrid compounds possess synergistic HDAC inhibition and antioxidant capacity. The best compound was screened by HDAC inhibition assay and free radical scavenging assay, including DPPH and ORAC assays. The immunomodulatory effects and *in vivo* neuroprotective effects of screened compounds were further studied to evaluate the efficacy for treatment of AD (*cf.* Chapter 3).

To further investigate the role of oxidative stress in the progression of AD, a class of neuroprotectants were designed by hybridizing of vitamin K derivative and several common antioxidants, including ferulic acid, melatonin, lipoic acid, and trolox. These novel neuroprotectants were expected to show more potent protection against oxytosis with improved antioxidant capacity. The best compound was selected mainly based on oxytosis assay and was further studied in ferroptosis and ATP depletion assays. The synergistic effects of vitamin K derivatives and antioxidants were studied by comparison to their equimolar mixture in the ferroptosis and ATP depletion assays. The mode of action of selected compound will be investigated by cellular ROS scavenging and western blot assays. Their immunomodulatory effects and *in vivo* neuroprotective effects will be further studied to evaluate the efficacy for treatment of AD (*cf.* Chapter 4.1).

Furthermore, the mechanism of quinones to produce neuroprotective effects against oxidative stress remains unclear. We have designed a series of quinone derivatives based on five different quinone structures to study the structure-activity relationships of their antioxidant capacity and neuroprotective effects against oxytosis. The antioxidant capacity was evaluated by ORAC assay and neuroprotective effects were studied by glutamate induced oxytosis in HT22 murine neuronal cells. The screened quinone structures can be a useful guidance for further developing of more potent neuroprotectants for treatment of neurodegenerative diseases (*cf.* Chapter 4.2).

For the second purpose, to uncover the role of HDAC6 in the progression of neurodegenerative diseases, we have designed a series of photoswitchable HDAC6 inhibitors as molecular tools for the mechanism study. Two series of photoswitchable HDAC6 inhibitors were designed based on 3-

arylazindole and azoquinoline, respectively. The photophysicochemical properties of target compounds were characterized by UV-vis spectroscopy, and corresponding *cis*-isomers of compounds with moderate thermal stability were further tested in HDAC inhibition assay (*cf.* Chapter 4.3).

3. Published Article: Melatonin- and Ferulic Acid-Based HDAC6 Selective Inhibitors Exhibit Pronounced Immunomodulatory Effects *In Vitro* and Neuroprotective Effects in a Pharmacological Alzheimer's Disease Mouse Model

Melatonin- and Ferulic Acid-Based HDAC6 Selective Inhibitors Exhibit Pronounced Immunomodulatory Effects *In Vitro* and Neuroprotective Effects in a Pharmacological Alzheimer's Disease Mouse Model

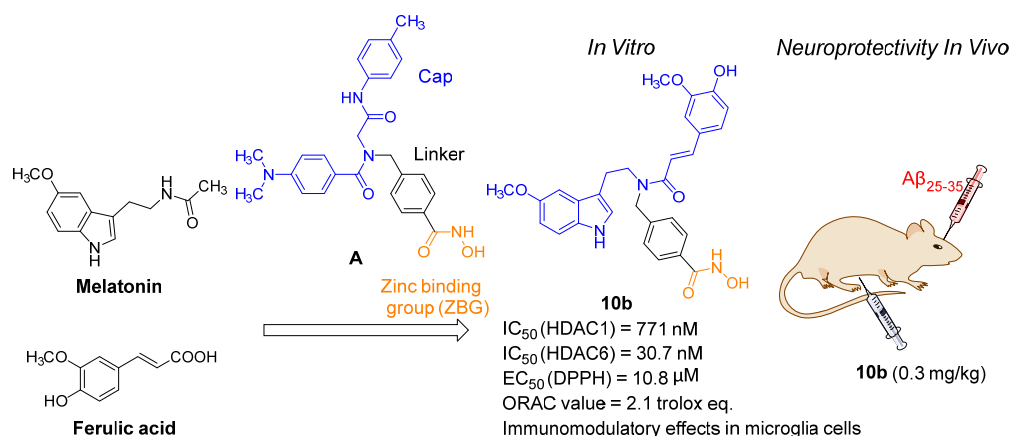
Feng He, C. James Chou, Matthias Scheiner, Eleonora Poeta, Natalia Yuan Chen, Sandra Gunesch, Matthias Hoffmann, Christoph Sotriffer, Barbara Monti, Tangui Maurice,* and Michael Decker*



Cite This: <https://doi.org/10.1021/acs.jmedchem.0c01940>



Read Online



Copyright (2021) American Chemical Society. Reproduced with permission.

Author contributions

Prof. Dr. Michael Decker supervised the whole study.

Feng He and Prof. Dr. Michael Decker designed all target compounds

Feng He, under the supervision of Prof. Dr. Michael Decker, performed the synthesis of all target compounds as well as the evaluation of their antioxidant and metal chelation capacities.

Prof. Dr. C. James Chou performed the HDAC inhibition assay.

Matthias Scheiner and Dr. Matthias Hoffmann performed the *in vivo* animal studies under the supervision of Dr. Tangui Maurice.

Elenora Poeta performed the immunomodulation study under the supervision of Prof. Dr. Barbara Monti.

Natalia Yuan Chen performed the docking study under the supervision of Prof. Dr. Christoph Sotriffer. Dr. Sandra Gunesch performed the neurotoxicity and neuroprotection assays.

3.1. Introduction

Histone deacetylases (HDACs) play essential roles in the progression of neurodegenerative disorders, including AD. Besides, HDACs show tightly relationships to other targets for AD research, like oxidative stress, metal chelation, tau protein phosphorylation, and $A\beta$ -aggregation. For example, hydroxamic acid-based HDACs inhibitors exhibited enhanced protection from oxidative stress through HDAC-independent mechanism or metal chelation.⁷⁹ The inhibition of HDAC6 results in tau acetylation and modulates tau phosphorylation.⁸⁰ Several HDACs inhibitors are able to lower $A\beta$ level in mouse models of AD or reverse $A\beta$ -induced deficits in synaptic plasticity.⁸¹ In view of the comprehensive physiological effects of HDACs on several AD related targets and the HDAC-independent mechanism regarding to AD, HDACs may be a perfect pointcut to design multi-target-directed ligands (MTDLs) which can modulate relevant targets involved in the pathological network for the effective treatment of AD.

Natural products melatonin and ferulic acid have shown promising pharmaceutical effects potentially beneficial in AD, such as antioxidant effects, neuroprotection and neurogenesis promotion.⁸²⁻⁸⁵ In this study, we chemically merged the structures of melatonin and ferulic acid into HDAC6 inhibitor **A** to develop novel multi-target-directed drug candidates for AD with the aim to combine effects in a synergistic manner without losing affinity and selectivity at HDAC6. Accordingly, 15 target compounds have been designed (**Figure 3.1**), synthesized and preliminarily bio-evaluated *in vitro* and *in vivo*.

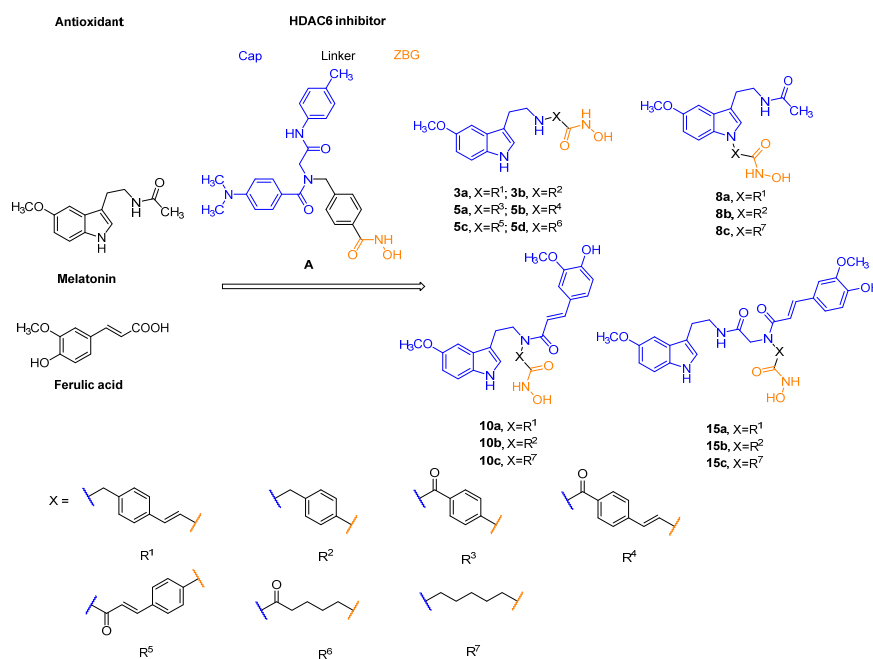


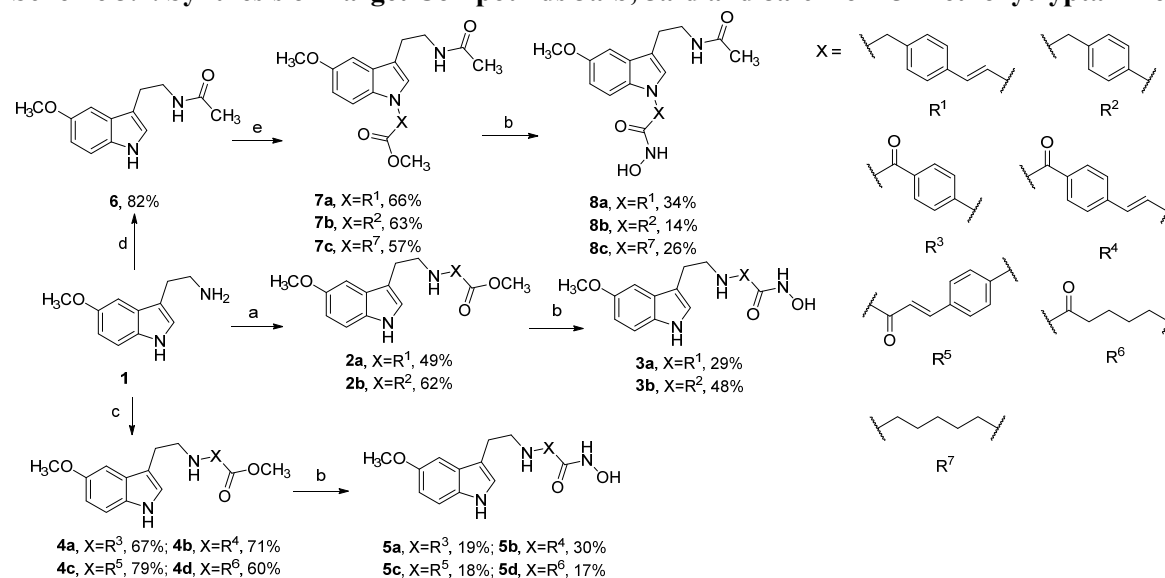
Figure 3.1. Design of melatonin- and ferulic acid-based HDAC inhibitors.

3.2. Synthesis

As described in **Scheme 3.1**, the synthesis of target compounds **3a-b** and **5a-d** starts from the introduction of various ester linker groups to 5-methoxytryptamine (**1**) through nucleophilic substitution. The synthesis of compounds **8a-c** starting with nucleophile substitution between various ester linker groups and melatonin (**6**). Afterwards, the hydroxamate groups were obtained in NH₂OH-KOH methanol solution from respective methyl ester intermediates. In **Scheme 3.2**, the core step to synthesize compounds **10a-c** was the introduction of ferulic acid moiety to intermediates **2a-c**, respectively. The ferulic acid was activated by excess ethyl chloroformate, meanwhile, the phenolic hydroxy group was esterified but could be hydrolyzed in following NH₂OH-KOH methanol solution during the formation of hydroxamate group. 5-Methoxytryptamine (**1**) reacted with Boc-Gly-OH and the boc protecting group was removed to afford intermediate **12**. Subsequently, compounds **15a-c** were obtained through an according procedure by synthesis of compounds **10a-c**, respectively.

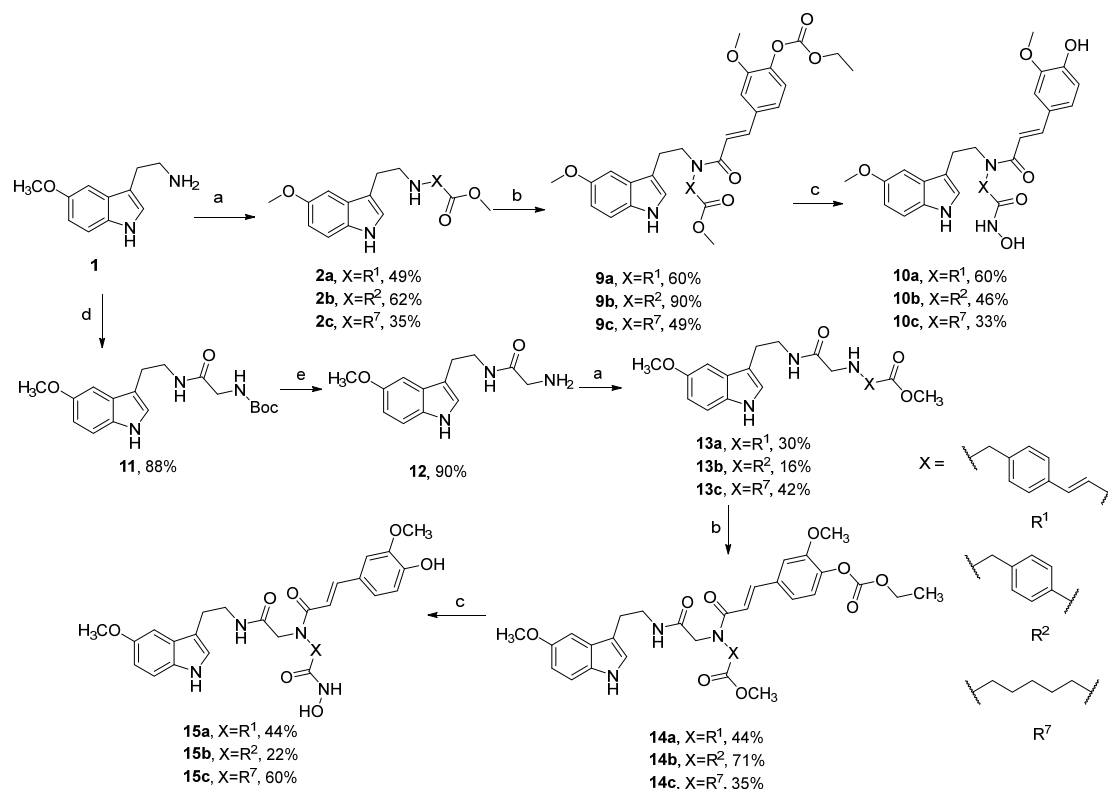
Besides, the temperature-dependent occurrence of *cis/trans* amide bond rotamers of tertiary amide compounds **10a-c** and **15a-c** is a well-known phenomenon, which produced troubles to characterize the structures of corresponding target compounds due to two sets of NMR signals.

Scheme 3.1. Synthesis of Target Compounds **3a-b**, **5a-d** and **8a-c** from 5-Methoxytryptamine (**1**)^a



^aReagents and conditions: (a) methyl (E)-3-(4-(bromomethyl)phenyl)acrylate for **2a**, methyl 4-(bromomethyl)benzoate for **2b**, K₂CO₃, THF, H₂O, reflux; (b) NH₂OH·HCl, KOH, MeOH, r.t.; (c) (E)-4-(3-methoxy-3-oxoprop-1-en-1-yl)benzoic acid for **4a**, 4-(methoxycarbonyl)benzoic acid for **4b**, (E)-3-(4-(methoxycarbonyl)-phenyl)acrylic acid for **4c**, 6-methoxy-6-oxohexanoic acid for **4d**, TBTU, TEA, THF, r.t.; (d) acetic anhydride, DCM, 0 °C to r.t.; (e) i) methyl (E)-3-(4-(bromomethyl)phenyl)acrylate for **7a**, methyl 4-(bromomethyl)benzoate for **7b**, methyl 6-bromohexanoate for **7c**, t-BuOK, THF, reflux; ii) SOCl₂, MeOH, r.t.

Scheme 3.2. Synthesis of Target Compounds 10a-c and 15a-c from 5-Methoxytryptamine (1)^a



^aReagents and conditions: (a) methyl (E)-3-(4-(bromomethyl)phenyl)acrylate for **13a**, methyl 4-(bromomethyl)benzoate for **13b**, methyl 6-bromohexanoate for **13c**, K₂CO₃, THF, H₂O, reflux; (b) ferulic acid, ethyl chloroformate, TEA, dried THF, 0 °C; (c) NH₂OH·HCl, KOH, MeOH, r.t.; (d) Boc-Gly-OH, EDCI, DMAP, TEA, THF, r.t.; (e) 10% TFA in DCM, r.t.

3.3. Biological Evaluation

HDACs Inhibition. In preliminary screening for the inhibition of target compounds against HDAC3 and HDAC6, the IC₅₀s of potent HDAC inhibitors were measured and shown in **Table 3.1**. Among them, compounds **8b** and **10b** showed the most potent HDAC6 inhibition, which are 57-fold and 53-fold selectivity over HDAC3, respectively. Besides, compounds **3a** and **5b** shown potent inhibition to HDAC3 with IC₅₀ of 5.1 and 3.6 nM, respectively. To further confirm the selective inhibition of HDAC6, the IC₅₀s against other subtypes of HDACs of compounds **8b** and **10b** were measured and are listed in **Table 3.2**. Both of them still show highly selective inhibition (more than 20-fold compared to other subtypes) toward HDAC6, and their selectivities are higher than reference compound ACY1215. Moreover, the cellular potency of compounds **8b** and **10b** were examined in HT22 cells by Western blot assay (**Figure 3.2**). Compound **8b** and **10b** selectively induced the increase of acetylated tubulin (AcTub), indicating that both compounds **8b** and **10b** are selectively inhibiting HDAC6 activity in cellular environment.

Furthermore, computational docking studies were carried out to identify the putative binding modes of compounds **8b** and **10b** for HDAC6 (PDB: 6DVM). The docking results are presented in **Figure 3.3**, detailed description can be find in He *et al.*³² or appendix I for both compounds. The results indicate

Table 3.1. Structures, *In Vitro* HDAC (HDAC3, HDAC6) Inhibitory, DPPH Radical Scavenging Activities and ORAC Values of Target Compounds.

Compound	R	IC ₅₀ HDAC3 [nM] or Inhibition [%] at 1 μM (pIC ₅₀ ± SEM) (n=2)	IC ₅₀ HDAC6 [nM] or Inhibition [%] at 1 μM (pIC ₅₀ ± SEM) (n=2)	Selectivity Ratio to HDAC6	DPPH Radical Scavenging Activity EC ₅₀ [μM] ^b	ORAC (trolox equivalents) ^c	
ACY1215	-	51.0 ^a	4.7 ^a	11	255 ± 20.2	0.5 ± 0.1	
Melatonin	-	-	-	-	> 6 mM	2.0 ± 0.3	
Ferulic acid	-	-	-	-	13.7 ± 0.5	3.1 ± 0.3	
3a		5.1 (8.29 ± 0.09)	21.4 (7.67 ± 0.03)	< 1	17.1 ± 2.8	2.4 ± 0.1	
3b		26%	43%	-	66.7 ± 8.8	3.0 ± 0.2	
5a		87%	88%	-	62.0 ± 1.0	2.4 ± 0.2	
5b		3.6 (8.45 ± 0.05)	19.1 (7.72 ± 0.03)	< 1	25.2 ± 1.9	2.0 ± 0.4	
5c		19.7 (7.71 ± 0.11)	33.7 (7.47 ± 0.06)	< 1	65.0 ± 5.8	2.0 ± 0.1	
5d		25%	-69%	-	292 ± 2.1	3.0 ± 0.2	
8a		182 (6.74 ± 0.08)	68.8 (7.16 ± 0.05)	3	31.4 ± 6.5	1.4 ± 0.1	
8b		641 (6.19 ± 0.09)	11.2 (7.95 ± 0.06)	57	56.3 ± 9.6	1.6 ± 0.2	
8c		494 (6.31 ± 0.10)	52.3 (7.28 ± 0.04)	9	262 ± 29.3	1.6 ± 0.3	
10a		163 (6.79 ± 0.06)	25.6 (7.59 ± 0.06)	6	8.5 ± 0.8	1.0 ± 0.2	
10b		1,613 (5.79 ± 0.16)	30.7 (7.51 ± 0.06)	53	10.8 ± 1.9	2.1 ± 0.3	
10c		811 (6.09 ± 0.10)	353 (6.45 ± 0.04)	2	8.9 ± 0.9	2.8 ± 0.1	
15a		108 (6.97 ± 0.09)	53.2 (7.27 ± 0.04)	2	8.3 ± 0.4	1.2 ± 0.4	
15b		-14%	19%	-	15.2 ± 1.3	1.6 ± 0.2	
15c		121 (6.92 ± 0.10)	57.0 (7.24 ± 0.03)	2	19.1 ± 1.1	3.2 ± 0.4	

^aData from ref ⁸⁶;

^bData are the mean (n=3) ± SD;

^cData is expressed as Trolox equivalents and are the mean (n=3) ± SD.

that binding of the capping groups to the L1 loop pocket can be assumed to be the likely reason for HDAC6 selectivity, in line with the elegant crystallographic analyses presented by Porter *et al.*⁸⁷

Table 3.2. Inhibitory Activities of Compounds 8b and 10b at HDAC1 - 4 and HDAC6 - 9

HDAC classes	Subtype	8b		10b	
		IC ₅₀ [nM] (pIC ₅₀ ± SEM) (n=2)	Selectivity Ratio to HDAC6	IC ₅₀ [nM] (pIC ₅₀ ± SEM) (n=2)	Selectivity Ratio to HDAC6
Class I	HDAC1	262 (6.58 ± 0.07)	23	771 (6.11 ± 0.09)	25
	HDAC2	336 (6.47 ± 0.09)	30	2851 (5.55 ± 0.41)	93
	HDAC3	641 (6.19 ± 0.09)	57	1613 (5.79 ± 0.16)	53
	HDAC8	838 (6.08 ± 0.23)	75	3590 (5.45 ± 0.54)	117
Class IIa	HDAC4	3431 (5.47 ± 0.06)	306	> 10 μM	> 326
	HDAC7	1653 (5.78 ± 0.10)	148	> 10 μM	> 326
Class IIb	HDAC9	362 (6.44 ± 0.11)	32	> 10 μM	> 326
	HDAC6	11.2 (7.59 ± 0.06)	-	30.7 (7.51 ± 0.06)	-

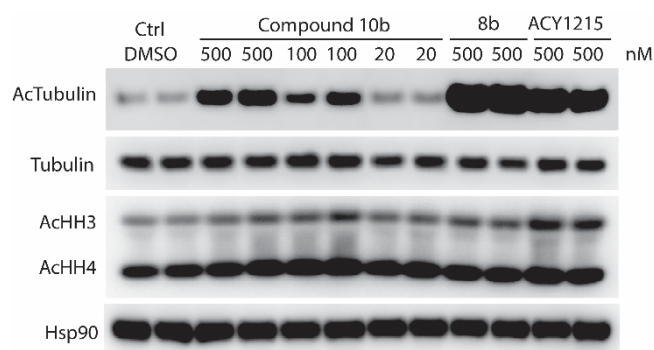


Figure 3.2. Western blot analysis of acetylated tubulin (AcTubulin), acetylated histone H3 (AcHH3), acetylated histone H4 (AcHH4) and Hsp90 in HT22 cell lines after 24 h treatment with compounds **10b** (500, 100 and 20 nM) and **8b** (500 nM) using ACY1215 (500 nM) as positive control. Tubulin was used as a loading control.

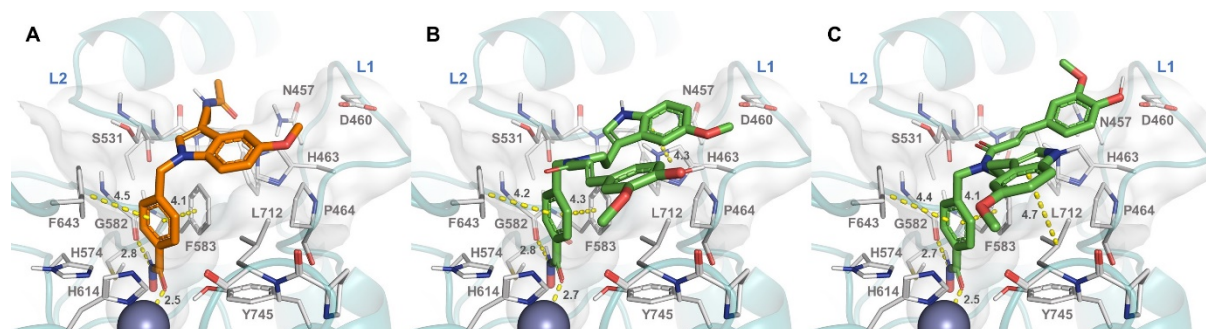


Figure 3.3. Proposed binding modes of compounds **8b** (A) and **10b** (B, C) at the active site of HDAC6. The two alternative binding modes shown for **10b** correspond to the best-ranked result (B) and the most populated cluster

of the docking results (C). Distances are given in Å, selected interactions are highlighted with dashed lines. The Zn²⁺ ion is represented as a grey sphere. Loops 1 and 2 are denoted as L1 and L2. The deep active-site pocket is visualized with a transparent light-grey surface.

Antioxidant Capacities. Free radicals readily damage DNA, lipids, and proteins affecting the cellular function.⁸⁸ DPPH assay and ORAC assay are widely used methods to evaluate antioxidant capacities based on their electron transfer (ET) and hydrogen atom transfer (HAT) capacities, respectively.⁸⁹ According to the data in **Table 3.1**, compounds **8b** and **10b** are not only potent HDAC6 selective inhibitors, but also potent antioxidants. Especially compound **10b**, which shows comparable radical scavenging capacity to ferulic acid and melatonin in DPPH and ORAC assays, respectively.

Neurotoxicity. The low neurotoxicity is essential property for the application of HDAC inhibitors as CNS-targeting therapeutics. Thus, we tested our target compounds in HT22 hippocampal nerve cells for neurotoxicity. As shown in **Figure 3.4**, Compound **10b** shows no significant neurotoxicity, and slight neurotoxic effects were observed for compound **8b** and reference compound ACY1215.

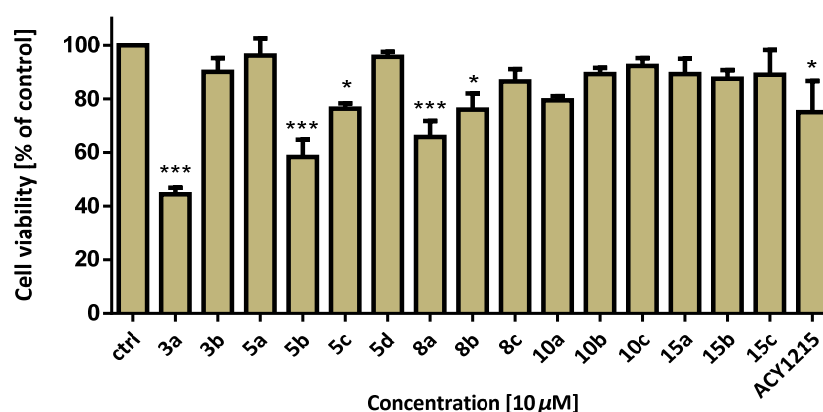


Figure 3.4. Neurotoxicity of target compounds in HT-22 cells at 10 μM. Statistical analysis was performed applying One-way ANOVA followed by Dunnett's multiple comparison post-test. Levels of significance: ****p*<0.001, **p*<0.05 referring to control cells treated with DMSO.

Immunomodulatory Effect. Recent studies have demonstrated that HDAC6 inhibitor tubastatin A alleviates LPS-induced neuroinflammation, representing a new strategy to counteract inflammation and consequently neurodegenerative progression.⁹⁰ Herein, we tested the possible immunomodulatory effects of compounds **8b**, **10b**, and the control ACY1215 in N9 microglial cells. As shown in **Figure 3.5**, compound **10b** strongly reduces nitrite accumulation (F) and IL1β release (I) compared to compound **8b** and control ACY1215, as well as iNOS expression induced by LPS-mediated microglia activation (L). Moreover, compound **10b** increases the expression of phagocytic protein TREM2 (O) and TGFβ2 (R), indicating an immunomodulatory effect that switching neurotoxic M1 to neuroprotective M2 microglia.

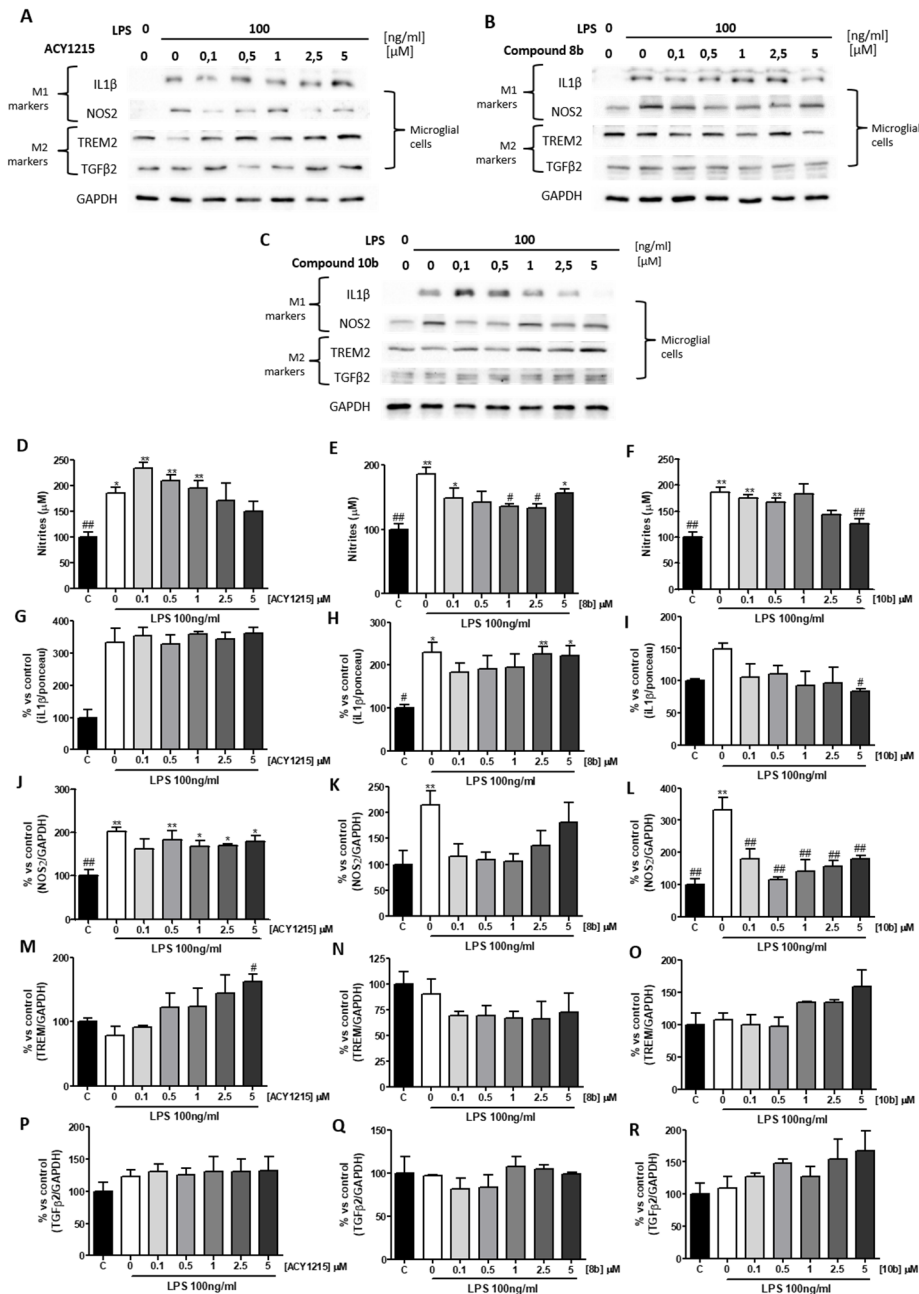


Figure 3.5. Effect of compounds **8b**, **10b** and control ACY1215 on murine N9 cells induced in a M1 activation state by LPS (100 ng/mL) treatment. IL1 β release in N9-conditioned medium and expression of iNOS, TREM2 and TGF β 2 were analyzed by Western blot after 24 h treatment with LPS in presence of increasing concentrations (0.1, 0.5, 1, 2.5 and 5 μ M) of compounds ACY1215 (A), **8a** (B) and **10b** (C). Nitric oxide release was evaluated through Griess reaction in media conditioned for 24 h by microglial cells treated with LPS in presence of compounds ACY1215 (D), **8a** (E) and **10b** (F); as shown in **Figure 3.5F**, only compound **10b** induced a significant reduction of NO release, with the strongest effect at 5 μ M. Additionally, IL1 β release (G, H, I) and iNOS expression (J, K, L), both markers of M1 neurotoxic microglia, strongly decreased in presence of increasing concentrations of compound **10b** (I, L) compared to LPS-treated control; in parallel, expression of M2 microglial markers TREM2 (O) and TGF β 2 (R) increased in cells co-treated by LPS-**10b** compound suggesting a shift from

neurotoxic M1 to neuroprotective M2 microglia. No significant differences on iNOS (M1 marker), TREM and *TGF β 2* (M2 marker) expression were observed in N9 cells after treatment with ACY1215 and compound **8b** compared to LPS-treated ones. All quantitative data are presented as means \pm S.E. from at last 3 independent experiments. Statistical significance between different treatments was calculated with GRAPHPAD PRISM 6 (La Jolla, California, USA) by using one-way analysis of variance (ANOVA) followed by post-hoc comparison through Bonferroni's test. * $p < 0.05$; ** $p < 0.01$ compared to un-treated control; # $p < 0.05$; ### $p < 0.01$ compared to LPS-treated control.

In Vivo Studies. Compound **10b** and the control ACY1214 were chosen to evaluate their neuroprotective properties in an *A β ₂₅₋₃₅*-induced *in vivo* model of AD in mice. As shown in **Figure 3.6A** and **C**, compound **10b** significantly attenuated the *A β ₂₅₋₃₅*-induced spontaneous alternation deficits at 0.3 mg/kg compared to 1 mg/kg of ACY1215. Furthermore, compound **10b** showed superior protection against both *A β ₂₅₋₃₅*-induced spontaneous alternation and passive avoidance deficits compared to an equimolar (0.7 μ M) mixture of the three entities ACY-1215, melatonin, and ferulic acid (**Figure 3.6E** and **Figure 3.7C**), showing the pronounced effects of the hybrid molecule.

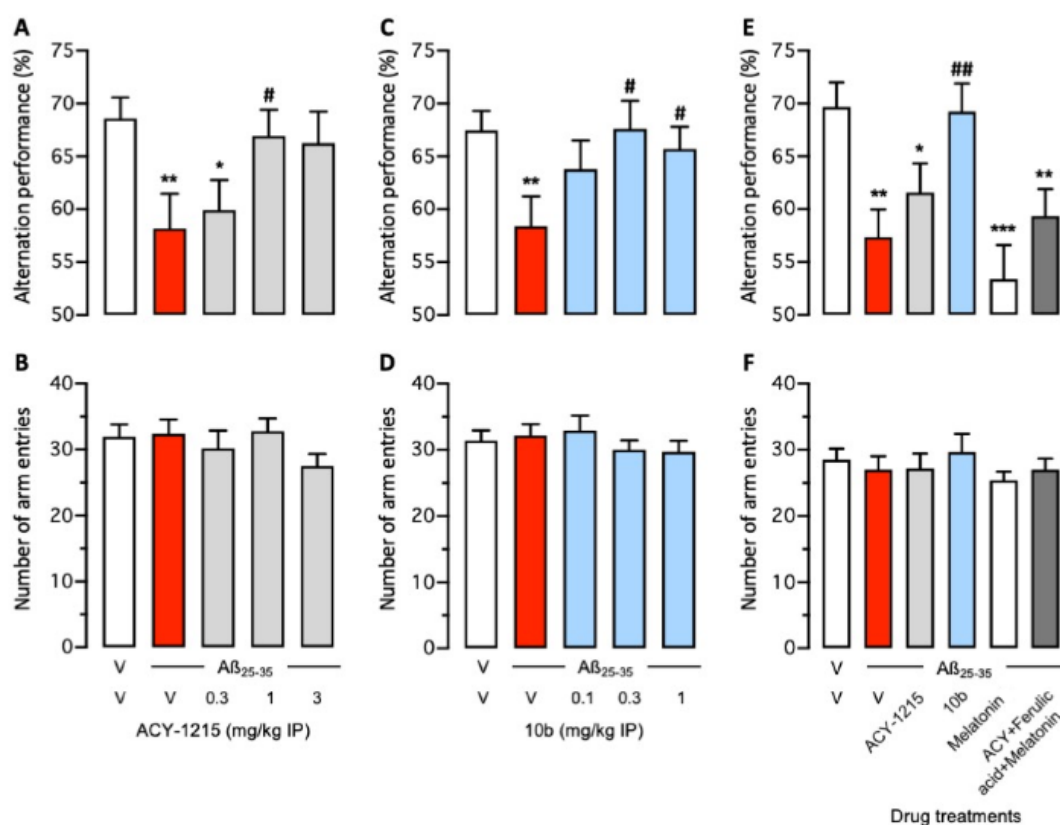


Figure 3.6. Effects of compound on *A β ₂₅₋₃₅*-induced spontaneous alternation deficit in mice. Mice received *A β ₂₅₋₃₅* (9 nmol icv) or vehicle solution (3 μ L icv) on day 1 and compounds (A, B) ACY1215 or (C, D) **10b**, in the 0.1–3 mg/kg ip dose range, o.d., from days 1 to 7. In (E, F), the effect of a drug combination with equimolar doses of ACY-1215 (0.3 mg/kg), melatonin (0.16 mg/kg) and ferulic acid (0.13 mg/kg) was compared to the efficacy of the hybrid molecule. Mice were then tested for spontaneous alternation performance in the YMT in day 8. Top panel (A, C, E): Spontaneous alternation performance; lower panel (B, D, F): number of arm entries. Data show mean \pm SEM with $n = 12-22$ per group. ANOVA: $F_{(4,76)} = 2.81$, $p < 0.05$ in A; $F_{(4,86)} = 2.68$, $p < 0.05$ in B; $F_{(4,76)} = 1.16$,

$p > 0.05$ in C; $F_{(4,86)} = 0.581$, $p > 0.05$ in D; $F_{(5,76)} = 6.20$, $p < 0.0001$ in E; $F_{(5,76)} = 0.554$, $p > 0.05$ in F. * $p < 0.05$, ** $p < 0.01$, *** $p < 0.001$ vs (V + V)-treated group. # $p < 0.05$, ## $p < 0.01$ vs ($A\beta_{25-35}$ + V)-treated group; Dunnett's test.

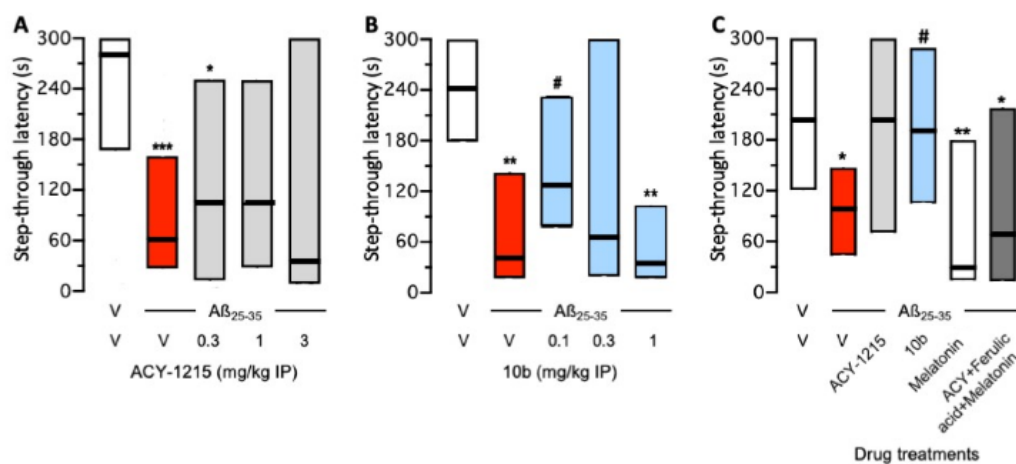


Figure 3.7. Effects of compounds on $A\beta_{25-35}$ -induced passive avoidance deficits in mice. Mice received $A\beta_{25-35}$ (9 nmol icv) or vehicle solution (3 μ L icv) on day 1 and compounds (A) ACY1215 and (B) **10b**, in the 0.1–3 mg/kg ip dose range, o.d., from days 1 to 7. Animals were trained in the passive avoidance test on day 9, and retention (step-through latency) was analyzed on day 10. Data show median and interquartile range with $n = 10-21$ per group. Kruskal-Wallis ANOVA: $H = 10.76$, $p < 0.05$ in A; $H = 16.59$, $p < 0.01$ in B; $H = 14.25$, $p < 0.05$ in C. * $p < 0.05$, ** $p < 0.01$, *** $p < 0.001$ vs (V + V)-treated group. # $p < 0.05$ vs ($A\beta_{25-35}$ + V)-treated group; Dunn's test.

3.4. Conclusions

Multi-target-directed ligands (MTDL) hold a great potential to resolve complex diseases like neurodegeneration and cancer. In this work, HDAC inhibitors as a new emerging direction for treatment of neurodegenerative diseases, were redesigned through MTDL strategy by incorporating the structures of melatonin and ferulic acid. In total 15 target compounds have been designed (in **Figure 3.1**), synthesized (in **Scheme 3.1** and **3.2**) and biologically evaluated in several *in vitro* and *in vivo* assays. Compound **10b** was identified as the most selective and potent HDAC6 inhibitor in both enzyme-based and cellular HDAC inhibition assays (in **Table 3.1** and **Figure 3.2**). Compound **10b** also scavenges the DPPH radical comparable to ferulic acid and possesses comparable ORAC value to melatonin. All *in vitro* data indicates compound **10b** as a potent HDAC6 inhibitor with additional antioxidant capacities. Moreover, compound **10b** shows an immunomodulatory effect (in **Figure 3.3**), leading to a reduction in LPS-induced microglia inflammation and a switch from neurotoxic M1 to neuroprotective M2 microglial phenotype. Furthermore, it shows pronounced attenuation of spatial working memory and long-term memory alteration in an *in vivo* AD mouse model induced by icv $A\beta_{25-35}$ peptide injection (in **Figure 3.4** and **3.5**) at very low doses, thereby proving neuroprotective properties. The superior *in vivo* efficacy of compound **10b** may indicate a synergistic effect between HDAC6 inhibition and its antioxidant activities, which suggests **10b** is a potential drug candidate for treatment of Alzheimer's disease. In another hand, the tertiary amide-based HDAC6-selective inhibitor described herein shows that HDAC6 inhibitors can not only be merged with melatonin and ferulic acid moieties, and as well

maintain potent HDAC6 selective inhibition and the antioxidant properties, but also represent a suitable scaffold to develop neuroprotective compounds *in vivo*, with potentially neurodegenerative disease-modifying properties. (For full article see He *et al.*³² or **Appendix I**)

4. Unpublished Work

4.1. Design, Synthesis and Bio-Evaluation of Hybrid Neuroprotectants based on Vitamin K Derivatives for Treatment of Neurodegenerative Disorders

Author Contributions

Prof. Dr. Michael Decker supervised the whole study.

Feng He and Prof. Dr. Michael Decker designed all target compounds.

Feng He, under the supervision of Prof. Dr. Michael Decker, performed the synthesis of all target compounds as well as the evaluation of their antioxidant capacities.

Julian Hofmann, under the supervision of Prof. Dr. Michael Decker, performed the neuroprotection assays.

4.1.1. Introduction

There are many pathological hallmarks in the progression of neurodegenerative disorders, including abnormal protein aggregation, neuroinflammation, oxidative stress, and nerve cell death.^{10, 91} Alzheimer's disease (AD) is one of the most prominent neurodegenerative disorders, and β -amyloid ($A\beta$) aggregation was considered as the primary cause of AD. However, clinical trials focusing on therapeutic candidates that targeting $A\beta$ had a 99.6% failure rate between 2002 and 2012, which renders researchers reconsider the abnormal protein aggregation hypothesis and shift their interests to other important hallmarks like neuroinflammation and oxidative stress.⁴

Oxytosis is an oxidative stress-dependent regulated cell-death pathway highly relevant to neurological disorders, including AD.^{91, 92} The Salk lab has screened out curcumin derivative J147 and fisetin derivative CMS121 through initial screens based on the oxytosis pathway, and both of them are in or near clinical trials for treatment of AD.³⁵ The development of novel neuroprotectants can not only yield drug candidates for the treatment of neurodegenerative diseases, but also can be useful molecular tools to uncover new aging and disease pathway. Using this approach and molecular hybridization strategy, our group has identified multiple neuroprotectants based on flavonoids,^{42, 43, 93} tetrahydroisoquinazoline,⁴⁴ tacrine,⁹⁴ curcumin,⁴⁶ and synthetic derivatives, some of which even show pronounced neuroprotective effects *in vivo*, indicating oxytosis assay is an effective approach to discover drug candidates for treatment of neurodegenerative disorders.

The Chou group at the Medical University of South Carolina has studied the structure-activity relationship of vitamin K derivatives with neuroprotective effects against oxytosis. Based on menaquinones (VK2), compound **1** with an amine group showed improved neuroprotective effects and compound **2** with a benzyl group connected with the amine exhibited more potent neuroprotection and lower neurotoxicity (**Figure 4.1.1**).⁴⁸ The Segal group has developed a series of naphthoquinone-tryptophan-based hybrids with inhibition of amyloids and tau- derived PHD finger protein 6 (PHF6)

peptide fibrils aggregation, showing potential treatment of AD.^{95, 96} Ferulic acid, melatonin, trolox and lipoic acid are antioxidants which have shown promising pharmacological effects potentially beneficial for AD treatment, but they all failed to protect HT22 hippocampal nerve cells from oxytosis at low micromolar concentration.^{14, 42, 43} Herein, we report the synthesis and pharmacological evaluation of a family of hybrid neuroprotectants, rationally designed by molecular hybridization of the structures of vitamin K derivative **2** and antioxidants like ferulic acid, melatonin, trolox, and lipoic acid, to obtain novel molecules with multifunctional antioxidant and neuroprotective properties (**Figure 4.1.2**).

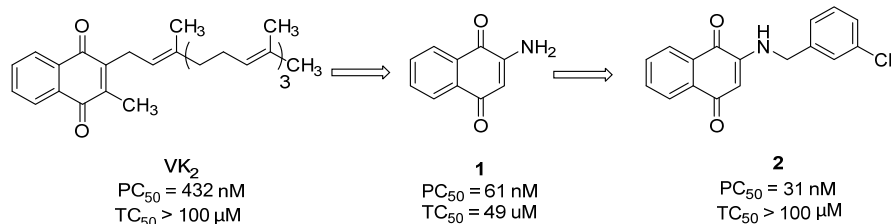


Figure 4.1.1. Development of vitamin derivatives from the Chou group.⁴⁸

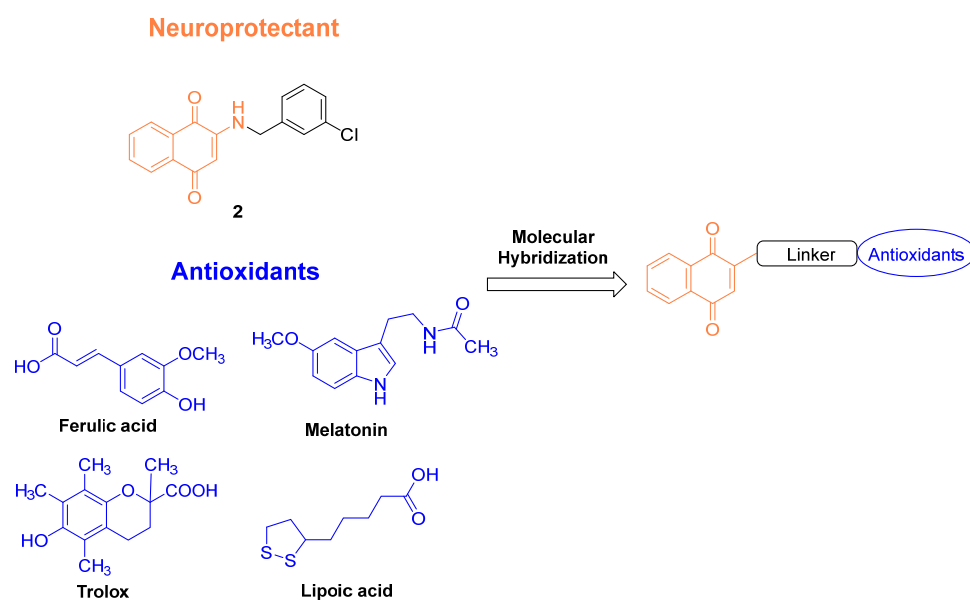
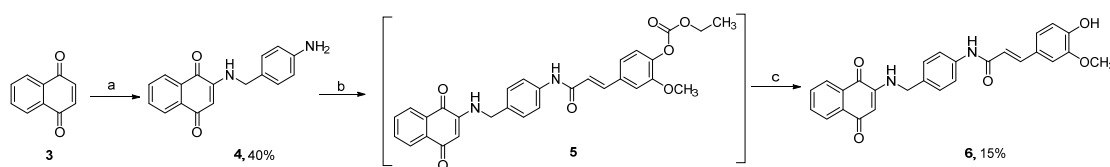


Figure 4.1.2. Design of hybrid vitamin K derivatives.

4.1.2. Results and Discussion

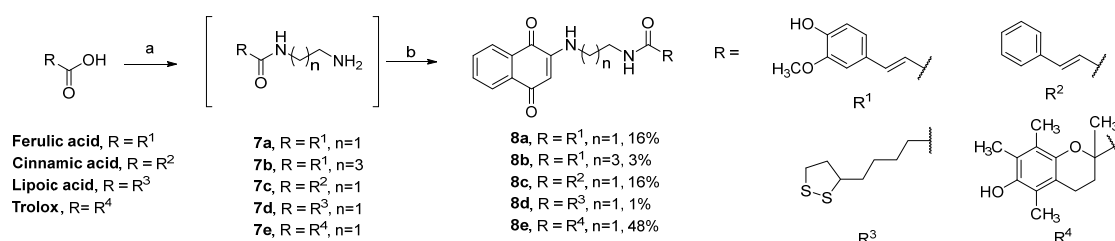
Chemistry. In **Scheme 4.1.1**, the synthesis of first target compound **6** is described starting from 1,4-naphthoquinone (**3**). 1,4-Naphthoquinone (**3**) undergoes a Michael addition reaction with 4-(aminomethyl)aniline to afford intermediate **4** at r.t. Ferulic acid was activated by ethyl chloroformate and reacted with primary amine **4** to afford intermediate **5**, which was subsequently hydrolyzed under basic solution to produce compound **6**. Compounds **8a-e** were synthesized by similar methods from corresponding acids, which is described in **Scheme 4.1.2**. In short, acids like ferulic acid, cinnamic acid, lipoic acid, and trolox were activated by HBTU and reacted with ethylenediamine (**7a, 7c-e**) or butane-1,4-diamine (**7b**) to produce corresponding intermediates **7a-e**. Without further purification, intermediates **7a-e** reacted with 1,4-naphthoquinone in ethanol through Michael addition reaction to yield compounds **8a-e**.

Scheme 4.1.1. Synthesis of Compound 6 from 1,4-Naphthoquinone (3)^a



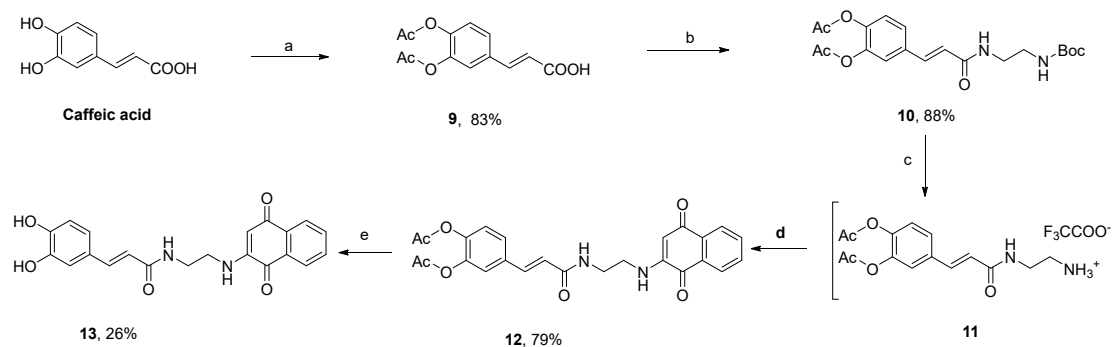
^aReagents and conditions: (a) 4-(aminomethyl)aniline, EtOH, r.t.; (b) ferulic acid, ethyl chloroformate, TEA, THF, 0 °C to r.t.; (c) KOH, MeOH, r.t.

Scheme 4.1.2. Synthesis of Compound 8a-e from the Corresponding Acids^a



^aReagents and conditions: (a) ethylenediamine for 7a and 7c-e, butane-1,4-diamine for 7b, HBTU, TEA, DCM, r.t.; (b) 1,4-naphthoquinone, EtOH, r.t.

Scheme 4.1.3. Synthesis of Compound 13 from Caffeic Acid^a

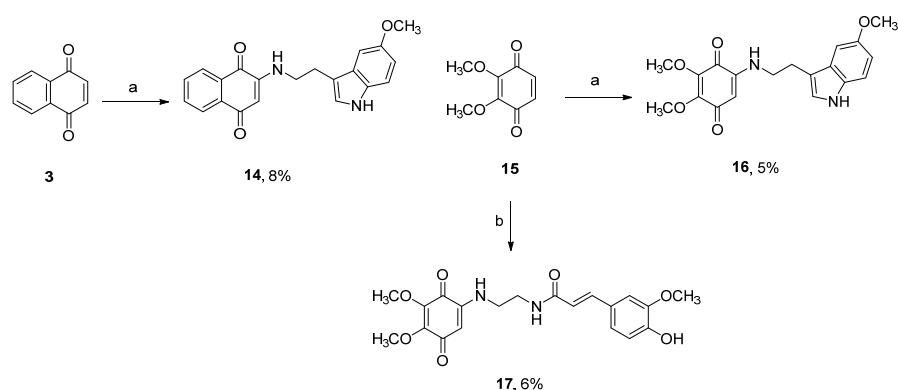


^aReagents and conditions: (a) Ac₂O, pyridine, r.t.; (b) i) ethylenediamine, Boc₂O, TFA, MeOH, 0 °C to r.t.; ii) ethyl chloroformate, TEA, THF, 0 °C to r.t.; (c) TFA, DCM, r.t.; (d) 1,4-naphthoquinone, TEA, EtOH, r.t.; (e) KOH, MeOH, r.t.

The synthesis of caffeic acid hybrid compound **13** was more complex due to the high reactivity of the catechol group, and is described in **Scheme 4.1.3**. The catechol group was firstly protected with acetyl groups by reacting with acetic anhydride in pyridine. The protected caffeic acid **9** was activated by ethyl chloroformate and subsequently reacted with single Boc group protected ethylenediamine to produce intermediate **10**. The boc group of intermediate **10** was removed in TFA-DCM solution and then reacted with 1,4-naphthoquinone to afford intermediate **12** directly without further purification. The final step was removing the acetyl groups in intermediate **12** and compound **13** was obtained with a total yield of 15%.

The synthesis of compounds **14**, **16**, and **17** is described in **Scheme 4.1.4**. Compounds **14** and **16** were obtained from 5-methoxytryptamine by reacting with 1,4-naphthoquinone and 2,3-dimethoxycyclohexa-2,5-diene-1,4-dione, respectively. Compound **17** was obtained by analogue Michael addition reaction with 2,3-dimethoxycyclohexa-2,5-diene-1,4-dione and intermediate **8a**.

Scheme 4.1.4. Synthesis of Compound 14, 16, and 17 from 1,4-Naphthoquinone and 2,3-Dimethoxycyclohexa-2,5-diene-1,4-dione^a



^aReagents and conditions: (a) 5-methoxytryptamine, EtOH, r.t. (b) i) ferulic acid, ethylenediamine, HBTU, TEA, DCM, r.t.; ii) EtOH, r.t.

Neuroprotection against oxytosis. Oxytosis is an oxidative stress induced cell death pathway and the assay was performed in glutamate treated murine hippocampal HT22 cells. Based on the most potent neuroprotective compound **2** from the Chou group,⁴⁸ we firstly designed compound **6** using the benzyl group as linker connecting 1,4-naphthoquinone with a ferulic acid moiety. In the oxytosis assay, compounds were incubated together with 5 mM glutamate treated HT22 cells for 24 h. However, the method from Chou group was slightly modified, in which compounds and 10 mM glutamate treated HT22 cells were incubated for 3 h. This difference rendered reference **2** shows significant neuroprotection at 10 μ M, but loses the activity at 5 μ M (**Figure 4.1.3**). Compound **6** shows no significant neuroprotection at both 5 and 10 μ M, neither compound **8b** with a four carbon linker, on the contrary, compound **8a** with a two carbon linker shows highly potent neuroprotection at 5 μ M. Subsequently, we maintained the two carbon linker and designed compound **8c** hybridizing with cinnamic acid and **13** hybridizing with caffeic acid to check the significance of phenolic acid groups. Compound **8c** loses the neuroprotection at both 5 and 10 μ M and compound **13** loses activity at 5 μ M, which indicates ferulic acid is the most suitable moiety to improve the neuroprotection against glutamate insult compared to cinnamic acid and caffeic acid. Meanwhile, we changed ferulic acid to some other common antioxidants like melatonin, trolox, and lipoic acid, among them, trolox hybrid compound **8e** and melatonin hybrid compound **14** show comparable neuroprotection with **8b** at both 5 and 10 μ M. Ubiquinone with a similar quinone structure was expected to exhibit similar neuroprotection against glutamate toxicity, but two hybrid compounds **16** and **17** failed to protect HT22 cells from oxytosis. Overall, we screened out hybrid compounds **8b**, **8e**, and **15** showing more potent neuroprotection compared to reference compound **2**, which we consider worth to be further studied.

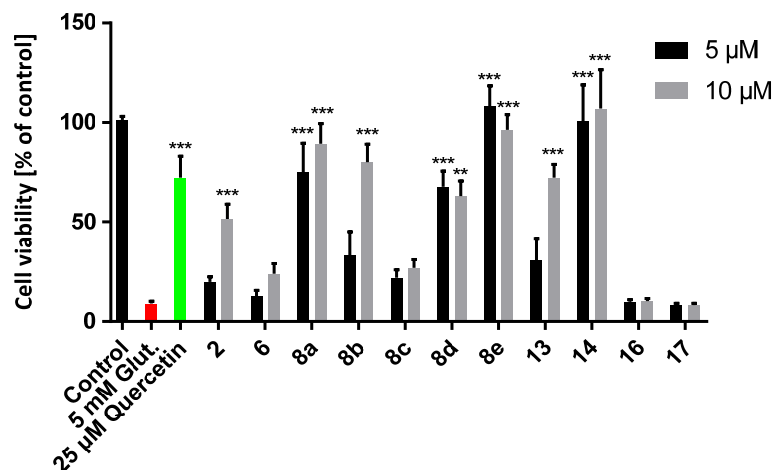


Figure 4.1.3. Neuroprotection of hybrid vitamin K derivatives at 5 and 10 μM against glutamate induced oxytosis in HT22 cells. 25 μM Quercetin served as a positive control (green) while 5 mM glutamate was used to induce toxicity (red). Data is presented as means \pm SEM of three independent experiments and results refer to untreated control cells (black). Statistical analysis was rendered using One-way ANOVA followed by Dunnett's multiple comparison posttest referring to cells treated with 5 mM glutamate. Levels of significance: ** $p < 0.01$, *** $p < 0.001$.

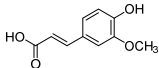
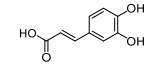
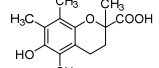
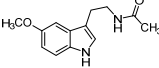
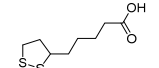
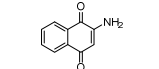
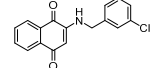
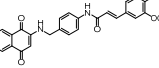
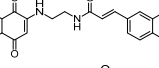
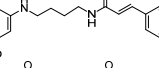
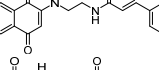
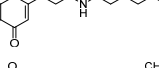
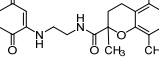
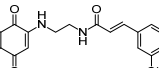
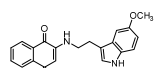
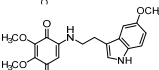
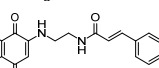
Physicochemical Antioxidant Parameters. All hybrid compounds were designed to maintain the antioxidant capacity from their parent antioxidants and to show improved antioxidant capacity compared to normal vitamin K derivatives. 2,2-Diphenyl-1-picrylhydrazyl radical (DPPH) and oxygen radical absorbance capacity (ORAC) assays were used to evaluate the antioxidant capacity of hybrid compounds.

The DPPH scavenging assay is an electron transfer (ET)-based assay measure an antioxidant's reducing capacity. In the DPPH scavenging assay, four ferulic acid hybrids (**5**, **8a**, **8b** and **17**) show potent and similar capacity to scavenging the DPPH radical, with EC_{50} s of 29.0, 26.1, 27.2, 28.4 μM , respectively, but not as potent as ferulic acid ($EC_{50} = 19.7 \mu\text{M}$) (**Table 4.1.1**), indicating that the derivatization of ferulic acid would slightly decrease its antioxidant capacity, and neither the linker groups or quinone structures could contribute to scavenge the DPPH radical. In line with the report from the Chou group,⁴⁸ both reference compounds **2** and **3** show no capacity to scavenge the DPPH radical. Compounds **8e** and **13** show the most potent radical scavenging capacity, with EC_{50} s of 15.4 and 9.0 μM , respectively, which is comparable to their parent compounds trolox and caffeic acid. As expected, melatonin, lipoic acid, cinnamic acid derivatives and all ubiquinone derivatives are not active in reducing DPPH due to their lack of phenolic acid groups.

ORAC assay is a hydrogen atom transfer (HAT)-based assay that quantifies hydrogen atom donating capacity, using fluorescein (FL) as the fluorescent probe and AAPH as a peroxy radical initiator. In the ORAC assay, most of the target compounds exhibit pronounced radical scavenging capacity with ORAC values ranging from 1.6 (**8e**) to 3.6 (**13** and **17**), respectively. Similar to melatonin, the reference compound **2** shows no capacity to scavenge DPPH radical, but indeed scavenge peroxy radicals

effectively (ORAC value = 1.5), which is comparable to compounds **8e** and **14**. Compounds **13** and **17** show the most potent antioxidant capacity in ORAC assay with the same ORAC value of 3.5, while their neuroprotective effects are not significant at 5 μ M. The ORAC values of compounds **2**, **8c** and **8d** could not be determined because of the high fluorescence they have on their own.

Table 4.1.1. Structures and Physicochemical Antioxidant Parameters of Target Compounds in DPPH and ORAC assays.

Compound	Structure	DPPH Radical Scavenging Activity EC ₅₀ [μ M]	ORAC (trolox equivalents)
Ferulic acid		19.7 \pm 0.5	3.2 \pm 0.3
Caffeic acid		8.0 \pm 0.5	4.8 \pm 0.4
Trolox		13.3 \pm 2.6	-
Melatonin		NA ^a	2.0 \pm 0.3
Lipoic acid		NA ^a	NA ^a
1		NA ^a	1.5 \pm 0.2
2		NA ^a	ND ^b
6		29.0 \pm 3.6	2.7 \pm 0.3
8a		26.1 \pm 1.5	3.1 \pm 0.4
8b		27.2 \pm 2.9	2.2 \pm 0.2
8c		NA ^a	ND ^b
8d		NA ^a	ND ^b
8e		15.4 \pm 1.9	1.6 \pm 0.2
13		9.0 \pm 0.7	3.5 \pm 0.4
14		NA ^a	1.8 \pm 0.2
16		NA ^a	3.0 \pm 0.4
17		28.4 \pm 1.2	3.5 \pm 0.5

^aNot active.

^bNot determined due to interference with their own fluorescence.

In summary, compounds **8b**, **8e**, and **15** show promising neuroprotection in oxytosis assay, and also show potent antioxidant capacities in both DPPH and ORAC assays, except compound **15** which is only active in ORAC assay. Reference compound **2** exhibits similar radical scavenging capacity with melatonin, which can be a reason for its potent neuroprotection in oxytosis assay. No obvious relationship can be observed between their neuroprotective effects and corresponding antioxidant capacities, which can be due to the difference of their membrane permeability, and is in fact often observed in related studies.^{42, 97}

Neuroprotection against Oxytosis, Ferroptosis and ATP Depletion. Encouraged by the potent neuroprotective effects and pronounced antioxidant capacities of compounds **8a**, **8e** and **13**, the lower concentrations in oxytosis assay (**Figure 4.1.4A**, D, G, J), ferroptosis assay (**Figure 4.1.4B**, E, H, K) and ATP depletion assay (**Figure 4.1.4C**, F, I, L) were further tested to get a more complete picture of their neuroprotective effects.

In the oxytosis assay, compounds **8a** (**Figure 4.1.4D**) and **13** (**Figure 4.1.4J**) show comparable neuroprotective effects to compound **2** (**Figure 4.1.4A**), and they all lose protection at 1.56 μM and concentrations lower than 1.56 μM . Relatively spoken, compound **8e** still shows significant protection at 1.56 and 0.75 μM , which is the most potent hybrid compound.

Ferroptosis is another regulated cell-death pathway quite similar to oxytosis and was identified in transformed fibroblasts in 2012 by the Stockwell group.³⁸ They developed compounds erastin and RSL3 as inducer for ferroptosis, and RSL3 was verified as an inhibitor of glutathione peroxidase 4 (GPx4), which could lead to an increase in lipid peroxidation.^{98, 99} Similar to the results in the oxytosis assay, compounds **8a** (**Figure 4.1.4E**) and **13** (**Figure 4.1.4K**) show comparable neuroprotective effects to reference compound **2** (**Figure 4.1.4B**), and they also lose protection at 1.56 μM and concentrations lower than 1.56 μM . More remarkably, compound **8e** maintain significant neuroprotection at 0.38 μM , the lowest concentration we have tested.

Iodoacetic acid (IAA) is an irreversible inhibitor of the glycolytic enzyme glyceraldehyde 3-phosphate dehydrogenase (G3PDH). The IAA insult in HT22 cells leads to ATP depletion and have been commonly used in screens for neuroprotective compounds.^{40, 43} As shown in **Figure 4.1.4C**, F, and L, compounds **2**, **8a**, and **13** possess comparable neuroprotective effects in the ATP depletion assay, and compound **8e** exhibit the most potent protection against IAA insults even at 0.38 μM .

Overall, after a series of screens with multiple neuroprotection assays including oxytosis, ferroptosis, and ATP depletion, compounds **8a** and **13** are comparable to reference compound **2**. Compared with reference compound **2**, compound **8e** shows more pronounced neuroprotective effects at submicromolar concentrations, indicating an improved efficacy after hybridization with trolox. Encouraged by the superior neuroprotective effects of compound **8e**, further studies about its cellular ROS scavenging capacity, immunomodulatory effects, and *in vivo* neuroprotective effects are currently ongoing.

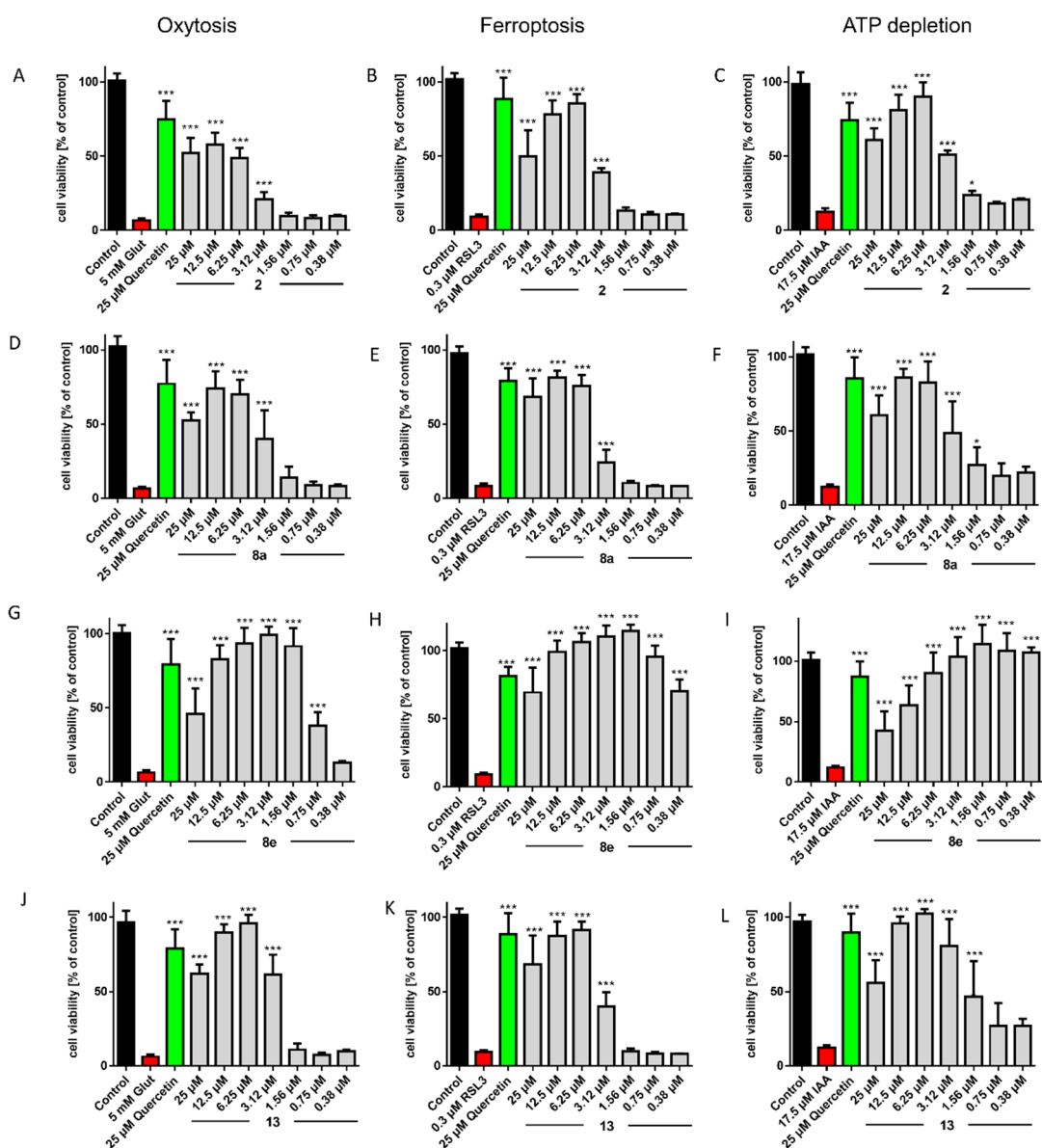


Figure 4.1.4. Neuroprotection of compounds **2**, **8a**, **8e**, and **13** at 0.8 - 25 μM against 5 mM glutamate induced oxytosis (A, D, G, J), 0.3 μM RSL3 induced ferroptosis (B, E, H, K), and 17.5 μM iodoacetic acid (IAA) induced ATP depletion (C, F, I, L) in HT22 hippocampal nerve cells. Data is presented as means \pm SD of three independent experiments and results refer to untreated control cells (black). Statistical analysis was rendered using One-way ANOVA followed by Dunnett's multiple comparison posttest referring to cells treated with 5 mM glutamate (A, D, G, J), 0.3 μM RSL3 (B, E, H, K) or 17.5 μM IAA (C, F, I, L). Levels of significance: * $p < 0.05$, ** $p < 0.01$, *** $p < 0.001$.

Synergistic effects. The highly potent neuroprotective effects of compound **8e** in ferroptosis and ATP depletion assays have intrigued our great interests on the synergistic effects between vitamin K derivatives and trolox. Therefore, we chose compound **1**, which is the core structure of all our target compounds, as a new reference to compare the neuroprotection between compound **8e** and the mixture of compound **1** and trolox. In the ferroptosis assay, compound **1** shows significant protection at 1.56 μM and higher concentrations, while the cell viability decrease at 25 μM probably due to the neurotoxicity

(**Figure 4.1.5A**), which is in line with the report from the Chou group ($TC_{50} = 49 \mu M$).⁴⁸ Trolox exhibits no protection at 0.38 – 25 μM (**Figure 4.1.5C**), on the contrary, the equimolar mixture of compound **1** and trolox already show an effect at 0.15 μM (**Figure 4.1.5E**), which is much more potent than compound **1**. The improved neuroprotective effects of the mixture indicating the combination of compound **1** and trolox possesses synergistic effects to protect HT22 cells from RSL3 insults. Compound **8e** (**Figure 4.1.5G**) shows comparable protection at all tested concentrations to the mixture of compound **1** and trolox (**Figure 4.1.5E**), demonstrating the hybridization have maintained the synergistic effects between vitamin K derivatives and trolox.

In the IAA induced ATP depletion assay, trolox shows slight but significant protection at 1.5 μM and higher concentrations, and the cells viability was improved from 25% to 52% at 25 μM (**Figure 4.1.5D**). Compounds **1**, **8e** and the equimolar mixture of **1** and trolox show highly potent protection even at lowest tested concentration of 0.075 μM , further tests at lower concentrations are currently ongoing. The protection of compound **1** decrease at 6.25 μM and loses the protection at 12.5 μM , indicating significant neurotoxicity to HT22 cells. The mixture of compound **1** and trolox also shows significant neurotoxicity at concentrations higher than 12.5 μM , while the cell viability of compound **8e** treatment shows a slight decrease at much higher concentration of 25 μM .

All in all, we screened the trolox hybrid compound **8e**, which exhibits pronounced antioxidant activities and was identified as the most potent hybrid compound against oxytosis at 0.75 μM , against ferroptosis even at 0.15 μM , and against ATP depletion at 0.075 μM . Trolox and vitamin K derivative **1** show significant synergistic effects in protecting HT22 cells from ferroptosis, moreover, compound **8e** maintains the synergistic effects and shows lower neurotoxicity.

Pan-Assay Interference Compounds (PAINS) Exclusion Assay. The quinone compounds contain the potential reactive “Michael acceptor” and will be recognized as a promiscuous pan-assay interference compound (PAINS) by most of the in silico filters. The Chou group has used a PAINS exclusion assay with 2-mercaptoethanol to confirm that amination of the naphthoquinone could deactivate the “Michael acceptor”.¹⁰⁰ Here, we use the similar method to test the reactivity of our quinone compounds with 2-mercaptoethanol (BME) in PBS (pH 7.4). Compounds 1,4-naphthoquinone (**3**) and 2,3-dimethoxy-5-methylcyclohexa-2,5-diene-1,4-dione (**U0**) are the core structures of vitamin K and ubiquinone, respectively, and can react with BME rapidly in 5 min. While our hybrid compounds **8a** and **17** show no reactivity with BME at all over 6 hours period (**Appendix II**). This study further confirms that not only the amination of naphthoquinone, but also the ubiquinone, will lose the reactivity with thiol.

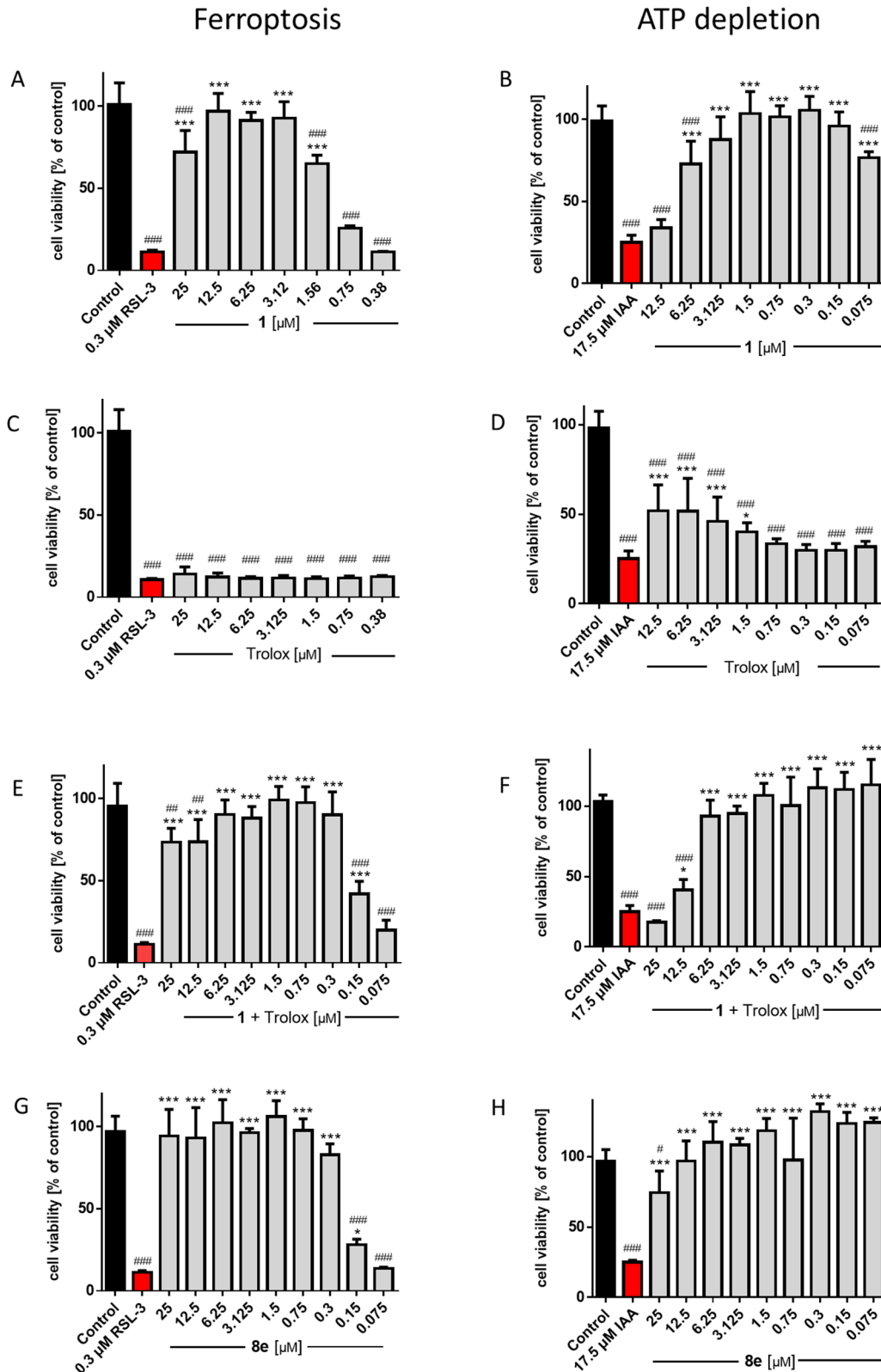


Figure 4.1.5. Neuroprotective effects of compound **8e** and the controls 2-amino-1,4-naphthoquinone (**1**), trolox, and the equimolar mixture of **1** and trolox (**1 + Trolox**) in ferroptosis (A, C, E, G) and ATP depletion (B, D, F, H) assays at 0.075 – 25 μ M. Data is presented as means \pm SD of three independent experiments and results refer to untreated control cells (black). Statistical analysis was rendered using One-way ANOVA followed by Dunnett's

multiple comparison posttest. * $p < 0.05$, ** $p < 0.01$, *** $p < 0.001$ vs 0.3 μM RSL3 (A, C, E, G) or 17.5 μM IAA treated group (B, D, F, H). # $p < 0.01$, ## $p < 0.01$, ### $p < 0.001$ vs control group.

4.1.3. Conclusions

In summary, based on molecular hybridization of vitamin K derivative and common antioxidants, we have designed and synthesized 10 novel hybrid neuroprotectants. With a preliminary oxytosis based screen, we identified the trolox hybrid compound **8e** to possess highly potent neuroprotective effects in glutamate induced oxytosis and RSL3 induced ferroptosis at submicromolar concentrations, and can protect HT22 cell from IAA induced ATP depletion at nanomolar range. Moreover, we found the combination of trolox and vitamin K derivative **1** possesses synergistic effects in protecting HT22 cells from ferroptosis, and the hybrid compound **8e** exhibits comparable protection compared with the combination. Compound **8e** also shows pronounced antioxidant capacity in both DPPH and ORAC assays, with EC_{50} of 15.4 μM and ORAC value of 1.6, respectively. Encouraged by the promising neuroprotective effects and antioxidant capacity of compound **8e**, further *in vitro* immunomodulatory effects and *in vivo* studies are ongoing.

4.1.4. Experimental Section

General Chemistry. Common reagents and solvents were purchased from commercial suppliers and used without further purification unless otherwise stated. Tetrahydrofuran (THF) was distilled from sodium-benzophenone under an argon atmosphere. Reaction progress was monitored using analytical thin layer chromatography (TLC) on precoated silica gel GF254 plates (Macherey Nagel GmbH & Co. KG, Düren, Germany), and spots were detected under UV light (254 nm and 366 nm). Compounds were purified with flash column chromatography with a silica gel with a particle size of 40–63 μM (VWR chemicals, Leuven, Belgium) as the stationary phase and petroleum ether/ethyl acetate or dichloromethane/methanol mixtures as eluent systems. Nuclear magnetic resonance spectra were measured on a Bruker AV-400 NMR instrument (Bruker, Karlsruhe, Germany) in deuterated solvents ($\text{DMSO-}d_6$, CDCl_3 , $\text{MeOD-}d_4$). Chemical shifts are expressed in ppm relative to $\text{DMSO-}d_6$, CDCl_3 , or $\text{MeOD-}d_4$ (2.50/7.26/3.31 for ^1H ; 39.52/77.16/49.00 for ^{13}C). Uncorrected melting points were measured using a Stuart melting point apparatus SMP30.

Measurements for verification and purity of the compounds were performed by LC/MS (from Shimadzu), comprising a DGU-20A3R controller, pump LC-20AB, degasser DGU-20A, and SPD-20A UV/Vis detector. ESI ionization was accomplished by an LCMS-2020 single quadrupole mass spectrometer. As a stationary phase, for analytical purpose, a Synergi 4U fusion-RP 80 Å (150 × 4.6 mm) column and for preparative purpose, a Synergi 4U fusion-RP 80 Å (250 × 10.0 mm) were used. As a mobile phase, a gradient of MeOH/water (both containing 0.1% formic acid) (phase 1/phase 2) was used. The compounds were dissolved in MeOH and filtered through syringe filters. Method: $V(1)/(V(1) + V(2)) = \text{from } 5 \text{ to } 90\% \text{ over } 10 \text{ min}$, $V(1)/(V(1) + V(2)) = 90\% \text{ for } 5 \text{ min}$, $V(1)/(V(1) + V(2)) = \text{from } 90 \text{ to } 5\% \text{ over } 3 \text{ min}$. Methods were performed with a flow rate of 1.0 mL/min. Compounds were detected at $\lambda = 254 \text{ nm}$, and target compounds were $\geq 95\%$ pure.

2-((4-Aminobenzyl)amino)naphthalene-1,4-dione (4)

4-(Aminomethyl)aniline (0.46 g, 3.79 mmol) was added to a solution of 1,4-naphthoquinone (0.60 g, 3.79 mmol) in ethanol, then stirred at room temperature for 1 h. The mixture was concentrated under vacuum and purified with column chromatography to afford red solid 0.42 g, yield 40%. Brown solid, yield 40%. ¹H NMR (400 MHz, CDCl₃): δ 8.12 (d, *J* = 7.7 Hz, 1H), 8.06 (d, *J* = 7.6 Hz, 1H), 7.74 (t, *J* = 7.3 Hz, 1H), 7.63 (t, *J* = 7.5 Hz, 1H), 7.13 (d, *J* = 8.3 Hz, 2H), 6.70 (d, *J* = 8.3 Hz, 2H), 6.10 (s, 1H), 5.83 (s, 1H), 4.25 (d, *J* = 5.5 Hz, 2H), 3.74 (s, 2H) ppm. ¹³C NMR (101 MHz, CDCl₃): δ 183.0, 181.9, 147.7, 146.4, 134.7, 133.7, 132.0, 130.6, 129.2, 126.3, 126.2, 125.5, 115.4, 101.4, 46.6 ppm. LRMS (ESI+) *m/z* calcd for [C₁₇H₁₅N₂O₂]⁺: 279.11, found: 279.10 [M+H]⁺.

(E)-N-(4-(((1,4-Dioxo-1,4-dihydronaphthalen-2-yl)amino)methyl)phenyl)-3-(4-hydroxy-3-methoxyphenyl)acrylamide (5)

Triethylamine (0.55 g, 5.39 mmol) and ethyl chloroformate (0.35 g, 3.23 mmol) were added to a solution of ferulic acid (0.31 g, 1.62 mmol) in 20 mL THF at 0 °C and stirred for 10 min. Then intermediate **4** (0.30 g, 1.08 mmol) was added to the mixture and stirred at r.t. for 1 h. The mixture was concentrated under vacuum, then the residue was redissolved in DCM and washed with water and brine. The organic phase was dried over Na₂SO₄ and concentrated under vacuum to afford red solid. The red solid was then dissolved in methanol and KOH (0.12 g, 2.16 mmol) was added to the mixture. After stirring at r.t. for 10 min, the mixture was extracted with DCM and washed with water and brine. Dried over Na₂SO₄ and purified with column chromatography to afford red solid 75 mg, yield 15%. ¹H NMR (400 MHz, DMSO-*d*₆): δ 10.08 (s, 1H), 9.51 (s, 1H), 8.13 (t, *J* = 6.4 Hz, 1H), 8.00 (d, *J* = 7.6 Hz, 1H), 7.91 (d, *J* = 7.6 Hz, 1H), 7.81 (t, *J* = 7.5 Hz, 1H), 7.73 (t, *J* = 7.5 Hz, 1H), 7.66 (d, *J* = 8.3 Hz, 2H), 7.48 (d, *J* = 15.6 Hz, 1H), 7.31 (d, *J* = 8.3 Hz, 2H), 7.18 (s, 1H), 7.06 (d, *J* = 8.1 Hz, 1H), 6.82 (d, *J* = 8.1 Hz, 1H), 6.63 (d, *J* = 15.6 Hz, 1H), 5.59 (s, 1H), 4.41 (d, *J* = 6.3 Hz, 2H), 3.83 (s, 3H) ppm. ¹³C NMR (101 MHz, DMSO-*d*₆): δ 182.1, 181.8, 164.4, 149.1, 148.9, 148.3, 141.1, 139.0, 135.3, 133.5, 132.7, 132.4, 130.9, 128.1 (2C), 126.7, 126.4, 125.8, 122.5, 119.7 (2C), 119.3, 116.2, 111.3, 100.9, 56.0, 45.3 ppm. LRMS (ESI+) *m/z* calcd for [C₂₇H₂₃N₂O₅]⁺: 455.15, found: 455.10 [M+H]⁺. HPLC: *t*_R = 12.1 min, purity 96.4%. mp = 209-210 °C.

(E)-N-(2-(((1,4-Dioxo-1,4-dihydronaphthalen-2-yl)amino)ethyl)-3-(4-hydroxy-3-methoxyphenyl)acrylamide (8a)

TEA (0.48 g, 4.74 mmol) and HBTU (0.66 g, 1.73 mmol) were added to a solution of ferulic acid (0.31 g, 1.58 mmol) in 20 mL DCM and stirred at room temperature for 1 h. The mixture was added dropwise to a solution of ethylenediamine (0.48 g, 7.97 mmol) in 10 mL DCM and stirred at room temperature for 1 h. The mixture was then concentrated under vacuum till the excess of ethylenediamine was removed. 1,4-Naphthoquinone (0.50 g, 3.16 mmol) in 20 mL ethanol was added to the residue and stirred for 1 h. The mixture was concentrated under vacuum and purified with column chromatography to afford orange solid 100 mg, yield 16%. ¹H NMR (400 MHz, DMSO-*d*₆): δ 9.48 (s, 1H), 8.25 (t, *J* = 5.8 Hz, 1H), 8.07 – 8.02 (m, 1H), 8.02 – 7.96 (m, 1H), 7.88 (td, *J* = 7.5, 1.2 Hz, 1H), 7.78 (td, *J* = 7.5,

1.2 Hz, 1H), 7.65 (t, $J = 5.8$ Hz, 1H), 7.41 (d, $J = 15.7$ Hz, 1H), 7.18 (d, $J = 1.7$ Hz, 1H), 7.05 (dd, $J = 8.2, 1.7$ Hz, 1H), 6.84 (d, $J = 8.1$ Hz, 1H), 6.46 (d, $J = 15.7$ Hz, 1H), 5.86 (s, 1H), 3.86 (s, 3H), 3.47 (q, $J = 6.0$ Hz, 2H), 3.35 (q, $J = 6.2$ Hz, 2H) ppm. ^{13}C NMR (101 MHz, DMSO- d_6): δ 181.9, 166.6, 149.2, 148.8, 148.3, 139.9, 135.3, 133.6, 132.7, 130.8, 126.8, 126.3, 125.8, 122.1, 119.0, 116.1, 111.3, 100.1, 56.0, 42.7, 37.4 ppm. LRMS (ESI+) m/z calcd for $[\text{C}_{22}\text{H}_{21}\text{N}_2\text{O}_5]^+$: 393.14, found: 393.10 $[\text{M}+\text{H}]^+$. HPLC: $t_{\text{R}} = 11.0$ min, purity 95.9%. mp = 194-196 °C.

(E)-N-(4-((1,4-Dioxo-1,4-dihydronaphthalen-2-yl)amino)butyl)-3-(3-hydroxy-4-methoxyphenyl)acrylamide (8b)

Compound **8b** was prepared from ferulic acid, 1,4-butanediamine and 1,4-naphthoquinone in a similar manner as described for compound **8a**. Red solid, yield 3%. ^1H NMR (400 MHz, DMSO- d_6): δ 9.40 (s, 1H), 8.02 – 7.91 (m, 3H), 7.82 (t, $J = 7.5$ Hz, 1H), 7.72 (t, $J = 7.5$ Hz, 1H), 7.57 (t, $J = 6.0$ Hz, 1H), 7.31 (d, $J = 15.7$ Hz, 1H), 7.11 (d, $J = 1.4$ Hz, 1H), 6.98 (dd, $J = 8.1, 1.5$ Hz, 1H), 6.79 (d, $J = 8.1$ Hz, 1H), 6.43 (d, $J = 15.7$ Hz, 1H), 5.71 (s, 1H), 3.80 (s, 3H), 3.27 – 3.13 (m, 4H), 1.70 – 1.56 (m, 2H), 1.56 – 1.46 (m, 2H) ppm. ^{13}C NMR (101 MHz, DMSO- d_6): δ 182.1, 181.7, 165.8, 149.0, 148.7, 148.3, 139.3, 135.3, 133.7, 132.6, 130.9, 126.9, 126.3, 125.8, 122.0, 119.5, 116.1, 111.2, 99.8, 56.0, 42.1, 38.8, 27.2, 25.4 ppm. LRMS (ESI+) m/z calcd for $[\text{C}_{24}\text{H}_{25}\text{N}_2\text{O}_5]^+$: 421.17, found: 421.10 $[\text{M}+\text{H}]^+$. HPLC: $t_{\text{R}} = 14.1$ min, purity 96.3%. mp = 181-183 °C.

N-(2-((1,4-Dioxo-1,4-dihydronaphthalen-2-yl)amino)ethyl)cinnamamide (8c)

Compound **8c** was prepared from cinnamic acid, ethylenediamine and 1,4-naphthoquinone in a similar manner as described for compound **8a**. Brown solid, yield 16%. ^1H NMR (400 MHz, DMSO- d_6): δ 8.35 (t, $J = 5.8$ Hz, 1H), 7.99 (dd, $J = 7.7, 1.0$ Hz, 1H), 7.94 (dd, $J = 7.6, 1.0$ Hz, 1H), 7.83 (td, $J = 7.5, 1.3$ Hz, 1H), 7.73 (td, $J = 7.5, 1.3$ Hz, 1H), 7.61 (t, $J = 5.9$ Hz, 1H), 7.58 – 7.55 (m, 2H), 7.46 (d, $J = 15.8$ Hz, 1H), 7.41 (d, $J = 7.6$ Hz, 2H), 7.39 – 7.37 (m, 1H), 6.60 (d, $J = 15.8$ Hz, 1H), 5.81 (s, 1H), 3.44 (q, $J = 6.1$ Hz, 2H), 3.31 (q, $J = 6.1$ Hz, 2H) ppm. ^{13}C NMR (101 MHz, DMSO- d_6): δ 181.9 (2C), 166.1, 149.2, 139.5, 135.3, 135.3, 133.6, 132.7, 130.8, 130.0, 129.4 (2C), 128.0 (2C), 126.3, 125.8, 122.3, 100.1, 42.6, 37.5 ppm. LRMS (ESI+) m/z calcd for $[\text{C}_{21}\text{H}_{19}\text{N}_2\text{O}_3]^+$: 347.13, found: 347.10 $[\text{M}+\text{H}]^+$. HPLC: $t_{\text{R}} = 11.8$ min, purity 99.8%. mp = 226-228 °C.

N-(2-((1,4-Dioxo-1,4-dihydronaphthalen-2-yl)amino)ethyl)-5-(1,2-dithiolan-3-yl)pentanamide (8d)

Compound **8d** was prepared from 1,4-naphthoquinone and lipoic acid in a similar manner as described for compound **8a**. Orange solid 24 mg, yield 3%. ^1H NMR (400 MHz, DMSO- d_6): δ 8.10 – 7.90 (m, 3H), 7.89 – 7.79 (m, 1H), 7.73 (t, $J = 6.8$ Hz, 1H), 7.51 (s, 1H), 5.76 (s, 1H), 3.61 – 3.49 (m, 1H), 3.26 – 3.19 (m, 2H), 3.19 – 3.11 (m, 1H), 3.11 – 3.02 (m, 1H), 2.42 – 2.29 (m, 1H), 2.06 (t, $J = 5.9$ Hz, 2H), 1.90 – 1.74 (m, 1H), 1.68 – 1.56 (m, 1H), 1.56 – 1.22 (m, 7H) ppm. ^{13}C NMR (101 MHz, DMSO- d_6): δ 181.9, 173.2, 149.2, 147.7, 135.3, 133.6, 132.7, 130.8, 126.3, 125.8, 100.0, 56.5, 46.0, 42.6, 38.5, 37.3, 35.7, 34.6, 28.7, 25.4 ppm. LRMS (ESI+) m/z calcd for $[\text{C}_{20}\text{H}_{25}\text{N}_2\text{O}_3\text{S}_2]^+$: 405.12 found: 405.05 $[\text{M}+\text{H}]^+$. HPLC: $t_{\text{R}} = 10.6$ min, purity 95.6%. mp = 164-165 °C.

***N*-(2-((1,4-Dioxo-1,4-dihydronaphthalen-2-yl)amino)ethyl)-6-hydroxy-2,5,7,8-tetramethylchromane-2-carboxamide (8e)**

Compound **8e** was prepared from trolox, ethylenediamine and 1,4-naphthoquinone in a similar manner as described for compound **8a**. Orange solid 43 mg, yield 48%. ¹H NMR (400 MHz, CDCl₃): δ 8.10 (dd, *J* = 7.7, 0.7 Hz, 1H), 8.08 – 8.04 (m, 1H), 7.74 (td, *J* = 7.6, 1.3 Hz, 1H), 7.64 (td, *J* = 7.6, 1.2 Hz, 1H), 6.75 (t, *J* = 6.1 Hz, 1H), 6.26 (s, 1H), 5.64 (s, 1H), 3.79 – 3.62 (m, 1H), 3.54 – 3.41 (m, 2H), 3.27 – 3.18 (m, 2H), 2.69 – 2.48 (m, 2H), 2.47 – 2.36 (m, 1H), 2.14 (s, 3H), 2.11 (s, 3H), 2.03 (s, 3H), 1.92 – 1.83 (m, 1H), 1.55 (s, 3H) ppm. ¹³C NMR (101 MHz, CDCl₃): δ 183.0, 181.3, 175.9, 148.2, 145.7, 144.1, 134.7, 133.5, 132.1, 130.5, 126.3, 126.2, 121.8, 121.7, 119.3, 118.0, 100.8, 78.4, 43.3, 37.6, 29.6, 24.7, 20.5, 12.2, 12.0, 11.3 ppm. LRMS (ESI+) *m/z* calcd for [C₂₆H₂₉N₂O₅]⁺: 449.20, found: 449.10 [M+H]⁺. HPLC: *t*_R = 12.0 min, purity 96.9%.

***(E)*-3-(3,4-diacetoxyphenyl)acrylic acid (9)**

Acetic anhydride (0.56 g, 5.50 mmol) was added to a solution of caffeic acid (0.10 g, 0.55 mmol) in 5 mL pyridine and stirred at r.t. over night. The mixture was neutralized to pH 6, then excess water was added and extracted with DCM. The organic phase was combined and washed with water and brine, dried over Na₂SO₄ and concentrated under vacuum to afford white solid 0.12 g, yield 83%. ¹H NMR (400 MHz, DMSO-*d*₆): δ 12.46 (s, 1H), 7.68 – 7.61 (m, 2H), 7.58 (d, *J* = 16.0 Hz, 1H), 7.32 (d, *J* = 8.3 Hz, 1H), 6.54 (d, *J* = 16.0 Hz, 1H), 2.30 (s, 3H), 2.29 (s, 3H) ppm. ¹³C NMR (101 MHz, DMSO-*d*₆): δ 168.7, 168.6, 167.8, 143.8, 142.8, 142.6, 133.6, 127.2, 124.6, 123.5, 120.8, 20.8, 20.8 ppm. LRMS (ESI+) *m/z* calcd for [C₁₃H₁₃O₆]⁺: 265.06 found: 265.00 [M+H]⁺. HPLC: *t*_R = 10.4 min.

***(E)*-4-(3-((2-((tert-butoxycarbonyl)amino)ethyl)amino)-3-oxoprop-1-en-1-yl)-1,2-phenylene diacetate (10)**

TEA (0.38 g, 3.79 mmol) and ethyl chloroformate (0.20 g, 1.89 mmol) were added to a solution of intermediate **9** (0.50 g, 1.89 mmol) in 20 mL THF and stirred at 0 °C for 10 min. tert-Butyl (2-aminoethyl)carbamate (0.36 g, 2.27 mmol) prepared from ethylenediamine, Boc₂O, and TFA was added to the mixture and stirred at r.t. for 1 h. The mixture was concentrated under vacuum and purified with column chromatography to afford white solid 0.68 g, yield 88%. ¹H NMR (400 MHz, CDCl₃): δ 7.55 (d, *J* = 15.6 Hz, 1H), 7.37 (dd, *J* = 8.4, 1.9 Hz, 1H), 7.33 (d, *J* = 1.8 Hz, 1H), 7.20 (d, *J* = 8.3 Hz, 1H), 6.60 (s, 1H), 6.34 (d, *J* = 15.6 Hz, 1H), 5.06 (s, 1H), 3.53 – 3.46 (m, 2H), 3.41 – 3.28 (m, 2H), 2.32 (s, 3H), 2.31 (s, 3H), 1.46 (s, 9H) ppm. ¹³C NMR (101 MHz, CDCl₃): δ 168.1, 168.1, 166.1, 155.23, 143.0, 142.4, 139.1, 133.8, 126.1, 123.8, 122.4, 121.9, 79.9, 50.8 (2C), 28.4 (3C), 20.7, 20.6 ppm. LRMS (ESI+) *m/z* calcd for [C₂₀H₂₇N₂O₇]⁺: 407.17 found: 407.15 [M+H]⁺. HPLC: *t*_R = 10.7 min.

***(E)*-4-(3-((2-((1,4-dioxo-1,4-dihydronaphthalen-2-yl)amino)ethyl)amino)-3-oxoprop-1-en-1-yl)-1,2-phenylene diacetate (12)**

1 mL TFA was added dropwise to a solution of intermediate **10** (0.20 g, 0.50 mmol) in 10 mL DCM and stirred at r.t. for 30 min. The mixture was concentrated under vacuum to afford crude intermediate **11**. Intermediate **11** and TEA (51 mg, 0.50 mmol) were added to a solution of 1,4-naphthoquinone (0.16

g, 1.00 mmol) in 5 mL DCM and stirred at r.t. for 30 min. The mixture was concentrated under vacuum and purified with column chromatography to afford intermediate orange solid 0.18 g, yield 79%. ¹H NMR (400 MHz, DMSO-*d*₆): δ 8.35 (t, *J* = 5.7 Hz, 1H), 7.99 (d, *J* = 7.5 Hz, 1H), 7.95 (d, *J* = 7.5 Hz, 1H), 7.83 (td, *J* = 7.5, 1.0 Hz, 1H), 7.73 (td, *J* = 7.5, 1.0 Hz, 1H), 7.61 (t, *J* = 5.9 Hz, 1H), 7.54 – 7.48 (m, 2H), 7.45 (d, *J* = 15.8 Hz, 1H), 7.31 (d, *J* = 8.2 Hz, 1H), 6.58 (d, *J* = 15.8 Hz, 1H), 5.82 (s, 1H), 3.43 (dd, *J* = 12.0, 6.0 Hz, 2H), 3.33 – 3.27 (m, 2H), 2.30 (s, 3H), 2.29 (s, 3H) ppm. ¹³C NMR (101 MHz, DMSO-*d*₆): δ 181.9, 168.7, 168.6, 165.9, 149.2, 143.2, 142.8, 137.8, 135.3, 134.2, 133.8, 133.6, 132.7, 130.9, 126.4, 126.3, 125.8, 124.6, 123.4, 122.8, 100.2, 42.5, 37.5, 20.82, 20.81 ppm. LRMS (ESI+) *m/z* calcd for [C₂₅H₂₃N₂O₇]⁺: 463.14 found: 463.05 [M+H]⁺. HPLC: *t*_R = 11.3 min.

(E)-3-(3,4-dihydroxyphenyl)-N-(2-((1,4-dioxo-1,4-dihydronaphthalen-2-yl)amino)ethyl)acrylamide (13)

KOH (64 mg, 1.14 mmol) in 2 mL methanol was added dropwise to a solution of intermediate **12** (0.26 g, 0.57 mmol) in 8 mL methanol and stirred at r.t. for 10 min. The mixture was acidified to pH 4 and concentrated under vacuum. The raw product was purified with column chromatography to afford orange solid 55 mg, yield 26%. ¹H NMR (400 MHz, DMSO-*d*₆): δ 9.41 (s, 1H), 9.18 (s, 1H), 8.31 (t, *J* = 5.7 Hz, 1H), 8.02 – 7.97 (m, 1H), 7.96 – 7.91 (m, 1H), 7.83 (td, *J* = 7.5, 1.1 Hz, 1H), 7.73 (td, *J* = 7.5, 1.1 Hz, 1H), 7.62 (t, *J* = 5.8 Hz, 1H), 7.28 (d, *J* = 15.7 Hz, 1H), 6.97 (d, *J* = 1.9 Hz, 1H), 6.85 (dd, *J* = 8.2, 1.8 Hz, 1H), 6.76 (d, *J* = 8.1 Hz, 1H), 6.31 (d, *J* = 15.7 Hz, 1H), 5.80 (s, 1H), 3.41 (dd, *J* = 11.8, 5.9 Hz, 2H), 3.30 (dd, *J* = 11.8, 5.9 Hz, 2H) ppm. ¹³C NMR (101 MHz, DMSO-*d*₆): δ 181.9, 181.9, 166.7, 149.2, 147.9, 146.0, 140.0, 135.3, 133.6, 132.7, 130.9, 126.7, 126.4, 125.8, 120.9, 118.5, 116.3, 114.4, 100.1, 42.7, 37.4 ppm. LRMS (ESI+) *m/z* calcd for [C₂₁H₁₉N₂O₅]⁺: 379.12 found: 379.05 [M+H]⁺. HPLC: *t*_R = 10.5 min, purity = 97.9%. mp = 259-261 °C.

2-((2-(5-methoxy-1H-indol-3-yl)ethyl)amino)naphthalene-1,4-dione (14)

Compound **14** was prepared from 5-methoxytryptamine and 1,4-naphthoquinone in a similar manner as described for intermediate **4**. Red solid, yield 8%. ¹H NMR (400 MHz, CDCl₃): δ 8.01 (dd, *J* = 7.7, 1.2 Hz, 2H), 7.92 (dd, *J* = 7.7, 1.2 Hz, 1H), 7.63 (td, *J* = 7.6, 1.3 Hz, 1H), 7.51 (td, *J* = 7.5, 1.2 Hz, 1H), 7.18 (d, *J* = 1.2 Hz, 1H), 6.97 (d, *J* = 2.0 Hz, 1H), 6.94 (d, *J* = 2.3 Hz, 1H), 6.80 (dd, *J* = 8.8, 2.4 Hz, 1H), 5.95 (s, 1H), 5.70 (s, 1H), 3.78 (s, 3H), 3.41 (q, *J* = 6.6 Hz, 2H), 3.03 (t, *J* = 6.8 Hz, 2H) ppm. ¹³C NMR (101 MHz, CDCl₃): δ 183.0, 181.8, 154.2, 147.9, 134.7, 133.7, 131.9, 131.6, 130.5, 127.4, 126.2, 126.2, 123.0, 112.7, 112.2, 111.8, 100.9, 100.3, 55.9, 42.5, 24.2 ppm. LRMS (ESI+) *m/z* calcd for [C₂₁H₁₉N₂O₃]⁺: 347.13, found: 347.10 [M+H]⁺. HPLC: *t*_R = 12.1 min, purity 95.9%. mp = 166-167 °C.

2,3-Dimethoxy-5-((2-(5-methoxy-1H-indol-3-yl)ethyl)amino)cyclohexa-2,5-diene-1,4-dione (16)

Compound **16** was prepared from 2,3-dimethoxycyclohexa-2,5-diene-1,4-dione and 5-methoxytryptamine in a similar manner as described for intermediate **4**. Brown solid 23 mg, yield 5%. ¹H NMR (400 MHz, CDCl₃): δ 8.17 (s, 1H), 7.29 (d, *J* = 8.8 Hz, 1H), 7.05 (d, *J* = 2.2 Hz, 1H), 7.01 (d, *J* = 2.2 Hz, 1H), 6.90 (dd, *J* = 8.8, 2.4 Hz, 1H), 5.94 (s, 1H), 5.35 (s, 1H), 4.17 (s, 3H), 3.89 (s, 3H), 3.84 (s, 3H), 3.42 (q, *J* = 6.6 Hz, 2H), 3.08 (t, *J* = 6.8 Hz, 2H) ppm. ¹³C NMR (101 MHz, CDCl₃): δ 181.3,

180.4, 154.2, 148.6, 145.8, 140.3, 131.6, 127.4, 123.0, 112.6, 112.2, 111.6, 100.3, 95.1, 61.4, 61.1, 56.0, 42.7, 24.1 ppm. LRMS (ESI+) m/z calcd for $[C_{19}H_{21}N_2O_5]^+$: 357.14 found: 357.05 $[M+H]^+$. HPLC: t_R = 10.7 min, purity 97.6%. mp = 108-110 °C.

(E)-N-(2-((4,5-dimethoxy-3,6-dioxocyclohexa-1,4-dien-1-yl)amino)ethyl)-3-(4-hydroxy-3-methoxyphenyl)acrylamide (17)

Compound **17** was prepared from 2,3-dimethoxycyclohexa-2,5-diene-1,4-dione and ferulic acid in a similar manner as described for compound **8a**. Purple solid 40 mg, yield 6%. 1H NMR (400 MHz, DMSO- d_6): δ 9.46 (brs, 1H), 8.24 – 8.10 (m, 1H), 7.44 (t, J = 5.9 Hz, 1H), 7.35 (d, J = 15.7 Hz, 1H), 7.13 (d, J = 1.8 Hz, 1H), 7.00 (dd, J = 8.2, 1.8 Hz, 1H), 6.80 (d, J = 8.1 Hz, 1H), 6.40 (d, J = 15.7 Hz, 1H), 5.33 (s, 1H), 4.00 (s, 3H), 3.81 (s, 3H), 3.76 (s, 3H), 3.35 (q, J = 6.1 Hz, 2H), 3.19 (q, J = 6.1 Hz, 2H) ppm. ^{13}C NMR (101 MHz, DMSO- d_6): δ 180.6, 180.6, 166.6, 148.8, 148.4, 148.3, 147.0, 141.1, 139.9, 126.7, 122.1, 119.0, 116.1, 111.3, 94.5, 61.3, 61.1, 56.0, 42.8, 37.4 ppm. LRMS (ESI+) m/z calcd for $[C_{20}H_{23}N_2O_7]^+$: 403.14 found: 403.05 $[M+H]^+$. HPLC: t_R = 9.8 min, purity 97.9%. mp = 75-77 °C.

DPPH Assay. To determine the antioxidant capacities, 2,2-diphenyl-1-picrylhydrazyl (DPPH) radical assay was used as previously described.¹⁰¹ A stock solution (200 μ M) of DPPH was freshly prepared in MeOH. Compounds were dissolved in MeOH (5 mM) as stock solution. To start the reaction, 50 μ L of the DPPH stock solution were added to 100 μ L diluted compound or pure methanol as negative control. The 96-well-plate was incubated at room temperature in the dark for 30 min and absorbance was then determined with a microplate reader at 517 nm. The experiments were performed in triplicates. A dilution series of the compound served as a blank to the particular compound and was subtracted from each measurement point. The scavenging potency is expressed as the concentration that scavenged 50% of the DPPH free radicals (EC_{50}) determined *via* nonlinear regression curve.

ORAC Assay. We used the ORAC-Fluorescein method of Ou *et al.*¹⁰² partially modified by Dávalos *et al.*¹⁰³ that uses fluorescein (FL) as a fluorescent probe, (\pm)-6-hydroxy-2,5,7,8-tetramethyl-chromane-2-carboxylic acid (Trolox) as reference and compound 2,2'-azobis(amidinopropane) dihydrochloride (AAPH) as peroxy radical generator. Reactions were performed in 75 mM PBS buffer (pH 7.4), and the final reaction mixture volume was 200 μ L at 37 °C. Derivatives at the desired concentrations (20 μ L) and FL (120 μ L, 70 nM, final concentration) solutions were mixed in a black 96-well microplate (SARSTEDT) and pre-incubated for 15 min at 37 °C. Subsequently, AAPH solution (60 μ L, 12 mM, final concentration) was added rapidly and the plate was placed in a TECAN microplate reader to measure the fluorescence (485 nm excitation and 510 nm emission filters) intensity every two min for 90 min. Samples were measured at two different concentrations (2 and 4 μ M). A blank (FL + AAPH in PBS) and a calibration curve of trolox (1, 2, 4, 6, 8, 10, 12 and 15 μ M) were included in each experiment. All samples were prepared in duplicate and three independent assays were performed for each compound. The area under the fluorescence decay curve (fluorescence *vs* time) (AUC) was calculated as

$$AUC = 1 + \sum_{i=1}^{i=45} f_i / f_0$$

where f_0 is the initial fluorescence reading at 0 min and f_i is the fluorescence reading at time $2i$ min. The net AUC corresponding to a sample was calculated by subtracting the AUC corresponding to the blank (Net AUC = AUC_{antioxidant} – AUC_{blank}). Linear regression equations were calculated by plotting the net AUC against the trolox antioxidant standard concentration ($R^2 > 0.99$). ORAC-FL values were expressed as trolox equivalents by using the standard curve calculated for each assay, where the ORAC-FL value of Trolox was taken as 1, plot the Trolox standard curve and interpolate it to determine sample ORAC values.

Neuroprotection Assays. HT-22 cells were grown in Dulbecco's Modified Eagle Medium (DMEM, Sigma Aldrich) supplemented with 10% (v/v) heat-inactivated fetal calf serum (FCS) and 1% (v/v) penicillin-streptomycin. Cells were subcultured every two days and incubated at 37 °C with 5% CO₂ in a humidified incubator. Compounds were dissolved in DMSO (Sigma Aldrich) and diluted with medium. Generally, 80% confluent cells were seeded with 5000 cells per well into sterile 96-well plates and were incubated for 24 hours. For the neurotoxicity assay, previous medium was removed and 10 μ M of the compound was added to the wells. 0.05% DMSO in DMEM served as control. Cells were incubated for 24 hours. MTT solution (4 mg/mL in PBS) was diluted 1:10 with medium and added to the wells after removal of previous medium. Cells were incubated for 3 hours when the supernatant was removed and lysis buffer (10% SDS) was applied. The next day, absorbance at 560 nm was determined with a multiwell plate photometer (Tecan – SpectraMax 250). Experiments were performed in triplicates. Results are presented as percentage to untreated control cells. Data is expressed as means \pm SD of three different independent experiments. Analysis was accomplished using GraphPad Prism 7 Software applying oneway ANOVA followed by Dunnett's multiple comparison posttest. Levels of significance: * $p < 0.05$; ** $p < 0.01$; *** $p < 0.001$.

For the oxytosis assay, 5 mM glutamate (monosodium-*L*-glutamate, Sigma Aldrich) together with respective compounds were added to the cells and incubated for 24 h. 25 μ M quercetin (Sigma Aldrich) together with 5 mM glutamate served as a positive control. After 24 h incubation, cell viability was determined using a colorimetric MTT assay as described above.

For the ferroptosis assay, 3×10^3 cells per well were seeded into sterile 96-well plates and incubated overnight. The next day medium was exchanged with fresh medium and 0.3 μ M RSL3 was added with vehicle (DMSO) to induce oxidative stress, or together with diluted compounds solutions for protection. After 24 h, cell viability was determined using a colorimetric MTT assay.

For the ATP depletion assay, 3×10^3 cells per well were seeded into sterile 96-well plates and incubated overnight. The next day medium was exchanged with fresh medium. 17.5 μ M iodoacetic acid (IAA) was added with vehicle (DMSO) as negative control, or together with respective compounds for protection. After 2 h incubation at 37 °C in the incubator, medium was aspirated, and fresh medium was applied and only the compounds at the same respective concentrations were added without IAA. After 24 h, cell viability was determined using a colorimetric MTT assay.

4.2. Structure-Activity Relationship (SAR) Study of Quinones as Free Radical Scavengers and Neuroprotectants

Author Contributions

Prof. Dr. Michael Decker supervised the whole study.

Feng He and Prof. Dr. Michael Decker designed all target compounds.

Feng He, under the supervision of Prof. Dr. Michael Decker, performed the synthesis of all target compounds as well as the evaluation of their antioxidant capacities.

Julian Hofmann, under the supervision of Prof. Dr. Michael Decker, performed the neuroprotection assays.

4.2.1. Introduction

Mitochondrial dysfunction is an important hallmark for neurodegenerative disorders resulting in ATP depletion, halting the activities of enzymes of electron transport chain (ETC), generation of reactive oxygen species (ROS), reduction of mitochondrial DNA (mtDNA) and caspase 3 release.⁸ Therefore, mitochondria targeting drug discovery holds promising potential to prevent the progression of neurodegenerative diseases.

Quinones are a family of compounds having two α,β -dienonic carbonyl groups in the same six-membered ring. The biological effects of quinones have been reported for decades and several quinones including CoQ10 (**1**, Ubiquinone), idebenone (**2**), MitoQ10 (**3**), and troloxamide quinone (**4**, EPI-589) which are under clinical evaluation toward mitochondrial diseases in phases II to IV (**Figure 4.2.1**).¹⁰⁴ The application of quinones in drug discovery has been comprehensively reviewed in several recent publications.¹⁰⁴⁻¹⁰⁷ More specifically, CoQ10 (**1**) has not been reported of any clinical benefits for the treatment of mitochondrial diseases,¹⁰⁸ while idebenone (**2**) as its water-soluble analog was approved in the EU for the treatment of Leber's hereditary optic neuropathy (LHON).¹⁰⁹ MitoQ10 (**3**) was designed based on the membrane potential-dependent accumulation of methyl-triphenylphosphonium (MTPP) cations in mitochondria and was found to accumulate 200-fold within the mitochondrial matrix to prevent lipid peroxidation.¹¹⁰ Troloxamide quinone (**4**, EPI-589) is now in phase II clinical trial for treatment of Parkinson's disease. The Melchiorre group has identified polyamine-quinone-based multi-target directed ligand (MTDL) memoquin (**5**), which showed pronounced activities targeting to acetylcholinesterase (AChE) and BACE-1 enzymes, amyloid β ($A\beta$), and oxidative processes.^{15, 111} Thymoquinone (**6**) is the main constituent of the oil extracted from *Nigella sativa* seeds, which was reported as a potent superoxide anion scavenger and was neuroprotective against $A\beta$ -induced neurotoxicity.^{112, 113} Anthraquinone-based compound **7** was reported by the Tonelli group as multi-target compounds against $A\beta$ aggregation, PHF6 tau fragment, AChE enzyme and MAO B for treatment of Alzheimer's disease (AD).¹¹⁴

Moreover, compounds **8** and **9** were identified as potent neuroprotectants in oxytosis assay with low neurotoxicity based on the structure-activity relationship (SAR) study of vitamin K by the Chou group.⁴⁸ Oxytosis is an oxidative stress-dependent regulated cell-death pathway highly relevant to neurological disorders, including Alzheimer's disease (AD). It is interesting to compare different kinds of quinones regarding their antioxidant capacity and neuroprotective effects. Thus, we have designed and synthesized a series of quinone derivatives based on the fore-mentioned quinones (**Figure 4.2.2**). We started with the amination of ubiquinone structure, which possesses two methoxyl groups in the benzoquinone (**10a-b**, **11a-f**). Compounds **12a-d**, **13a-d**, **14a-d**, and **15a-d** were derivated from EPI-589 (**4**), memoquin (**5**), thymoquinone (**6**), and anthraquinone (**7**), respectively. Their antioxidant capacity was evaluated by oxygen radical absorbance capacity (ORAC) assay, and neuroprotective effects were studied by oxytosis assay in HT22 hippocampal cells.

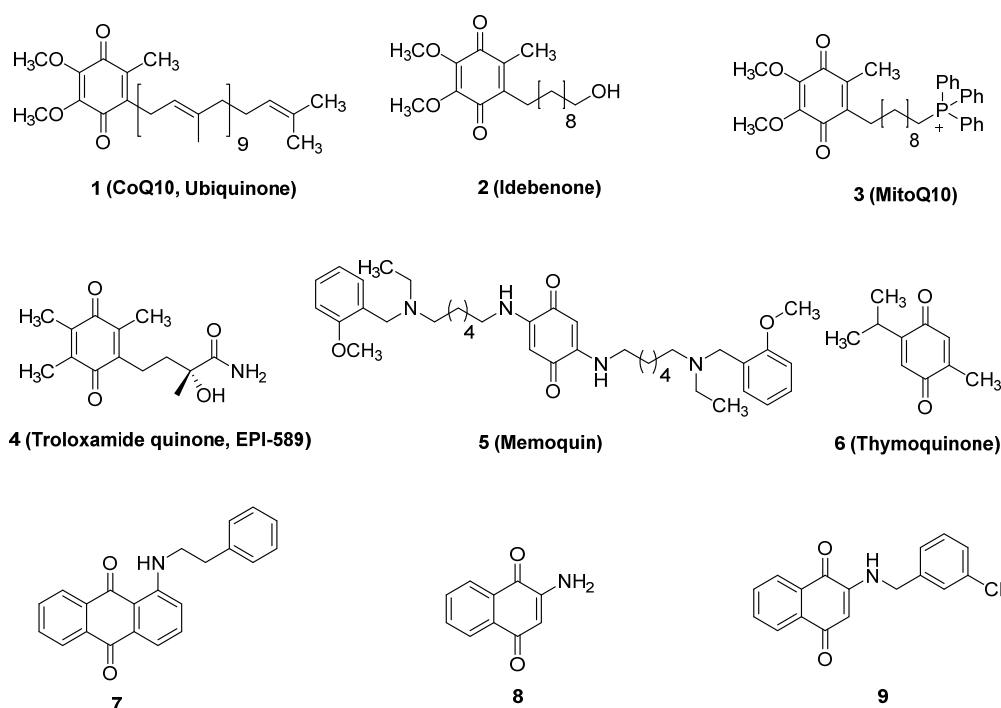


Figure 4.2.1. A selection of quinones correlated to neurodegenerative disorders.

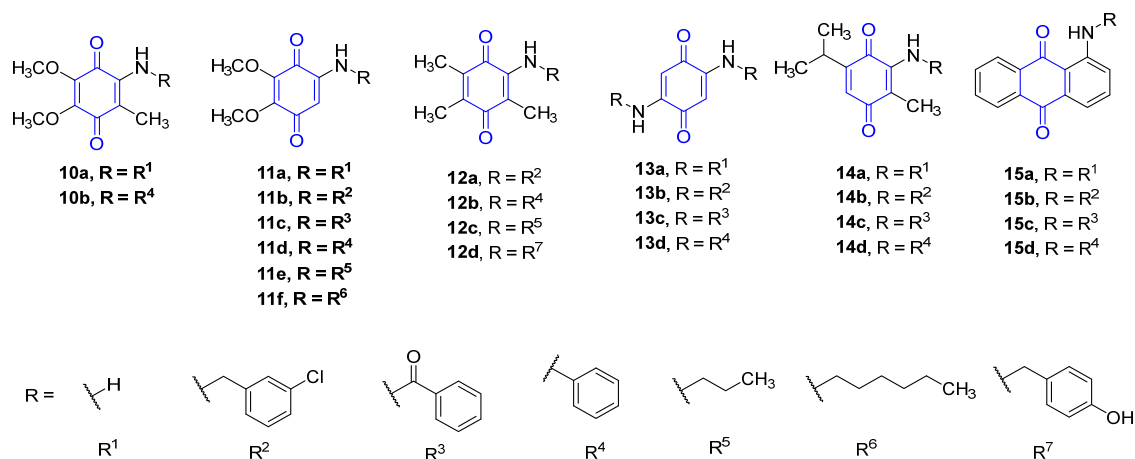
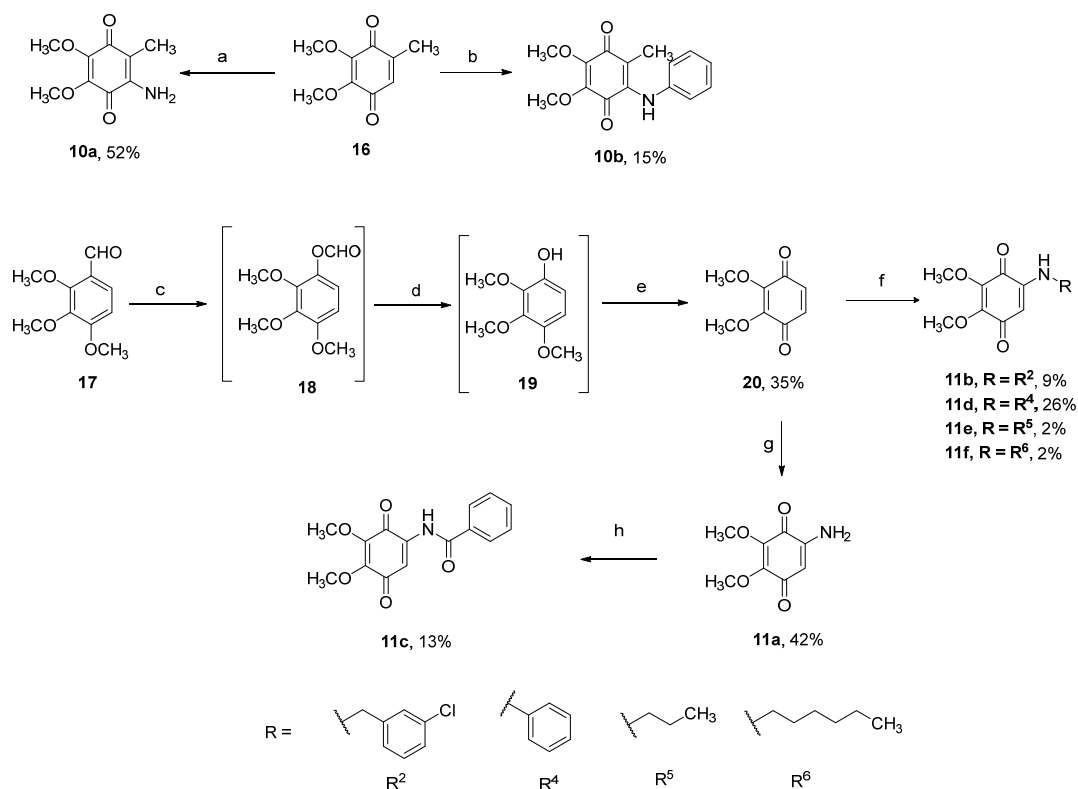


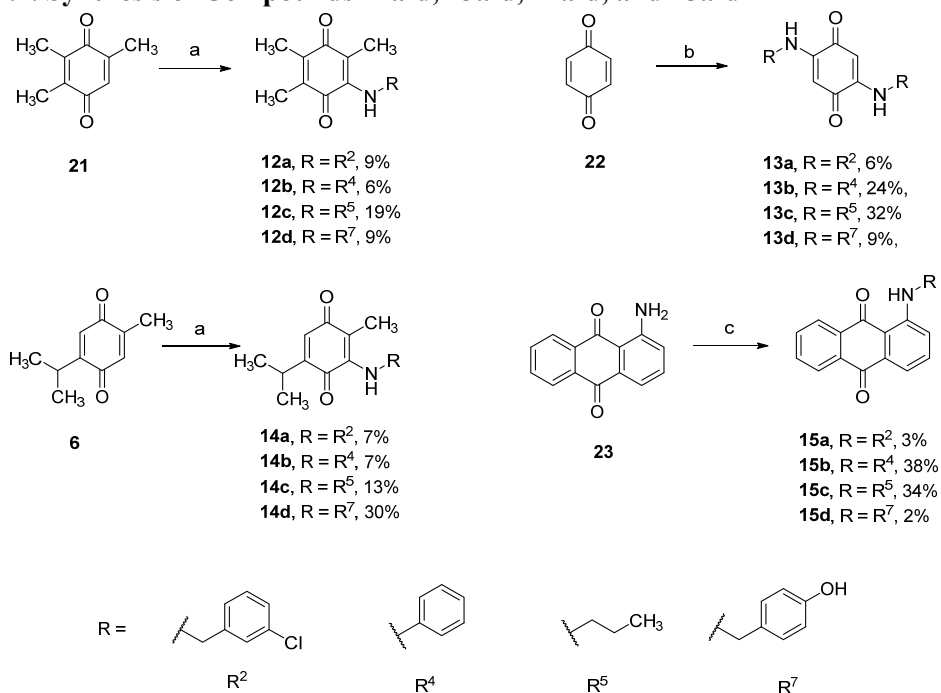
Figure 4.2.2. Structures of designed target quinone compounds.

Scheme 4.2.1. Synthesis of Ubiquinone Derivatives 10a-b, 11a-f^a



^aReagents and conditions: (a) NaN₃, 12 M HCl aq., H₂O, MeOH, 50 °C; (b) aniline, H₂O, r.t.; (c) m-CPBA, DCM, 0 °C; (d) KOH, MeOH, r.t.; (e) ceric ammonium nitrate, silica gel, DCM, r.t.; (f) 3-chlorophenylmethanamine for **11b**, aniline for **11d**, propan-1-amine for **11e**, hexan-1-amine for **11f** EtOH, r.t.; (g) NaN₃, AcOH, H₂O, THF, r.t.; (h) benzyl chloride, TEA, THF, 55 °C.

Scheme 4.2.2. Synthesis of Compounds 12a-d, 13a-d, 14a-d, and 15a-d^a



^aReagents and conditions: (a) (3-chlorophenyl)methanamine at r.t. for **12a** and **14a**, aniline at 90 °C for **12b** and **14b**, propan-1-amine at r.t. for **12c** and **14c**, 4-(aminomethyl)phenol at r.t. for **12d** and **14d**, EtOH; (b) 3-chlorophenylmethanamine for **13a**, aniline for **13b**, propan-1-amine for **13c**, 4-(aminomethyl)phenol for **13d**, air,

EtOH, r.t.; (c) i) 1-(bromomethyl)-3-chlorobenzene for **15a**, iodobenzene for **15b**, K₂CO₃, DMF, 80 °C; ii) 1-bromopropane for **15c**, *t*-BuOK, DMF, 80 °C; iii) 4-hydroxybenzaldehyde for **15d**, MeOH, AcOH, MgSO₄, NaBH₃CN, r.t.

4.2.2. Results and Discussion

Chemistry. In **Scheme 4.2.1**, the synthesis of ubiquinone derivatives **10a-b** and **11a-f** is described starting from 2,3-dimethoxy-1,4-benzoquinone (**16**) and 2,3,4-trimethoxybenzaldehyde (**17**), respectively. Compound **10a** was synthesized from 2,3-dimethoxy-5-methylcyclohexa-2,5-diene-1,4-dione (**16**) and sodium azide in acidic medium by similar method as described previously.¹¹⁵ Compound **10b** was obtained through Michael addition reaction between **16** and aniline in water.^{116,117} Intermediate **20** was synthesized from 2,3,4-trimethoxybenzaldehyde (**17**) as previously described.¹¹⁸ Briefly, the synthesis start with a Baeyer–Villiger oxidation of compound **17**, followed by hydrolysis of the crude formate ester (**18**). 2,3-Dimethoxy-1,4-benzoquinone (**20**) was obtained by oxidation of the intermediate **19** by ceric ammonium nitrate on silica. The amination of intermediate **20** was performed by a similar method to compound **10a**, in which 12 M HCl was replaced with acetic acid. Subsequent coupling reaction of compound **10a** using benzoic chloride provided compound **10c**. Compound **10b** and **10d-f** were synthesized from intermediate **20** and corresponding amines by Michael addition reaction in ethanol.

The synthesis of compounds **12a-d**, **13a-d**, **14a-d**, and **15a-d**, respectively is described in **Scheme 4.2.2**. Compounds **12a-d** and **14a-d** were obtained by Michael addition reaction from compounds **21** and **6**, respectively. The only difference was the synthesis of compounds **12b** and **14b**, which needed to be performed at 90 °C instead of room temperature due to the low reactivity of aniline. The synthesis of compounds **13a-d** was found to be exceptionally selective with corresponding amines and produced only bis-substituted 1,4-benzoquinones in position 2 and 5 under aerobic conditions, and the target compounds can be simply filtered and recrystallized from the reaction mixture.¹¹⁹ However, compound **13b** was insoluble in DMSO and most organic solvents, which rendered it could not be characterized and further tested. The synthesis of compounds **15a-c** was carried out in DMF with K₂CO₃ and corresponding halides at 80 °C, while compound **15d** was obtained by reductive amination from 1-aminoanthraquinone (**23**) and 4-hydroxybenzaldehyde.

Physicochemical Antioxidant Parameters. Oxygen radical absorbance capacity (ORAC) assay was used to evaluate the antioxidant capacity of quinone derivatives. 2,2-Azobis(2-amidino-propane)dihydrochloride (AAPH) is a peroxy radical (ROO·) generator in the ORAC assay. We focused on the ubiquinone derivatives (**10a-b**, **11a-f**) at the beginning. Compounds **6**, **8**, **9**, **16**, **21**, **23**, and melatonin were used as reference compounds. All ubiquinone derivatives showed potent antioxidant capacity in scavenging peroxy radicals with ORAC values ranging from 0.8 (**11c**) to 3.6 (**10b**), respectively. Compounds **10a** and **10b** exhibit comparable ORAC values to compounds **11a** and **11d**, indicating that the methyl group in ortho-position of the amine is not necessary for its radical scavenging

capacity. Compounds **11a** and **11c** are not as active as other ubiquinone derivatives, which indicates the benefit of electron-donating groups to improve the radical scavenging capacity.

Table 4.2.1. Antioxidant Activities of Quinone Derivatives Determined in the ORAC Assay.

Compound	Structure	ORAC (trolox equivalents)	Compound	Structure	ORAC (trolox equivalents)
Melatonin		2.6 ± 0.1	12a		0.3 ± 0.1
6		0.2 ± 0.2	12b		2.9 ± 0.2
8		1.5 ± 0.2	12c		0.6 ± 0.1
9		ND ^b	12d		4.5 ± 0.6
16		0.4 ± 0.2	13a		NA ^a
21		NA ^a	13c		2.0 ± 0.2
23		ND ^b	13d		2.9 ± 0.6
10a		2.2 ± 0.3	14a		0.6 ± 0.2
10b		3.6 ± 0.3	14b		2.5 ± 0.2
11a		2.0 ± 0.3	14c		1.0 ± 0.2
11b		1.3 ± 0.2	14d		3.5 ± 0.6
11c		0.8 ± 0.2	15a		NA ^a
11d		2.9 ± 0.4	15b		0.4 ± 0.1
11e		2.7 ± 0.4	15c		1.1 ± 0.1
11f		1.9 ± 0.2	15d		ND ^b

^aNot active.

^bNot determined due to interference with their own fluorescence.

According to the potent neuroprotective effects of compound **9** from the Chou group, we used the same (3-chlorophenyl)methanamine group to design new quinone derivatives **11b**, **12a**, **13a**, **14a**, and **15a**, while all of them show no or slight antioxidant capacity, except compound **11b** possessing an ORAC value of 1.3. Based on the high ORAC values of compounds **10b** and **11e**, respectively, we subsequently introduced the same phenyl and n-propyl groups and obtained compounds **12a-b**, **13a-b**, **14a-b**, and **15a-b**. The antioxidant capacity indeed improved, especially for benzene derivatives like compounds **12b** and **14b**, with ORAC values of 2.9 and 2.5, respectively, which are comparable to reference compound melatonin. Given the low water solubility of compounds **13a-b** and **15a**, compounds **12d**, **13d**, **14d**, and **15d** were designed with phenolic acid groups introduced to improve the solubility and radical scavenging capacity. As expected, compounds **12d**, **13d**, and **14d** show highly potent antioxidant capacity with ORAC values of 4.5, 2.9, and 3.5, respectively, while the ORAC value of compound **15d** could not be determined due to interference with its own fluorescence. All data is shown in **Table 4.2.1**.

In summary, the amination of quinones could enhance their antioxidant capacity, moreover, anthraquinone derivatives (**15a-d**) show lower antioxidant capacity compared with other quinones. Compounds **12a-d** show comparable ORAC values to compound **14a-d**, respectively, indicating that thymoquinone derivatives (**14a-d**) show similar structure-activity relationship with trimethyl-1,4-benzoquinone derivatives (**12a-d**) for antioxidant capacities.

Activity in the Oxytosis Assay. The potent neuroprotective effects of vitamin K derivatives encouraged us to further study the SAR of quinones with neuroprotection against oxytosis to identify more potent quinone neuroprotectants. In the oxytosis assay of the Salk lab, compounds were incubated together with 5 mM glutamate treated HT22 cells for 24 h. However, the method from the Chou group was slightly modified, with compounds and 10 mM glutamate treated HT22 cells been incubated for 3 h. This difference rendered compound **2** showing no significant neuroprotection at 5 μ M. As shown in **Figure 4.2.3**, compounds **16**, **10a-b** and **11a-f** based on ubiquinone show no or low neuroprotection at 5 μ M except compounds **11c** and **11d**. This result is not related to the reported structure-activity relationships of vitamin K derivatives.⁴⁸ Both compounds **11c** and **11d** possess electron withdrawing groups, which indicates that electron withdrawing groups can improve the neuroprotective effects of ubiquinone derivatives. Compounds **13a** and **13c-d** based on memoquin and **15a-d** based on anthraquinone show no neuroprotection at 5 μ M, which indicates that memoquin and anthraquinone are not suitable lead compounds for neuroprotectants. Encouragingly, compounds **12a-d** and **14a-d** together with their corresponding mother compounds 2,3,5-trimethyl-1,4-benzoquinone and thymoquinone show highly potent neuroprotection at 5 μ M, which makes them more potent than vitamin K and ubiquinone derivatives, respectively. However, no obvious difference can be observed between **12a-d**, neither with **14a-d**, which might be due to the high concentration tested. Compounds **12a-d** and **14a-d** are worth to be further studied especially at lower concentrations.

Pan-Assay Interference Compounds (PAINS) Exclusion Assay. The PAINS exclusion assay was done for quinone derivatives by a similar way as for hybrid vitamin K derivatives and results are described in **Appendix III**. Compounds **21** and **6** without amine group attached show high reactivity with 2-mercaptoethanol (BME), and corresponding derivatives with amine groups (**12c** and **14c**) do not react with BME in 6 hours. Same results were observed in the reactions of compounds **11e**, **13c** 1-aminoanthraquinone (**23**) and **15c**, which indicating that none of designed these aminated quinone compounds are pan-assay interference compounds (PAINS).

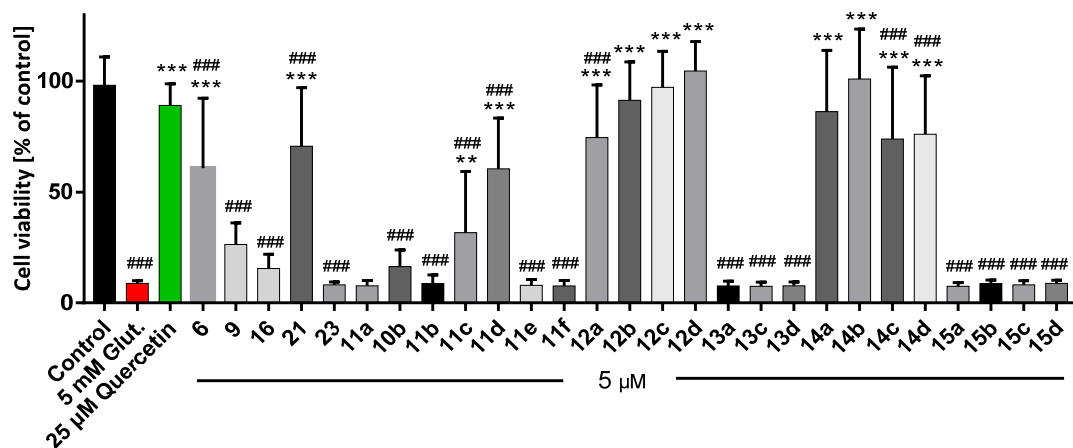


Figure 4.2.3. Neuroprotection of quinone derivatives at 5 μM against glutamate induced oxytosis in HT22 cells. 25 μM Quercetin served as a positive control (green) while 5 mM glutamate was used to induce toxicity (red). Data is presented as means \pm SD of three independent experiments and results refer to untreated control cells (black). Statistical analysis was rendered using One-way ANOVA followed by Dunnett's multiple comparison posttest referring to cells treated with 5 mM glutamate. ** $p < 0.01$, *** $p < 0.001$ vs 5 mM glutamate treated group. ### $p < 0.001$ vs control group.

4.2.3. Conclusions

In summary, the structure-activity relationship of quinone derivatives with antioxidant capacity and neuroprotective effects has been preliminarily studied. Inspired by vitamin K derivatives, five kinds of different quinones including ubiquinone, 2,3,5-trimethyl-1,4-benzoquinone, memoquin, thymoquinone, and anthraquinone derivatives have been designed and their antioxidant capacity and neuroprotective effects have been evaluated by ORAC and oxytosis assays, respectively. 2,3,5-Trimethyl-1,4-benzoquinone (**12a-d**) and thymoquinone derivatives (**14a-d**) were identified as potent antioxidants with ORAC values ranging from 0.3 to 4.5, and as more potent neuroprotectants compared with other quinones like vitamin K, ubiquinone, 2,3,5-trimethyl-1,4-benzoquinone, memoquin, thymoquinone, and anthraquinone derivatives, which could be used as lead compounds for further mechanistic study and regarding drug discovery for treatment of neurodegenerative disease.

4.2.4. Experimental Section

For general information see in section 4.1.4.

2-Amino-5,6-dimethoxy-3-methylcyclohexa-2,5-diene-1,4-dione (10a)

NaN₃ (1.07 g, 16.47 mmol) was dissolved in 3 mL water and acidified with 0.5 mL 12 M HCl. The NaN₃ solution was added to a solution of 2,3-dimethoxy-5-methylcyclohexa-2,5-diene-1,4-dione **16** (0.50 g, 2.74 mmol) in 20 mL MeOH and stirred at 50°C for 1 h. The mixture was then neutralized to pH = 8, excess water was added to the mixture and extracted with ethyl acetate twice. The organic phase was combined and dried over Na₂SO₄, then concentrated with vacuum and purified with column chromatography to afford black solid 0.28 g, yield 52%. ¹H NMR (400 MHz, CDCl₃): δ 4.81 (brs, 2H), 4.11 (s, 3H), 3.90 (s, 3H), 1.83 (s, 3H) ppm. ¹³C NMR (101 MHz, CDCl₃): δ 181.8, 180.6, 147.0, 142.4, 140.3, 107.2, 61.36, 61.1, 8.5 ppm. LRMS (ESI+) *m/z* calcd for [C₉H₁₂NO₄]⁺: 198.07 found: 198.05 [M+H]⁺. HPLC: *t_R* = 7.8 min, purity 98.8%. mp = 108-110 °C.

2,3-Dimethoxy-5-methyl-6-(phenylamino)cyclohexa-2,5-diene-1,4-dione (10b)

Anilin (0.10 g, 1.10 mmol) was added to a solution of 2,3-dimethoxy-5-methylcyclohexa-2,5-diene-1,4-dione **16** (0.20 g, 1.10 mmol) in 10 mL water and stirred at r.t. over night. The mixture was extracted with ethyl acetate, dried over Na₂SO₄, purified with column chromatography to afford black oil 45 mg, yield 15%. ¹H NMR (400 MHz, CDCl₃): δ 7.33 (t, *J* = 7.8 Hz, 2H), 7.18 (s, 1H), 7.12 (t, *J* = 7.4 Hz, 1H), 6.95 (d, *J* = 7.9 Hz, 2H), 4.15 (s, 3H), 3.95 (s, 3H), 1.58 (s, 3H) ppm. ¹³C NMR (101 MHz, CDCl₃): δ 183.4, 181.9, 147.1, 140.6, 139.5, 139.2, 128.9 (2C), 124.2, 122.3 (2C), 112.6, 61.4, 61.2, 12.9 ppm. LRMS (ESI+) *m/z* calcd for [C₁₅H₁₆NO₄]⁺: 274.10 found: 274.05 [M+H]⁺. HPLC: *t_R* = 14.5 min, purity 98.4%. mp = 65-67 °C.

2,3-Dimethoxycyclohexa-2,5-diene-1,4-dione (20)

A solution of 2,3,4-trimethoxybenzaldehyde **17** (0.50 g, 2.55 mmol) in CH₂Cl₂ (10 mL) was added slowly to a solution of *m*-CPBA (77 wt%, 0.69 g, 3.06 mmol) in CH₂Cl₂ (1 mL) at 0 °C and the mixture allowed to warm to r.t. and stirred for 3 h. Saturated aqueous NaHCO₃ (10 mL) was then added and the layers were separated. The organic phase was washed with 10% (w/v) aqueous Na₂S₂O₃, dried over Na₂SO₄ and evaporated to provide crude formate ester **18** as yellow oil. This residue was re-dissolved in MeOH (10 mL), KOH (0.29 g, 5.10 mmol) was added and the mixture stirred at r.t. for 5 min. The reaction was then acidified to pH 1 using 6.0 M aqueous HCl and diluted with CH₂Cl₂. The layers were separated and the aqueous phase was extracted with CH₂Cl₂ (4x). The combined organic fractions were dried over Na₂SO₄ and evaporated to provide the crude phenol **19** as orange oil. The material was carried forward without further purification. A solution of ceric ammonium nitrate (1.49 g, 2.71 mmol) in H₂O (5 mL) was added to a flask charged with silica gel (3.0 g). CH₂Cl₂ (60 mL) was added, followed by a solution of the above crude product **19** in CH₂Cl₂ (50 mL) and the mixture being stirred at r.t. for 1.5 h. The silica was then removed by filtration, rinsing with CH₂Cl₂. The layers of the filtrate were separated and the aqueous phase was extracted with CH₂Cl₂ (2x). The combined organic fractions were evaporated. The residue was purified by flash column chromatography to provide **20** as red solid 0.15 g, yield 35%. ¹H NMR (400 MHz, CDCl₃): δ 6.63 (s, 2H), 4.04 (s, 6H) ppm. LRMS (ESI+) *m/z* calcd for [C₈H₉O₄]⁺: 169.04 found: 169.10 [M+H]⁺.

5-Amino-2,3-dimethoxycyclohexa-2,5-diene-1,4-dione (11a)

NaN₃ (1.16 g, 17.80 mmol) was dissolved in 3 mL water and acidified with 1 mL AcOH. The NaN₃ solution was added to a solution of intermediate **20** (0.50 g, 2.97 mmol) in 20 mL MeOH and stirred at r.t. for 1 h. The mixture was then neutralized to pH = 8, excess water was added to the mixture and extracted with ethyl acetate twice. The organic phase was combined and dried over Na₂SO₄, then concentrated with vacuum and purified with column chromatography to afford black solid 0.23 g, yield 42%. ¹H NMR (400 MHz, CDCl₃): δ 5.48 (s, 1H), 5.09 (s, 2H), 4.07 (s, 3H), 3.81 (s, 3H) ppm. ¹³C NMR (101 MHz, CDCl₃): δ 182.2, 180.6, 147.6, 145.9, 140.7, 99.1, 61.40, 61.1 ppm. LRMS (ESI+) *m/z* calcd for [C₈H₁₀NO₄]⁺: 184.05 found: 184.05 [M+H]⁺. HPLC: *t_R* = 6.7 min, purity = 99.3%. mp = 125-127 °C.

N-(4,5-Dimethoxy-3,6-dioxocyclohexa-1,4-dien-1-yl)benzamide (11c)

TEA (0.56 g, 5.50 mmol) and benzoylchloride (0.77 g, 5.50 mmol) were added dropwise to a solution of **11a** (0.20 g, 1.10 mmol) in 10 mL dry THF, then stirred at 55 °C for 30 min. Excess water was added to quench the reaction and the mixture was extracted with ethyl acetate. The organic phase was combined, dried over Na₂SO₄ and purified with column chromatography to afford orange solid 40 mg, yield 13%. ¹H NMR (400 MHz, CDCl₃): δ 8.98 (s, 1H), 7.91 (d, *J* = 7.5 Hz, 2H), 7.63 (t, *J* = 7.3 Hz, 1H), 7.58 – 7.52 (m, 3H), 4.17 (s, 3H), 3.99 (s, 3H) ppm. ¹³C NMR (101 MHz, CDCl₃) δ 184.1, 180.3, 165.6, 146.7, 141.7, 137.1, 133.1, 133.0, 129.1, 127.3, 112.4, 61.6, 61.4 ppm. LRMS (ESI+) *m/z* calcd for [C₁₅H₁₄NO₅]⁺: 288.08 found: 288.00 [M+H]⁺. HPLC: *t_R* = 11.2 min, purity 99.1%. mp = 134-136 °C.

5-((3-Chlorobenzyl)amino)-2,3-dimethoxycyclohexa-2,5-diene-1,4-dione (11b)

(3-Chlorophenyl)methanamine (0.17 g, 1.19 mmol) was added to a solution of intermediate **20** (0.20 g, 1.19 mmol) in ethanol and stirred for 2 h. The mixture was concentrated under vacuum and purified with column chromatography to afford brown solid 32 mg, yield 9%. ¹H NMR (400 MHz, CDCl₃): δ 7.24 – 7.20 (m, 2H), 7.18 (s, 1H), 7.08 (t, *J* = 4.0 Hz, 1H), 6.04 (s, 1H), 5.21 (s, 1H), 4.20 (d, *J* = 5.9 Hz, 2H), 4.08 (s, 3H), 3.80 (s, 3H) ppm. ¹³C NMR (101 MHz, CDCl₃): δ 181.5, 180.4, 148.3, 145.4, 140.5, 137.8, 135.0, 130.3, 128.4, 127.5, 125.6, 96.4, 61.4, 61.1, 46.3 ppm. LRMS (ESI+) *m/z* calcd for [C₁₅H₁₅ClNO₄]⁺: 308.06 found: 308.00 [M+H]⁺. HPLC: *t_R* = 11.2 min, purity = 96.1%. mp = 132-134 °C.

2,3-Dimethoxy-5-(phenylamino)cyclohexa-2,5-diene-1,4-dione (11d)

Compound **11d** was prepared from intermediate **20** and aniline in a similar manner as described for compound **11b**. Black solid, yield 26%. ¹H NMR (400 MHz, CDCl₃): δ 7.46 (s, 1H), 7.44 – 7.38 (m, 2H), 7.25 – 7.17 (m, 3H), 6.00 (s, 1H), 4.20 (s, 3H), 3.94 (s, 3H) ppm. ¹³C NMR (101 MHz, CDCl₃): δ 182.4, 180.8, 148.0, 142.2, 140.6, 137.4, 129.7 (2C), 125.6, 122.2 (2C), 98.0, 61.5, 61.2 ppm. LRMS (ESI+) *m/z* calcd for [C₁₄H₁₄NO₄]⁺: 260.08 found: 260.05 [M+H]⁺. HPLC: *t_R* = 11.1 min, purity 98.3%. mp = 110-112 °C.

2,3-Dimethoxy-5-(propylamino)cyclohexa-2,5-diene-1,4-dione (11e)

Compound **11e** was prepared from intermediate **20** and 1-propylamine in a similar manner as described for compound **11b**. Black solid, yield 2%. ¹H NMR (400 MHz, CDCl₃): δ 5.73 (s, 1H), 5.21

(s, 1H), 4.09 (s, 3H), 3.78 (s, 3H), 2.99 (q, $J = 6.8$ Hz, 2H), 1.66 – 1.55 (m, 2H), 0.92 (t, $J = 7.4$ Hz, 3H) ppm. ^{13}C NMR (101 MHz, CDCl_3): δ 181.2, 180.6, 148.6, 145.9, 140.3, 95.0, 61.4, 61.1, 44.4, 21.5, 11.5 ppm. LRMS (ESI+) m/z calcd for $[\text{C}_{11}\text{H}_{16}\text{NO}_4]^+$: 226.10 found: 226.05 $[\text{M}+\text{H}]^+$. HPLC: $t_{\text{R}} = 9.5$ min, purity 95.8%. mp = 81-83 °C.

5-(Hexylamino)-2,3-dimethoxycyclohexa-2,5-diene-1,4-dione (11f)

Compound **11f** was prepared from intermediate **20** and hexylamin in a similar manner as described for compound **11b**. Brown solid, yield 2%. ^1H NMR (400 MHz, CDCl_3): δ 5.72 (s, 1H), 5.20 (s, 1H), 4.09 (s, 3H), 3.78 (s, 3H), 3.01 (q, $J = 6.8$ Hz, 2H), 1.62 – 1.51 (m, 2H), 1.34 – 1.21 (m, 6H), 0.83 (t, $J = 6.8$ Hz, 3H) ppm. ^{13}C NMR (101 MHz, CDCl_3): δ 181.2, 180.6, 148.6, 145.9, 140.2, 94.9, 61.4, 61.1, 42.8, 31.4, 28.1, 26.7, 22.5, 14.0 ppm. LRMS (ESI+) m/z calcd for $[\text{C}_{14}\text{H}_{22}\text{NO}_4]^+$: 268.15 found: 268.10 $[\text{M}+\text{H}]^+$. HPLC: $t_{\text{R}} = 12.0$ min, purity 99.0%. mp = 84-86 °C.

2-((3-Chlorobenzyl)amino)-3,5,6-trimethylcyclohexa-2,5-diene-1,4-dione (12a)

(3-Chlorophenyl)methanamine (140 mg, 1.00 mmol) was added to a solution of 2,5,6-trimethyl-1,4-benzoquinone **21** (150 mg, 1.00 mmol) in 15 mL EtOH, then stirred at 70 °C overnight. The mixture was concentrated and purified with column chromatography to afford brown solid 37 mg, yield 13%. ^1H NMR (400 MHz, CDCl_3): δ 7.32 – 7.26 (m, 3H), 7.18 – 7.14 (m, 1H), 4.62 (s, 2H), 2.05 (s, 3H), 2.04 (s, 3H), 2.00 (s, 3H) ppm. ^{13}C NMR (101 MHz, CDCl_3): δ 186.4, 184.6, 143.6, 143.5, 141.1, 136.1, 134.8, 130.2, 127.9, 127.1, 125.0, 110.0, 48.4, 13.1, 12.0, 10.6 ppm. LRMS (ESI+) m/z calcd for $[\text{C}_{16}\text{H}_{17}\text{ClNO}_2]^+$: 290.09 found: 290.05 $[\text{M}+\text{H}]^+$. HPLC: $t_{\text{R}} = 13.1$ min, purity 99.3%. mp = 90-91 °C.

2,3,5-Trimethyl-6-(phenylamino)cyclohexa-2,5-diene-1,4-dione (12b)

2,5,6-Trimethyl-1,4-benzoquinone **21** (0.10 g, 0.67 mmol) and aniline (62 mg, 0.67 mmol) were refluxed in 5 mL ethanol for two days. The mixture was concentrated and purified with column chromatography to afford 5 mg brown solid, yield 3%. ^1H NMR (400 MHz, CDCl_3): δ 7.23 (t, $J = 7.9$ Hz, 2H), 7.02 – 6.98 (m, 2H), 6.83 (d, $J = 7.9$ Hz, 2H), 2.00 (s, 3H), 1.97 (s, 3H), 1.54 (s, 3H) ppm. ^{13}C NMR (101 MHz, CDCl_3): δ 187.2, 184.9, 143.3, 140.1, 136.8, 128.8 (2C), 123.6 (2C), 121.8 (2C), 116.0, 13.3, 13.0, 12.0 ppm. LRMS (ESI+) m/z calcd for $[\text{C}_{15}\text{H}_{16}\text{NO}_2]^+$: 242.11, found: 242.10 $[\text{M}+\text{H}]^+$. HPLC: $t_{\text{R}} = 12.6$ min, purity 95.3%. mp = 86-88 °C.

2,3,5-Trimethyl-6-(propylamino)cyclohexa-2,5-diene-1,4-dione (12c)

Compound **12c** was prepared from 2,5,6-trimethyl-1,4-benzoquinone **21** and 1-propylamin in a similar manner as described for compound **12a**. Purple solid, yield 19%. ^1H NMR (400 MHz, CDCl_3): δ 5.27 (brs, 1H), 3.33 (t, $J = 7.1$ Hz, 2H), 2.00 (s, 3H), 1.96 (s, 3H), 1.89 (s, 3H), 1.61 – 1.49 (m, 2H), 0.90 (t, $J = 7.4$ Hz, 3H) ppm. ^{13}C NMR (101 MHz, CDCl_3): δ 186.3, 184.8, 143.9, 143.7, 135.7, 108.5, 47.0, 24.1, 13.1, 11.9, 11.2, 10.6 ppm. LRMS (ESI+) m/z calcd for $[\text{C}_{12}\text{H}_{18}\text{NO}_2]^+$: 208.13, found: 208.10 $[\text{M}+\text{H}]^+$. HPLC: $t_{\text{R}} = 12.3$ min, purity 95.5%. mp = 51-52 °C.

2-((4-Hydroxybenzyl)amino)-3,5,6-trimethylcyclohexa-2,5-diene-1,4-dione (12d)

Compound **12d** was prepared from 2,5,6-trimethyl-1,4-benzoquinone **21** and 4-(aminomethyl)phenol in a similar manner as described for compound **12a**. Purple solid 16 mg, yield 9%. ^1H NMR (400 MHz,

CDCl₃): δ 7.05 (d, J = 8.4 Hz, 2H), 6.75 (d, J = 8.4 Hz, 2H), 5.57 (s, 1H), 5.21 (s, 1H), 4.47 (s, 2H), 2.00 (s, 3H), 1.96 (s, 3H), 1.90 (s, 3H) ppm. ¹³C NMR (101 MHz, CDCl₃): δ 186.6, 184.7, 155.3, 143.9, 143.7, 136.0, 130.9, 128.7 (2C), 115.8 (2C), 109.3, 48.8, 13.2, 11.9, 10.7 ppm. LRMS (ESI+) m/z calcd for [C₁₆H₁₈NO₃]⁺: 272.12, found: 272.10 [M+H]⁺. HPLC: t_R = 11.5 min, purity 95.1%. mp = 133-135 °C.

2,5-Bis((3-chlorobenzyl)amino)cyclohexa-2,5-diene-1,4-dione (13a)

(3-Chlorophenyl)methanamine (260 mg, 1.85 mmol) was added to a solution of 1,4-benzoquinone (100 mg, 0.93 mmol) in EtOH and stirred violently at room temperature, the solution was left to exposure in the air. The red precipitation was filtered and washed with petrolether and EtOH, then dried to afford yellow solid 21 mg, yield 6%. ¹H NMR (400 MHz, DMSO-*d*₆): δ 8.32 (t, J = 6.7 Hz, 2H), 7.40 – 7.38 (m, 2H), 7.36 (d, J = 7.6 Hz, 2H), 7.34 – 7.30 (m, 2H), 7.29 – 7.24 (m, 2H), 5.22 (s, 2H), 4.38 (d, J = 6.7 Hz, 4H) ppm. ¹³C NMR (101 MHz, DMSO-*d*₆): δ 178.4 (2C), 151.2 (2C), 140.6 (2C), 133.6 (2C), 130.8 (2C), 127.6 (2C), 127.6 (2C), 126.4 (2C), 93.9 (2C), 44.9 (2C) ppm. mp = 232-234 °C.

2,5-Bis(propylamino)cyclohexa-2,5-diene-1,4-dione (13c)

Compound **13c** was prepared from 1,4-benzoquinone and 1-propylamine in a similar manner as described for compound **13a**. Red solid 0.13 g, yield 32%. ¹H NMR (400 MHz, DMSO-*d*₆): δ 7.71 (t, J = 5.8 Hz, 2H), 5.25 (s, 2H), 3.10 (q, J = 6.7 Hz, 4H), 1.65 – 1.48 (m, 4H), 0.87 (t, J = 7.4 Hz, 6H) ppm. ¹³C NMR (101 MHz, DMSO-*d*₆): δ 177.8 (2C), 151.9 (2C), 92.4 (2C), 43.9 (2C), 21.4 (2C), 11.8 (2C) ppm. LRMS (ESI+) m/z calcd for [C₁₂H₁₈N₂O₂]⁺: 223.14, found: 223.15 [M+H]⁺. HPLC: t_R = 10.5 min, purity 97.3%. mp = 167-169 °C.

2,5-Bis((4-hydroxybenzyl)amino)cyclohexa-2,5-diene-1,4-dione (13d)

Compound **13d** was prepared from 1,4-benzoquinone and 4-(aminomethyl)phenol in a similar manner as described for compound **13a**. Yellow solid 0.13 g, yield 20%. ¹H NMR (400 MHz, DMSO-*d*₆): δ 9.30 (s, 2H), 8.14 (t, J = 5.5 Hz, 2H), 7.10 (d, J = 8.4 Hz, 4H), 6.71 (d, J = 8.4 Hz, 4H), 5.20 (s, 2H), 4.24 (d, J = 5.4 Hz, 4H) ppm. ¹³C NMR (101 MHz, DMSO-*d*₆): δ 178.1 (2C), 157.0 (2C), 151.4 (2C), 129.1 (4C), 127.9 (2C), 115.7 (4C), 93.5 (2C), 45.2 (2C) ppm. LRMS (ESI+) m/z calcd for [C₂₀H₁₉N₂O₄]⁺: 351.13, found: 351.15 [M+H]⁺. mp = 255-256 °C.

3-((3-Chlorobenzyl)amino)-5-isopropyl-2-methylcyclohexa-2,5-diene-1,4-dione (14a)

Compound **14a** was prepared from thymoquinone and (3-chlorophenyl) methanamine in a similar manner as described for compound **12a**. Black solid 26 mg, yield 7%. ¹H NMR (400 MHz, CDCl₃): δ 7.26 – 7.17 (m, 3H), 7.10 – 7.06 (m, 1H), 6.35 (s, 1H), 5.65 (s, 1H), 4.56 (s, 2H), 2.97 – 2.84 (m, 1H), 1.94 (s, 3H), 1.05 (d, J = 6.9 Hz, 6H) ppm. ¹³C NMR (101 MHz, CDCl₃): δ 187.0, 184.4, 150.1, 144.2, 141.0, 134.9, 132.9, 130.2, 128.0, 127.1, 125.0, 109.7, 48.5, 26.6, 21.3 (2C), 10.2 ppm. LRMS (ESI+) m/z calcd for [C₁₇H₁₉ClNO₂]⁺: 304.10, found: 304.05 [M+H]⁺. HPLC: t_R = 13.3 min, purity 99.3%. mp = 65-66 °C.

5-Isopropyl-2-methyl-3-(phenylamino)cyclohexa-2,5-diene-1,4-dione (14b)

Compound **14b** was prepared from thymoquinone and aniline in a similar manner as described for compound **12b**. Purple solid, yield 7%. ¹H NMR (400 MHz, CDCl₃): δ 7.28 – 7.21 (m, 2H), 7.05 – 6.98

(m, 2H), 6.86 (d, $J = 7.7$ Hz, 2H), 6.43 (d, $J = 1.2$ Hz, 1H), 3.05 – 2.91 (m, 1H), 1.53 (s, 3H), 1.10 (s, 3H), 1.08 (s, 3H) ppm. ^{13}C NMR (101 MHz, CDCl_3): δ 187.7, 184.7, 150.8, 140.7, 139.9, 132.7, 128.8 (2C), 123.9, 122.1 (2C), 115.5, 26.7, 21.4 (2C), 12.9 ppm. LRMS (ESI+) m/z calcd for $[\text{C}_{16}\text{H}_{18}\text{NO}_2]^+$: 256.13, found: 256.10 $[\text{M}+\text{H}]^+$. HPLC: $t_{\text{R}} = 12.8$ min, purity 97.6%. mp = 62-64 °C.

5-Isopropyl-2-methyl-3-(propylamino)cyclohexa-2,5-diene-1,4-dione (14c)

Compound **14c** was prepared from thymoquinone and 1-propylamine in a similar manner as described for compound **12a**. Purple solid, yield 13%. ^1H NMR (400 MHz, CDCl_3): δ 6.33 (s, 1H), 3.37 (t, $J = 7.1$ Hz, 2H), 2.95 – 2.80 (m, 1H), 2.00 (s, 3H), 1.63 – 1.48 (m, 2H), 1.03 (d, $J = 6.9$ Hz, 6H), 0.91 (t, $J = 7.4$ Hz, 3H) ppm. ^{13}C NMR (101 MHz, CDCl_3): δ 186.8, 184.7, 149.7, 144.5, 133.2, 108.2, 47.0, 26.5, 24.1, 21.3 (2C), 11.2, 10.2 ppm. LRMS (ESI+) m/z calcd for $[\text{C}_{13}\text{H}_{20}\text{NO}_2]^+$: 222.14, found: 222.10 $[\text{M}+\text{H}]^+$. HPLC: $t_{\text{R}} = 12.6$ min, purity 98.6%. mp = 32-34 °C.

3-((4-Hydroxybenzyl)amino)-5-isopropyl-2-methylcyclohexa-2,5-diene-1,4-dione (14d)

Compound **14d** was prepared from thymoquinone and 4-(aminomethyl)phenol in a similar manner as described for compound **12a**. Black solid, yield 30%. ^1H NMR (400 MHz, CDCl_3): δ 7.07 (d, $J = 8.3$ Hz, 2H), 6.78 (d, $J = 8.4$ Hz, 2H), 6.35 (s, 1H), 5.55 (s, 2H), 4.51 (s, 2H), 2.99 – 2.79 (m, 1H), 2.01 (s, 3H), 1.03 (d, $J = 6.9$ Hz, 6H) ppm. ^{13}C NMR (101 MHz, CDCl_3): δ 187.2, 184.5, 155.5, 150.0, 144.5, 133.1, 130.5, 128.7 (2C), 115.9 (2C), 108.8, 48.8, 26.6, 21.3 (2C), 10.3 ppm. LRMS (ESI+) m/z calcd for $[\text{C}_{17}\text{H}_{20}\text{NO}_3]^+$: 286.14, found: 286.10 $[\text{M}+\text{H}]^+$. HPLC: $t_{\text{R}} = 11.8$ min, purity 95.2%. mp = 136-138 °C.

1-((3-Chlorobenzyl)amino)anthracene-9,10-dione (15a)

K_2CO_3 (760 mg, 5.40 mmol) and (3-chlorophenyl)methanamine (368 mg, 1.84 mmol) were added to a solution of 1-aminoanthraquinone (400 mg, 1.79 mmol) in 5 mL DMF, then stirred at 80 °C overnight. Excess water was added to the mixture, red solid was precipitated and filtered. The red solid was then purified with column chromatography and recrystallization in a solution of petrolether : EtOAc = 100 : 1 to afford red solid 19 mg, yield 3%. ^1H NMR (400 MHz, CDCl_3): δ 10.18 (s, 1H), 8.37 – 8.30 (m, 1H), 8.31 – 8.24 (m, 1H), 7.85 – 7.73 (m, 2H), 7.67 (d, $J = 6.8$ Hz, 1H), 7.57 – 7.50 (m, 1H), 7.39 (s, 1H), 7.33 – 7.29 (m, 3H), 6.98 (d, $J = 8.5$ Hz, 1H), 4.61 (s, 2H) ppm. ^{13}C NMR (101 MHz, CDCl_3): δ 183.6, 183.0, 135.4, 134.8, 134.0, 133.2, 130.9, 130.2, 128.9, 127.7 (2C), 127.1, 126.8 (3C), 124.9 (2C), 118.1, 116.4, 100.0, 46.5 ppm. LRMS (ESI+) m/z calcd for $[\text{C}_{21}\text{H}_{15}\text{ClNO}_2]^+$: 348.07, found: 348.05 $[\text{M}+\text{H}]^+$. HPLC: $t_{\text{R}} = 14.6$ min, purity 97.3%. mp = 228-230 °C.

1-(Phenylamino)anthracene-9,10-dione (15b)

Compound **15b** was prepared from 1-aminoanthraquinone and iodobenzene in a similar manner as described for compound **15a**. Red solid 51 mg, yield 38%. ^1H NMR (400 MHz, CDCl_3): δ 11.28 (s, 1H), 8.24 (d, $J = 7.7$ Hz, 1H), 8.19 (dd, $J = 7.5, 0.7$ Hz, 1H), 7.75 – 7.60 (m, 3H), 7.46 – 7.37 (m, 2H), 7.34 (t, $J = 7.8$ Hz, 2H), 7.24 (d, $J = 7.8$ Hz, 2H), 7.14 (t, $J = 7.3$ Hz, 1H) ppm. ^{13}C NMR (101 MHz, CDCl_3): δ 185.5, 183.5, 149.3, 139.4, 135.0, 134.9, 134.7, 134.1, 133.3, 133.1, 129.6 (2C), 126.9, 126.9, 125.2, 124.2 (2C), 120.0, 117.8, 114.2 ppm. LRMS (ESI+) m/z calcd for $[\text{C}_{20}\text{H}_{14}\text{NO}_2]^+$: 300.09, found: 300.05 $[\text{M}+\text{H}]^+$. HPLC: $t_{\text{R}} = 14.7$ min, purity 99.4%. mp = 145-146 °C.

1-(Propylamino)anthracene-9,10-dione (15c)

t-BuOK (101 mg, 0.90 mmol) and 1-bromopropan were added to a solution of 1-aminoanthraquinone (0.10 g, 0.45 mmol) in 2 mL DMF and stirred at 80 °C for 4 h. Excess water was added to the mixture and extracted with EA. The combined organic phase was washed with water and brine, dried over Na₂SO₄, concentrated under vacuum and purified with column chromatography to afford red solid 41 mg, yield 34%. ¹H NMR (400 MHz, CDCl₃): δ 9.69 (s, 1H), 8.23 – 8.13 (m, 2H), 7.72 – 7.58 (m, 2H), 7.53 (d, *J* = 7.1 Hz, 1H), 7.47 (t, *J* = 7.9 Hz, 1H), 7.01 (d, *J* = 8.4 Hz, 1H), 3.24 (t, *J* = 7.0 Hz, 2H), 1.85 – 1.65 (m, 2H), 1.02 (t, *J* = 7.4 Hz, 3H) ppm. ¹³C NMR (101 MHz, CDCl₃): δ 185.0, 183.8, 151.5, 135.3, 135.0, 134.7, 133.9, 133.1, 132.9, 126.7, 126.7, 118.2, 115.9, 113.1, 45.0, 22.4, 11.7 ppm. LRMS (ESI+) *m/z* calcd for [C₁₇H₁₆NO₂]⁺: 266.11, found: 266.05 [M+H]⁺. HPLC: *t*_R = 14.3 min, purity 96.5%. mp = 147-148 °C. (Ref. Labbook FH-III-94)

1-((4-Hydroxybenzyl)amino)anthracene-9,10-dione (15d)

MgSO₄ (1.0 g, 8.33 mmol), 4-hydroxybenzaldehyde (0.28 g, 2.25 mmol), and 1 mL AcOH were added to a solution of AQ (0.50 g, 2.25 mmol) in 40 mL MeOH, then stirred at r.t. over night. NaBH₃CN (0.70 g, 11.25 mmol) was added to the mixture and stirred at r.t. for 6 h. The insoluble solid was filtered out and washed with MeOH. MeOH solution was collected and concentrated under vacuum. The residue was redissolved in ethyl acetate and washed with water and brine, dried over Na₂SO₄, purified with column chromatography to afford red solid 18 mg, yield 2%. ¹H NMR (400 MHz, DMSO-*d*₆): δ 9.91 (t, *J* = 5.4 Hz, 1H), 9.39 (s, 1H), 8.22 – 8.16 (m, 1H), 8.13 (dd, *J* = 7.7, 1.0 Hz, 1H), 7.89 (td, *J* = 7.5, 1.3 Hz, 1H), 7.84 (td, *J* = 7.5, 1.2 Hz, 1H), 7.65 – 7.59 (m, 1H), 7.44 (d, *J* = 7.2 Hz, 1H), 7.29 – 7.18 (m, 3H), 6.77 (d, *J* = 8.4 Hz, 2H), 4.49 (d, *J* = 5.5 Hz, 2H) ppm. ¹³C NMR (101 MHz, DMSO-*d*₆): δ 184.6, 183.3, 157.1, 151.5, 136.0, 135.0, 134.8, 134.4, 134.0, 132.8, 129.2 (2C), 128.8, 126.9, 126.7, 119.4, 115.9 (2C), 115.7, 112.7, 46.2 ppm. LRMS (ESI+) *m/z* calcd for [C₂₁H₁₆NO₃]⁺: 330.11, found: 330.05 [M+H]⁺. HPLC: *t*_R = 13.3 min, purity 96.7%. mp = 227-229 °C.

ORAC assay and Oxytosis assay were performed as described before (Chapter 4.1.4).

4.3. Design, Synthesis, Photophysical Characterization and Bio-Evaluation of Photoswitchable HDAC6 Inhibitors

Author Contributions

Prof. Dr. Michael Decker supervised the whole study.

Feng He and Prof. Dr. Michael Decker designed all target compounds

Feng He, under the supervision of Prof. Dr. Michael Decker, performed the synthesis of all target compounds as well as the photophysical characterization.

Prof. Dr. C. James Chou performed HDACs inhibition assay.

4.3.1. Introduction

Chemotherapy is one of the crucial strategies for the treatment of cancer, while the systemic distribution of chemotherapeutic drugs decreases their efficacy and induces severe side effects due to non-selective toxicity.¹²⁰ Photopharmacological agents exhibit light-dependent biological activity and may have promising potential in the development of cancer therapy with reduced side-effects benefiting from high spatiotemporal control of light usage.¹²¹ Histone deacetylase 6 (HDAC6) have been reported to be a potential target for further investigation regarding therapeutic applications in autoimmune disorders and neurodegenerative diseases and as an anticancer agent, alone or in combination with other approved drugs.¹²² Photoswitchable HDAC inhibitors have been developed previously and showed promising potential for chemotherapy and optical control of epigenetic states.^{73, 75, 77}

In this work, encouraged by the potent HDAC6 inhibition of melatonin derived compound **A** from our previous study,³² we have designed two series of photochromic HDAC6 inhibitors incorporate with 3-arylaZOindole photoswitch (**Figure 4.3.1a**). The 3-arylaZOindole photoswitch can switch from *trans*-isomer to *cis*-isomer by irradiation at 400 nm light instead of commonly used 365 nm UV light, which is better tolerated in cells-based pharmacological assays.¹²³ HDAC inhibitors normally include a zinc binding group (ZBG, e.g., hydroxamic acid), a linker mimicking the lysine chain, and a cap group, which is usually an aromatic group that can interact with the external surface of the enzyme.⁸⁷ Compounds **6a-f** were firstly designed by adopting 3-arylaZOindole group as the cap group to investigate the different effects of *cis/trans* isomers in the surface of HDAC6 binding site. The thermal stabilities of their *cis*-isomers are essential properties, which can decide their further application. Long thermal lifetimes are convenient for biological evaluation and are desired for applications such as molecular storage or logic devices, respectively.¹²⁴ Fast relaxing photoswitchable molecules are preferably used in real-time optical information transmitting materials or in *in vivo* studies.^{125, 126} The thermal half-lives of *cis*-isomers of compounds **6a-f** in DMSO are ranging from 0.7 – 150.2 min (**Table 4.3.1**), respectively. However, their thermal half-lives decrease to 0.1 – 2.2 min in buffer solution, which renders them inconvenient for further biological evaluation. Compounds **9a-b** were designed with multiple fluorinated substituents to produce a pull-pull system, expecting an improvement on thermal stability.

To rationally design “*cis-on*” molecules, compounds **11a-b** and **14a-f** were designed by using phenylazo group as the linker to make their corresponding *cis*-isomers own more suitable length of linker instead of *trans*-isomer with rigid and longer linker group, which were expected to produce more potent and highly selective HDAC6 inhibition with the *cis*-isomers. In total sixteen 3-arylazaindole-based target compounds have been synthesized and photophysical characterized. Some of their *cis*-isomers show good thermal stabilities in DMSO, but none of them is stable enough in the buffer solution, which makes them inconvenient for further biological evaluation. To avoid the fast isomerization of *cis*-isomers, we further designed a new series of photoswitchable HDAC6 inhibitors based on an azoquinoline photoswitch (**2**) and HDAC6 inhibitor **B** (Figure 4.3.1b).¹²⁷ Accordingly, azoquinoline photoswitches show similar photophysical properties to azobenzene, and the half-lives of corresponding *cis*-isomers mainly depend on the push-pull system of substitution, not the solvents.¹²⁸ Similar to the design strategy of compounds **11a-b** and **14a-f**, azoquinoline-based compounds **17**, **19a-b**, **21a-b**, **23** and **26** used phenylazo group as the linker and were expected to produce a *cis-on* effect. More specifically, compounds **19a-b** and **26** maintain the amino groups to produce push-pull effects with para benzoyl groups, which makes them possess the ability of visible light conversion.

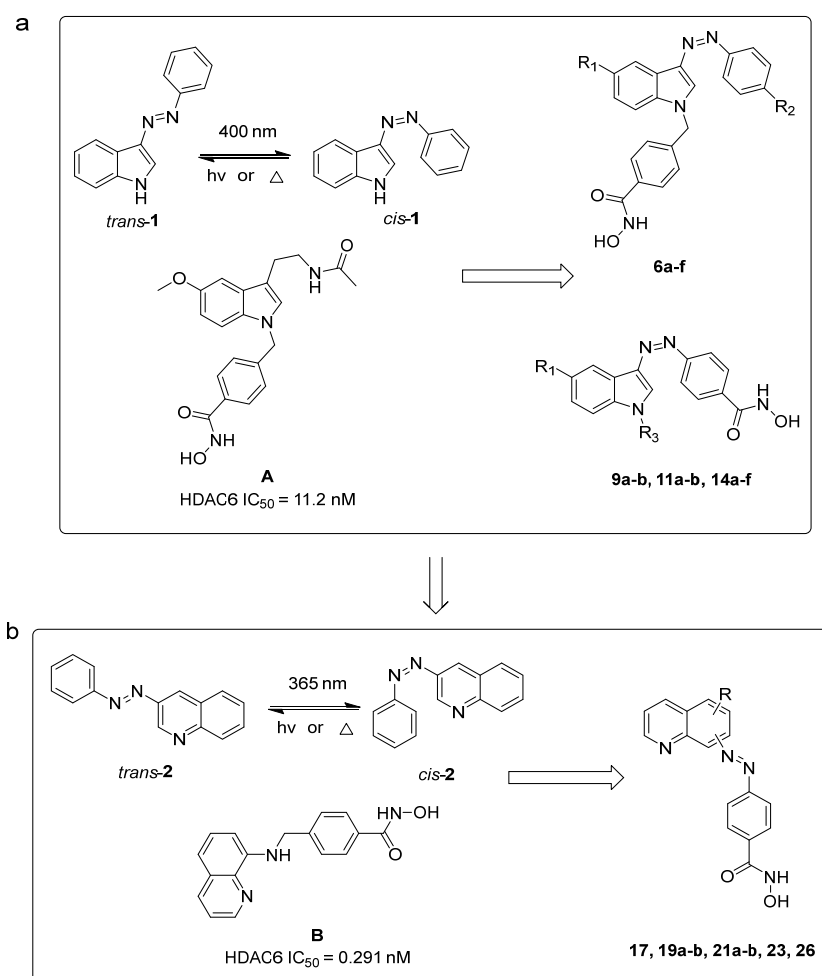
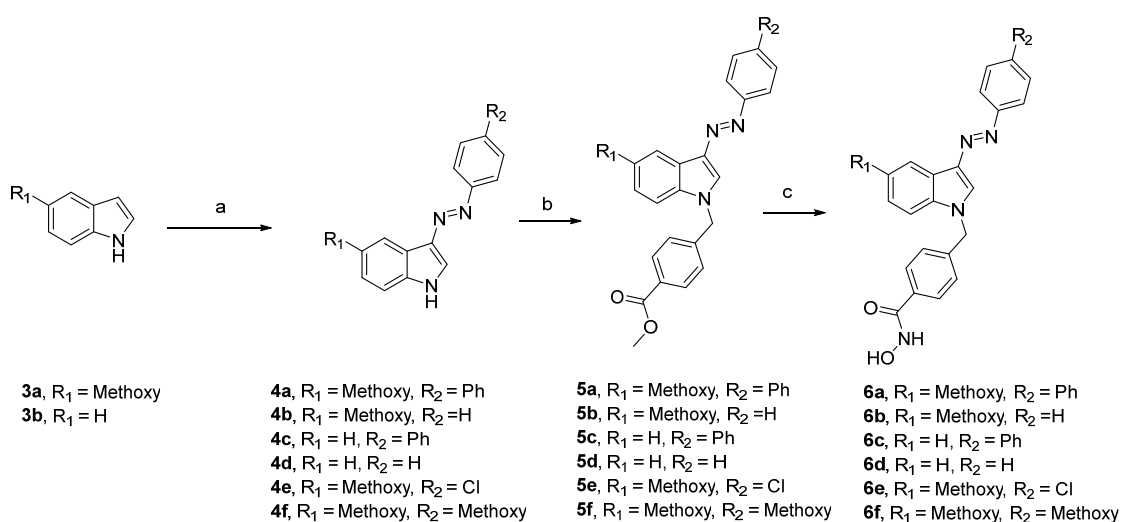


Figure 4.3.1. Design of photoswitchable HDAC6 inhibitors

4.3.2. Results and Discussion

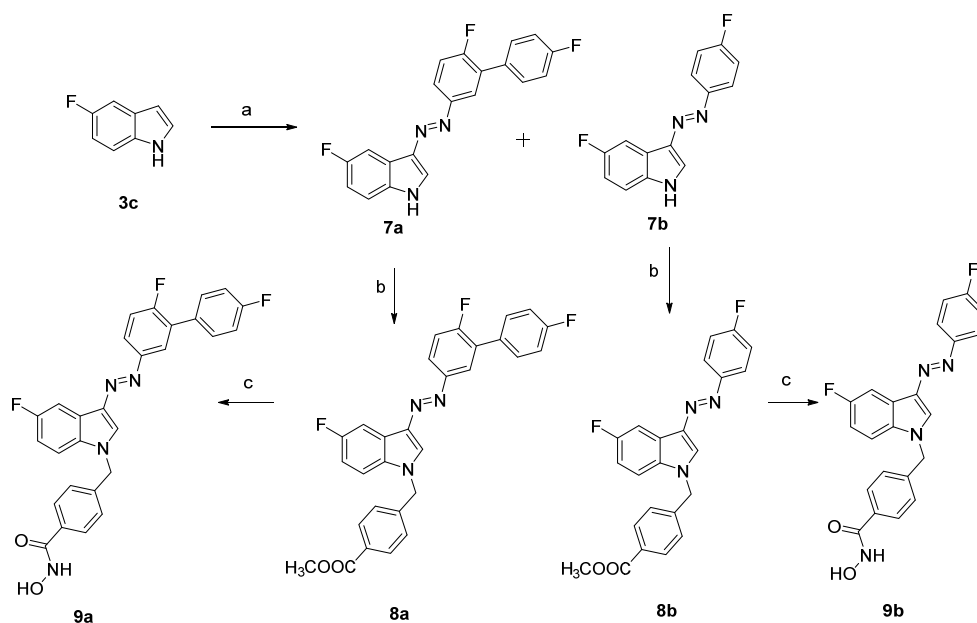
Chemistry. The synthesis of compounds **6a-f** starting from indole or 5-methoxyindole is described in **Scheme 4.3.1**. Intermediates **4a-f** were synthesized through corresponding diazonium salts, followed by substitution with methyl 4-(bromomethyl)benzoate in DMF at 80 °C to afford corresponding ester intermediates **5a-f**. More specifically, biphenyl intermediates **4a** and **4c** are byproduct during the synthesis of intermediates **4b** and **4d**, respectively. Target compounds **6a-f** were obtained in the usual way from corresponding ester intermediate **5a-f**, NH₂OH-HCl, and KOH in methanol. In **Scheme 4.3.2**, the synthesis of two fluoride compounds **9a-b** is described, which is similar to the synthesis of compounds **6a-b**.

Scheme 4.3.1. Synthesis of Compounds 6a-f^a



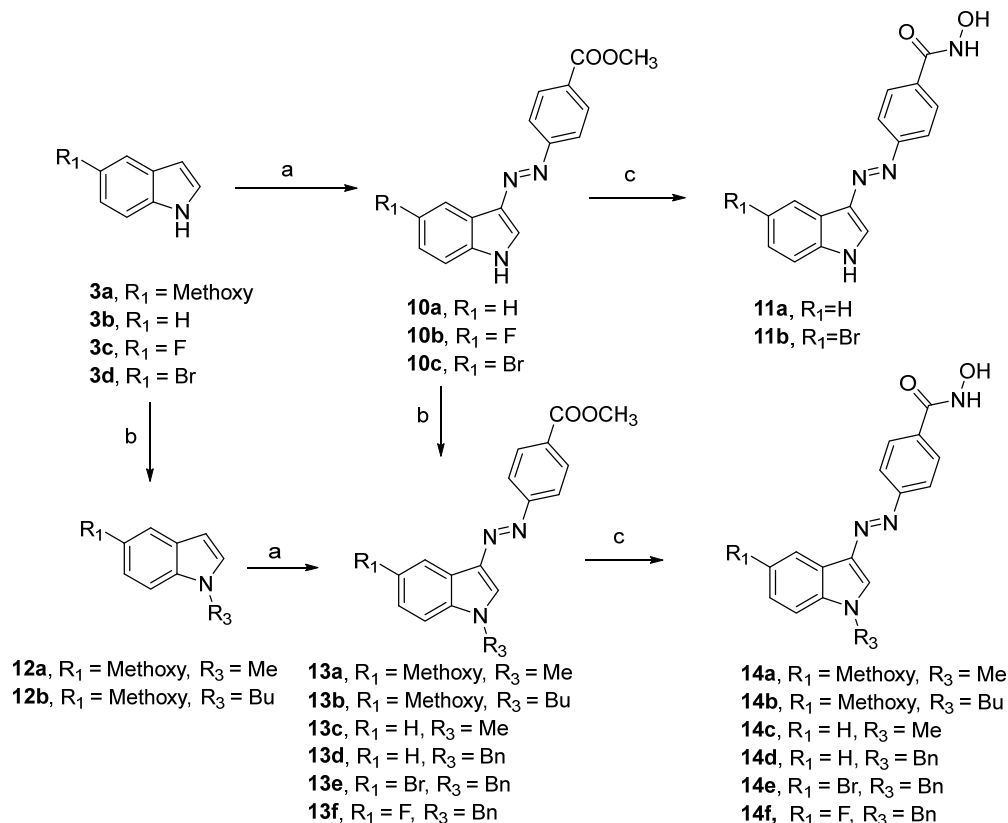
^aReagents and Conditions: (a) i) corresponding para-substituted aniline, 50% HBF₄ aq., NaNO₂ aq., -15 °C; ii) sat. Na₂CO₃ aq, MeOH, 0 °C, 30% - 60%; (b) methyl 4-(bromomethyl) benzoate, K₂CO₃, DMF, 80 °C, 63% - 92%; (c) NH₂OH-HCl, KOH, MeOH, r.t., 20% - 55%.

Scheme 4.3.2. Synthesis of Compounds 9a-b^a



^aReagents and Conditions: (a) i) 4-fluoroaniline, 50% HBF₄ aq., NaNO₂ aq., -15 °C; ii) sat. Na₂CO₃ aq, MeOH, 0 °C, 22% - 31%; (b) methyl 4-(bromomethyl) benzoate, K₂CO₃, DMF, 80 °C, 87% - 99%; (c) NH₂OH-HCl, KOH, MeOH, r.t., 26% - 37%.

Scheme 4.3.3. Synthesis of Compounds 11a-b and 14a-f^a



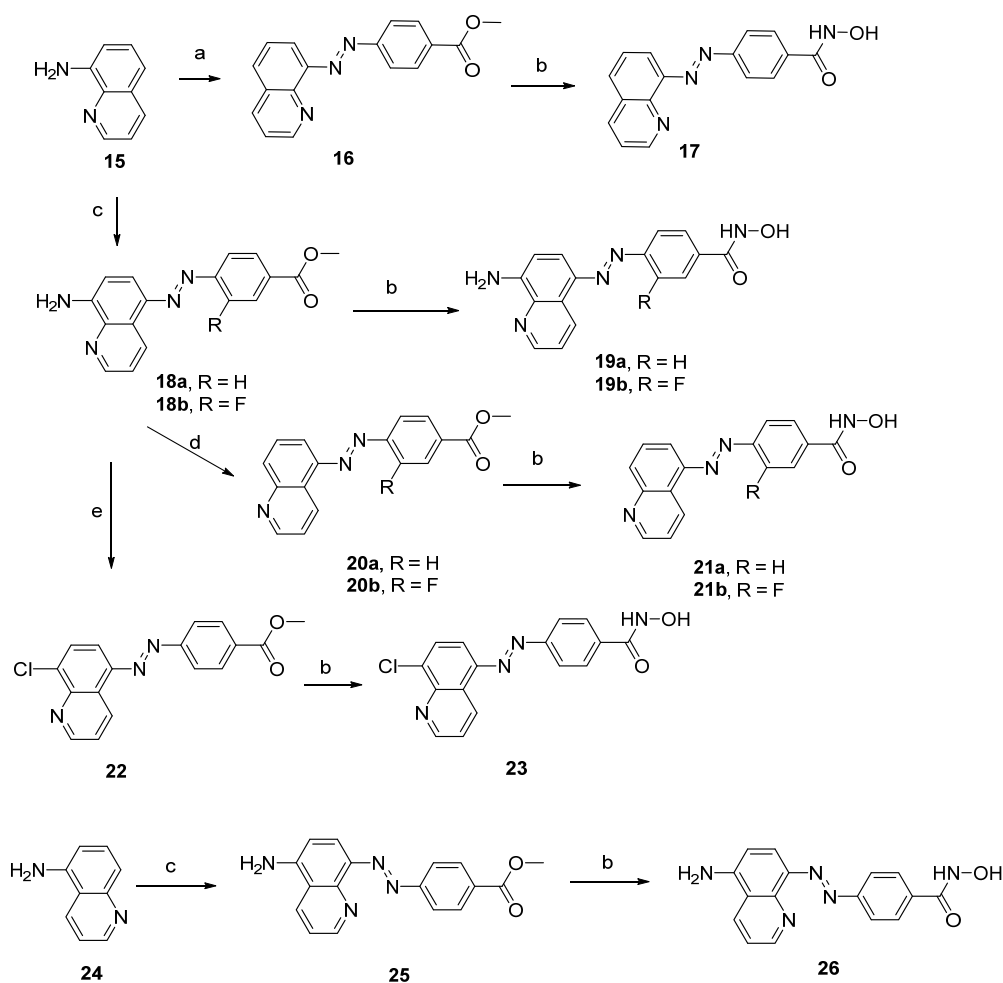
^aReagents and Conditions: (a) methyl 4-aminobenzoate, 50% HBF₄ aq., NaNO₂ aq., -15 °C; ii) sat. Na₂CO₃ aq, MeOH, 0 °C, 40% - 60%; (b) corresponding halide, K₂CO₃, DMF, 80 °C, 70% - 90%; (c) NH₂OH-HCl, KOH, MeOH, r.t., 20% - 50%.

Scheme 4.3.3 describes the synthesis of compounds **11a-b** and **14a-f** starting from 5-substituted indoles. Intermediates **10a-c** were synthesized through diazonium salts by a similar method with the synthesis of intermediates **4a-f**. Intermediates **12a-b** were synthesized from **3a** by reacting with iodomethane and 1-bromobutane, respectively, subsequent azo coupling reaction with diazonium salts afforded intermediates **13a-b**. Intermediates **10a-c** reacted with iodomethane or benzyl bromide in a suspension of K₂CO₃ in DMF to afford intermediates **13c-f**. Compounds **11a-b** and **14a-f** were obtained from corresponding ester intermediates by a similar method with the synthesis of other target compounds, and also the target compounds described in **Scheme 4.3.4**.

In **Scheme 4.3.4**, the synthesis of azoquinoline-based compounds **17**, **19a-b**, **21a-b**, **23** and **26** is described. The synthesis of compounds **17**, **19a-b**, **21a-b** and **23** started from 8-aminoquinoline, while the synthesis of compound **26** started from 5-aminoquinoline. Intermediate **16** was synthesized by Mills reaction from 8-aminoquinoline and the nitroso intermediate was prepared from methyl 4-aminobenzoate. Intermediates **18a-b** were obtained by azo coupling reaction from 8-aminoquinoline and corresponding diazonium salts prepared from methyl 4-aminobenzoate and methyl 4-amino-3-

fluorobenzoate, respectively. The reductive deamination of intermediates **18a-b** was performed through diazonium salts and the subsequent reduction by copper powder to afford intermediates **20a-b**. The transformation of arylamine intermediate **18a** to aryl halide intermediate **22** was performed via NaNO_2 and concentrated hydrogen chloride in DMSO. Intermediate **25** was synthesized from 5-aminoquinoline (**24**) by a similar method with the synthesis of intermediate **18a**. All target compounds were obtained in a similar method from corresponding ester intermediates with $\text{NH}_2\text{OH}\cdot\text{HCl}$, and KOH in methanol.

Scheme 4.3.4. Synthesis of Compounds **17**, **19a-b**, **21a-b**, **23** and **26**^a

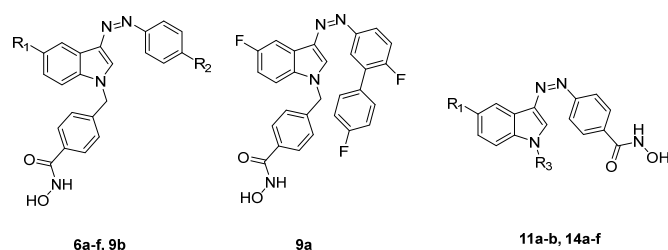


^aReagents and Conditions: (a) i) methyl 4-aminobenzoate, oxone, DCM, water, r.t.; ii) TFA, AcOH, r.t., 3%; (b) $\text{NH}_2\text{OH}\cdot\text{HCl}$, KOH , MeOH, r.t., 14% - 42%; (c) i) methyl 4-aminobenzoate for **18a**, methyl 4-amino-3-fluorobenzoate for **18b**, 50% HBF_4 aq., NaNO_2 aq., -15 °C; ii) sat. Na_2CO_3 aq., MeOH, 0 °C, 62% - 71%; (d) i) 50% HBF_4 aq., NaNO_2 aq., -15 °C; ii) copper powder, NaNO_2 aq., water, r.t., 6% - 7%; (e) 37% HCl , NaNO_2 , DMSO, r.t., 12%.

Photophysical Properties. Photophysical characterization of photoswitchable compounds is essential to screen suitable compounds for further tests, which were evaluated by UV/vis spectroscopy. In total 23 target compounds have been designed, synthesized and photophysicochemically characterized. As shown in **Table 4.3.1**, 3-arylaZOindole-based compounds **6a-f**, **9a-b**, **11a-b**, and **14a-f** can achieve the maximal photoconversion from *trans*-isomers to *cis*-isomer by irradiation at 385 nm UV light, except NH-containing compounds **11a-b**, which switch from *trans*

to *cis* by irradiation at 400 nm. By irradiation at 530 nm green light, their *cis*-isomers show highest conversion to corresponding *trans*-isomers. Besides, half-lives of their *cis*-isomers in both DMSO and buffer are presented. Interestingly, the half-lives are highly dependent on their substitution pattern and the solvents. For example, the half-lives of *cis*-isomers of compounds **10a-b** in DMSO are too short to be measured, which is probably due to the different isomerization pathway between substituted and NH-containing compounds reported by Simeth *et al.*¹²⁹ Compound **9b** possesses the longest half-life (848.9 min) of its *cis*-isomer in DMSO, while the half-life decrease to 1.5 min in buffer. The short half-lives in buffer can be observed in all 3-arylaazoindole-based compounds, which was probably caused by the proton-transfer mechanism in protic solvents of 3-arylaazoindole photoswitches.¹²⁹

Table 4.3.1. Structures of 3-arylaazoindole-based target compounds, and their half-lives of respective *cis*-isomers in DMSO or HDAC buffer, at 30 °C and in darkness.^a



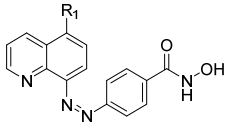
Compound	R ₁	R ₂	R ₃	λ_{\max} of <i>trans</i> (π - π^*) [nm]	ϵ of <i>trans</i> (π - π^*) [$\times 10^3$ M ⁻¹ cm ⁻¹]	λ_{\max} of <i>cis</i> (n- π^*) [nm] ^a	ϵ of <i>cis</i> (n- π^*) [$\times 10^3$ M ⁻¹ cm ⁻¹] ^a	$t_{1/2}$ in DMSO [min]	$t_{1/2}$ in buffer [min]
6a	-OCH ₃	-Ph	-	383	15.1	461	3.3	2.3	2.2
6b	-OCH ₃	-H	-	375	18.9	nd	nd	56.9	0.1
6c	-H	-Ph	-	385	19.5	462	4.0	5.5	0.9
6d	-H	-H	-	372	23.3	nd	nd	150.2	0.4
6e	-OCH ₃	-Cl	-	382	18.7	nd	nd	0.7	0.7
6f	-OCH ₃	-OCH ₃	-	383	22.6	423	4.3	63.2	0.6
9a	-	-	-	377	20.1	456	4.1	99.9	0.9
9b	-F	-F	-	366	22.4	411	2.8	848.9	1.5
11a	-H	-	-H	386	41.8	nd	nd	<0.1	<0.1
11b	-Br	-	-H	381	17.8	nd	nd	<0.1	<0.1
14a	-OCH ₃	-	-Me	401	16.1	nd	nd	0.9	<0.1
14b	-OCH ₃	-	-Bu	397	17.7	nd	nd	2.1	<0.1
14c	-H	-	-Me	394	13.9	nd	nd	5.8	<0.1
14d	-H	-	-Bn	381	23.2	nd	nd	34.6	0.2
14e	-Br	-	-Bn	380	20.1	nd	nd	159.5	3.2
14f	-F	-	-Bn	377	23.0	nd	nd	135.6	1.2

^a λ_{\max} (π - π^* , n- π^*) represents the wavelength at the maximal absorption of the π - π^* and n- π^* transition bands, respectively. The molar extinction coefficients ϵ (π - π^* , n- π^*) were calculated according to the Lambert-Beer formula. The tests were performed in HDAC assay buffer (pH 7.4), while all the n- π^* transition in buffer were too weak to be recognized, the n- π^* transition data were obtained in DMSO.

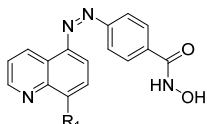
All 3-arylaazoindole-compounds are inconvenient for further pharmacological evaluation due to the fast isomerization of corresponding *cis*-isomers in buffer. Therefore, azoquinoline-based compounds **17**, **19a-b**, **21a-b**, **23** and **26** have been designed, synthesized and photophysical characterized. As

shown in **Table 4.3.2**, compounds **19a-b** and **26** possess push-pull electrical system and their maximal absorbance wavelength shows significant red shift, which render them be able to switch to corresponding *cis*-isomers by the irradiation of 455 nm blue light, on the other hand, this also speeds up the thermal-relaxation of their *cis*-isomers. Compounds **17**, **21a-b** and **23** can be switched between *cis* and *trans*-isomers with 365 and 455 nm light. Their half-lives of *cis*-isomers in buffer are higher than seven hours, which make them suitable for further pharmacological evaluation and allow their photostationary state percentage to be measured by HPLC. Consideration of the yield of *cis*-isomer, compound **PH6-22** possess highest 80%, which indicates the best photochemical properties.

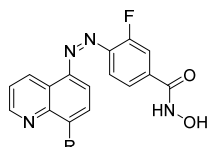
Table 4.3.2. Structures of quinolone-based target compounds, and their half-lives of respective *cis* isomers in DMSO or HDAC buffer, at 30 °C and in darkness.^a



17, 26



19a, 21a, 23



19b, 21b

Compound	R ₁	λ_{\max} of <i>trans</i> (π - π^*) [nm]	ϵ of <i>trans</i> (π - π^*) [$\times 10^3$ M ⁻¹ cm ⁻¹]	λ_{\max} of <i>cis</i> (n - π^*) [nm]	ϵ of <i>cis</i> (n - π^*) [$\times 10^3$ M ⁻¹ cm ⁻¹]	$t_{1/2}$ in DMSO [min]	$t_{1/2}$ in buffer [min]	PSS _{<i>trans</i>} (%)	PSS _{<i>cis</i>} (%)
17	-H	351	10.5	426	2.1	263	402.4	95	60
19a	-8-NH ₂	nd (477) ^b	nd (22.2) ^b	nd	nd	0.2	-	-	-
19b	-NH ₂	nd (493) ^b	nd (24.0) ^b	nd	nd	<0.1	-	-	-
21a	-H	346	10.3	nd (441) ^b	nd (2.1) ^b	324.9	718.6	94	75
21b	-H	356	14.4	nd	nd	113.1	481.2	96	65
23	-Cl	366	8.4	nd	nd	751.9	386.6	96	80
26	-NH ₂	448	10.0	nd	nd	2.0	<0.1	-	-

^a λ_{\max} (π - π^* , n - π^*) represents the wavelength at the maximal absorption of the π - π^* and n - π^* transition bands, respectively. The molar extinction coefficients ϵ (π - π^* , n - π^*) were calculated according to the Lambert-Beer formula. The tests were performed in HDAC assay buffer (pH 7.4). Photostationary state (PSS) percentages after irradiation with operational wavelengths determined by liquid chromatography using the wavelength at the isosbestic point as the detecting wavelength.

^bThe data in brackets were obtained in DMSO.

In **Figure 2** and **3**, the photophysical properties of 3-arylazoinole-based compound **9b** and azoquinoline-based compound **23** are shown as examples. Compound **9b** can be switched between *cis* and *trans*-isomers with 385 and 530 nm light in both DMSO and buffer (**Figure 2a** and **2b**), while compound **23** can be switched between *cis* and *trans*-isomers with 365 and 455 nm light (**Figure 3a** and **3b**). All target compounds show no significant photodecomposition after 15 cycles of *cis/trans* conversion except compound **19a**. The photophysical properties of other target compounds can be found in **Appendix IV**.

HDAC inhibition. Compounds **17**, **21a-b**, **23** possess relatively thermal-stable *cis*-isomers in buffer solution ($t_{1/2}$ = 386.6 – 751.9 min), which render them suitable for HDAC inhibition assay to test the inhibition of both *trans* and *cis*-isomers. As shown in **Table 2**, all target compounds show sub-micromolar range inhibition toward HDAC6 and micromolar range inhibition toward HDAC3 with or

without 365 nm UV light irradiation. Unfortunately, there is no obvious difference between the *trans*-isomers and corresponding *cis*-isomers, and all of target compounds are not as potent as reference compound **B**. This result is probably due to the highly tolerance of linker groups in HDAC inhibitors, which is not sensitive enough to the *trans-cis* conversion. In other words, azo group as the linker of HDAC inhibitor is invalid to produce the *cis*-on effect in the current design.

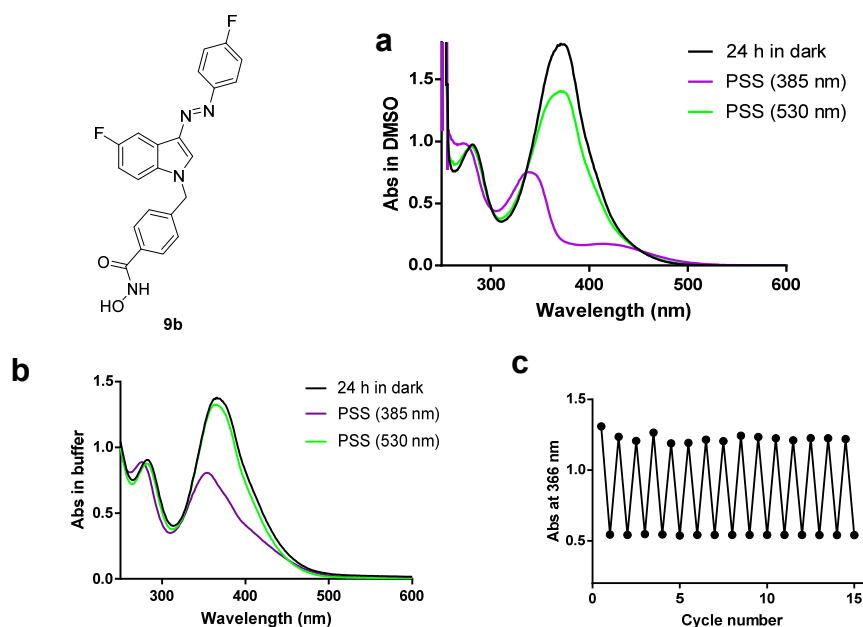


Figure 4.3.2. Photophysical properties of compound **9b** (61.6 μ M). Absorption spectra of PSS at the dark-adapted state and after irradiation with 385 nm (to *cis*) and 530 nm (to *trans*) for 1 min in DMSO (a) and HDAC assay buffer (pH 7.4) (b). 15 cycles of 385 nm/530 nm light irradiation performed without significant photodecomposition in buffer (c).

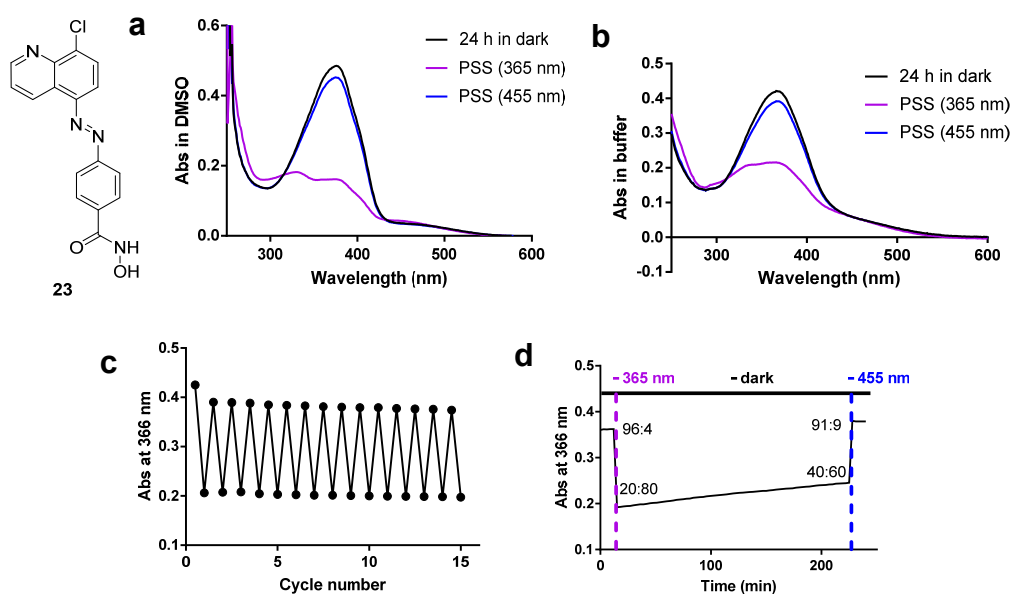
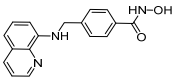
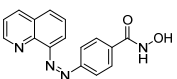
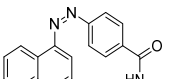
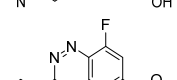
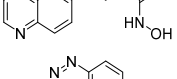


Figure 4.3.3. Photophysical properties of compound **23** (50 μ M). Absorption spectra of PSS at the dark-adapted state and after irradiation with 365 nm (to *cis*) and 455 nm (to *trans*) for 1 min in DMSO (a) and HDAC assay buffer (pH7.4) (b). 15 cycles of 365 nm/455 nm light irradiation performed without significant

photodecomposition in buffer (c). Stability measurement of *cis*-isomer during 210 min in darkness at 30 °C, HPLC ratios of *trans*- vs *cis*-isomer show in corresponding time point (d).

Table 4.3.2. Structures and *In Vitro* HDAC (HDAC3 and HDAC6) Inhibition of Compounds 17, 21a-b, and 23

Compound	Structure	HDAC6 IC ₅₀ [nM]	HDAC6 UV IC ₅₀ [nM]	HDAC3 IC ₅₀ [nM]	HDAC3 UV IC ₅₀ [nM]
B		28.72	17.64	666.1	751.4
17		719.7	742.3	3746	4404
21a		660.0	886.0	2072	2527
21b		654.8	357.3	2389	3472
23		499.5	411.2	2230	1272

4.3.3. Conclusions

Two series of photoswitchable HDAC6 inhibitors were designed based on 3-arylaazoindole and azoquinoline, respectively, in order to develop novel molecular tools to uncover the role of HDAC6 in the progression of neurodegenerative diseases. Based on their photophysicochemical properties, azoquinoline compounds possess more thermally stable *cis*-isomers in buffer solution, which were further tested in enzyme-based HDAC inhibition assay. Four tested azoquinoline-based compounds show moderate selectivity toward HDAC6 over HDAC3 at sub-micromolar range. However, minor differences in activities were observed between *trans*-isomers and corresponding *cis*-isomers. Hence, 3-arylaazoindole- and azoquinoline-based HDAC inhibitors are not appropriate solutions to design photoswitchable HDAC inhibitors as molecular tools. Nevertheless, this work has thoroughly studied the substituent effects on 3-arylaazoindole and azoquinoline photoswitches based on 23 novel photoswitchable molecules, and the obtained structure-photophysicochemical properties relationship could be a direction for other researchers and other applications.

4.3.4. Experimental section

For general information see in section 4.1.4. UV/vis spectra and experiments were made on a Varian Cary 50 Bio UV/vis spectrophotometer using Hellma (type 100-QS) cuvettes (10 mm light path).

(E'-3-([1,1'-Biphenyl]-4-yl)diazenyl)-5-methoxy-1H-indole (4a)

2 mL saturated Na₂CO₃ aqueous was added to a solution of 5-methoxyindole (0.5 g, 3.40 mmol) in 15 mL MeOH to maintain pH 8-9. The diazonium salt (0.65 g, 3.40 mmol) prepared in the usual way

from aniline (1.0 g, 10.74 mmol), 3.25 mL 50% HBF₄ aq. and 1 mL 43% NaNO₂ aq. was added gradually to the mixture at 0 °C and stirred for 2 h. Then solvent was removed under vacuum, the residue was dissolved in DCM and washed with water and brine, dried over Na₂SO₄, finally purified with column chromatography to afford yellow solid 0.13 g, yield 12%. ¹H NMR (400 MHz, CDCl₃): δ 8.43 (s, 1H), 8.15 (d, *J* = 2.6 Hz, 1H), 7.93 (d, *J* = 7.5 Hz, 2H), 7.81 (d, *J* = 7.7 Hz, 2H), 7.50 – 7.35 (m, 5H), 7.23 (d, *J* = 8.8 Hz, 1H), 7.18 (s, 1H), 6.89 (dd, *J* = 8.8, 2.6 Hz, 1H), 3.86 (s, 3H) ppm. ¹³C NMR (101 MHz, CDCl₃): δ 156.9, 154.2, 142.1, 132.5, 131.0, 130.4, 129.2 (2C), 129.1, 129.0 (2C), 128.8, 128.8 (2C), 122.1 (2C), 120.5, 114.2, 111.7, 105.6, 55.8 ppm. LRMS (ESI+) *m/z* calcd for [C₂₁H₁₈N₃O]⁺: 328.14, found: 328.20 [M+H]⁺.

(E)-5-Methoxy-3-(phenyldiazenyl)-1H-indole (4b)

Intermediate **4b** was prepared from 5-methoxyindole in the same reaction with the production of intermediate **4a**. Dark red solid, yield 74%. ¹H NMR (400 MHz, CDCl₃): δ 8.58 (brs, 1H), 8.14 (d, *J* = 2.5 Hz, 1H), 8.00 (d, *J* = 2.7 Hz, 1H), 7.94 – 7.87 (m, 2H), 7.58 – 7.49 (m, 2H), 7.45 – 7.37 (m, 1H), 7.33 – 7.27 (m, 1H), 7.04 – 6.92 (m, 1H), 3.95 (s, 3H) ppm. ¹³C NMR (101 MHz, CDCl₃): δ 156.7, 153.8, 136.8, 131.2, 131.0, 129.1, 129.0 (2C), 121.8 (2C), 119.4, 114.2, 112.1, 104.9, 55.8 ppm. LRMS (ESI+) *m/z* calcd for [C₁₅H₁₄N₃O]⁺: 252.11, found: 252.15 [M+H]⁺.

(E)-3-([1,1'-Biphenyl]-4-yl)diazenyl)-1H-indole (4c)

Intermediate **4c** was prepared from 1H-indole in a similar manner as described for intermediate **4a**. Red solid, yield 13%. ¹H NMR (400 MHz, CDCl₃): δ 8.75 – 8.66 (m, 1H), 8.60 (brs, 1H), 8.05 (d, *J* = 7.3 Hz, 2H), 7.94 (d, *J* = 7.5 Hz, 2H), 7.60 – 7.49 (m, 5H), 7.46 – 7.33 (m, 4H) ppm. ¹³C NMR (101 MHz, CDCl₃): δ 154.2, 141.7, 135.5, 132.5, 130.9, 129.3 (2C), 129.2, 129.0 (2C), 128.8 (2C), 124.6, 123.7, 123.4, 122.1 (2C), 120.0, 115.8, 111.0 ppm. LRMS (ESI+) *m/z* calcd for [C₂₀H₁₆N₃]⁺: 298.13, found: 298.15 [M+H]⁺.

(E)-3-(Phenyldiazenyl)-1H-indole (4d)

Intermediate **4d** was prepared from 1H-indole in the same reaction with the production of intermediate **4c**. Dark red solid, yield 64%. ¹H NMR (400 MHz, CDCl₃): δ 8.67 – 8.55 (m, 2H), 8.02 (d, *J* = 2.6 Hz, 1H), 7.93 (d, *J* = 7.9 Hz, 2H), 7.54 (t, *J* = 7.7 Hz, 2H), 7.47 – 7.31 (m, 4H) ppm. ¹³C NMR (101 MHz, CDCl₃): δ 153.8, 136.9, 136.3, 130.6, 129.2, 129.0 (2C), 124.4, 123.1, 123.1, 121.9 (2C), 118.9, 111.4 ppm. LRMS (ESI+) *m/z* calcd for [C₁₄H₁₂N₃]⁺: 222.10, found: 222.15 [M+H]⁺.

(E)-5-Methoxy-3-((4-methoxyphenyl)diazenyl)-1H-indole (4e)

Intermediate **4e** was prepared from 5-methoxyindole in a similar manner as described for intermediate **4a**. Red solid, yield 41%. ¹H NMR (400 MHz, CDCl₃): δ 8.47 (brs, 1H), 7.99 (d, *J* = 2.5 Hz, 1H), 7.91 (d, *J* = 2.9 Hz, 1H), 7.73 (d, *J* = 8.6 Hz, 2H), 7.37 (d, *J* = 8.6 Hz, 2H), 7.19 (d, *J* = 8.8 Hz, 1H), 6.90 (dd, *J* = 8.8, 2.6 Hz, 1H), 3.84 (s, 3H) ppm. ¹³C NMR (101 MHz, CDCl₃): δ 156.8, 136.8, 134.6, 131.4, 131.2, 129.1 (2C), 123.0 (2C), 114.3, 112.2, 104.9, 55.8 ppm. LRMS (ESI+) *m/z* calcd for [C₁₅H₁₃ClN₃O]⁺: 286.07, found: 286.10 [M+H]⁺.

(E)-5-Methoxy-3-((4-methoxyphenyl)diazenyl)-1H-indole (4f)

Intermediate **4f** was prepared from 5-methoxyindole and *p*-anisidine in a similar manner as described for intermediate **4a**. Red solid, yield 50%. ¹H NMR (400 MHz, CDCl₃): δ 8.51 (brs, 1H), 8.13 (d, *J* = 2.3 Hz, 1H), 7.94 (s, 1H), 7.89 (d, *J* = 8.8 Hz, 2H), 7.29 (d, *J* = 8.8 Hz, 1H), 7.04 (d, *J* = 8.8 Hz, 2H), 6.98 (dd, *J* = 8.8, 2.5 Hz, 1H), 3.94 (s, 3H), 3.91 (s, 3H) ppm. ¹³C NMR (101 MHz, CDCl₃): δ 160.6, 156.5, 148.0, 136.6, 131.2, 129.8, 123.3 (2C), 119.6, 114.2 (2C), 114.1, 112.1, 104.8, 55.8, 55.6 ppm. LRMS (ESI+) *m/z* calcd for [C₁₆H₁₆N₃O₂]⁺: 282.12, found: 282.15 [M+H]⁺.

Methyl (E)-4-((3-([1,1'-biphenyl]-4-yl)diazanyl)-5-methoxy-1H-indol-1-yl)methyl)benzoate (5a)

K₂CO₃ (0.11 g, 0.8 mmol) was added to a solution of **4a** (0.13 g, 0.4 mmol) in 5 mL DMF, then methyl 4-(bromomethyl)benzoate (0.11 g, 0.48 mmol) was added to the mixture and stirred at 70 °C for 2 h. Excess water was added to the mixture and extracted with ethyl acetate. The combined organic phase was washed with water and brine, dried over Na₂SO₄, and purified with column chromatography to afford red solid 70 mg, yield 37%. ¹H NMR (400 MHz, CDCl₃) δ 8.19 (d, *J* = 2.6 Hz, 1H), 7.89 (d, *J* = 8.3 Hz, 2H), 7.75 – 7.67 (m, 2H), 7.52 – 7.45 (m, 2H), 7.42 – 7.30 (m, 6H), 7.29 – 7.22 (m, 2H), 7.06 (d, *J* = 8.2 Hz, 1H), 6.99 (d, *J* = 8.9 Hz, 1H), 6.83 (dd, *J* = 8.9, 2.6 Hz, 1H), 5.37 (s, 2H), 3.85 (s, 3H), 3.82 (s, 3H). ¹³C NMR (101 MHz, CDCl₃): δ 166.6, 157.2, 154.1, 142.2, 133.0, 131.9, 131.3 (2C), 130.3 (2C), 129.7, 129.5, 129.2, 128.9, 128.9 (2C), 128.7, 128.2 (2C), 126.0 (2C), 122.0 (2C), 119.8, 114.0, 111.2, 105.5, 55.9, 52.2, 48.1. LRMS (ESI+) *m/z* calcd for [C₃₀H₂₆N₃O₃]⁺: 476.19, found: 476.20 [M+H]⁺.

Methyl (E)-4-((3-([1,1'-biphenyl]-4-yl)diazanyl)-1H-indol-1-yl)methyl)benzoate (5b)

Intermediate **5b** was prepared from **4b** in a similar manner as described for intermediate **5a**. Red solid, yield 83%. ¹H NMR (400 MHz, CDCl₃): δ 8.64 (d, *J* = 7.8 Hz, 1H), 7.90 (d, *J* = 8.3 Hz, 2H), 7.83 (d, *J* = 7.9 Hz, 2H), 7.53 – 7.45 (m, 2H), 7.42 – 7.31 (m, 5H), 7.31 – 7.18 (m, 3H), 7.14 – 7.04 (m, 3H), 5.41 (s, 2H), 3.82 (s, 3H) ppm. ¹³C NMR (101 MHz, CDCl₃): δ 166.6, 154.1, 146.3, 142.2, 136.9, 133.1, 131.4 (2C), 130.3 (2C), 129.7, 129.5, 129.2, 128.9 (3C), 128.2 (2C), 126.0 (2C), 124.5, 123.7, 123.6, 122.0 (2C), 119.4, 110.4, 52.2, 48.0 ppm. LRMS (ESI+) *m/z* calcd for [C₂₉H₂₄N₃O₂]⁺: 446.18, found: 446.20 [M+H]⁺.

Methyl (E)-4-((5-Methoxy-3-(phenyldiazanyl)-1H-indol-1-yl)methyl)benzoate (5c)

Intermediate **5c** was prepared from **4c** in a similar manner as described for intermediate **5a**. Yellow solid, yield 88%. ¹H NMR (400 MHz, DMSO-*d*₆): δ 8.56 (s, 1H), 7.97 (d, *J* = 2.6 Hz, 1H), 7.94 (d, *J* = 8.3 Hz, 2H), 7.82 (d, *J* = 7.3 Hz, 2H), 7.54 (t, *J* = 7.7 Hz, 2H), 7.46 – 7.39 (m, 4H), 6.92 (dd, *J* = 8.9, 2.6 Hz, 1H), 5.65 (s, 2H), 3.83 (s, 3H), 3.82 (s, 3H) ppm. ¹³C NMR (101 MHz, DMSO-*d*₆): δ 166.4, 156.9, 153.6, 143.0, 136.8, 135.1, 131.8, 130.1 (2C), 129.7 (2C), 129.5, 129.4, 127.9 (2C), 121.8 (2C), 120.1, 113.7, 112.4, 105.2, 55.9, 52.6, 50.0 ppm. LRMS (ESI+) *m/z* calcd for [C₂₄H₂₂N₃O₃]⁺: 400.16, found: 400.20 [M+H]⁺.

Methyl (E)-4-((3-(phenyldiazanyl)-1H-indol-1-yl)methyl)benzoate (5d)

Intermediate **5d** was prepared from **4d** in a similar manner as described for intermediate **5a**. Red solid, yield 84%. ¹H NMR (400 MHz, CDCl₃): δ 8.63 (d, *J* = 7.1 Hz, 1H), 8.03 (d, *J* = 8.2 Hz, 2H), 7.97 (s,

1H), 7.90 (d, $J = 7.6$ Hz, 2H), 7.52 (t, $J = 7.7$ Hz, 2H), 7.44 – 7.24 (m, 6H), 5.47 (s, 2H), 3.93 (s, 3H). ^{13}C NMR (101 MHz, CDCl_3): δ 166.5, 141.1, 136.8, 136.0, 133.8, 130.3 (2C), 130.1, 129.2, 129.0 (2C), 126.9 (2C), 124.4, 123.4, 123.2, 121.8 (2C), 120.0, 109.9, 100.0, 52.2, 50.5. LRMS (ESI+) m/z calcd for $[\text{C}_{23}\text{H}_{20}\text{N}_3\text{O}_2]^+$: 370.15, found: 370.15 $[\text{M}+\text{H}]^+$.

Methyl (E)-4-((3-((4-chlorophenyl)diazenyl)-5-methoxy-1H-indol-1-yl)methyl)benzoate (5e)

Intermediate **5e** was prepared from **4e** in a similar manner as described for intermediate **5a**. Yellow solid, yield 90%. ^1H NMR (400 MHz, CDCl_3): δ 8.10 (d, $J = 2.4$ Hz, 1H), 8.03 (d, $J = 8.2$ Hz, 2H), 7.94 (s, 1H), 7.83 (d, $J = 8.6$ Hz, 2H), 7.47 (d, $J = 8.5$ Hz, 2H), 7.27 (d, $J = 9.0$ Hz, 2H), 7.15 (d, $J = 8.9$ Hz, 1H), 6.95 (dd, $J = 8.9, 2.5$ Hz, 1H), 5.43 (s, 2H), 3.93 (s, 6H) ppm. ^{13}C NMR (101 MHz, CDCl_3): δ 166.5, 157.0, 140.9, 135.7, 134.5, 134.5, 131.8, 130.4 (2C), 130.2, 129.1 (2C), 126.8 (2C), 123.0 (2C), 114.1, 110.9, 105.2, 55.8, 52.2, 50.7 ppm. LRMS (ESI+) m/z calcd for $[\text{C}_{24}\text{H}_{21}\text{ClN}_3\text{O}_3]^+$: 434.12, found: 434.15 $[\text{M}+\text{H}]^+$. (Ref. Labbook FH-II-34)

Methyl (E)-4-((5-methoxy-3-((4-methoxyphenyl)diazenyl)-1H-indol-1-yl)methyl)benzoate (5f)

Intermediate **5f** was prepared from **4f** and methyl 4-(bromomethyl)benzoate in a similar manner as described for intermediate **5a**. Red oil, yield 41%. ^1H NMR (400 MHz, CDCl_3): δ 8.03 (d, $J = 2.1$ Hz, 1H), 7.91 (d, $J = 8.3$ Hz, 2H), 7.81 – 7.74 (m, 3H), 7.16 (d, $J = 8.2$ Hz, 2H), 7.03 (d, $J = 8.9$ Hz, 1H), 6.96 – 6.90 (m, 2H), 6.83 (dd, $J = 8.9, 2.5$ Hz, 1H), 5.32 (s, 2H), 3.83 (s, 3H), 3.82 (s, 3H), 3.80 (s, 3H) ppm. ^{13}C NMR (101 MHz, CDCl_3): δ 166.6, 160.6, 156.7, 141.3, 140.4, 135.6, 132.9, 131.8, 130.3 (2C), 130.0, 126.8 (2C), 123.2 (2C), 120.6, 114.2 (2C), 113.9, 110.7, 105.1, 55.8, 55.5, 52.2, 50.6. LRMS (ESI+) m/z calcd for $[\text{C}_{25}\text{H}_{24}\text{N}_3\text{O}_4]^+$: 430.17, found: 430.20 $[\text{M}+\text{H}]^+$.

(E)-4-((3-([1,1'-Biphenyl]-4-yl)diazenyl)-5-methoxy-1H-indol-1-yl)methyl)-N-hydroxybenzamide (6a)

KOH (28 g, 509 mmol) in 70 mL MeOH was added to a stirred solution of $\text{NH}_2\text{OH}\cdot\text{HCl}$ (23.35 g, 343 mmol) in 120 mL MeOH at room temperature. After 30 min, white precipitate was filtered out to afford NH_2OK methanol solution. **5a** (70 mg, 0.15 mmol) was added to 10 mL NH_2OK methanol solution, the mixture was stirred at room temperature for 3 h. The solvent was evaporated under vacuum, the residue was dissolved with 5 mL water and then adjusted to pH 6-7 by hydrochloric acid. The precipitate was filtered and dried, then purified with column chromatography to afford light red solid 44 mg, yield 86%. ^1H NMR (400 MHz, $\text{DMSO}-d_6$): δ 11.13 (s, 1H), 9.00 (s, 1H), 8.10 (d, $J = 2.3$ Hz, 1H), 7.70 – 7.63 (m, 6H), 7.58 – 7.55 (m, 3H), 7.49 (t, $J = 7.4$ Hz, 2H), 7.45 – 7.34 (m, 2H), 7.07 (d, $J = 8.0$ Hz, 2H), 6.96 (dd, $J = 8.7, 2.1$ Hz, 1H), 5.59 (s, 2H), 3.85 (s, 3H) ppm. ^{13}C NMR (101 MHz, $\text{DMSO}-d_6$): δ 166.3, 154.0, 147.3, 132.6, 131.9, 131.8, 131.6 (2C), 129.8, 129.7, 129.6 (2C), 129.5, 129.3, 128.82, 128.79 (2C), 127.82, 127.79 (2C), 126.5 (2C), 121.8 (2C), 119.4, 113.8, 105.4, 55.9, 47.6. LRMS (ESI+) m/z calcd for $[\text{C}_{29}\text{H}_{25}\text{N}_4\text{O}_3]^+$: 477.18, found: 477.20 $[\text{M}+\text{H}]^+$. HPLC (method A): $t_R = 13.8$ min, purity 98.5%. mp = 160–162 °C.

(E)-N-Hydroxy-4-((5-methoxy-3-(phenyldiazenyl)-1H-indol-1-yl)methyl)benzamide (6b)

Compound **6b** was prepared from **5b** in a similar manner as described for compound **6a**. Yellow solid, yield 43%. ^1H NMR (400 MHz, $\text{DMSO}-d_6$): δ 11.17 (s, 1H), 9.02 (s, 1H), 8.55 (s, 1H), 7.96 (d, $J = 2.0$

Hz, 1H), 7.82 (d, $J = 7.8$ Hz, 2H), 7.73 (d, $J = 7.9$ Hz, 2H), 7.54 (t, $J = 7.6$ Hz, 2H), 7.47 (d, $J = 8.9$ Hz, 1H), 7.44 – 7.37 (m, 3H), 6.93 (dd, $J = 8.8, 2.0$ Hz, 1H), 5.59 (s, 2H), 3.82 (s, 3H) ppm. ^{13}C NMR (101 MHz, DMSO- d_6): δ 164.4, 156.9, 153.6, 140.6, 136.8, 135.0, 132.7, 131.8, 129.7 (2C), 129.4, 127.8 (2C), 127.7 (2C), 121.8 (2C), 120.0, 113.7, 112.4, 105.1, 55.9, 50.0 ppm. LRMS (ESI+) m/z calcd for $[\text{C}_{23}\text{H}_{21}\text{N}_4\text{O}_3]^+$: 401.15, found: 401.15 $[\text{M}+\text{H}]^+$. HPLC (method A): $t_{\text{R}} = 12.6$ min, purity 99.6%. mp = 160–162 °C.

(E)-4-((3-([1,1'-Biphenyl]-4-yl)diazenyl)-1H-indol-1-yl)methyl)-N-hydroxybenzamide (6c)

Compound **6c** was prepared from **5c** in a similar manner as described for compound **6a**. Yellow solid, yield 33%. ^1H NMR (400 MHz, DMSO- d_6): δ 11.13 (s, 1H), 9.00 (s, 1H), 8.67 – 8.48 (m, 1H), 7.72 – 7.67 (m, 4H), 7.65 (d, $J = 8.2$ Hz, 2H), 7.60 – 7.54 (m, 3H), 7.53 – 7.46 (m, 3H), 7.38 (t, 1H), 7.36 – 7.30 (m, 2H), 7.09 (d, $J = 8.1$ Hz, 2H), 5.62 (s, 2H) ppm. ^{13}C NMR (101 MHz, DMSO- d_6): δ 164.3, 154.0, 147.1, 140.7, 136.9, 132.8, 132.4, 131.7, 129.9, 129.6 (2C), 129.5, 129.4, 128.8 (2C), 127.83, 127.81 (2C), 126.5 (2C), 124.9, 124.0, 123.1, 121.9 (2C), 118.9, 111.8, 47.5 ppm. LRMS (ESI+) m/z calcd for $[\text{C}_{28}\text{H}_{23}\text{N}_4\text{O}_2]^+$: 447.17, found: 447.20 $[\text{M}+\text{H}]^+$. HPLC (method A): $t_{\text{R}} = 13.7$ min, purity 95.3%. mp = 158–160 °C.

(E)-N-Hydroxy-4-((3-(phenyldiazenyl)-1H-indol-1-yl)methyl)benzamide (6d)

Compound **6d** was prepared from **5d** in a similar manner as described for compound **6a**. Red solid, yield 77%. ^1H NMR (400 MHz, DMSO- d_6): δ 11.17 (s, 1H), 9.02 (s, 1H), 8.63 (s, 1H), 8.48 – 8.36 (m, 1H), 7.83 (d, $J = 7.4$ Hz, 2H), 7.73 (d, $J = 8.2$ Hz, 2H), 7.60 – 7.51 (m, 3H), 7.46 – 7.39 (m, 3H), 7.33 – 7.26 (m, 2H), 5.64 (s, 2H) ppm. ^{13}C NMR (101 MHz, DMSO- d_6): δ 164.4, 153.7, 140.6, 136.9, 136.8, 135.2, 132.8, 129.7 (2C), 129.6, 127.8 (2C), 127.7 (2C), 124.5, 123.5, 123.0, 121.8 (2C), 119.4, 111.5, 49.8 ppm. LRMS (ESI+) m/z calcd for $[\text{C}_{22}\text{H}_{19}\text{N}_4\text{O}_2]^+$: 371.14, found: 371.20 $[\text{M}+\text{H}]^+$. HPLC (method A): $t_{\text{R}} = 12.7$ min, purity 99.6%. mp = 168–169 °C.

(E)-4-((3-((4-Chlorophenyl)diazenyl)-5-methoxy-1H-indol-1-yl)methyl)-N-hydroxybenzamide (6e)

Compound **6e** was prepared from **5e** in a similar manner as described for compound **6a**. Yellow solid, yield 56%. ^1H NMR (400 MHz, DMSO- d_6): δ 11.17 (s, 1H), 9.02 (s, 1H), 8.58 (s, 1H), 7.94 (d, $J = 2.5$ Hz, 1H), 7.84 (d, $J = 8.6$ Hz, 2H), 7.72 (d, $J = 8.2$ Hz, 2H), 7.58 (d, $J = 8.6$ Hz, 2H), 7.47 (d, $J = 8.9$ Hz, 1H), 7.40 (d, $J = 8.2$ Hz, 2H), 6.93 (dd, $J = 8.9, 2.5$ Hz, 1H), 5.60 (s, 2H), 3.81 (s, 3H) ppm. ^{13}C NMR (101 MHz, DMSO- d_6): δ 164.3, 157.0, 152.3, 140.5, 137.4, 135.1, 133.5, 132.8, 131.8, 129.7 (2C), 127.8 (2C), 127.7 (2C), 123.4 (2C), 120.0, 113.8, 112.5, 105.2, 55.9, 50.0 ppm. LRMS (ESI+) m/z calcd for $[\text{C}_{23}\text{H}_{20}\text{ClN}_4\text{O}_3]^+$: 435.11, found: 435.15 $[\text{M}+\text{H}]^+$. HPLC (method A): $t_{\text{R}} = 13.3$ min, purity 99.8%. mp = 167–168 °C.

(E)-N-hydroxy-4-((5-methoxy-3-((4-methoxyphenyl)diazenyl)-1H-indol-1-yl)methyl)benzamide (6f)

Compound **6f** was prepared from **5f** in a similar manner as described for compound **6a**. Brown solid, yield 53%. ^1H NMR (400 MHz, DMSO- d_6): δ 11.17 (s, 1H), 9.02 (s, 1H), 8.45 (s, 1H), 7.95 (s, 1H), 7.81 (d, $J = 7.9$ Hz, 2H), 7.72 (d, $J = 7.4$ Hz, 2H), 7.45 (d, $J = 8.2$ Hz, 1H), 7.39 (d, $J = 7.3$ Hz, 2H), 7.09 (d, $J = 8.0$ Hz, 2H), 6.91 (d, $J = 7.6$ Hz, 1H), 5.57 (s, 2H), 3.85 (s, 3H), 3.81 (s, 3H) ppm. ^{13}C NMR (101

MHz, DMSO-*d*₆): δ 164.4, 160.6, 156.6, 147.8, 140.8, 135.5, 134.7, 132.7, 131.7, 127.8 (2C), 127.6 (2C), 123.3 (2C), 120.2, 114.8 (2C), 113.5, 112.3, 105.1, 55.9, 55.9, 49.9 ppm. LRMS (ESI+) *m/z* calcd for [C₂₄H₂₃N₄O₄]⁺: 431.16, found: 431.20 [M+H]⁺. HPLC (method A): *t*_R = 12.7 min, purity 99.3%. mp = 159–160 °C.

(E)-3-((4',6-Difluoro-[1,1'-biphenyl]-3-yl)diazanyl)-5-fluoro-1H-indole (7a)

Intermediate **7a** was prepared from 5-fluoro-1H-indole (**3c**) and 4-fluoroaniline in a similar manner as described for intermediate **4a**. Red solid, yield 31%. ¹H NMR (400 MHz, DMSO-*d*₆): δ 12.50 (s, 1H), 8.25 – 8.13 (m, 3H), 7.94 – 7.82 (m, 2H), 7.56 – 7.44 (m, 3H), 7.41 – 7.33 (m, 2H), 7.17 (td, *J* = 9.2, 2.7 Hz, 1H) ppm. ¹³C NMR (101 MHz, DMSO-*d*₆): δ 163.3 (d, *J* = 248.0 Hz), 162.8 (d, *J* = 247.0 Hz), 159.7 (d, *J* = 235.0 Hz), 143.23, 132.92, 132.14 (d, *J* = 8.6 Hz, 2C), 127.26, 127.23, 123.98 (d, *J* = 8.6 Hz, 2C), 119.49, 119.38, 116.57 (d, *J* = 23.1 Hz, 2C), 116.35 (d, *J* = 22.0 Hz, 2C), 113.7 (d, *J* = 9.7 Hz), 112.7 (d, *J* = 26.0 Hz), 108.1 (d, *J* = 25.2 Hz) ppm. LRMS (ESI+) *m/z* calcd for [C₂₀H₁₃F₃N₃]⁺: 352.10, found: 352.15 [M+H]⁺.

(E)-5-Fluoro-3-((4-fluorophenyl)diazanyl)-1H-indole (7b)

Intermediate **7b** was prepared from 5-fluoro-1H-indole (**3c**) and 4-fluoroaniline in the same reaction with the production of intermediate **7a**. Red solid, yield 22%. ¹H NMR (400 MHz, DMSO-*d*₆): δ 12.21 (s, 1H), 8.44 (d, *J* = 3.1 Hz, 1H), 8.09 (dd, *J* = 9.8, 2.6 Hz, 1H), 7.92 – 7.85 (m, 2H), 7.52 (dd, *J* = 8.8, 4.6 Hz, 1H), 7.39 – 7.32 (m, 2H), 7.14 (td, *J* = 9.2, 2.7 Hz, 1H) ppm. ¹³C NMR (101 MHz, DMSO-*d*₆): δ 162.8 (d, *J* = 246.5 Hz), 159.4 (d, *J* = 234.8 Hz), 150.29 (d, *J* = 2.8 Hz), 135.65 (d, *J* = 4.3 Hz), 135.57, 133.66, 123.75 (d, *J* = 8.7 Hz, 2C), 118.59 (d, *J* = 11.0 Hz), 116.46 (d, *J* = 22.7 Hz, 2C), 114.04 (d, *J* = 9.7 Hz), 112.30 (d, *J* = 25.9 Hz), 107.56 (d, *J* = 25.0 Hz) ppm. LRMS (ESI+) *m/z* calcd for [C₁₄H₁₀F₂N₃]⁺: 258.08, found: 258.20 [M+H]⁺.

Methyl (E)-4-((3-((4',6-difluoro-[1,1'-biphenyl]-3-yl)diazanyl)-5-fluoro-1H-indol-1-yl)methyl)benzoate (8a)

Intermediate **8a** was prepared from **7a** and methyl 4-(bromomethyl)benzoate in a similar manner as described for intermediate **5a**. Yellow solid, yield 90%. ¹H NMR (400 MHz, CDCl₃): δ 8.27 (dd, *J* = 9.5, 2.5 Hz, 1H), 7.92 (d, *J* = 8.2 Hz, 2H), 7.73 – 7.66 (m, 2H), 7.49 – 7.41 (m, 2H), 7.10 (t, *J* = 8.6 Hz, 2H), 7.07 – 7.01 (m, 5H), 6.95 (td, *J* = 8.9, 2.5 Hz, 1H), 5.37 (s, 2H), 3.83 (s, 3H) ppm. ¹³C NMR (101 MHz, CDCl₃): δ 166.5, 163.6 (d, *J* = 228.4 Hz), 163.4 (d, *J* = 225.1 Hz), 160.3 (d, *J* = 238.8 Hz), 150.4 (d, *J* = 2.8 Hz), 150.4, 146.2, 141.7, 133.3, 133.1 (d, *J* = 8.4 Hz, 2C), 130.4 (2C), 129.9, 125.8 (2C), 125.2 (d, *J* = 3.6 Hz), 123.7 (d, *J* = 8.5 Hz, 2C), 119.6 (d, *J* = 11.1 Hz), 115.8 (d, *J* = 22.7 Hz, 2C), 115.6 (d, *J* = 21.8 Hz, 2C), 112.7 (d, *J* = 26.3 Hz), 111.2 (d, *J* = 9.5 Hz), 108.9 (d, *J* = 25.6 Hz), 52.2, 48.1 ppm. LRMS (ESI+) *m/z* calcd for [C₂₉H₂₁F₃N₃O₂]⁺: 500.15, found: 500.20 [M+H]⁺.

Methyl (E)-4-((5-fluoro-3-((4-fluorophenyl)diazanyl)-1H-indol-1-yl)methyl)benzoate (8b)

Intermediate **8b** was prepared from **7b** and methyl 4-(bromomethyl)benzoate in a similar manner as described for intermediate **5a**. Yellow solid, yield 87%. ¹H NMR (400 MHz, CDCl₃): δ 8.19 – 8.13 (m, 1H), 7.96 – 7.92 (m, 2H), 7.88 (s, 1H), 7.81 – 7.75 (m, 2H), 7.16 (d, *J* = 8.5 Hz, 2H), 7.12 – 7.04 (m,

3H), 6.94 (td, $J = 8.9, 2.6$ Hz, 1H), 5.35 (s, 2H), 3.83 (s, 3H) ppm. ^{13}C NMR (101 MHz, CDCl_3): δ 166.5, 163.4 (d, $J = 249.4$ Hz), 160.0 (d, $J = 238.3$ Hz), 150.11 (d, $J = 3.1$ Hz), 140.7, 135.5 (d, $J = 4.5$ Hz), 134.9, 133.3, 130.4 (2C), 130.3, 126.8 (2C), 123.6 (d, $J = 8.6$ Hz, 2C), 120.2 (d, $J = 11.2$ Hz), 115.9 (d, $J = 22.8$ Hz, 2C), 112.6 (d, $J = 26.4$ Hz), 110.8 (d, $J = 9.7$ Hz), 108.8 (d, $J = 25.2$ Hz), 52.3, 50.8 ppm. LRMS (ESI+) m/z calcd for $[\text{C}_{23}\text{H}_{18}\text{F}_2\text{N}_3\text{O}_2]^+$: 406.13, found: 406.15 $[\text{M}+\text{H}]^+$.

(E)-4-((3-((4',6-Difluoro-[1,1'-biphenyl]-3-yl)diazenyl)-5-fluoro-1H-indol-1-yl)methyl)-N-hydroxybenzamide (9a)

Compound **9a** was prepared from **8a** in a similar manner as described for compound **6a**. Brown solid, yield 26%. ^1H NMR (400 MHz, $\text{DMSO}-d_6$): δ 11.15 (s, 1H), 9.01 (s, 1H), 8.25 (dd, $J = 9.7, 1.9$ Hz, 1H), 7.79 – 7.69 (m, 4H), 7.66 (d, $J = 7.8$ Hz, 2H), 7.57 (d, $J = 5.0$ Hz, 1H), 7.47 – 7.29 (m, 4H), 7.25 – 7.16 (m, 1H), 7.08 (d, $J = 7.7$ Hz, 2H), 5.62 (s, 2H) ppm. ^{13}C NMR (101 MHz, $\text{DMSO}-d_6$): δ 164.3, 163.3 (d, $J = 247.9$ Hz), 162.9 (d, $J = 246.8$ Hz), 162.3 (d, $J = 233.2$ Hz), 150.5 (d, $J = 2.5$ Hz), 147.3, 140.4, 133.9 (d, $J = 8.5$ Hz, 2C), 133.5, 132.52, 132.49, 127.8 (2C), 126.5 (2C), 125.6 (d, $J = 2.9$ Hz), 124.0 (d, $J = 8.7$ Hz, 2C), 119.0 (d, $J = 11.0$ Hz), 116.5 (d, $J = 22.8$ Hz, 2C), 116.1 (d, $J = 21.9$ Hz, 2C), 113.4 (d, $J = 9.7$ Hz), 112.9 (d, $J = 26.0$ Hz), 108.1 (d, $J = 25.4$ Hz), 47.7 ppm. LRMS (ESI+) m/z calcd for $[\text{C}_{28}\text{H}_{20}\text{F}_3\text{N}_4\text{O}_2]^+$: 501.15, found: 501.25 $[\text{M}+\text{H}]^+$. HPLC (method A): $t_R = 14.0$ min, purity 97.1 %. mp = 133–135 °C.

(E)-4-((5-Fluoro-3-((4-fluorophenyl)diazenyl)-1H-indol-1-yl)methyl)-N-hydroxybenzamide (9b)

Compound **9b** was prepared from **8b** in a similar manner as described for compound **6a**. Brown solid, 81 mg, yield 37%. ESI-MS m/z : 407.15 $[\text{M}+\text{H}]^+$. ^1H NMR (400 MHz, $\text{DMSO}-d_6$): δ 11.18 (s, 1H), 9.03 (s, 1H), 8.69 (s, 1H), 8.12 (dd, $J = 9.6, 2.6$ Hz, 1H), 7.95 – 7.86 (m, 2H), 7.73 (d, $J = 8.3$ Hz, 2H), 7.61 (dd, $J = 9.0, 4.4$ Hz, 1H), 7.47 – 7.30 (m, 4H), 7.17 (td, $J = 9.1, 2.6$ Hz, 1H), 5.64 (s, 2H) ppm. ^{13}C NMR (101 MHz, $\text{DMSO}-d_6$): δ 164.3, 163.0 (d, $J = 247.0$ Hz), 159.7 (d, $J = 236.3$ Hz), 150.2 (d, $J = 2.9$ Hz), 140.4, 138.1, 134.8 (d, $J = 4.2$ Hz), 133.5, 132.8, 127.8 (2C), 127.7 (2C), 123.9 (d, $J = 8.9$ Hz, 2C), 119.5 (d, $J = 10.8$ Hz), 116.5 (d, $J = 22.7$ Hz, 2C), 113.0 (d, $J = 10.3$ Hz), 112.5 (d, $J = 25.5$ Hz), 107.9 (d, $J = 24.6$ Hz), 50.1 ppm. LRMS (ESI+) m/z calcd for $[\text{C}_{22}\text{H}_{17}\text{F}_2\text{N}_4\text{O}_2]^+$: 407.12, found: 407.15 $[\text{M}+\text{H}]^+$. HPLC (method A): $t_R = 13.2$ min, purity 96.6 %. mp = 121–123 °C.

Methyl (E)-4-((1H-indol-3-yl)diazenyl)benzoate (10a)

Intermediate **10a** was prepared from 1H-indole (**3b**) and methyl 4-aminobenzoate in a similar manner as described for intermediate **4a**. Red solid, yield 63%. ESI-MS m/z : 280.10 $[\text{M}+\text{H}]^+$. ^1H NMR (400 MHz, $\text{DMSO}-d_6$): δ 12.29 (s, 1H), 8.48 (s, 1H), 8.45 – 8.37 (m, 1H), 8.11 (d, $J = 8.4$ Hz, 2H), 7.90 (d, $J = 8.4$ Hz, 2H), 7.52 (d, $J = 7.7$ Hz, 1H), 7.35 – 7.24 (m, 2H), 3.89 (s, 3H) ppm. ^{13}C NMR (101 MHz, $\text{DMSO}-d_6$): δ 166.4, 156.7, 137.3, 136.6, 136.1, 130.9 (2C), 129.5, 124.7, 123.5, 122.8, 121.8 (2C), 118.4, 112.9, 52.7 ppm. LRMS (ESI+) m/z calcd for $[\text{C}_{16}\text{H}_{14}\text{N}_3\text{O}_2]^+$: 280.10, found: 280.10 $[\text{M}+\text{H}]^+$.

Methyl (E)-4-((5-fluoro-1H-indol-3-yl)diazenyl)benzoate (10b)

Intermediate **10b** was prepared from 5-fluoro-1H-indole (**3c**) and methyl 4-aminobenzoate in a similar manner as described for intermediate **4a**. Red solid, yield 85%. ^1H NMR (400 MHz, CDCl_3): δ 8.66 (s,

1H), 8.16 (dd, $J = 9.5, 2.5$ Hz, 1H), 8.10 (d, $J = 8.5$ Hz, 2H), 8.04 (d, $J = 3.1$ Hz, 1H), 7.84 (d, $J = 8.5$ Hz, 2H), 7.27 (dd, $J = 8.8, 4.3$ Hz, 1H), 7.01 (td, $J = 8.9, 2.6$ Hz, 1H), 3.88 (s, 3H) ppm. ^{13}C NMR (101 MHz, CDCl_3): δ 166.9, 160.1 (d, $J = 238.5$ Hz), 133.20, 133.15, 132.7, 130.6 (2C), 130.2, 121.7 (2C), 113.1, 112.8, 112.3, 112.2, 108.64 (d, $J = 25.4$ Hz), 52.2 ppm. LRMS (ESI+) m/z calcd for $[\text{C}_{16}\text{H}_{13}\text{FN}_3\text{O}_2]^+$: 298.09, found: 298.15 $[\text{M}+\text{H}]^+$.

Methyl (E)-4-((5-bromo-1H-indol-3-yl)diazenyl)benzoate (10c)

Intermediate **10c** was prepared from 5-bromo-1H-indole (**3d**) and methyl 4-aminobenzoate in a similar manner as described for intermediate **4a**. Red solid, yield 68%. ^1H NMR (400 MHz, $\text{DMSO}-d_6$): δ 12.47 (s, 1H), 8.55 (s, 1H), 8.54 (d, $J = 1.9$ Hz, 1H), 8.11 (d, $J = 8.5$ Hz, 2H), 7.92 (d, $J = 8.5$ Hz, 2H), 7.53 – 7.49 (m, 1H), 7.47 – 7.43 (m, 1H), 3.90 (s, 3H) ppm. ^{13}C NMR (101 MHz, $\text{DMSO}-d_6$): δ 166.3, 156.4, 136.9, 136.0, 135.6, 130.9 (2C), 129.8, 127.2, 124.8, 122.0 (2C), 119.8, 116.0, 115.1, 52.7. LRMS (ESI+) m/z calcd for $[\text{C}_{16}\text{H}_{13}\text{BrN}_3\text{O}_2]^+$: 358.01, found: 358.00 $[\text{M}+\text{H}]^+$.

(E)-4-((1H-indol-3-yl)diazenyl)-N-hydroxybenzamide (11a)

Compound **11a** was prepared from **10a** in a similar manner as described for compound **6a**. Brown solid, yield 40%. ^1H NMR (400 MHz, $\text{DMSO}-d_6$): δ 12.23 (brs, 1H), 11.39 (brs, 1H), 8.46 – 8.39 (m, 2H), 8.18 (s, 1H), 7.92 (d, $J = 8.4$ Hz, 2H), 7.85 (d, $J = 8.5$ Hz, 2H), 7.52 (d, $J = 7.7$ Hz, 1H), 7.34 – 7.23 (m, 2H) ppm. ^{13}C NMR (101 MHz, $\text{DMSO}-d_6$): δ 163.8, 155.4, 137.2, 136.4, 135.3, 132.9, 128.5 (2C), 124.5, 123.3, 122.8, 121.6 (2C), 118.4, 112.9. LRMS (ESI+) m/z calcd for $[\text{C}_{15}\text{H}_{13}\text{N}_4\text{O}_2]^+$: 281.10, found: 281.10 $[\text{M}+\text{H}]^+$. HPLC (method A): $t_R = 11.0$ min, purity 96.7%. mp = 151–153 °C.

(E)-4-((5-bromo-1H-indol-3-yl)diazenyl)-N-hydroxybenzamide (11b)

Compound **11b** was prepared from **10c** in a similar manner as described for compound **6a**. Brown solid, yield 28%. ^1H NMR (400 MHz, $\text{DMSO}-d_6$): δ 12.40 (brs, 1H), 11.32 (brs, 1H), 8.58 – 8.47 (m, 2H), 8.18 (s, 1H), 7.93 (d, $J = 8.4$ Hz, 2H), 7.86 (d, $J = 8.4$ Hz, 2H), 7.50 (d, $J = 8.5$ Hz, 1H), 7.44 (d, $J = 7.2$ Hz, 1H) ppm. ^{13}C NMR (101 MHz, $\text{DMSO}-d_6$): δ 155.1, 136.2, 135.9, 135.3, 133.24, 133.21, 128.5 (2C), 127.1, 124.7, 121.7 (2C), 119.8, 115.8, 115.0 ppm. LRMS (ESI+) m/z calcd for $[\text{C}_{15}\text{H}_{12}\text{BrN}_4\text{O}_2]^+$: 359.01, found: 359.05 $[\text{M}+\text{H}]^+$. HPLC (method A): $t_R = 12.2$ min, purity 99.2%. mp = 179–181 °C.

5-Methoxy-1-methyl-1H-indole (12a)

K_2CO_3 (0.94 g, 6.8 mmol) was added to a solution of 5-methoxyindole (0.50 g, 3.4 mmol) in 10 mL of DMF at room temperature. After 10 min, CH_3I (0.95 g, 6.8 mmol) was added dropwise to the solution. Then the solution was stirred at r.t. for 1 h. Excess water was added to the solution, then extracted with EtOAc. The combined organic phase was washed with water and brine, dried over Na_2SO_4 and purified with column chromatography to afford white solid 0.40 g, yield 61%. ^1H NMR (400 MHz, CDCl_3): δ 7.24 (d, $J = 8.8$ Hz, 1H), 7.12 (d, $J = 2.3$ Hz, 1H), 7.05 (d, $J = 3.0$ Hz, 1H), 6.92 (dd, $J = 8.8, 2.3$ Hz, 1H), 6.43 (d, $J = 3.0$ Hz, 1H), 3.88 (s, 3H), 3.79 (s, 3H) ppm. LRMS (ESI+) m/z calcd for $[\text{C}_{10}\text{H}_{12}\text{NO}]^+$: 162.08, found: 162.15 $[\text{M}+\text{H}]^+$.

1-Butyl-5-methoxy-1H-indole (12b)

Intermediate **12b** was prepared from 5-methoxyindole (**3a**) and 1-brombutane in a similar manner as described for intermediate **12a**. Colorless oil, yield 84%. ¹H NMR (400 MHz, CDCl₃): δ 7.26 (d, *J* = 8.9 Hz, 1H), 7.12 (d, *J* = 2.4 Hz, 1H), 7.09 (d, *J* = 3.0 Hz, 1H), 6.90 (dd, *J* = 8.8, 2.3 Hz, 1H), 6.43 (d, *J* = 3.0 Hz, 1H), 4.11 (t, *J* = 7.1 Hz, 1H), 3.88 (s, 3H), 1.90 – 1.78 (m, 1H), 1.43 – 1.31 (m, 2H), 0.96 (t, *J* = 7.4 Hz, 1H) ppm. LRMS (ESI+) *m/z* calcd for [C₁₃H₁₈NO]⁺: 204.13, found: 204.20 [M+H]⁺.

Methyl (E)-4-((5-methoxy-1-methyl-1H-indol-3-yl)diazenyl)benzoate (13a)

Intermediate **13a** was prepared from **12a** and methyl 4-aminobenzoate in a similar manner as described for intermediate **4a**. Red solid, yield 9%. ESI-MS *m/z*: 324.15 [M+H]⁺. ¹H NMR (400 MHz, DMSO-*d*₆): δ 8.41 (s, 1H), 8.10 (d, *J* = 8.6 Hz, 2H), 7.96 (d, *J* = 2.5 Hz, 1H), 7.89 (d, *J* = 8.6 Hz, 2H), 7.52 (d, *J* = 8.9 Hz, 1H), 7.01 (dd, *J* = 8.9, 2.6 Hz, 1H), 3.92 (s, 3H), 3.89 (s, 3H), 3.84 (s, 3H) ppm. ¹³C NMR (101 MHz, DMSO-*d*₆): δ 166.4, 157.3, 156.7, 139.1, 135.3, 132.9, 130.9 (2C), 129.2, 121.8 (2C), 119.4, 113.7, 112.2, 105.2, 55.9, 52.6, 34.0 ppm. LRMS (ESI+) *m/z* calcd for [C₁₈H₁₈N₃O₃]⁺: 324.13, found: 324.20 [M+H]⁺.

Methyl (E)-4-((1-butyl-5-methoxy-1H-indol-3-yl)diazenyl)benzoate (13b)

Intermediate **13b** was prepared from **12b** and methyl 4-aminobenzoate in a similar manner as described for intermediate **4a**. Orange solid, yield 28%. ¹H NMR (400 MHz, CDCl₃): δ 8.18 (d, *J* = 8.4 Hz, 2H), 8.11 (d, *J* = 2.6 Hz, 1H), 7.94 (s, 1H), 7.90 (d, *J* = 8.4 Hz, 2H), 7.29 (d, *J* = 2.0 Hz, 1H), 7.01 (dd, *J* = 8.9, 2.5 Hz, 1H), 4.21 (t, *J* = 7.1 Hz, 2H), 3.97 (s, 3H), 3.95 (s, 3H), 2.00 – 1.87 (m, 2H), 1.51 – 1.36 (m, 2H), 1.00 (t, *J* = 7.4 Hz, 3H) ppm. ¹³C NMR (101 MHz, CDCl₃): δ 167.0, 157.11, 157.10, 140.0, 135.4, 131.7, 130.6 (2C), 129.5, 121.4 (2C), 113.9, 110.70, 110.68, 105.2, 55.9, 52.1, 47.1, 31.9, 20.1, 13.6 ppm. LRMS (ESI+) *m/z* calcd for [C₂₁H₂₄N₃O₃]⁺: 366.17, found: 366.20 [M+H]⁺.

Methyl (E)-4-((1-methyl-1H-indol-3-yl)diazenyl)benzoate (13c)

Intermediate **13c** was prepared from **10a** and iodomethane in a similar manner as described for intermediate **12a**. Orange solid, yield 85%. ESI-MS *m/z*: 294.15 [M+H]⁺. ¹H NMR (400 MHz, CDCl₃): δ 8.51 – 8.45 (m, 1H), 8.08 (d, *J* = 8.4 Hz, 2H), 7.85 (s, 1H), 7.82 (d, *J* = 8.4 Hz, 2H), 7.31 – 7.28 (m, 3H), 3.87 (s, 3H), 3.84 (s, 3H) ppm. ¹³C NMR (101 MHz, CDCl₃): δ 166.9, 156.7, 137.5, 136.2 (2C), 130.6 (2C), 129.7, 124.4, 123.5, 123.3, 121.5 (2C), 118.4, 109.6, 52.1, 33.6 ppm. LRMS (ESI+) *m/z* calcd for [C₁₇H₁₆N₃O₂]⁺: 294.12, found: 294.15 [M+H]⁺.

Methyl (E)-4-((1-benzyl-1H-indol-3-yl)diazenyl)benzoate (13d)

Intermediate **13d** was prepared from **10a** and benzyl bromide in a similar manner as described for intermediate **12a**. Yellow solid, yield 54%. ¹H NMR (400 MHz, CDCl₃): δ 8.65 – 8.56 (m, 1H), 8.18 (d, *J* = 8.5 Hz, 2H), 8.01 (s, 1H), 7.92 (d, *J* = 8.5 Hz, 2H), 7.41 – 7.34 (m, 6H), 7.27 (dd, *J* = 6.1, 4.3 Hz, 2H), 5.42 (s, 2H), 3.97 (s, 3H). ¹³C NMR (101 MHz, CDCl₃): δ 166.9, 156.8, 137.1, 136.3, 135.6, 135.5, 130.6 (2C), 129.8, 129.1 (2C), 128.3, 127.3 (2C), 124.5, 123.6, 123.4, 121.6 (2C), 119.6, 110.1, 52.2, 50.9. LRMS (ESI+) *m/z* calcd for [C₂₃H₂₀N₃O₂]⁺: 370.15, found: 370.20 [M+H]⁺.

Methyl (E)-4-((1-benzyl-5-bromo-1H-indol-3-yl)diazenyl)benzoate (13e)

Intermediate **13e** was prepared from **10c** and benzyl bromide in a similar manner as described for intermediate **12a**. Yellow solid, yield 59%. ¹H NMR (400 MHz, CDCl₃): δ 8.62 (d, *J* = 1.8 Hz, 1H), 8.11 (d, *J* = 8.4 Hz, 2H), 7.92 (s, 1H), 7.82 (d, *J* = 8.4 Hz, 2H), 7.40 (d, *J* = 7.1 Hz, 2H), 7.37 – 7.21 (m, 5H), 5.32 (s, 2H), 3.86 (s, 3H) ppm. ¹³C NMR (101 MHz, CDCl₃): δ 166.2, 156.5, 136.1, 135.9, 135.7, 135.2, 130.7 (2C), 130.1, 129.2 (2C), 128.5, 128.3, 127.4, 127.2 (2C), 125.9, 121.7 (2C), 117.0, 111.7, 51.1, 50.3 ppm. LRMS (ESI+) *m/z* calcd for [C₂₃H₁₉BrN₃O₂]⁺: 370.15, found: 370.20 [M+H]⁺.

Methyl (E)-4-((1-benzyl-5-fluoro-1H-indol-3-yl)diazenyl)benzoate (13f)

Intermediate **13f** was prepared from **10b** and benzyl bromide in a similar manner as described for intermediate **12a**. Yellow solid, yield 85%. ESI-MS *m/z*: 388.20 [M+H]⁺. ¹H NMR (400 MHz, CDCl₃) δ 8.18 (dd, *J* = 9.5, 2.6 Hz, 1H), 8.08 (d, *J* = 8.3 Hz, 2H), 7.93 (s, 1H), 7.81 (d, *J* = 8.3 Hz, 2H), 7.33 – 7.21 (m, 3H), 7.20 – 7.12 (m, 3H), 6.97 (td, *J* = 8.9, 2.5 Hz, 1H), 5.31 (s, 2H), 3.87 (s, 3H). ¹³C NMR (101 MHz, CDCl₃): δ 166.9, 160.2 (d, *J* = 238.8 Hz), 156.5, 136.5, 135.3, 133.5, 131.8, 130.6 (2C), 130.0, 129.2 (2C), 128.5, 127.2 (2C), 125.8, 121.6 (2C), 112.7 (d, *J* = 26.4 Hz), 111.1 (d, *J* = 9.6 Hz), 108.8 (d, *J* = 25.2 Hz), 52.2, 51.2 ppm. LRMS (ESI+) *m/z* calcd for [C₂₃H₁₉FN₃O₂]⁺: 388.14, found: 388.20 [M+H]⁺.

(E)-N-Hydroxy-4-((5-methoxy-1-methyl-1H-indol-3-yl)diazenyl)benzamide (14a)

Compound **14a** was prepared from **13a** in a similar manner as described for compound **6a**. Brown solid, yield 20%. ¹H NMR (400 MHz, DMSO-*d*₆): δ 11.29 (brs, 1H), 9.12 (brs, 1H), 8.37 (s, 1H), 7.96 (s, 1H), 7.91 (d, *J* = 8.0 Hz, 2H), 7.83 (d, *J* = 8.1 Hz, 2H), 7.51 (d, *J* = 7.6 Hz, 1H), 7.00 (d, *J* = 6.5 Hz, 1H), 3.92 (s, 3H), 3.84 (s, 3H) ppm. ¹³C NMR (101 MHz, DMSO-*d*₆): δ 164.2, 157.1, 155.3, 138.4, 135.0, 132.8, 132.7, 128.4 (2C), 121.5 (2C), 119.5, 113.6, 112.1, 105.1, 55.9, 33.9 ppm. LRMS (ESI+) *m/z* calcd for [C₁₇H₁₇N₄O₃]⁺: 325.12, found: 325.15 [M+H]⁺. HPLC (method A): *t*_R = 11.6 min, purity 98.9%. mp = 151–153 °C.

(E)-4-((1-Butyl-5-methoxy-1H-indol-3-yl)diazenyl)-N-hydroxybenzamide (14b)

Compound **14b** was prepared from **13b** in a similar manner as described for compound **6a**. Brown solid, yield 56%. ¹H NMR (400 MHz, DMSO-*d*₆): δ 11.19 (brs, 1H), 9.11 (brs, 1H), 8.42 (s, 1H), 7.96 (s, 1H), 7.91 (d, *J* = 8.1 Hz, 2H), 7.84 (d, *J* = 8.1 Hz, 2H), 7.56 (d, *J* = 7.9 Hz, 1H), 6.98 (d, *J* = 7.1 Hz, 1H), 4.37 – 4.17 (m, 2H), 3.84 (s, 3H), 1.91 – 1.76 (m, 2H), 1.42 – 1.25 (m, 2H), 0.92 (t, *J* = 6.9 Hz, 3H) ppm. ¹³C NMR (101 MHz, DMSO-*d*₆): δ 157.0, 155.4, 137.6, 135.1, 132.0, 129.5, 128.4 (2C), 121.5 (2C), 119.6, 113.6, 112.2, 105.2, 100.0, 55.9, 46.6, 32.0, 19.9, 14.0 ppm. LRMS (ESI+) *m/z* calcd for [C₂₀H₂₃N₄O₃]⁺: 367.17, found: 367.20 [M+H]⁺. HPLC (method A): *t*_R = 12.8 min, purity 95.4%. mp = 127–129 °C.

(E)-N-Hydroxy-4-((1-methyl-1H-indol-3-yl)diazenyl)benzamide (14c)

Compound **14c** was prepared from **13c** in a similar manner as described for compound **6a**. Brown solid, yield 40%. ¹H NMR (400 MHz, DMSO-*d*₆): δ 11.30 (s, 1H), 9.09 (s, 1H), 8.49 – 8.40 (m, 2H), 7.92 (d, *J* = 8.4 Hz, 2H), 7.84 (d, *J* = 8.4 Hz, 2H), 7.60 (d, *J* = 7.9 Hz, 1H), 7.38 (t, *J* = 7.3 Hz, 1H), 7.32

(t, $J = 7.4$ Hz, 1H), 3.95 (s, 3H) ppm. ^{13}C NMR (101 MHz, DMSO- d_6): δ 155.3, 138.5, 137.8, 135.2, 132.9, 128.5 (2C), 124.6, 123.7, 122.9, 121.5 (2C), 118.9, 111.2, 33.8 ppm. LRMS (ESI+) m/z calcd for $[\text{C}_{16}\text{H}_{15}\text{N}_4\text{O}_2]^+$: 295.11, found: 295.10 $[\text{M}+\text{H}]^+$. HPLC (method A): $t_{\text{R}} = 11.6$ min, purity 95.1%. mp = 162–164 °C.

(E)-4-((1-Benzyl-1H-indol-3-yl)diazenyl)-N-hydroxybenzamide (14d)

Compound **14d** was prepared from **13d** in a similar manner as described for compound **6a**. Brown solid, yield 68%, purity 96.2%. ^1H NMR (400 MHz, DMSO- d_6): δ 11.31 (s, 1H), 9.09 (s, 1H), 8.66 (s, 1H), 8.51 – 8.38 (m, 1H), 7.93 (d, $J = 8.4$ Hz, 2H), 7.86 (d, $J = 8.4$ Hz, 2H), 7.64 – 7.58 (m, 1H), 7.41 – 7.34 (m, 4H), 7.33 – 7.26 (m, 3H), 5.59 (s, 2H) ppm. ^{13}C NMR (101 MHz, DMSO- d_6): δ 155.3, 137.8, 137.4, 137.0, 135.5, 133.1, 132.0, 129.2 (2C), 128.5 (2C), 128.3, 127.8 (2C), 124.7, 123.7, 123.0, 121.6 (2C), 119.3, 111.7, 50.2 ppm. LRMS (ESI+) m/z calcd for $[\text{C}_{22}\text{H}_{19}\text{N}_4\text{O}_2]^+$: 371.14, found: 371.15 $[\text{M}+\text{H}]^+$. HPLC (method A): $t_{\text{R}} = 12.7$ min, purity 97.3%. mp = 169–170 °C.

(E)-4-((1-Benzyl-5-bromo-1H-indol-3-yl)diazenyl)-N-hydroxybenzamide (14e)

Compound **14e** was prepared from **13e** in a similar manner as described for compound **6a**. Brown solid, yield 55%. ^1H NMR (400 MHz, DMSO- d_6): δ 11.29 (brs, 1H), 9.11 (brs, 1H), 8.73 (s, 1H), 8.55 (s, 1H), 7.93 (d, $J = 8.1$ Hz, 2H), 7.88 (d, $J = 8.1$ Hz, 2H), 7.61 (d, $J = 6.7$ Hz, 1H), 7.46 (d, $J = 7.1$ Hz, 1H), 7.42 – 7.33 (m, 5H), 5.60 (s, 2H) ppm. ^{13}C NMR (101 MHz, DMSO- d_6): δ 155.1, 138.6, 137.1, 135.8, 134.4, 133.4, 129.3 (2C), 128.5 (2C), 128.4, 127.9, 127.8 (2C), 127.2, 124.9, 121.8 (2C), 120.6, 116.4, 113.9, 50.4 ppm. LRMS (ESI+) m/z calcd for $[\text{C}_{22}\text{H}_{18}\text{BrN}_4\text{O}_2]^+$: 449.05, found: 449.10 $[\text{M}+\text{H}]^+$. HPLC (method A): $t_{\text{R}} = 13.5$ min, purity 97.9%. mp = 167–168 °C.

(E)-4-((1-Benzyl-5-fluoro-1H-indol-3-yl)diazenyl)-N-hydroxybenzamide (14f)

Compound **14f** was prepared from **13f** in a similar manner as described for compound **6a**. Brown solid, yield 26%. ESI-MS m/z : 389.20 $[\text{M}+\text{H}]^+$. ^1H NMR (400 MHz, DMSO- d_6): δ 11.34 (s, 1H), 9.14 (s, 1H), 8.71 (s, 1H), 8.12 (dd, $J = 9.6, 2.6$ Hz, 1H), 7.92 (d, $J = 8.6$ Hz, 2H), 7.88 (d, $J = 8.6$ Hz, 2H), 7.62 (dd, $J = 8.9, 4.3$ Hz, 1H), 7.38 – 7.34 (m, 4H), 7.32 – 7.27 (m, 1H), 7.17 (td, $J = 9.1, 2.6$ Hz, 1H), 5.58 (s, 2H) ppm. ^{13}C NMR (101 MHz, DMSO- d_6): δ 164.3, 159.9 (d, $J = 236.4$ Hz), 155.1, 138.9, 137.1, 135.2, 133.6, 133.2, 129.3 (2C), 128.5 (2C), 128.4, 127.8 (2C), 121.7 (2C), 119.4 (d, $J = 10.9$ Hz), 113.2 (d, $J = 9.4$ Hz), 112.7 (d, $J = 26.0$ Hz), 108.1 (d, $J = 25.2$ Hz), 50.5 ppm. LRMS (ESI+) m/z calcd for $[\text{C}_{22}\text{H}_{18}\text{FN}_4\text{O}_2]^+$: 389.13, found: 389.20 $[\text{M}+\text{H}]^+$. HPLC (method A): $t_{\text{R}} = 12.9$ min, purity 99.8%. mp = 171–173 °C.

Methyl (E)-4-(quinolin-8-yl)diazenylbenzoate (16)

Oxone (8.14 g, 13.24 mmol) in 30 mL water was added to methyl 4-aminobenzoate (1.00 g, 6.62 mmol) in 30 mL dichloromethane at r.t. for 4 h. The organic phase was washed with water and brine, dried over Na_2SO_4 , and concentrated to afford light green solid methyl 4-nitrosobenzoate. 8-Aminoquinoline (0.50 g, 3.47 mmol) was added to the light green solid, subsequently, a mixture of 20 mL AcOH and 10 mL TFA was added and stirred at r.t. over night. Solvents were removed afterwards, the residue was extracted with ethyl acetate and washed with water and brine. The organic phase was dried over Na_2SO_4

and purified with column chromatography to afford red solid 30 mg, yield 3%. ¹H NMR (400 MHz, CDCl₃): δ 9.09 (dd, *J* = 4.1, 1.6 Hz, 1H), 8.20 (dd, *J* = 8.3, 1.5 Hz, 1H), 8.15 (d, *J* = 8.5 Hz, 2H), 8.02 (d, *J* = 8.5 Hz, 2H), 7.94 (d, *J* = 8.0 Hz, 1H), 7.80 (d, *J* = 7.5 Hz, 1H), 7.59 (t, *J* = 7.8 Hz, 1H), 7.48 (dd, *J* = 8.3, 4.2 Hz, 1H), 3.90 (s, 3H) ppm. ¹³C NMR (101 MHz, CDCl₃): δ 166.6, 155.6, 151.6, 149.2, 144.5, 136.4, 132.1, 131.5, 130.6 (2C), 129.2, 126.5, 123.2 (2C), 121.9, 116.2, 52.4 ppm. LRMS (ESI+) *m/z* calcd for [C₁₇H₁₄N₃O₂]⁺: 292.10, found: 292.15 [M+H]⁺.

(E)-N-Hydroxy-4-(quinolin-8-yl diazenyl)benzamide (17)

Compound **17** was prepared from intermediate **16** in a similar manner as described for compound **6a**. Red solid, yield 42%. ¹H NMR (400 MHz, DMSO-*d*₆): δ 9.10 (d, *J* = 2.8 Hz, 1H), 8.54 (d, *J* = 8.1 Hz, 1H), 8.24 – 8.20 (m, 1H), 8.18 (s, 3H), 8.06 – 8.00 (m, 3H), 7.78 (t, *J* = 7.9 Hz, 2H), 7.71 (dd, *J* = 8.2, 4.1 Hz, 1H) ppm. ¹³C NMR (101 MHz, DMSO-*d*₆): δ 164.0, 157.6, 154.3, 151.9, 149.3, 143.9, 136.9, 132.2, 129.3, 128.7 (2C), 127.0, 123.3 (2C), 122.8, 116.3 ppm. LRMS (ESI+) *m/z* calcd for [C₁₆H₁₃N₄O₂]⁺: 293.10, found: 293.15 [M+H]⁺. HPLC (method A): *t*_R = 7.3 min, purity 95.9%. mp = 88–90 °C.

Methyl (E)-4-((8-aminoquinolin-5-yl) diazenyl)benzoate (18a)

Intermediate **18a** was prepared from 8-aminoquinoline (**15**) and methyl 4-aminobenzoate in a similar manner as described for intermediate **4a**. Red solid, yield 68%. ¹H NMR (400 MHz, DMSO-*d*₆): δ 9.26 (dd, *J* = 8.6, 1.7 Hz, 1H), 8.86 (dd, *J* = 4.1, 1.7 Hz, 1H), 8.14 – 8.10 (m, 2H), 8.06 (d, *J* = 8.7 Hz, 1H), 8.03 – 7.97 (m, 2H), 7.72 (dd, *J* = 8.6, 4.1 Hz, 1H), 7.35 (s, 2H), 7.00 (d, *J* = 8.7 Hz, 1H), 3.90 (s, 3H) ppm. ¹³C NMR (101 MHz, DMSO-*d*₆): δ 166.4, 156.3, 151.9, 148.3, 136.3, 136.1, 131.9, 130.9 (2C), 129.8, 128.8, 124.1, 122.5 (2C), 117.7, 108.9, 52.7 ppm. LRMS (ESI+) *m/z* calcd for [C₁₇H₁₅N₄O₂]⁺: 307.11, found: 307.15 [M+H]⁺.

Methyl (E)-4-((8-aminoquinolin-5-yl) diazenyl)-3-fluorobenzoate (18b)

Intermediate **18b** was prepared from 8-aminoquinoline (**15**) and methyl 4-amino-3-fluorobenzoate in the similar procedure as described for intermediate **4a**. Red solid, yield 62%. ¹H NMR (400 MHz, DMSO-*d*₆): δ 9.26 (dd, *J* = 8.6, 1.6 Hz, 1H), 8.87 (dd, *J* = 4.1, 1.6 Hz, 1H), 8.07 (d, *J* = 8.8 Hz, 1H), 7.99 (t, *J* = 8.2 Hz, 1H), 7.88 – 7.86 (m, 1H), 7.84 (s, 1H), 7.73 (dd, *J* = 8.6, 4.1 Hz, 1H), 7.54 (s, 2H), 7.01 (d, *J* = 8.8 Hz, 1H), 3.90 (s, 3H). ¹³C NMR (101 MHz, DMSO-*d*₆): δ 165.4 (d, *J* = 2.6 Hz), 158.2 (d, *J* = 253.9 Hz), 152.7, 148.3, 144.5 (d, *J* = 6.9 Hz), 136.6, 136.2, 131.9, 130.9 (d, *J* = 7.3 Hz), 128.9, 126.2 (d, *J* = 3.3 Hz), 124.3, 119.0, 118.4, 118.0 (d, *J* = 21.7 Hz), 109.1, 53.0 ppm. LRMS (ESI+) *m/z* calcd for [C₁₇H₁₄FN₄O₂]⁺: 325.10, found: 325.10 [M+H]⁺.

(E)-4-((8-Aminoquinolin-5-yl) diazenyl)-N-hydroxybenzamide (19a)

Compound **19a** was prepared from **18a** in a similar manner as described for compound **6a**. Red solid, yield 24%. ¹H NMR (400 MHz, DMSO-*d*₆): δ 11.34 (s, 1H), 9.35 – 9.20 (m, 1H), 9.10 (s, 1H), 8.86 (d, *J* = 2.6 Hz, 1H), 8.03 (d, *J* = 8.7 Hz, 1H), 7.94 (s, 4H), 7.70 (dd, *J* = 8.5, 4.1 Hz, 1H), 7.24 (s, 2H), 6.99 (d, *J* = 8.7 Hz, 1H) ppm. ¹³C NMR (101 MHz, DMSO-*d*₆): δ 164.2, 160.1, 155.0, 151.5, 148.2, 136.3, 136.0, 133.3, 132.0, 128.5 (2C), 123.9, 122.2 (2C), 117.2, 108.8 ppm. LRMS (ESI+) *m/z* calcd for

$[C_{16}H_{14}N_5O_2]^+$: 308.11, found: 308.05 $[M+H]^+$. HPLC (method A): t_R = 10.8 min, purity 96.5%. mp = 237-239 °C.

(E)-4-((8-Aminoquinolin-5-yl)diazenyl)-3-fluoro-N-hydroxybenzamide (19b)

Compound **19b** was prepared from **18b** in a similar manner as described for compound **6a**. Brown solid, yield 24%. 1H NMR (400 MHz, DMSO- d_6): δ 11.42 (s, 1H), 9.27 (d, J = 8.2 Hz, 1H), 8.86 (d, J = 2.3 Hz, 1H), 8.05 (d, J = 8.7 Hz, 1H), 7.95 (t, J = 8.0 Hz, 1H), 7.82 – 7.65 (m, 3H), 7.42 (s, 2H), 7.01 (d, J = 8.7 Hz, 1H) ppm (one exchangeable proton not observed). ^{13}C NMR (101 MHz, DMSO- d_6): δ 167.50, 158.37 (d, J = 253.8 Hz), 152.17, 148.28, 143.01 (d, J = 6.9 Hz), 136.38 (d, J = 25.7 Hz, 2C), 134.5, 131.98, 128.76, 124.18, 123.93 (d, J = 3.8 Hz), 118.29 (d, J = 11.1 Hz, 2C), 115.84 (d, J = 20.6 Hz), 108.98 ppm. LRMS (ESI+) m/z calcd for $[C_{16}H_{13}FN_5O_2]^+$: 325.10, found: 326.05 $[M+H]^+$. HPLC (method A): t_R = 11.5 min, purity 97.9%. mp = 203-205 °C.

Methyl (E)-4-(quinolin-5-yl diazenyl)benzoate (20a)

18a (0.20 g, 0.65 mmol) was added to 2 mL of 50% HBF₄ aq. at -15 °C, then NaNO₂ (71 mg, 0.98 mmol) in 1 mL water was added dropwise. The mixture was stirred at -15 °C for 30 min, then the precipitate was filtered out and washed with cold Et₂O and the mixture of Et₂O - MeOH (1:1) to afford the dizonium salt. The dizonium salt was then suspended in 2 mL water and added to copper powder (0.42 g, 6.5 mmol), subsequently, NaNO₂ (0.24 g, 3.25 mmol) in 1 mL water was added. The mixture was stirred at r.t. over night. Afterwards, the mixture was extracted with ethyl acetate and purified with column chromatography to afford red solid 12 mg, yield 6%. 1H NMR (400 MHz, CDCl₃): δ 9.30 (d, J = 8.5 Hz, 1H), 9.06 (d, J = 3.6 Hz, 1H), 8.33 (d, J = 7.9 Hz, 1H), 8.27 (d, J = 8.2 Hz, 2H), 8.09 (d, J = 8.3 Hz, 2H), 7.98 (d, J = 7.6 Hz, 1H), 7.85 (t, J = 8.0 Hz, 1H), 7.61 (dd, J = 8.5, 4.1 Hz, 1H), 4.01 (s, 3H) ppm. ^{13}C NMR (101 MHz, CDCl₃): δ 166.4, 155.6, 155.3, 150.7, 147.2, 132.9, 132.8, 132.3, 130.8 (2C), 129.36, 127.0, 123.0 (2C), 122.0, 112.9, 52.4 ppm. LRMS (ESI+) m/z calcd for $[C_{17}H_{14}N_3O_2]^+$: 292.10, found: 292.15 $[M+H]^+$.

Methyl (E)-3-fluoro-4-(quinolin-5-yl diazenyl)benzoate (20b)

Intermediate **20b** was prepared from **18b** in the similar procedure as described for intermediate **20a**. Red solid, yield 7%. 1H NMR (400 MHz, CDCl₃): δ 9.32 (d, J = 8.4 Hz, 1H), 9.07 (d, J = 3.1 Hz, 1H), 8.38 (d, J = 8.3 Hz, 1H), 8.04 (d, J = 7.6 Hz, 1H), 8.03 – 7.97 (m, 2H), 7.95 – 7.90 (m, 1H), 7.87 (t, J = 8.0 Hz, 1H), 7.64 (dd, J = 8.6, 4.2 Hz, 1H), 4.01 (s, 3H) ppm. ^{13}C NMR (101 MHz, CDCl₃): δ 165.4, 159.5 (d, J = 259.5 Hz), 153.2, 151.2, 148.7, 147.5, 143.5 (d, J = 7.2 Hz), 134.0, 132.0, 129.0, 126.9, 125.6 (d, J = 3.8 Hz), 122.3, 118.7 (d, J = 21.9 Hz), 118.2, 113.4, 52.7 ppm. LRMS (ESI+) m/z calcd for $[C_{17}H_{13}FN_3O_2]^+$: 310.09, found: 310.10 $[M+H]^+$.

(E)-N-hydroxy-4-(quinolin-5-yl diazenyl)benzamide (21a)

Compound **21a** was prepared from **20a** in a similar manner as described for compound **6a**. Red solid, 26 mg, yield 20%. 1H NMR (400 MHz, DMSO- d_6): δ 11.43 (s, 1H), 9.30 (d, J = 8.2 Hz, 1H), 9.07 (d, J = 2.7 Hz, 1H), 8.35 – 8.23 (m, 1H), 8.13 (t, J = 8.9 Hz, 2H), 8.03 (d, J = 8.3 Hz, 2H), 7.94 (d, J = 4.0 Hz, 2H), 7.76 (dd, J = 8.4, 4.0 Hz, 1H). ^{13}C NMR (101 MHz, DMSO- d_6): δ 154.1, 152.0, 148.6, 147.1,

135.9, 133.5, 132.1, 129.8, 128.7, 126.5, 123.5 (2C), 123.2, 112.9 ppm. LRMS (ESI+) m/z calcd for $[C_{16}H_{13}N_4O_2]^+$: 293.10, found: 293.15 $[M+H]^+$. HPLC (method A): t_R = 9.6 min, purity 97.4%. mp = 218-220 °C.

(E)-3-fluoro-N-hydroxy-4-(quinolin-5-yl)diazanylbenzamide (21b)

Compound **21b** was prepared from **20b** in a similar manner as described for compound **6a**. Brown solid, 10 mg, yield 33%. 1H NMR (400 MHz, DMSO- d_6): δ 9.26 (s, 1H), 9.06 (s, 1H), 8.29 (s, 1H), 8.03 (s, 1H), 7.97 – 7.60 (m, 6H) ppm (one exchangeable proton not observed). ^{13}C NMR (101 MHz, DMSO- d_6): δ 162.3, 159.5 (d, J = 256.9 Hz), 157.6, 152.0, 148.6, 147.3, 141.9 (d, J = 12.0 Hz), 134.0, 132.1, 129.8, 126.6, 124.0, 123.3, 118.8, 116.2 (d, J = 21.4 Hz), 113.3 ppm. LRMS (ESI+) m/z calcd for $[C_{16}H_{12}FN_4O_2]^+$: 311.09, found: 311.05 $[M+H]^+$. HPLC (method A): t_R = 11.3 min, purity 96.1%. mp = 182-183 °C.

Methyl (E)-4-((8-chloroquinolin-5-yl)diazanyl)benzoate (22)

18a (0.30 g, 0.98 mmol) was added to a solution of sodium nitrite (0.29 g, 3.92 mmol) in 3 mL DMSO, then 0.5 mL of 37% HCl was added dropwise to the mixture and stirred at r.t. over night. Excess water was added, red solid was precipitated and filtered, then purified with column chromatography to afford red solid 38 mg, yield 12%. 1H NMR (400 MHz, $CDCl_3$): δ 9.28 (dd, J = 8.5, 1.5 Hz, 1H), 9.09 (dd, J = 4.1, 1.5 Hz, 1H), 8.17 (d, J = 8.4 Hz, 2H), 7.99 (d, J = 8.4 Hz, 2H), 7.91 – 7.81 (m, 2H), 7.61 (dd, J = 8.5, 4.2 Hz, 1H), 3.91 (s, 3H) ppm. ^{13}C NMR (101 MHz, $CDCl_3$): δ 166.3, 155.5, 155.05, 147.0, 146.1, 137.4, 134.0, 132.9, 131.5, 130.8 (2C), 128.8, 123.2 (2C), 115.8, 114.9, 52.5 ppm. LRMS (ESI+) m/z calcd for $[C_{17}H_{13}ClN_3O_2]^+$: 326.06, found: 326.10 $[M+H]^+$.

(E)-4-((8-chloroquinolin-5-yl)diazanyl)-N-hydroxybenzamide (23)

Compound **23** was prepared from intermediate **22** in a similar manner as described for compound **6a**. Red solid, yield 32%. 1H NMR (400 MHz, DMSO- d_6): δ 11.37 (s, 1H), 9.27 (d, J = 77.1 Hz, 2H), 8.33 – 7.68 (m, 8H) ppm. ^{13}C NMR (101 MHz, DMSO- d_6): δ 154.1, 152.6, 146.0, 144.2, 137.0, 136.0, 132.9, 130.02, 130.00, 128.7 (2C), 127.7, 124.0, 123.6 (2C), 113.0 ppm. LRMS (ESI+) m/z calcd for $[C_{16}H_{12}ClN_4O_2]^+$: 327.06, found: 327.10 $[M+H]^+$. HPLC (method A): t_R = 11.9 min, purity 95.3%. mp = 173-175 °C.

Methyl (E)-4-((5-aminoquinolin-8-yl)diazanyl)benzoate (25)

Intermediate **25** was prepared from 5-aminoquinoline (**24**) and methyl 4-aminobenzoate in a similar manner as described for intermediate **2a**. Brown solid, yield 71%. 1H NMR (400 MHz, DMSO- d_6): δ 9.05 (dd, J = 4.1, 1.4 Hz, 1H), 8.71 (dd, J = 8.5, 1.4 Hz, 1H), 8.13 (d, J = 8.4 Hz, 2H), 8.07 (d, J = 8.7 Hz, 1H), 7.96 (d, J = 8.5 Hz, 2H), 7.57 (dd, J = 8.5, 4.2 Hz, 1H), 7.40 (s, 2H), 6.83 (d, J = 8.8 Hz, 1H), 3.90 (s, 3H) ppm. ^{13}C NMR (101 MHz, DMSO- d_6): δ 166.4, 156.0, 152.6, 151.7, 146.2, 137.5, 132.8, 130.9 (2C), 129.8, 122.5 (2C), 120.4, 120.3, 116.8, 108.2, 52.7 ppm. LRMS (ESI+) m/z calcd for $[C_{17}H_{15}N_4O_2]^+$: 307.11, found: 307.10 $[M+H]^+$.

(E)-4-((5-aminoquinolin-8-yl)diazenyl)-N-hydroxybenzamide (26)

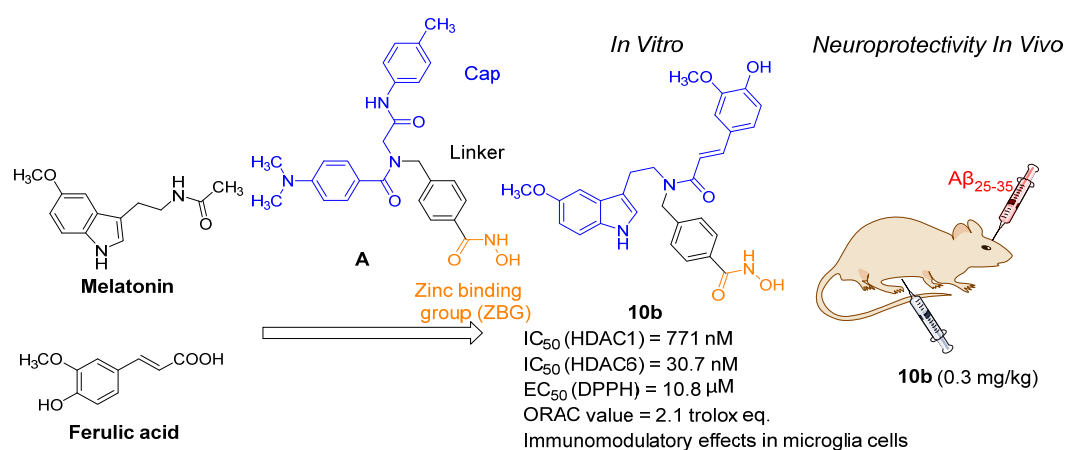
Compound **26** was prepared from intermediate **25** in a similar manner as described for compound **6a**. Black solid, yield 14%. ¹H NMR (400 MHz, DMSO-*d*₆): δ 9.02 (s, 1H), 8.69 (d, *J* = 8.1 Hz, 1H), 8.27 (s, 2H), 8.02 (d, *J* = 8.6 Hz, 1H), 7.94 (d, *J* = 8.4 Hz, 2H), 7.89 (d, *J* = 8.4 Hz, 2H), 7.53 (d, *J* = 4.5 Hz, 1H), 7.24 (s, 1H), 6.82 (d, *J* = 8.6 Hz, 1H) ppm (one exchangeable proton not observed). ¹³C NMR (101 MHz, DMSO-*d*₆): δ 164.7, 155.1, 151.9, 151.7, 146.8, 138.4, 136.1, 131.9, 128.5 (2C), 127.0 122.3 (2C), 120.1, 118.9, 107.7 ppm. LRMS (ESI+) *m/z* calcd for [C₁₆H₁₄N₅O₂]⁺: 308.11, found: 308.10 [M+H]⁺. HPLC (method A): *t*_R = 8.0 min, purity 95.0%. mp = 209-211 °C.

***In Vitro* HDACs Inhibition Fluorescence Assay.** All of the HDAC enzymes were bought from BPS Bioscience. *In vitro* HDAC inhibition assays were conducted as previously described with partial modification.¹³⁰ In brief, 20 μL of recombinant HDAC enzyme solution was mixed with various concentrations of tested compound (20 μL). Only for the measurement of corresponding *cis*-isomers, diluted compounds were treated with irradiation of 365 nm UV light for 2 min before being mixed with the enzymes. The mixture was incubated at 30 °C for 1 h, then 10 μL of fluorogenic substrate (Boc-Lys (acetyl)-AMC) was added. After incubation at 30 °C for 2 h, the catalysis was stopped by addition of 10 μL of developer containing trypsin. Thirty minutes later, fluorescence intensity was measured using a microplate reader at excitation and emission wavelengths of 360 and 460 nm, respectively. All samples were prepared in duplicate and minimum of two independent assays were performed for each compound. The inhibition ratios were calculated from the fluorescence intensity readings of tested wells relative to those of control wells, and the IC₅₀ curves and values were determined by GraphPad Prism 7, using the “log (inhibitor) vs. normalized response - variable slope” function.

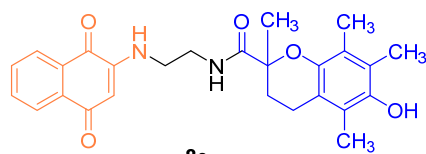
5. Summary

Most antioxidants reported so far only achieved limited success in AD clinical trials. Growing evidences suggest that merely targeting oxidative stress will not be sufficient to fight AD. While multi-target directed ligands could synergistically modulate different steps in the neurodegenerative process, offering a promising potential for treatment of this complex disease. The rationale of oxidative stress based MTDL strategy is that single molecules, endowed with antioxidant properties by incorporating with the pharmacophore of antioxidants, can produce additional neuroprotective effects against AD.

In the first project of this thesis (*cf.* Chapter 3), 15 target compounds have been designed by merging melatonin and ferulic acid into the cap group of a tertiary amide HDAC6 inhibitor. All target compounds were chemically synthesized and biologically evaluated by enzyme-based and cellular HDAC inhibition assays, DPPH and ORAC assays. Compound **10b** was screened as the best hybrid molecule exhibit potent HDAC6 inhibition ($IC_{50} = 30.7$ nM, 25-fold selectivity over HDAC1) and potent antioxidant capacity (DPPH $EC_{50} = 10.8$ μ M, ORAC value = 2.1 trolox eq.). Further immunomodulatory effects were evaluated in murine N9 cells, compound **10b** alleviated LPS-induced microglia inflammation and led to a switch from neurotoxic M1 to the neuroprotective M2 microglial phenotype. Moreover, compound **10b** show pronounced attenuation of spatial working memory and long-term memory damage in an *in vivo* AD mouse model induced by icv $A\beta_{25-35}$ peptide injection at dose of only 0.3 mg/kg, indicating its *in vivo* neuroprotective properties. Compound **10b** can be a potentially effective drug candidate for treatment of AD and its druggability worth to be further studied.



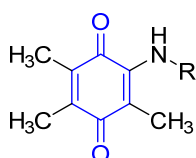
Furthermore, novel neuroprotectants based on molecular hybridization can be an effective approach to uncover the pathogenesis and signaling pathways of aging and neurodegenerative diseases. Based on the potent neuroprotective effects of vitamin K derivatives against oxytosis pathway, we have designed ten novel neuroprotectants by hybridizing with several common antioxidants, including ferulic acid, melatonin, lipoic acid, and trolox. The trolox hybrid compound exhibited the most potent neuroprotective effects in multiple neuroprotection assays. Besides, we identified the synergistic effects between trolox and vitamin K derivative, and our trolox hybrid compound showed comparable neuroprotection with the mixture of trolox and vitamin K derivative.



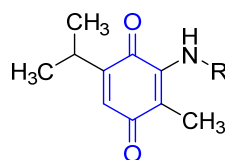
8e

EC₅₀ (DPPH) = 15.4 μM
 ORAC value = 1.6 trolox eq.
 Protect HT22 cells from
 oxytosis and ferroptosis at 0.75
 and 0.15 μM, respectively

Encouraged by the potent antioxidant capacity and neuroprotective effects of vitamin K hybrids, we have studied the structure-activity relationship of quinone derivatives with antioxidant capacity and neuroprotective effects to provide guidance for further design of novel neuroprotectants. We have designed and synthesized 24 quinone derivatives based on five kinds of different quinones including ubiquinone, 2,3,5-trimethyl-1,4-benzoquinone, memoquin, thymoquinone, and anthraquinone. Their antioxidant capacity and neuroprotective effects have been evaluated by ORAC and oxytosis assays, respectively. 2,3,5-Trimethyl-1,4-benzoquinone (**12a-d**) and thymoquinone derivatives (**14a-d**) were identified as potent antioxidants with ORAC values ranging from 0.3 to 4.5, respectively. Moreover, trimethylbenzoquinone and thymoquinone derivatives showed more potent neuroprotection than other quinones in oxytosis assay. Therefore, trimethylbenzoquinone and thymoquinone derivatives can be used as lead compounds for further mechanism study and drug discovery for treatment of neurodegenerative disease. No relationship between their antioxidant capacity and neuroprotective effects in HT22 cells could be observed.

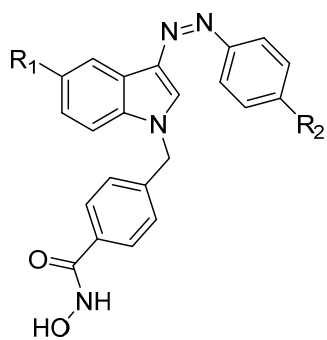


12a-d (Trimethylbenzoquinone derivatives)
 ORAC value = 0.3 - 4.5 trolox eq.
 Protect HT22 cells from oxytosis at 5 μM

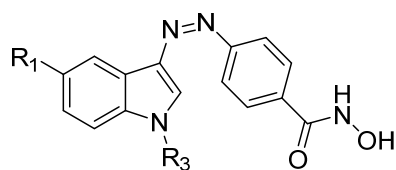


14a-d (Thymoquinone derivatives)
 ORAC value = 0.6 - 3.5 trolox eq.
 Protect HT22 cells from oxytosis at 5 μM

HDAC6 is a new emerging target showing great therapeutic potential to tackle neurodegenerative disorders, however, its mode of action in neurodegenerative progression remains unclear. We herein designed a series of photoswitchable HDAC inhibitors, which could be effective molecular tools due to the high spatial and temporal resolution. In total 23 target compounds were synthesized and photophysicochemically characterized. Azoquinoline-based compounds possess more thermally stable *cis*-isomers in buffer solution, which were further tested in enzyme-based HDAC inhibition assay. However, none of those tested compounds show significant differences in activities between *trans*-isomers and corresponding *cis*-isomers. Although the expected “*cis*-on” effect was not achieved, the substituent effects on 3-arylazoinole and azoquinoline photoswitches have been thoroughly investigated, and the obtained structure-photophysicochemical properties relationship could be a direction for other researchers and in other applications.

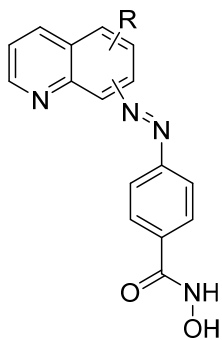


6a-f, 9a-b



11a-b, 14a-f

Cis-isomers are thermally unstable in buffer



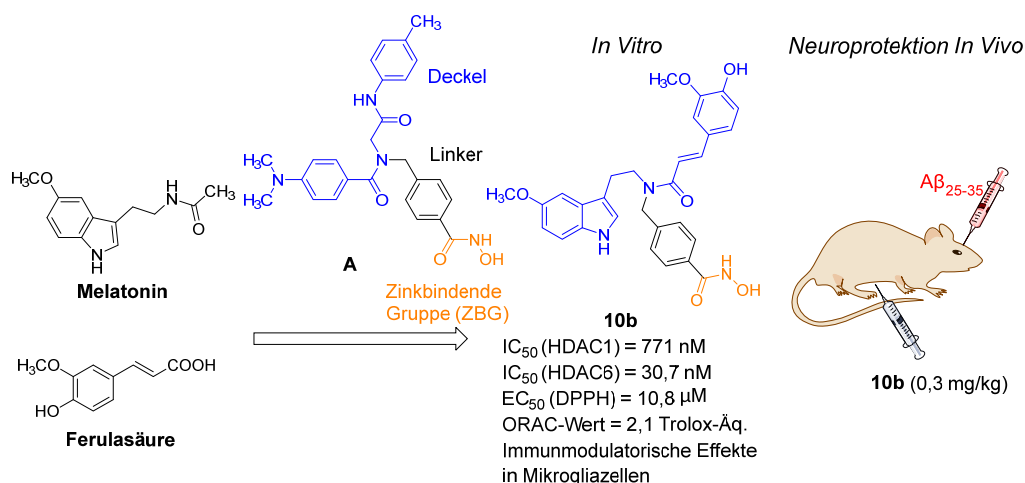
17, 19a-b, 21a-b, 23, 26

Cis-isomers are thermally stable in buffer, but no significant difference in activities between *trans* and *cis*-isomers was observed

6. Zusammenfassung

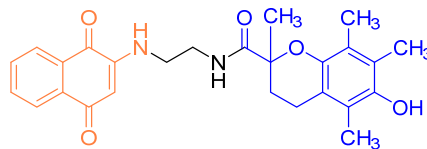
Die meisten bisher berichteten Antioxidantien erzielten in klinischen-Studien zur Alzheimer-Krankheit nur einen begrenzten Erfolg. Es gibt immer mehr Hinweise darauf, dass die bloße Bekämpfung von oxidativem Stress nicht ausreicht, um die Alzheimer-Krankheit zu bekämpfen. Während Multipotente Liganden verschiedene Schritte im neurodegenerativen Prozess synergistisch modulieren könnten und ein vielversprechendes Potenzial für die Behandlung dieser komplexen Krankheit bieten. Das Design für die Verbindungen basiert auf oxidativem Stress und der Multipotente Liganden Strategie ist, einzelnen Molekülen, die durch den Einbau in den Pharmakophor von Antioxidantien mit antioxidativen Eigenschaften ausgestattet sind, zusätzliche neuroprotektive Wirkungen gegen die Alzheimer-Krankheit haben können.

Im ersten Projekt dieser Dissertation (vgl. Kapitel 3) wurden 15 Zielverbindungen entworfen, indem Melatonin und Ferulasäure in die Deckel-Gruppe eines tertiären Amid-HDAC6-Inhibitors fusioniert wurden. Alle Zielverbindungen wurden chemisch synthetisiert und durch enzymbasierte und zelluläre HDAC-Inhibitionsassays, dem DPPH-Assay und dem ORAC-Assay biologisch untersucht. Verbindung **10b** wurde als bestes Hybridmolekül gescreent, das eine potente HDAC6-Hemmung ($IC_{50} = 30,7$ nM, 25-fache Selektivität gegenüber HDAC1) und eine starke antioxidative Kapazität (DPPH $EC_{50} = 10,8$ μ M, ORAC-Wert = 2,1 Trolox-Äq.) aufweist. Weitere immunmodulatorische Effekte wurden in murinen N9-Zellen untersucht. Hierbei linderte Verbindung **10b** die LPS-induzierte Mikroglia-Entzündung und führte zu einem Wechsel vom neurotoxischen M1- zum neuroprotektiven M2-Mikroglia-Phänotyp. Darüber hinaus zeigt Verbindung **10b** eine ausgeprägte Abschwächung des räumlichen Arbeitsgedächtnisses und eine Schädigung des Langzeitgedächtnisses in einem in vivo Alzheimer-Krankheit-Mausmodell, das durch icv $A\beta_{25-35}$ Peptidinjektion in einer Dosis von 0,3 mg/kg induziert wurde, was auf seine in vivo neuroprotektiven Eigenschaften hinweist. Verbindung **10b** kann ein potenzieller Wirkstoffkandidat zur Behandlung der Alzheimer-Krankheit sein, und eignet sich für weiterführende Studien.



Darüber hinaus können neuartige neuroprotektive Substanzen, die auf molekularer Hybridisierung basieren, ein effektiver Ansatz sein, um die Pathogenese und Signalwege des Alterns und

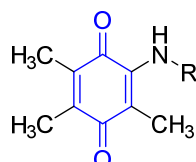
neurodegenerativer Erkrankungen zu behandeln. Basierend auf den starken neuroprotektiven Wirkungen von Vitamin-K-Derivaten gegen den Oxytoseweg, haben wir zehn neue Verbindungen entwickelt, indem wir Vitamin K mit mehreren Antioxidantien, darunter Ferulasäure, Melatonin, Liponsäure und Trolox, hybridisierten. Die Trolox-Hybridverbindung zeigte die stärksten neuroprotektiven Wirkungen in mehreren Neuroprotektionsassays. Außerdem haben wir die synergistischen Effekte zwischen Trolox und dem Vitamin-K-Derivat identifiziert, und unsere Trolox-Hybridverbindung zeigte eine vergleichbare Neuroprotektion mit der Mischung aus Trolox und Vitamin-K-Derivat.



8e

EC₅₀ (DPPH) = 15,4 μM
 ORAC-Wert = 1,6 Trolox-Äq.
 Schützen Sie HT22-Zellen vor
 Oxytose und Ferroptose bei
 0,75 und 0,15 mM, respektive

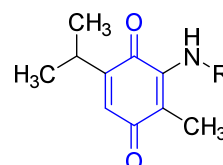
Ermutigt durch die starke antioxidative Kapazität und der neuroprotektiven Wirkung von Vitamin-K-Hybriden, haben wir die Struktur-Aktivitäts-Beziehung von Chinon-Derivaten mit der antioxidativen Kapazität und der neuroprotektiven Wirkungen untersucht, um Leitlinien für das weitere Design neuer neuroprotektive Verbindungen bereitzustellen. Wir haben 24 Chinon-Derivate entwickelt und synthetisiert, die auf fünf verschiedenen Chinonen basieren, darunter Ubichinon, 2,3,5-Trimethyl-1,4-Benzochinon, Memoquin, Thymochinon und Anthrachinon. Deren antioxidative Kapazität und neuroprotektive Wirkung wurden durch ORAC- bzw. Oxytose-Assays bewertet. 2,3,5-Trimethyl-1,4-benzochinon (**12a-d**) und Thymochinon-Derivate (**14a-d**) wurden als starke Antioxidantien mit ORAC-Werten zwischen 0,3 bzw. 4,5 identifiziert. Darüber hinaus zeigten Trimethylbenzochinon- und Thymochinon-Derivate im Oxytose-Assay eine stärkere Neuroprotektion als andere Chinone. Daher können Trimethylbenzochinon- und Thymochinon-Derivate als Leitverbindungen für die weitere Untersuchung des Mechanismus und die Wirkstoffforschung zur Behandlung neurodegenerativer Erkrankungen verwendet werden. Es konnte kein Zusammenhang zwischen deren antioxidativen Kapazität und der neuroprotektiven Wirkungen in HT22-Zellen beobachtet werden.



12a-d (Trimethylbenzochinon-Derivate)

ORAC-Wert = 0,3 - 4,5 Trolox-Äq.

Schützen Sie HT22-Zellen vor Oxytose bei 5 μM



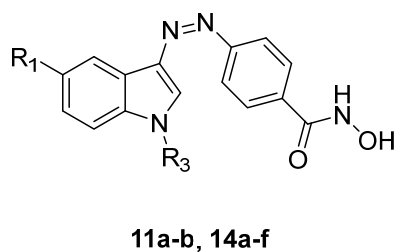
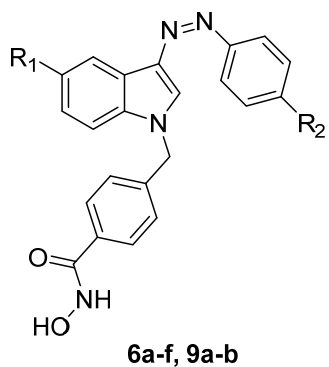
14a-d (Thymochinon-Derivate)

ORAC-Wert = 0,6 - 3,5 Trolox Äq.

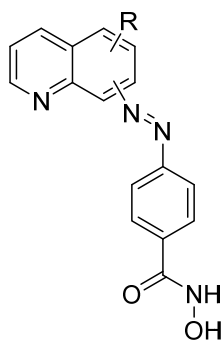
Schützen Sie HT22-Zellen vor Oxytose bei 5 μM

HDAC6 ist ein neues aufkommendes Target, das ein großes therapeutisches Potenzial zur Bekämpfung neurodegenerativer Erkrankungen aufweist, sein Wirkmechanismus bei

neurodegenerativer Progression bleibt jedoch unklar. Wir haben hier eine Reihe von photoschaltbaren HDAC-Inhibitoren entwickelt, die aufgrund der hohen räumlichen und zeitlichen Auflösung effektive molekulare Werkzeuge sein könnten. Insgesamt wurden 23 Zielverbindungen synthetisiert und photophysikochemisch charakterisiert. Die Verbindungen auf Azochinolinbasis besitzen thermisch stabilere *cis*-Isomere in Pufferlösung, die in einem enzymbasierten HDAC-Inhibitionsassay weiter getestet wurden. Keine dieser getesteten Verbindungen zeigt jedoch signifikante Unterschiede in der Aktivität zwischen *trans*-Isomeren und den entsprechenden *cis*-Isomeren. Obwohl der vermutete „*cis*-on“-Effekt nicht erreicht wurde, wurden die Substituenteneffekte auf 3-Arylazaindol- und Azochinolin-Photoschalter gründlich untersucht, und die erhaltene Beziehung zwischen Struktur und photophysikochemischen Eigenschaften könnte eine Richtung für andere Forscher und für andere Anwendungen sein.



Cis-Isomere sind in Puffer thermisch instabil



Cis-Isomere sind in Puffer thermisch stabil, aber es wurde kein signifikanter Aktivitätsunterschied zwischen *trans*- und *cis*-Isomeren beobachtet

7. Abbreviations

AAPH	2,2'-Azobis(amidinopropane) dihydrochloride
$A\beta$	Amyloid β
AChE	Acetylcholinesterase
AD	Alzheimer's disease
ALS	Amyotrophic lateral sclerosis
APP	Amyloid precursor protein
ARE	Antioxidant response element
ATF4	Activating transcription factor 4
Bach1	BTB domain and CNC homolog 1
BChE	Butyrylcholinesterase
DCM	Dichloromethane
DGR	Double glycine repeat
DMSO	Dimethylsulfoxide
DNA	Deoxyribonucleic acid
EDTA	Ethylenediaminetetraacetic acid
FL	Fluorescein
GPx4	Glutathione peroxidase 4
GSH	Glutathione
GST	Glutathione S-transferase
GSK3 β	Glycogen synthase kinase 3 β
HDAC	Histone deacetylase
HO-1	Heme oxygenase-1
HIF-1 α	Hypoxia-inducible factor
HSP-90	Hot shock protein 90
IL-1 β	Interleukin 1 beta
IND	Investigational new drug
iNOS	Inducible nitric oxide synthase
Keap1	Kelch-like ECH-associated protein 1
LOX	Lipoxygenase

LPS	Lipopolysaccharides
MTT	3-(4,5-Dimethylthiazol-2-yl)-2,5-diphenyltetrazolium bromide
MTDL	Multi-target-directed ligands
mp	Melting point
NAD ⁺	Nicotinamide adenine dinucleotide
NQO1	NAD(P)H quinone oxidoreductase-1
NFTs	Neurofibrillary tangles
NMDAR	<i>N</i> -Methyl-D-aspartate receptor
Nrf2	Nuclear factor erythroid 2-related factor
PBS	Phosphate buffered saline
PD	Parkinson's disease
PDE5	Phosphodiesterase 5
PDT	Photodynamic therapy
PHF6	PHD finger protein 6
PPI	Protein-protein interaction
ROS	Ractive oxygen species
TBTU	<i>O</i> -(benzotriazol-1-yl)- <i>N,N,N,N'</i> -tetra-methyluron-ium tetrafluoroborate
TEA	Trimethylamine
TFA	Trifluoroacetic acid
THF	Tetrahydrofuran
TG2	Transglutaminase 2
TREM2	Triggering receptor expressed on myeloid cells 2
Trolox	(±)-6-Hydroxy-2,5,7,8-tetramethylchromane-2-carboxylic acid
YMT	Y-maze test
ZBG	Zinc binding group

8. References

- (1) Christina, P. The state of the art of dementia research: new frontiers. *World Alzheimer report* **2018**, <https://doi.org/APO-260056>.
- (2) Terry, A. V., Jr.; Buccafusco, J. J. The cholinergic hypothesis of age and Alzheimer's disease-related cognitive deficits: recent challenges and their implications for novel drug development. *J. Pharmacol. Exp. Ther.* **2003**, *306* (3), 821-827.
- (3) Anu Kunnath, R.; Subham, D.; Alex, J.; Gurupur Gautham, S.; Angel Treasa, A.; Jayesh, M. Neurodegenerative pathways in Alzheimer's disease: A Review. *Curr. Neuropharmacol.* **2021**, *19* (5), 679-692.
- (4) Kametani, F.; Hasegawa, M. Reconsideration of amyloid hypothesis and tau hypothesis in Alzheimer's disease. *Front. Neurosci.* **2018**, *12*, 25.
- (5) Lozupone, M.; Solfrizzi, V.; D'Urso, F.; Di Gioia, I.; Sardone, R.; Dibello, V.; Stallone, R.; Liguori, A.; Ciritella, C.; Daniele, A.; Bellomo, A.; Seripa, D.; Panza, F. Anti-amyloid- β protein agents for the treatment of Alzheimer's disease: an update on emerging drugs. *Expert Opin. Emerg. Drugs* **2020**, *25* (3), 319-335.
- (6) Hooker, J. M. FDA approval of aducanumab divided the community but also connected and united it. *ACS Chem. Neurosci.* **2021**, doi: 10.1021/acscemneuro.1021c00393.
- (7) Wang, X.; Wang, W.; Li, L.; Perry, G.; Lee, H. G.; Zhu, X. Oxidative stress and mitochondrial dysfunction in Alzheimer's disease. *Biochim. Biophys. Acta* **2014**, *1842* (8), 1240-1247.
- (8) Wu, Y.; Chen, M.; Jiang, J. Mitochondrial dysfunction in neurodegenerative diseases and drug targets via apoptotic signaling. *Mitochondrion* **2019**, *49*, 35-45.
- (9) Wang, W.; Zhao, F.; Ma, X.; Perry, G.; Zhu, X. Mitochondria dysfunction in the pathogenesis of Alzheimer's disease: recent advances. *Mol. Neurodegener.* **2020**, *15* (1), 30.
- (10) Paula, A.; Rodrigo, A. C.; Catarina, O. Neuroinflammation, oxidative stress and the pathogenesis of Alzheimers disease. *Curr. Pharm. Des.* **2010**, *16* (25), 2766-2778.
- (11) Chan, A. M.; Fletcher, S. Shifting the paradigm in treating multi-factorial diseases: polypharmacological co-inhibitors of HDAC6. *RSC Med. Chem.* **2021**, *12* (2), 178-196.
- (12) Duce, J. A.; Bush, A. I. Biological metals and Alzheimer's disease: implications for therapeutics and diagnostics. *Prog. Neurobiol.* **2010**, *92* (1), 1-18.
- (13) Albertini, C.; Salerno, A.; de Sena Murteira Pinheiro, P.; Bolognesi, M. L. From combinations to multitarget-directed ligands: A continuum in Alzheimer's disease polypharmacology. *Med. Res. Rev.* **2020**, 1-28.
- (14) He, F.; Chou, C. J.; Scheiner, M.; Poeta, E.; Yuan Chen, N.; Gunesch, S.; Hoffmann, M.; Sottriffer, C.; Monti, B.; Maurice, T.; Decker, M. Melatonin- and ferulic acid-based HDAC6 selective inhibitors exhibit pronounced immunomodulatory effects in vitro and neuroprotective effects in a pharmacological Alzheimer's disease mouse model. *J. Med. Chem.* **2021**, *64* (7), 3794-3812.
- (15) Bolognesi, M. L.; Banzi, R.; Bartolini, M.; Cavalli, A.; Tarozzi, A.; Andrisano, V.; Minarini, A.;

Rosini, M.; Tumiatti, V.; Bergamini, C.; Fato, R.; Lenaz, G.; Hrelia, P.; Cattaneo, A.; Recanatini, M.; Melchiorre, C. Novel class of quinone-bearing polyamines as multi-target-directed ligands to combat Alzheimer's disease. *J. Med. Chem.* **2007**, *50* (20), 4882-4897.

(16) Zagorska, A.; Jaromin, A. Perspectives for new and more efficient multifunctional ligands for Alzheimer's disease therapy. *Molecules* **2020**, *25* (15), 3337.

(17) Takayoshi, S.; Yukihiro, I.; Naoki, M. Isoform-selective histone deacetylase inhibitors. *Curr. Pharm. Des.* **2008**, *14* (6), 529-544.

(18) Mottamal, M.; Zheng, S.; Huang, T.; Wang, G. Histone deacetylase inhibitors in clinical studies as templates for new anticancer agents. *Molecules* **2015**, *20* (3), 3898-3941.

(19) Graff, J.; Rei, D.; Guan, J. S.; Wang, W. Y.; Seo, J.; Hennig, K. M.; Nieland, T. J.; Fass, D. M.; Kao, P. F.; Kahn, M.; Su, S. C.; Samiei, A.; Joseph, N.; Haggarty, S. J.; Delalle, I.; Tsai, L. H. An epigenetic blockade of cognitive functions in the neurodegenerating brain. *Nature* **2012**, *483* (7388), 222-226.

(20) Cuadrado-Tejedor, M.; Oyarzabal, J.; Lucas, M. P.; Franco, R.; Garcia-Osta, A. Epigenetic drugs in Alzheimer's disease. *Biomol. Concepts* **2013**, *4* (5), 433-445.

(21) Mahady, L.; Nadeem, M.; Malek-Ahmadi, M.; Chen, K.; Perez, S. E.; Mufson, E. J. HDAC2 dysregulation in the nucleus basalis of Meynert during the progression of Alzheimer's disease. *Neuropathol. Appl. Neurobiol.* **2019**, *45* (4), 380-397.

(22) Govindarajan, N.; Rao, P.; Burkhardt, S.; Sananbenesi, F.; Schluter, O. M.; Bradke, F.; Lu, J.; Fischer, A. Reducing HDAC6 ameliorates cognitive deficits in a mouse model for Alzheimer's disease. *EMBO Mol. Med.* **2013**, *5* (1), 52-63.

(23) Zhang, L.; Sheng, S.; Qin, C. The Role of HDAC6 in Alzheimer's Disease. *J. Alzheimer's Dis.* **2013**, *33*, 283-295.

(24) LoPresti, P. HDAC6 in diseases of cognition and of neurons. *Cells* **2020**, *10* (1), 12.

(25) Thomas, E. A.; D'Mello, S. R. Complex neuroprotective and neurotoxic effects of histone deacetylases. *Journal of Neurochemistry* **2018**, *145* (2), 96-110.

(26) Chen, S.; Owens, G. C.; Makarenkova, H.; Edelman, D. B. HDAC6 regulates mitochondrial transport in hippocampal neurons. *PLoS One* **2010**, *5* (5), e10848.

(27) De Simone, A.; La Pietra, V.; Betari, N.; Petragani, N.; Conte, M.; Daniele, S.; Pietrobono, D.; Martini, C.; Petralla, S.; Casadei, R.; Davani, L.; Frabetti, F.; Russomanno, P.; Novellino, E.; Montanari, S.; Tumiatti, V.; Ballerini, P.; Sarno, F.; Nebbioso, A.; Altucci, L.; Monti, B.; Andrisano, V.; Milelli, A. Discovery of the first-in-class GSK-3 β /HDAC dual inhibitor as disease-modifying agent to combat Alzheimer's disease. *ACS Med. Chem. Lett.* **2019**, *10* (4), 469-474.

(28) Rabal, O.; Sanchez-Arias, J. A.; Cuadrado-Tejedor, M.; de Miguel, I.; Perez-Gonzalez, M.; Garcia-Barroso, C.; Ugarte, A.; Estella-Hermoso de Mendoza, A.; Saez, E.; Espelousin, M.; Ursua, S.; Haizhong, T.; Wei, W.; Musheng, X.; Garcia-Osta, A.; Oyarzabal, J. Design, synthesis, and biological evaluation of first-in-class dual acting histone deacetylases (HDACs) and phosphodiesterase 5 (PDE5) inhibitors

for the treatment of Alzheimer's disease. *J. Med. Chem.* **2016**, *59* (19), 8967-9004.

(29) He, F.; Ran, Y.; Li, X.; Wang, D.; Zhang, Q.; Lv, J.; Yu, C.; Qu, Y.; Zhang, X.; Xu, A.; Wei, C.; Chou, C. J.; Wu, J. Design, synthesis and biological evaluation of dual-function inhibitors targeting NMDAR and HDAC for Alzheimer's disease. *Bioorg. Chem.* **2020**, *103*, 104109.

(30) Xu, A.; He, F.; Zhang, X.; Li, X.; Ran, Y.; Wei, C.; James Chou, C.; Zhang, R.; Wu, J. Tacrine-hydroxamate derivatives as multitarget-directed ligands for the treatment of Alzheimer's disease: Design, synthesis, and biological evaluation. *Bioorg. Chem.* **2020**, *98*, 103721.

(31) Tseng, H. J.; Lin, M. H.; Shiao, Y. J.; Yang, Y. C.; Chu, J. C.; Chen, C. Y.; Chen, Y. Y.; Lin, T. E.; Su, C. J.; Pan, S. L.; Chen, L. C.; Wang, C. Y.; Hsu, K. C.; Huang, W. J. Synthesis and biological evaluation of acridine-based histone deacetylase inhibitors as multitarget agents against Alzheimer's disease. *Eur. J. Med. Chem.* **2020**, *192*, 112193.

(32) He, F.; Chou, C. J.; Scheiner, M.; Poeta, E.; Yuan Chen, N.; Gunesch, S.; Hoffmann, M.; Sottriffer, C.; Monti, B.; Maurice, T.; Decker, M. Melatonin- and ferulic acid-based HDAC6 selective inhibitors exhibit pronounced immunomodulatory effects in vitro and neuroprotective effects in a pharmacological Alzheimer's disease mouse model. *J. Med. Chem.* **2021**, *64* (7), 3794-3812.

(33) Basso, M.; Chen, H. H.; Tripathy, D.; Conte, M.; Apperley, K. Y. P.; De Simone, A.; Keillor, J. W.; Ratan, R.; Nebbioso, A.; Sarno, F.; Altucci, L.; Milelli, A. Designing dual transglutaminase 2/histone deacetylase inhibitors effective at halting neuronal death. *ChemMedChem* **2018**, *13* (3), 227-230.

(34) Hu, J.; An, B.; Pan, T.; Li, Z.; Huang, L.; Li, X. Design, synthesis, and biological evaluation of histone deacetylase inhibitors possessing glutathione peroxidase-like and antioxidant activities against Alzheimer's disease. *Bioorg. Med. Chem.* **2018**, *26* (21), 5718-5729.

(35) Maher, P.; Currais, A.; Schubert, D. Using the oxytosis/ferroptosis pathway to understand and treat age-associated neurodegenerative diseases. *Cell Chem. Biol.* **2020**, *27* (12), 1456-1471.

(36) Thomas, B.; Gazaryan, I. The status of Nrf2-based therapeutics: current perspectives and future prospects. *Neural. Regen. Res.* **2016**, *11* (11), 1708-1711.

(37) Tan, S.; Schubert, D.; Maher, P. Oxytosis: A novel form of programmed cell death. *Curr. Top. Med. Chem.* **2001**, *1* (6), 497-506.

(38) Dixon, S. J.; Lemberg, K. M.; Lamprecht, M. R.; Skouta, R.; Zaitsev, E. M.; Gleason, C. E.; Patel, D. N.; Bauer, A. J.; Cantley, A. M.; Yang, W. S.; Morrison, B., 3rd; Stockwell, B. R. Ferroptosis: an iron-dependent form of nonapoptotic cell death. *Cell* **2012**, *149* (5), 1060-1072.

(39) Chen, Q.; Prior, M.; Dargusch, R.; Roberts, A.; Riek, R.; Eichmann, C.; Chiruta, C.; Akaishi, T.; Abe, K.; Maher, P.; Schubert, D. A novel neurotrophic drug for cognitive enhancement and Alzheimer's disease. *PLoS One* **2011**, *6* (12), e27865.

(40) Chiruta, C.; Schubert, D.; Dargusch, R.; Maher, P. Chemical modification of the multitarget neuroprotective compound fisetin. *J. Med. Chem.* **2012**, *55* (1), 378-389.

(41) Currais, A.; Huang, L.; Goldberg, J.; Petrascheck, M.; Ates, G.; Pinto-Duarte, A.; Shokhirev, M. N.; Schubert, D.; Maher, P. Elevating acetyl-CoA levels reduces aspects of brain aging. *Elife* **2019**, *8*,

e47866.

(42) Schramm, S.; Huang, G.; Gunesch, S.; Lang, F.; Roa, J.; Hogger, P.; Sabate, R.; Maher, P.; Decker, M. Regioselective synthesis of 7-O-esters of the flavonolignan silibinin and SARs lead to compounds with overadditive neuroprotective effects. *Eur. J. Med. Chem.* **2018**, *146*, 93-107.

(43) Gunesch, S.; Hoffmann, M.; Kiermeier, C.; Fischer, W.; Pinto, A. F. M.; Maurice, T.; Maher, P.; Decker, M. 7-O-Esters of taxifolin with pronounced and overadditive effects in neuroprotection, anti-neuroinflammation, and amelioration of short-term memory impairment in vivo. *Redox Biol.* **2020**, *29*, 101378.

(44) Hoffmann, M.; Stiller, C.; Endres, E.; Scheiner, M.; Gunesch, S.; Sottriffer, C.; Maurice, T.; Decker, M. Highly selective butyrylcholinesterase inhibitors with tunable duration of action by chemical modification of transferable carbamate units exhibit pronounced neuroprotective effect in an Alzheimer's disease mouse model. *J. Med. Chem.* **2019**, *62* (20), 9116-9140.

(45) Scheiner, M.; Dolles, D.; Gunesch, S.; Hoffmann, M.; Nabissi, M.; Marinelli, O.; Naldi, M.; Bartolini, M.; Petralla, S.; Poeta, E.; Monti, B.; Falkeis, C.; Vieth, M.; Hubner, H.; Gmeiner, P.; Maitra, R.; Maurice, T.; Decker, M. Dual-acting cholinesterase-human cannabinoid receptor 2 ligands show pronounced neuroprotection in vitro and overadditive and disease-modifying neuroprotective effects in vivo. *J. Med. Chem.* **2019**, *62* (20), 9078-9102.

(46) Hofmann, J.; Ginex, T.; Espargaro, A.; Scheiner, M.; Gunesch, S.; Arago, M.; Stigloher, C.; Sabate, R.; Luque, F. J.; Decker, M. Azobioisosteres of curcumin with pronounced activity against amyloid aggregation, intracellular oxidative stress, and neuroinflammation. *Chemistry* **2021**, *27* (19), 6015-6027.

(47) Ates, G.; Goldberg, J.; Currais, A.; Maher, P. CMS121, a fatty acid synthase inhibitor, protects against excess lipid peroxidation and inflammation and alleviates cognitive loss in a transgenic mouse model of Alzheimer's disease. *Redox Biol.* **2020**, *36*, 101648.

(48) Josey, B. J.; Inks, E. S.; Wen, X.; Chou, C. J. Structure-activity relationship study of vitamin k derivatives yields highly potent neuroprotective agents. *J. Med. Chem.* **2013**, *56* (3), 1007-1022.

(49) Armstrong, M. M.; Freedman, C. J.; Jung, J. E.; Zheng, Y.; Kalyanaraman, C.; Jacobson, M. P.; Simeonov, A.; Maloney, D. J.; van Leyen, K.; Jadhav, A.; Holman, T. R. A potent and selective inhibitor targeting human and murine 12/15-LOX. *Bioorg. Med. Chem.* **2016**, *24* (6), 1183-1190.

(50) Prokai, L.; Oon, S.-M.; Prokai-Tatrai, K.; Abboud, K. A.; Simpkins, J. W. Synthesis and biological evaluation of 17 β -alkoxyestra-1,3,5(10)-trienes as potential neuroprotectants against oxidative stress. *J. Med. Chem.* **2001**, *44* (1), 110-114.

(51) Speer, R.; Ratan, R. R. Hypoxic adaptation in the nervous system: Promise for novel therapeutics for acute and chronic neurodegeneration. *Adv. Exp. Med. Biol.* **2016**, *903*, 221-243.

(52) Niccoli, T.; Kerr, F.; Snoeren, I.; Fabian, D.; Aleyakpo, B.; Ivanov, D.; Sofola-Adesakin, O.; Cryar, A.; Adcott, J.; Thornton, J.; Partridge, L. Activating transcription factor 4-dependent lactate dehydrogenase activation as a protective response to amyloid beta toxicity. *Brain Commun.* **2021**, *3* (2), fcab053.

- (53) Robledinos-Anton, N.; Fernandez-Gines, R.; Manda, G.; Cuadrado, A. Activators and inhibitors of NRF2: A review of their potential for clinical development. *Oxid. Med. Cell Longev.* **2019**, *2019*, 9372182.
- (54) Townsend, B. E.; Johnson, R. W. Sulforaphane induces Nrf2 target genes and attenuates inflammatory gene expression in microglia from brain of young adult and aged mice. *Exp. Gerontol.* **2016**, *73*, 42-48.
- (55) Truong, V. L.; Jun, M.; Jeong, W. S. Role of resveratrol in regulation of cellular defense systems against oxidative stress. *Biofactors* **2018**, *44* (1), 36-49.
- (56) Calkins, M. J.; Johnson, D. A.; Townsend, J. A.; Vargas, M. R.; Dowell, J. A.; Williamson, T. P.; Kraft, A. D.; Lee, J. M.; Li, J.; Johnson, J. A. The Nrf2/ARE pathway as a potential therapeutic target in neurodegenerative disease. *Antioxid. Redox Signal.* **2009**, *11* (3), 497-508.
- (57) Smirnova, N. A.; Kaidery, N. A.; Hushpulian, D. M.; Rakhman, II; Poloznikov, A. A.; Tishkov, V. I.; Karuppagounder, S. S.; Gaisina, I. N.; Pekcec, A.; Leyen, K. V.; Kazakov, S. V.; Yang, L.; Thomas, B.; Ratan, R. R.; Gazaryan, I. G. Bioactive flavonoids and catechols as Hif1 and Nrf2 protein stabilizers - implications for Parkinson's disease. *Aging Dis.* **2016**, *7* (6), 745-762.
- (58) Ahuja, M.; Ammal Kaidery, N.; Yang, L.; Calingasan, N.; Smirnova, N.; Gaisin, A.; Gaisina, I. N.; Gazaryan, I.; Hushpulian, D. M.; Kaddour-Djebbar, I.; Bollag, W. B.; Morgan, J. C.; Ratan, R. R.; Starkov, A. A.; Beal, M. F.; Thomas, B. Distinct Nrf2 signaling mechanisms of fumaric acid esters and their role in neuroprotection against 1-methyl-4-phenyl-1,2,3,6-tetrahydropyridine-induced experimental Parkinson's-like disease. *J. Neurosci.* **2016**, *36* (23), 6332-6351.
- (59) Gaisina, I. N.; Lee, S. H.; Kaidery, N. A.; Ben Aissa, M.; Ahuja, M.; Smirnova, N. N.; Wakade, S.; Gaisin, A.; Bourassa, M. W.; Ratan, R. R.; Nikulin, S. V.; Poloznikov, A. A.; Thomas, B.; Thatcher, G. R. J.; Gazaryan, I. G. Activation of Nrf2 and hypoxic adaptive response contribute to neuroprotection elicited by phenylhydroxamic acid selective HDAC6 inhibitors. *ACS Chem. Neurosci.* **2018**, *9* (5), 894-900.
- (60) Marcotte, D.; Zeng, W.; Hus, J. C.; McKenzie, A.; Hession, C.; Jin, P.; Bergeron, C.; Lugovskoy, A.; Enyedy, I.; Cuervo, H.; Wang, D.; Atmanene, C.; Roecklin, D.; Vecchi, M.; Vivat, V.; Kraemer, J.; Winkler, D.; Hong, V.; Chao, J.; Lukashev, M.; Silvian, L. Small molecules inhibit the interaction of Nrf2 and the Keap1 Kelch domain through a non-covalent mechanism. *Bioorg. Med. Chem.* **2013**, *21* (14), 4011-4019.
- (61) Armagan, G.; Sevgili, E.; Gurkan, F. T.; Kose, F. A.; Bilgic, T.; Dagci, T.; Saso, L. Regulation of the Nrf2 pathway by glycogen synthase kinase-3beta in MPP(+)-induced cell damage. *Molecules* **2019**, *24* (7), 1377.
- (62) Fuchter, M. J. On the promise of photopharmacology using photoswitches: A medicinal chemist's perspective. *J. Med. Chem.* **2020**, *63* (20), 11436-11447.
- (63) Blazquez-Castro, A.; Breitenbach, T.; Ogilby, P. R. Singlet oxygen and ROS in a new light: low-dose subcellular photodynamic treatment enhances proliferation at the single cell level. *Photochem.*

Photobiol. Sci. **2014**, *13* (9), 1235-1240.

(64) Klan, P.; Solomek, T.; Bochet, C. G.; Blanc, A.; Givens, R.; Rubina, M.; Popik, V.; Kostikov, A.; Wirz, J. Photoremovable protecting groups in chemistry and biology: reaction mechanisms and efficacy. *Chem. Rev.* **2013**, *113* (1), 119-191.

(65) Vorobev, A. Y.; Moskalensky, A. E. Long-wavelength photoremovable protecting groups: On the way to in vivo application. *Comput. Struct. Biotechnol. J.* **2020**, *18*, 27-34.

(66) Rodríguez-Soacha, D. A.; Decker, M. Photopharmacology in Alzheimer's disease. *Adv. Ther.* **2018**, *1* (3), 180037.

(67) Agnetta, L.; Decker, M., 11 - Photoresponsive Hybrid Compounds. In *Design of Hybrid Molecules for Drug Development*, Decker, M., Ed. Elsevier: 2017; pp 279-315.

(68) Hull, K.; Morstein, J.; Trauner, D. In vivo photopharmacology. *Chem. Rev.* **2018**, *118* (21), 10710-10747.

(69) Broichhagen, J.; Frank, J. A.; Trauner, D. A roadmap to success in photopharmacology. *Acc. Chem. Res.* **2015**, *48* (7), 1947-1960.

(70) Hoorens, M. W. H.; Szymanski, W. Reversible, spatial and temporal control over protein activity using light. *Trends Biochem. Sci.* **2018**, *43* (8), 567-575.

(71) Agnetta, L.; Kauk, M.; Canizal, M. C. A.; Messerer, R.; Holzgrabe, U.; Hoffmann, C.; Decker, M. A photoswitchable dualsteric ligand controlling receptor efficacy. *Angew Chem. Int. Ed. Engl.* **2017**, *56* (25), 7282-7287.

(72) Chen, X.; Wehle, S.; Kuzmanovic, N.; Merget, B.; Holzgrabe, U.; König, B.; Sotriffer, C. A.; Decker, M. Acetylcholinesterase inhibitors with photoswitchable inhibition of beta-amyloid aggregation. *ACS Chem. Neurosci.* **2014**, *5* (5), 377-389.

(73) Wutz, D.; Gluhacevic, D.; Chakrabarti, A.; Schmidt-kunz, K.; Robaa, D.; Erdmann, F.; Romier, C.; Sippl, W.; Jung, M.; König, B. Photochromic histone deacetylase inhibitors based on dithienylethenes and fulgimides. *Org. Biomol. Chem.* **2017**, *15* (22), 4882-4896.

(74) Weston, C. E.; Richardson, R. D.; Haycock, P. R.; White, A. J.; Fuchter, M. J. Arylazopyrazoles: azoheteroarene photoswitches offering quantitative isomerization and long thermal half-lives. *J. Am. Chem. Soc.* **2014**, *136* (34), 11878-11881.

(75) Szymanski, W.; Ourailidou, M. E.; Velema, W. A.; Dekker, F. J.; Feringa, B. L. Light-controlled histone deacetylase (HDAC) inhibitors: towards photopharmacological chemotherapy. *Chemistry* **2015**, *21* (46), 16517-16524.

(76) Weston, C. E.; Kramer, A.; Colin, F.; Yildiz, O.; Baud, M. G.; Meyer-Almes, F. J.; Fuchter, M. J. Toward photopharmacological antimicrobial chemotherapy using photoswitchable amidohydrolase inhibitors. *ACS Infect. Dis.* **2017**, *3* (2), 152-161.

(77) Reis, S. A.; Ghosh, B.; Hendricks, J. A.; Szantai-Kis, D. M.; Tork, L.; Ross, K. N.; Lamb, J.; Read-Button, W.; Zheng, B.; Wang, H.; Salhouse, C.; Haggarty, S. J.; Mazitschek, R. Light-controlled modulation of gene expression by chemical optoepigenetic probes. *Nat. Chem. Biol.* **2016**, *12* (5), 317-

323.

(78) Ieda, N.; Yamada, S.; Kawaguchi, M.; Miyata, N.; Nakagawa, H. (7-Diethylaminocoumarin-4-yl)methyl ester of suberoylanilide hydroxamic acid as a caged inhibitor for photocontrol of histone deacetylase activity. *Bioorg. Med. Chem.* **2016**, *24* (12), 2789-2793.

(79) Sartori, L.; Minucci, S. Tackling oxidative stress by a direct route: a new job for HDAC inhibitors? *Chem Biol* **2015**, *22* (4), 431-432.

(80) Noack, M.; Leyk, J.; Richter-Landsberg, C. HDAC6 inhibition results in tau acetylation and modulates tau phosphorylation and degradation in oligodendrocytes. *Glia* **2014**, *62* (4), 535-547.

(81) Sung, Y. M.; Lee, T.; Yoon, H.; DiBattista, A. M.; Song, J. M.; Sohn, Y.; Moffat, E. I.; Turner, R. S.; Jung, M.; Kim, J.; Hoe, H. S. Mercaptoacetamide-based class II HDAC inhibitor lowers Abeta levels and improves learning and memory in a mouse model of Alzheimer's disease. *Exp Neurol* **2013**, *239*, 192-201.

(82) Rosales-Corral, S. A.; Reiter, R. J.; Tan, D.-X.; Manchester, L. C.; Liu, X., Chapter 18 - Antioxidant and anti-inflammatory role of melatonin in Alzheimer's neurodegeneration. In *Aging*, Preedy, V. R., Ed. Academic Press: San Diego, 2014; pp 177-193.

(83) Nabavi, S. F.; Devi, K. P.; Malar, D. S.; Sureda, A.; Daglia, M.; Nabavi, S. M. Ferulic acid and Alzheimer's disease: promises and pitfalls. *Mini-Rev. Med. Chem.* **2015**, *15* (9), 776-788.

(84) Mihardja, M.; Roy, J.; Wong, K. Y.; Aquili, L.; Heng, B. C.; Chan, Y. S.; Fung, M. L.; Lim, L. W. Therapeutic potential of neurogenesis and melatonin regulation in Alzheimer's disease. *Ann. N. Y. Acad. Sci.* **2020**, *1478* (1), 43-62.

(85) Gu, L.; Cui, X.; Wei, W.; Yang, J.; Li, X. Ferulic acid promotes survival and differentiation of neural stem cells to prevent gentamicin-induced neuronal hearing loss. *Exp. Cell. Res.* **2017**, *360* (2), 257-263.

(86) Santo, L.; Hideshima, T.; Kung, A. L.; Tseng, J. C.; Tamang, D.; Yang, M.; Jarpe, M.; van Duzer, J. H.; Mazitschek, R.; Ogier, W. C.; Cirstea, D.; Rodig, S.; Eda, H.; Scullen, T.; Canavese, M.; Bradner, J.; Anderson, K. C.; Jones, S. S.; Raje, N. Preclinical activity, pharmacodynamic, and pharmacokinetic properties of a selective HDAC6 inhibitor, ACY-1215, in combination with bortezomib in multiple myeloma. *Blood* **2012**, *119* (11), 2579-2589.

(87) Porter, N. J.; Osko, J. D.; Diedrich, D.; Kurz, T.; Hooker, J. M.; Hansen, F. K.; Christianson, D. W. Histone deacetylase 6-selective inhibitors and the influence of capping groups on hydroxamate-zinc denticity. *J. Med. Chem.* **2018**, *61* (17), 8054-8060.

(88) Villaño, D.; Fernández-Pachón, M. S.; Moyá, M. L.; Troncoso, A. M.; García-Parrilla, M. C. Radical scavenging ability of polyphenolic compounds towards DPPH free radical. *Talanta* **2007**, *71* (1), 230-235.

(89) Huang, D.; Ou, B.; Prior, R. L. The Chemistry behind Antioxidant Capacity Assays. *J. Agr. Food Chem.* **2005**, *53* (6), 1841-1856.

(90) Song, Y.; Qin, L.; Yang, R.; Yang, F.; Kenechukwu, N. A.; Zhao, X.; Zhou, X.; Wen, X.; Li, L.

Inhibition of HDAC6 alleviating lipopolysaccharide-induced p38MAPK phosphorylation and neuroinflammation in mice. *Pharm. Biol.* **2019**, *57* (1), 263-268.

(91) Lewerenz, J.; Ates, G.; Methner, A.; Conrad, M.; Maher, P. Oxytosis/Ferroptosis-(Re-) Emerging Roles for Oxidative Stress-Dependent Non-apoptotic Cell Death in Diseases of the Central Nervous System. *Front Neurosci.* **2018**, *12*, 214.

(92) Shirlee, T.; David, S.; Pamela, M. Oxytosis: A novel form of programmed cell death. *Curr. Top. Med. Chem.* **2001**, *1* (6), 497-506.

(93) Gunesch, S.; Soriano-Castell, D.; Lamer, S.; Schlosser, A.; Maher, P.; Decker, M. Development and application of a chemical probe based on a neuroprotective flavonoid hybrid for target identification using activity-based protein profiling. *ACS Chem. Neurosci.* **2020**, *11* (22), 3823-3837.

(94) Scheiner, M.; Dolles, D.; Gunesch, S.; Hoffmann, M.; Nabissi, M.; Marinelli, O.; Naldi, M.; Bartolini, M.; Petralla, S.; Poeta, E.; Monti, B.; Falkeis, C.; Vieth, M.; Hübner, H.; Gmeiner, P.; Maitra, R.; Maurice, T.; Decker, M. Dual-acting cholinesterase–human cannabinoid receptor 2 ligands show pronounced neuroprotection in vitro and overadditive and disease-modifying neuroprotective effects in vivo. *J. Med. Chem.* **2019**, *62* (20), 9078-9102.

(95) Paul, A.; Viswanathan, G. K.; Mahapatra, S.; Balboni, G.; Pacifico, S.; Gazit, E.; Segal, D. Antagonistic activity of naphthoquinone-based hybrids toward amyloids associated with Alzheimer's disease and type-2 diabetes. *ACS Chem. Neurosci.* **2019**, *10* (8), 3510-3520.

(96) Frenkel-Pinter, M.; Tal, S.; Scherzer-Attali, R.; Abu-Hussien, M.; Alyagor, I.; Eisenbaum, T.; Gazit, E.; Segal, D. Naphthoquinone-tryptophan hybrid inhibits aggregation of the tau-derived peptide PHF6 and reduces neurotoxicity. *J. Alzheimers Dis.* **2016**, *51* (1), 165-178.

(97) Scheiner, M.; Hoffmann, M.; He, F.; Poeta, E.; Chatonnet, A.; Monti, B.; Maurice, T.; Decker, M. Selective pseudo-irreversible butyrylcholinesterase inhibitors transferring antioxidant moieties to the enzyme show pronounced neuroprotective efficacy in vitro and in vivo in an Alzheimer's disease mouse model. *J. Med. Chem.* **2021**, *64* (13), 9302-9320.

(98) Yang, W. S.; SriRamaratnam, R.; Welsch, M. E.; Shimada, K.; Skouta, R.; Viswanathan, V. S.; Cheah, J. H.; Clemons, P. A.; Shamji, A. F.; Clish, C. B.; Brown, L. M.; Girotti, A. W.; Cornish, V. W.; Schreiber, S. L.; Stockwell, B. R. Regulation of ferroptotic cancer cell death by GPX4. *Cell* **2014**, *156* (1-2), 317-331.

(99) Yang, W. S.; Stockwell, B. R. Synthetic lethal screening identifies compounds activating iron-dependent, nonapoptotic cell death in oncogenic-RAS-harboring cancer cells. *Chem. Biol.* **2008**, *15* (3), 234-245.

(100) Li, X.; Himes, R. A.; Prosser, L. C.; Christie, C. F.; Watt, E.; Edwards, S. F.; Metcalf, C. S.; West, P. J.; Wilcox, K. S.; Chan, S. S. L.; Chou, C. J. Discovery of the first vitamin K analogue as a potential treatment of pharmacoresistant seizures. *J. Med. Chem.* **2020**, *63* (11), 5865-5878.

(101) Sharma, O. P.; Bhat, T. K. DPPH antioxidant assay revisited. *Food Chem.* **2009**, *113* (4), 1202-1205.

- (102) Ou, B.; Hampsch-Woodill, M.; Prior, R. L. Development and validation of an improved oxygen radical absorbance capacity assay using fluorescein as the fluorescent probe. *J. Agr. Food Chem.* **2001**, *49* (10), 4619-4626.
- (103) Dávalos, A.; Gómez-Cordovés, C.; Bartolomé, B. Extending applicability of the oxygen radical absorbance capacity (ORAC–fluorescein) assay. *J. Agr. Food Chem.* **2004**, *52* (1), 48-54.
- (104) Weissig, V. Drug development for the therapy of mitochondrial diseases. *Trends Mol. Med.* **2020**, *26* (1), 40-57.
- (105) Silva, T. L.; de Azevedo, M. d. L. S. G.; Ferreira, F. R.; Santos, D. C.; Amatore, C.; Goulart, M. O. F. Quinone-based molecular electrochemistry and their contributions to medicinal chemistry: A look at the present and future. *Curr. Opin. Electrochem.* **2020**, *24*, 79-87.
- (106) Ferreira, V. F.; de Carvalho, A. S.; Ferreira, P. G.; Lima, C. G. S.; de, C. d. S. F. Quinone-based drugs: an important class of molecules in medicinal chemistry. *Med. Chem.* **2020**, *16*, 1-13.
- (107) Bolton, J. L.; Dunlap, T. Formation and biological targets of quinones: cytotoxic versus cytoprotective effects. *Chem. Res. Toxicol.* **2017**, *30* (1), 13-37.
- (108) Pfeffer, G.; Majamaa, K.; Turnbull, D. M.; Thorburn, D.; Chinnery, P. F. Treatment for mitochondrial disorders. *Cochrane Database Syst. Rev.* **2012**, *2012* (4), CD004426.
- (109) Lyseng-Williamson, K. A. Idebenone: A review in Leber's hereditary optic neuropathy. *Drugs* **2016**, *76* (7), 805-813.
- (110) Murphy, M. P.; Smith, R. A. Targeting antioxidants to mitochondria by conjugation to lipophilic cations. *Annu. Rev. Pharmacol. Toxicol.* **2007**, *47*, 629-656.
- (111) Cavalli, A.; Bolognesi, M. L.; Capsoni, S.; Andrisano, V.; Bartolini, M.; Margotti, E.; Cattaneo, A.; Recanatini, M.; Melchiorre, C. A small molecule targeting the multifactorial nature of Alzheimer's disease. *Angew Chem. Int. Ed. Engl.* **2007**, *46* (20), 3689-3692.
- (112) Badary, O. A.; Taha, R. A.; Gamal El-Din, A. M.; Abdel-Wahab, M. H. Thymoquinone is a potent superoxide anion scavenger. *Drug Chem. Toxicol.* **2003**, *26* (2), 87-98.
- (113) Alhebshi, A. H.; Gotoh, M.; Suzuki, I. Thymoquinone protects cultured rat primary neurons against amyloid β -induced neurotoxicity. *Biochem. Biophys. Res. Commun.* **2013**, *433* (4), 362-367.
- (114) Campora, M.; Canale, C.; Gatta, E.; Tasso, B.; Laurini, E.; Relini, A.; Pricl, S.; Catto, M.; Tonelli, M. Multitarget biological profiling of new naphthoquinone and anthraquinone-based derivatives for the treatment of Alzheimer's disease. *ACS Chem. Neurosci.* **2021**, *12* (3), 447-461.
- (115) Fieser, L. F.; Hartwell, J. L. The reaction of hydrazoic acid with the naphthoquinones. *J. Am. Chem. Soc.* **1935**, *57* (8), 1482-1484.
- (116) Patil, R.; Chadar, D.; Chaudhari, D.; Peter, J.; Nikalje, M.; Weyhermüller, T.; Salunke-Gawali, S. Synthesis and characterization of 2-(n-alkylamino)-1,4-naphthoquinone: Molecular structures of ethyl and hexyl derivatives. *J. Mol. Struct.* **2014**, *1075*, 345-351.
- (117) Tandon, V. K.; Maurya, H. K. 'On water': unprecedented nucleophilic substitution and addition reactions with 1,4-quinones in aqueous suspension. *Tetrahedron Lett.* **2009**, *50* (43), 5896-5902.

- (118) Twigg, D. G.; Baldassarre, L.; Frye, E. C.; Galloway, W.; Spring, D. R. Bioinspired total synthesis of bussealin E. *Org. Lett.* **2018**, *20* (6), 1597-1599.
- (119) Bayen, S.; Barooah, N.; Sarma, R. J.; Sen, T. K.; Karmakar, A.; Baruah, J. B. Synthesis, structure and electrochemical properties of 2,5-bis(alkyl/arylamino)1,4-benzoquinones and 2-arylamino-1,4-naphthoquinones. *Dyes Pigment.* **2007**, *75* (3), 770-775.
- (120) Bae, Y. H.; Park, K. Targeted drug delivery to tumors: myths, reality and possibility. *J. Control Release* **2011**, *153* (3), 198-205.
- (121) Hansen, M. J.; Velema, W. A.; de Bruin, G.; Overkleeft, H. S.; Szymanski, W.; Feringa, B. L. Proteasome inhibitors with photocontrolled activity. *ChemBiochem* **2014**, *15* (14), 2053-2057.
- (122) Kalin, J. H.; Bergman, J. A. Development and therapeutic implications of selective histone deacetylase 6 inhibitors. *J. Med. Chem.* **2013**, *56* (16), 6297-6313.
- (123) Crespi, S.; Simeth, N. A.; Bellisario, A.; Fagnoni, M.; Konig, B. Unraveling the thermal isomerization mechanisms of heteroaryl azoswitches: phenylazoindoles as case study. *J. Phys. Chem. A* **2019**, *123* (9), 1814-1823.
- (124) Andréasson, J.; Pischel, U.; Straight, S. D.; Moore, T. A.; Moore, A. L.; Gust, D. All-photonic multifunctional molecular logic device. *J. Am. Chem. Soc.* **2011**, *133* (30), 11641-11648.
- (125) García-Amorós, J.; Velasco, D. Recent advances towards azobenzene-based light-driven real-time information-transmitting materials. *Beilstein J. Org. Chem.* **2012**, *8*, 1003-1017.
- (126) Kienzler, M. A.; Reiner, A.; Trautman, E.; Yoo, S.; Trauner, D.; Isacoff, E. Y. A red-shifted, fast-relaxing azobenzene photoswitch for visible light control of an ionotropic glutamate receptor. *J. Am. Chem. Soc.* **2013**, *135* (47), 17683-17686.
- (127) Lee, H. Y.; Nepali, K.; Huang, F. I.; Chang, C. Y.; Lai, M. J.; Li, Y. H.; Huang, H. L.; Yang, C. R.; Liou, J. P. (N-Hydroxycarbonylbenzylamino)quinolines as selective histone deacetylase 6 inhibitors suppress growth of multiple myeloma in vitro and in vivo. *J. Med. Chem.* **2018**, *61* (3), 905-917.
- (128) Xu, Y.; Gao, C.; Andreasson, J.; Grotli, M. Synthesis and photophysical characterization of azoheteroarenes. *Org. Lett.* **2018**, *20* (16), 4875-4879.
- (129) Simeth, N. A.; Crespi, S.; Fagnoni, M.; Konig, B. Tuning the thermal isomerization of phenylazoindole photoswitches from days to nanoseconds. *J. Am. Chem. Soc.* **2018**, *140* (8), 2940-2946.
- (130) Heltweg, B.; Trapp, J.; Jung, M. In vitro assays for the determination of histone deacetylase activity. *Methods* **2005**, *36* (4), 332-337.

9. Appendix

Appendix I:

He, F.; Chou, C. J.; Scheiner, M.; Poeta, E.; Yuan Chen, N.; Gunesch, S.; Hoffmann, M.; Sotriffer, C.; Monti, B.; Maurice, T.; Decker, M. Melatonin- and ferulic acid-based HDAC6 selective inhibitors exhibit pronounced immunomodulatory effects in vitro and neuroprotective effects in a pharmacological Alzheimer's disease mouse model. *J. Med. Chem.* **2021**, *64* (7), 3794-3812.

<https://pubs.acs.org/doi/10.1021/acs.jmedchem.0c01940>

Appendix II:

Supporting Information for Chapter 4.1, including all LCMS data of target compounds and LCMS data of Pan-Assay Interference Compounds (PAINS) Exclusion Assay..

Appendix III:

Supporting Information for Chapter 4.2, including all LCMS data of target compounds and LCMS data of Pan-Assay Interference Compounds (PAINS) Exclusion Assay.

Appendix IV:

Supporting Information for Chapter 4.3, including all UV-vis spectra and LCMS data of target compounds.

Appendix V:

Curriculum Vitae.

Appendix I

He, F.; Chou, C. J.; Scheiner, M.; Poeta, E.; Yuan Chen, N.; Gunesch, S.; Hoffmann, M.; Sotriffer, C.; Monti, B.; Maurice, T.; Decker, M. Melatonin- and Ferulic Acid-Based HDAC6 Selective Inhibitors Exhibit Pronounced Immunomodulatory Effects In Vitro and Neuroprotective Effects in a Pharmacological Alzheimer's Disease Mouse Model. *J. Med. Chem.* **2021**, *64* (7), 3794-3812.

<https://pubs.acs.org/doi/10.1021/acs.jmedchem.0c01940>

Melatonin- and Ferulic Acid-Based HDAC6 Selective Inhibitors Exhibit Pronounced Immunomodulatory Effects *In Vitro* and Neuroprotective Effects in a Pharmacological Alzheimer's Disease Mouse Model

Feng He, C. James Chou, Matthias Scheiner, Eleonora Poeta, Natalia Yuan Chen, Sandra Gunesch, Matthias Hoffmann, Christoph Sotriffer, Barbara Monti, Tangui Maurice,* and Michael Decker*

Cite This: *J. Med. Chem.* 2021, 64, 3794–3812

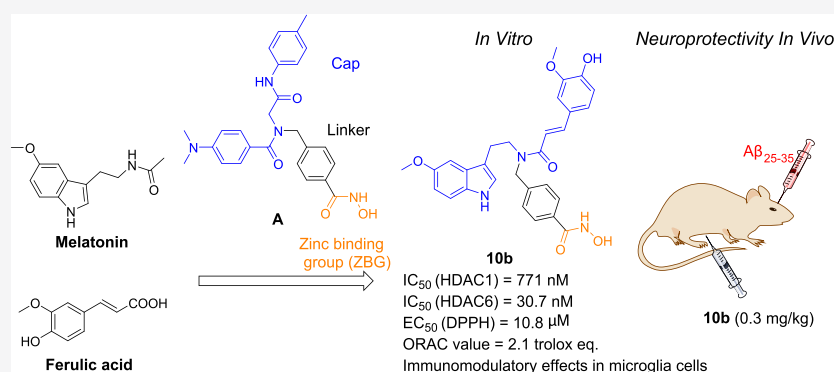
Read Online

ACCESS |

Metrics & More

Article Recommendations

Supporting Information



ABSTRACT: The structures of melatonin and ferulic acid were merged into tertiary amide-based histone deacetylase 6 (HDAC6) inhibitors to develop multi-target-directed inhibitors for neurodegenerative diseases to incorporate antioxidant effects without losing affinity and selectivity at HDAC6. Structure-activity relationships led to compound **10b** as a hybrid molecule showing pronounced and selective inhibition of HDAC6 (IC₅₀ = 30.7 nM, > 25-fold selectivity over other subtypes). This compound shows comparable DPPH radical scavenging ability to ferulic acid, comparable ORAC value to melatonin and comparable Cu²⁺ chelating ability to EDTA. It also lacks neurotoxicity on HT-22 cells, exhibits a pronounced immunomodulatory effect, and is active *in vivo* showing significantly higher efficacy in an AD mouse model to prevent both Aβ_{25–35}-induced spatial working and long-term memory dysfunction at lower dose (0.3 mg/kg) compared to positive control HDAC6 inhibitor ACY1215 and an equimolar mixture of the three entities ACY1215, melatonin and ferulic acid, suggesting potentially disease-modifying properties.

INTRODUCTION

Histone deacetylases (HDACs) are responsible for controlling gene expression by modulating the acetylation status of histone and some nonhistone proteins.¹ HDACs play essential roles in neurodevelopment, memory formation, and cognitive processes, and HDAC inhibitors have been validated as innovative agents for the treatment of neurodegenerative disorders, such as Alzheimer's disease (AD).² Among all 18 subtypes, HDAC6 is of particular interest as it contains two catalytic domains and is mainly cytoplasmic. Moreover, due to its cytoplasmic localization, HDAC6 rather targets nonhistone proteins, such as HSP-90, α-tubulin, β-catenin, and tau protein, which renders HDAC6 to be an interesting target for treatment of neurodegenerative diseases and several rare diseases like Rett syndrome and idiopathic pulmonary fibrosis.^{3–5} It is overexpressed in the brain of AD patients, especially in the cortex and hippocampus.⁶ HDAC6 enables tau protein deacetylation and

modulates tau protein phosphorylation, which aggregates to intracellular neurofibrillary tangles (NFTs) in AD patients.⁷ Phenylhydroxamic acid-based selective HDAC6 inhibitors can activate Nrf2 and hypoxic adaptive response, which contribute to neuroprotection *in vitro* and *in vivo*.⁸ 5-Aroylindole-based HDAC6 inhibitors showed neuroprotective activity by triggering ubiquitination and ameliorated the cognition impairment on a scopolamine-induced AD model in rats, a model reflecting the cholinergic deficit seen in the pathology.⁹ Lastly, given the importance in AD progression of a sustained

Received: November 9, 2020

Published: March 26, 2021



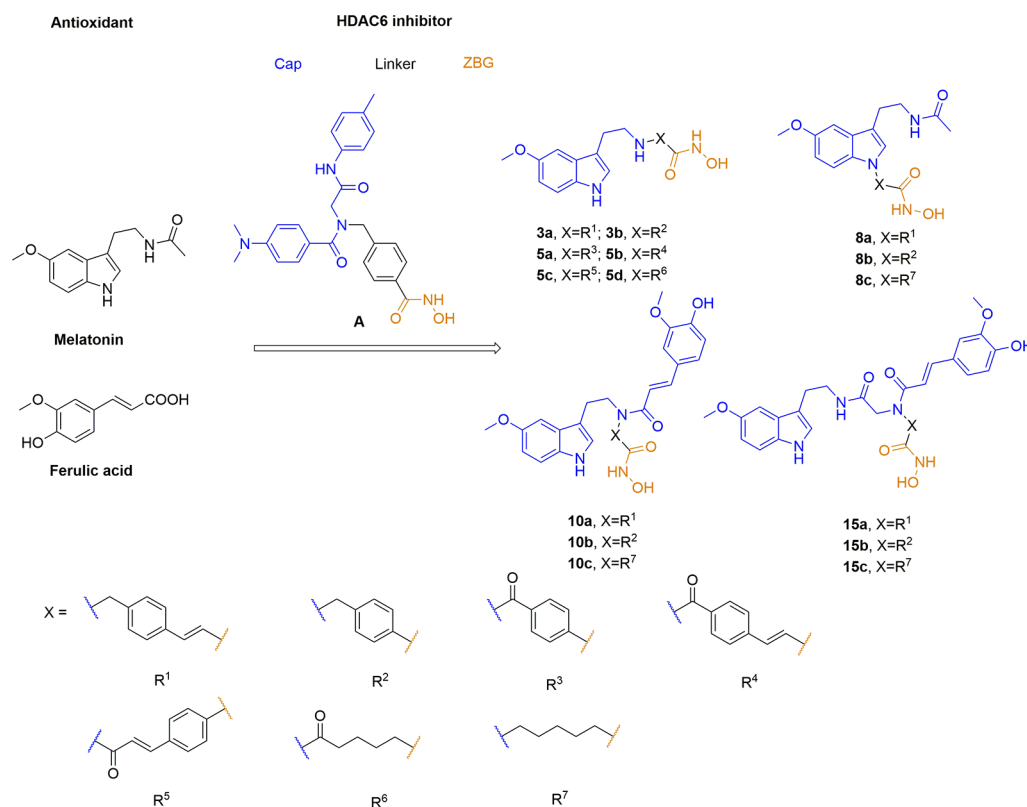


Figure 1. Design of melatonin- and ferulic acid-based HDAC inhibitors.

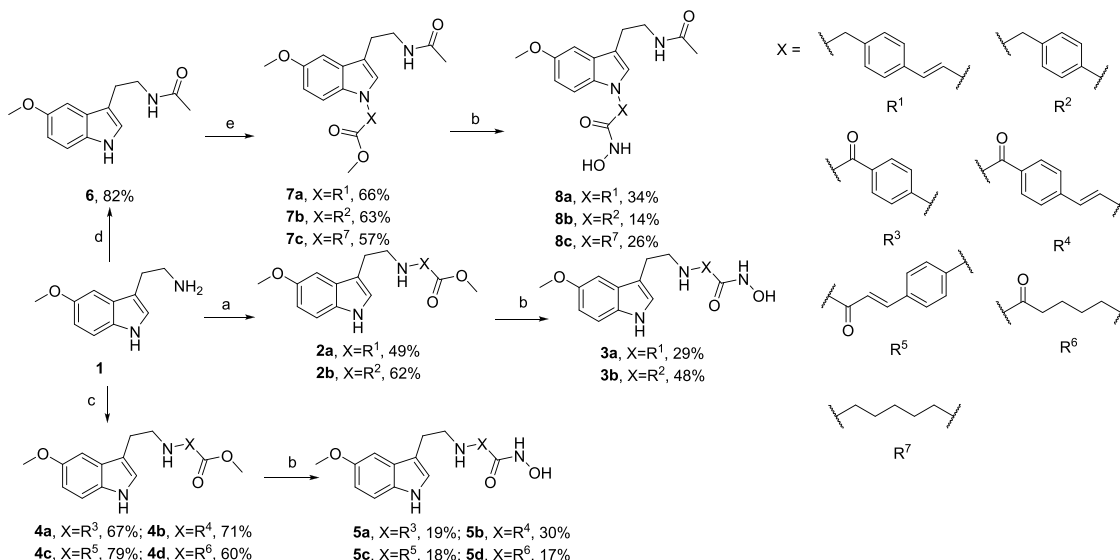
immune response (inflammation) and microglia-related mechanisms in $A\beta$ clearance and production,¹⁰ the potential immunomodulatory activity of HDACs through control of release of cytokines, as well as alteration of activity or function of CNS' macrophages (microglia) and dendritic cells, has been widely investigated.¹¹ Recent studies have demonstrated that manipulation of HDAC6 by tubastatin A (TBSA) alleviates LPS-induced neuroinflammation, representing a new strategy to counteract inflammation and consequently neurodegenerative progression in mice.¹²

Given the multifactorial nature of AD, multitarget compounds being able to simultaneously modulate multiple targets involved in the onset of the disease are promising to restore the physiological balance and generate sufficient therapeutic efficacy. There are several recent reviews covering the design of multitarget compounds.^{13–16} As a new approach for AD treatment, the pharmacophore model of HDAC inhibitors has been designed into multitarget compounds addressing several other related targets, which has been extensively discussed in several comprehensive reviews.^{17–20} Generally, HDAC inhibitors comprise a zinc binding group (ZBG, e.g., hydroxamic acid), a linker mimicking the lysine chain, and a cap group, usually an aromatic group that interacts with the external surface of the enzyme.²¹ Due to the high compatibility of the cap group, it can be replaced by different pharmacophores addressing a second target. The Oyarzabal group has reported HDAC and phosphodiesterase 5 (PDE5) dual-target inhibitor CM-414, which can rescue the impaired long-term potentiation evident in hippocampal slices from APP/PS1 mice and reverse cognitive deficits in Tg2576 mice.^{22–24} Simone *et al.* designed the first-in-class GSK-3 β -HDAC dual inhibitor showing disease-modifying effects *in vitro* for AD.²⁵ The Wu group recently published memantine-

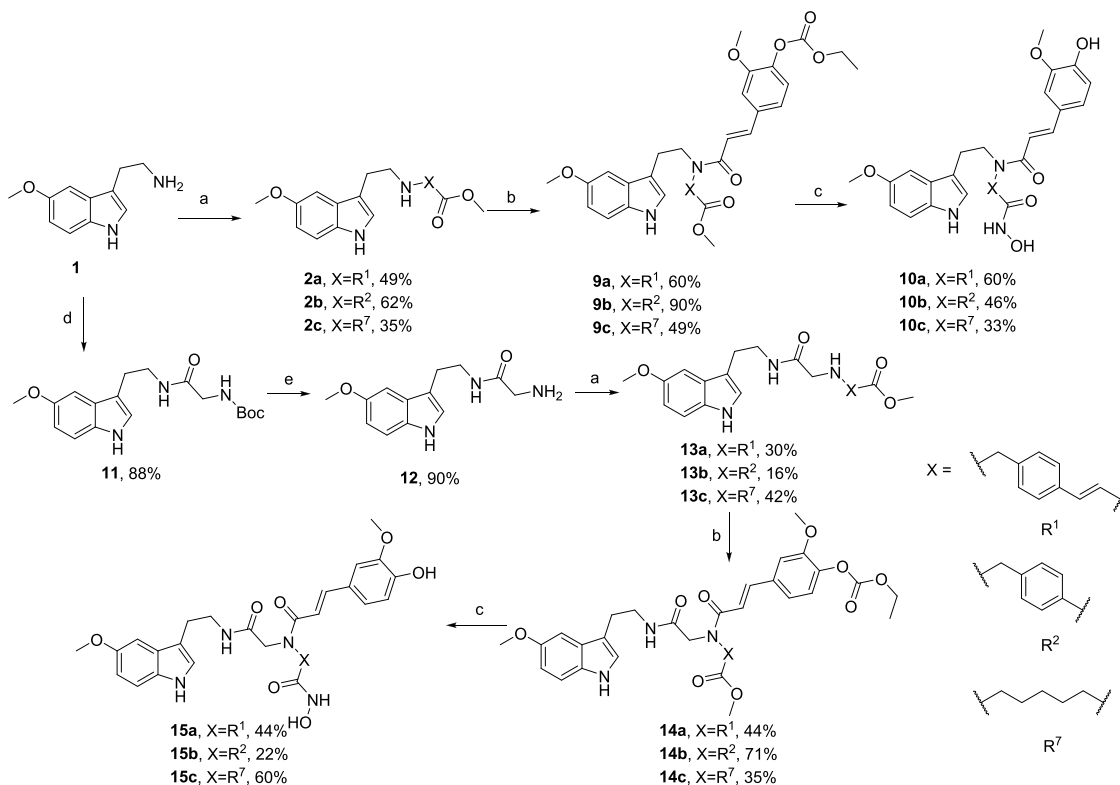
based HDAC-NMDAR and tacrine-based HDAC-ChEs multitarget inhibitors, which exhibit potent neuroprotection, antioxidant, and anti- $A\beta$ -aggregation activities.^{26,27} Tseng *et al.* designed HDAC-AChE multitarget inhibitors that enhance neurite outgrowth and show significant anti- $A\beta$ -aggregation activity.²⁸

Natural products melatonin and ferulic acid have shown promising pharmacological effects potentially beneficial for AD treatment, such as antioxidant effects, neuroprotection, and neurogenesis promotion.^{29–32} In the hippocampus of AD patients, increased melatonin receptor 1 (MT1) and decreased melatonin receptor 2 (MT2) expression has been observed.^{33,34} However, ferulic acid has low bio-availability and poor blood-brain-barrier penetration, melatonin possesses very short biological half time and lack of selectivity, which are present limitations for further clinical application.^{29,30} Nevertheless, pan-HDAC inhibitors based on ferulic acid, tryptamine, or tryptophan all show potent inhibitory activities.^{35–38} For instance, the tryptamine-based HDAC inhibitor panobinostat (LBH589) was approved by the FDA for the treatment of multiple myeloma in 2015.³⁹ In addition, we have recently reported that hybrids of ferulic and cinnamic acids with flavonoids shown pronounced neuroprotection *in vitro*, which also translates to *in vivo* activity. These activities are due to specific interactions with distinct mitochondrial targets.^{40,41}

In this study, we chemically merged the structures of melatonin and ferulic acid into HDAC6 inhibitor A to develop novel multitarget-directed drug candidates for AD with the aim to combine antioxidant effects in a synergistic manner without losing affinity at and selectivity toward HDAC6. Accordingly, 15 target compounds have been designed (Figure 1), synthesized, and bioevaluated. Compounds 3a and 3b were designed with two aromatic linker groups to replace the acetyl

Scheme 1. Synthesis of Target Compounds 3a–3b, 5a–5d and 8a–8c from 5-Methoxytryptamine (1)^a

^aReagents and conditions: (a) methyl (*E*)-3-(4-(bromomethyl)phenyl)acrylate for 2a, methyl 4-(bromomethyl)benzoate for 2b, K₂CO₃, THF, H₂O, reflux; (b) NH₂OH·HCl, KOH, MeOH, r.t.; (c) (*E*)-4-(3-methoxy-3-oxoprop-1-en-1-yl)benzoic acid for 4a, 4-(methoxycarbonyl)benzoic acid for 4b, (*E*)-3-(4-(methoxycarbonyl)phenyl)acrylic acid for 4c, 6-methoxy-6-oxohexanoic acid for 4d, TBTU, TEA, THF, r.t.; (d) acetic anhydride, DCM, 0 °C to r.t.; (e) (i) methyl (*E*)-3-(4-(bromomethyl)phenyl)acrylate for 7a, methyl 4-(bromomethyl)benzoate for 7b, methyl 6-bromohexanoate for 7c, *t*-BuOK, THF, reflux; (ii) SOCl₂, MeOH, r.t.; (f) ferulic acid, ethyl chloroformate, TEA, dried THF, 0 °C; (g) Boc-Gly-OH, EDCI, DMAP, TEA, THF, r.t.; (h) 10% TFA in DCM, r.t.

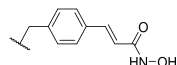
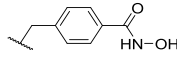
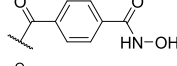
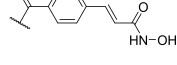
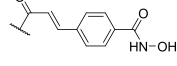
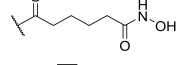
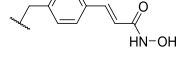
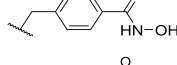
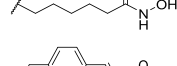
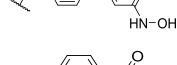
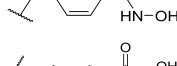
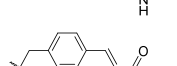
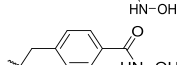
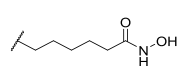
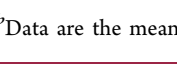
Scheme 2. Synthesis of Target Compounds 10a–10c and 15a–15c from 5-Methoxytryptamine (1)^a

^aReagents and conditions: (a) methyl (*E*)-3-(4-(bromomethyl)phenyl)acrylate for 13a, methyl 4-(bromomethyl)benzoate for 13b, methyl 6-bromohexanoate for 13c, K₂CO₃, THF, H₂O, reflux; (b) ferulic acid, ethyl chloroformate, TEA, dried THF, 0 °C; (c) NH₂OH·HCl, KOH, MeOH, r.t.; (d) Boc-Gly-OH, EDCI, DMAP, TEA, THF, r.t.; (e) 10% TFA in DCM, r.t.

group; similarly, compounds 5a–5d incorporate four linker groups in the same position and maintain the amide linkage to study SARs and evaluate the importance of the amide linkage.

The linker groups of compounds 8a–8c were introduced at the indole nitrogen atom, this design makes the linker groups not as long as the linker group in ethylamine position, and the

Table 1. Structures, *In Vitro* HDAC (HDAC3 and HDAC6) Inhibitory, DPPH Radical Scavenging Activities, and ORAC Values of Target Compounds

Compound	R	IC ₅₀ HDAC3 [nM] or Inhibition [%] at 1 μM (pIC ₅₀ ± SEM) (n=2)	IC ₅₀ HDAC6 [nM] or Inhibition [%] at 1 μM (pIC ₅₀ ± SEM) (n=2)	Selectivity Ratio to HDAC6	DPPH Radical Scavenging Activity EC ₅₀ [μM] ^b	ORAC (trolox equivalents) ^c
ACY1215	-	51.0 ^a	4.7 ^a	11	255 ± 20.2	0.5 ± 0.1
Melatonin	-	-	-	-	> 6 mM	2.0 ± 0.3
Ferulic acid	-	-	-	-	13.7 ± 0.5	3.1 ± 0.3
3a		5.1 (8.29 ± 0.09)	21.4 (7.67 ± 0.03)	< 1	17.1 ± 2.8	2.4 ± 0.1
3b		26%	43%	-	66.7 ± 8.8	3.0 ± 0.2
5a		87%	88%	-	62.0 ± 1.0	2.4 ± 0.2
5b		3.6 (8.45 ± 0.05)	19.1 (7.72 ± 0.03)	< 1	25.2 ± 1.9	2.0 ± 0.4
5c		19.7 (7.71 ± 0.11)	33.7 (7.47 ± 0.06)	< 1	65.0 ± 5.8	2.0 ± 0.1
5d		25%	-69%	-	292 ± 2.1	3.0 ± 0.2
8a		182 (6.74 ± 0.08)	68.8 (7.16 ± 0.05)	3	31.4 ± 6.5	1.4 ± 0.1
8b		641 (6.19 ± 0.09)	11.2 (7.95 ± 0.06)	57	56.3 ± 9.6	1.6 ± 0.2
8c		494 (6.31 ± 0.10)	52.3 (7.28 ± 0.04)	9	262 ± 29.3	1.6 ± 0.3
10a		163 (6.79 ± 0.06)	25.6 (7.59 ± 0.06)	6	8.5 ± 0.8	1.0 ± 0.2
10b		1,613 (5.79 ± 0.16)	30.7 (7.51 ± 0.06)	53	10.8 ± 1.9	2.1 ± 0.3
10c		811 (6.09 ± 0.10)	353 (6.45 ± 0.04)	2	8.9 ± 0.9	2.8 ± 0.1
15a		108 (6.97 ± 0.09)	53.2 (7.27 ± 0.04)	2	8.3 ± 0.4	1.2 ± 0.4
15b		-14%	19%	-	15.2 ± 1.3	1.6 ± 0.2
15c		121 (6.92 ± 0.10)	57.0 (7.24 ± 0.03)	2	19.1 ± 1.1	3.2 ± 0.4

^aData from ref 48. ^bData are the mean ($n = 3$) ± SD. ^cData are expressed as Trolox equivalents and are the mean ($n = 3$) ± SD.

structures are less flexible, which is supposed to produce higher HDAC6 selective inhibition. Melatonin and ferulic acid as the

cap group were merged into one entity for compounds **10a–10c** and **15a–15c** aiming to produce stronger HDAC6

Table 2. Inhibitory Activities of Compounds 8b and 10b at HDAC1–4 and HDAC6–9

HDAC classes	subtype	8b		10b	
		IC ₅₀ (nM) (pIC ₅₀ ± SEM) (n = 2)	selectivity ratio to HDAC6	IC ₅₀ (nM) (pIC ₅₀ ± SEM) (n = 2)	selectivity ratio to HDAC6
class I	HDAC1	262 (6.58 ± 0.07)	23	771 (6.11 ± 0.09)	25
	HDAC2	336 (6.47 ± 0.09)	30	2851 (5.55 ± 0.41)	93
	HDAC3	641 (6.19 ± 0.09)	57	1613 (5.79 ± 0.16)	53
	HDAC8	838 (6.08 ± 0.23)	75	3590 (5.45 ± 0.54)	117
class IIa	HDAC4	3431 (5.47 ± 0.06)	306	>10 μM	>326
	HDAC7	1653 (5.78 ± 0.10)	148	>10 μM	>326
	HDAC9	362 (6.44 ± 0.11)	32	>10 μM	>326
class IIb	HDAC6	11.2 (7.59 ± 0.06)		30.7 (7.51 ± 0.06)	

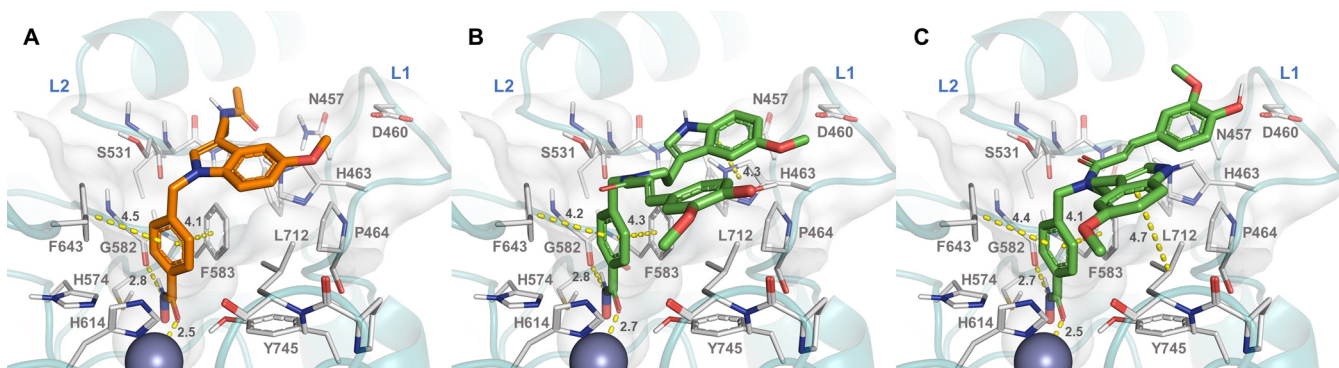


Figure 2. Proposed binding modes of compounds 8b (A) and 10b (B, C) at the active site of HDAC6. The two alternative binding modes shown for 10b correspond to the best-ranked result (B) and the most populated cluster of the docking results (C). Distances are given in Å; selected interactions are highlighted with dashed lines. The Zn²⁺ ion is represented as a grey sphere. Loops 1 and 2 are denoted as L1 and L2. The deep active-site pocket is visualized with a transparent light-grey surface.

selective inhibition and more pronounced antioxidant capacity.²¹

RESULTS AND DISCUSSION

Chemistry. In Scheme 1, the syntheses of target compounds 3a, 3b, 5a–5d, and 8a–8c are described starting from 5-methoxytryptamine (1). Corresponding linker groups were introduced to the ethylamine position of 5-methoxytryptamine (1) by stirring with potassium carbonate in a mixture of THF and water to afford intermediates 2a and 2b. The formation of dual-substituted byproducts lowered the yields of this step, especially the synthesis of intermediate 2c presented in Scheme 2. Amide condensation to form intermediates 4a–4d were carried out after corresponding carboxylic acids had been activated by TBTU and stirred with compound 1, which gave reasonable yields of 60–79%. Melatonin (6) formed by acetylation of compound 1 was refluxed with corresponding bromides and *t*-BuOK in THF; meanwhile, the ester groups were hydrolyzed. The obtained crude carboxyl intermediates were therefore esterified in methanol after activation with thionyl chloride to afford intermediates 7a–7c.

The key step to synthesize compounds 10a–10c was the introduction of a ferulic acid moiety, which was introduced into intermediates 2a–2c to produce the tertiary amides (Scheme 2). First, the carboxyl group of ferulic acid was activated by excess ethyl chloroformate; then the phenolic hydroxyl group was esterified and could be hydrolyzed in NH₂OH-KOH methanol solution during the formation of the hydroxamate group. BOC-Gly-OH reacted with 5-methoxytryptamine (1) after it had been activated with EDCI, and the Boc protecting group was removed in 10% TFA in dichloromethane to afford intermediate 12. Subsequently, compounds

15a–15c were obtained through procedures similar to the synthesis of compounds 10a–10c. All ester intermediates 2a, 2b, 4a–4d, 7a–7c, 9a–9c, and 14a–14c were converted to hydroxamic acid compounds 3a, 3b, 5a–5d, 8a–8c, 10a–10c, and 15a–15c, respectively, by NH₂OH-KOH in methanol. Purification of target compounds proved challenging because of a carboxylic acid byproduct formed and adsorbed on silica gel.

Due to the tertiary amide groups of compounds 10a–10c and 15a–15c, the occurrence of *cis/trans* amide bond rotamers was observed, which possess two sets of NMR signals, arising from the restricted rotation around the tertiary amide bond for each rotamer. Since this phenomenon had already been discussed in detail in several publications,^{42–44} variable temperature NMR studies (VT-NMR) for these compounds did not deem necessary.

Inhibition of HDACs. To evaluate selectivity toward HDAC6 and extent of inhibition, a fluorescence assay against HDAC3 and HDAC6 was applied to test the target molecules (Table 1).⁴⁵ At 1 μM, compounds 3b, 5a, 5d, and 15b show less potent inhibition of both HDAC3 and HDAC6 than all other target compounds. Compounds 3b, 5a, and 5d share similar lengths of linker groups, which are shorter than the cinnamate group in compounds 3a, 5b, and 5c, indicating that the longer linker (like a cinnamate group) is preferable. For comparison, compounds 8b and 10b show the highest selectivity values regarding HDAC6 inhibition, namely, 57-fold and 53-fold, respectively, over HDAC3. Interestingly, compounds 8b and 10b share the same phenylhydroxamic acid with different bulky capping groups, being in line with the other reported selective HDAC6 inhibitors.²¹ Also, due to the longer linker and its high flexibility, compounds 3a, 3b, and

5a–5d exhibit less selective inhibition of HDAC6 compared to the other compounds. On the contrary, compounds **3a** and **5b** show the most potent inhibition to HDAC3 with IC_{50} values of 5.1 and 3.6 nM, respectively, which is more pronounced than their inhibition of HDAC6. Compounds **5b** and **3a** with or without the amide linkage showed no differences in the extent of HDAC inhibition.

To further confirm selective inhibition of compounds **8b** and **10b** over other HDACs, their IC_{50} s at other Zn^{2+} -dependent HDACs (HDAC1–9) were measured (Table 2). Both compounds show highly selective inhibition (more than 23-fold over other subtypes) toward HDAC6, and their selectivity values are higher than those of reference compound ACY1215. The results further validate the importance of phenylhydroxamic acid with bulky capping groups to yield pronounced HDAC6 selective inhibition.

Computational docking studies were carried out to identify putative binding modes of compounds **8b** and **10b** for HDAC6. The protein structure from the crystallographically determined complex of HDAC6 with reference compound **A** (PDB: 6DVM)²¹ was used for this purpose. For compound **8b**, a well-clustered top-ranked docking result was obtained in which the phenylhydroxamate binds to the deep active-site tunnel in a previously reported conformation.^{21,46,47} The hydroxamate shows a monodentate coordination to the zinc ion at 2.5 Å and a hydrogen-bonding interaction with Gly582 at 2.8 Å distance (Figure 2A). The phenyl linker is sandwiched in the tunnel between Phe583 and Phe643 at 4.1 and 4.5 Å, respectively. The melatonin-based capping group is positioned in a pocket at the outer rim of the active site, flanked by the L1 loop. The indole moiety is oriented toward His463 and Pro464, while the extended amide might accept a hydrogen bond from Asn457. For compound **10b**, two binding modes appear feasible for the capping groups, which are placed above the pocket flanked by loop L1 but can be switched in their orientation (Figure 2B,C). In the best binding pose according to the DSX scoring function⁴⁹ (cf. the Supporting Information for further details), aromatic interactions of the indole moiety with His463 appear to be feasible, whereas the hydroxymethoxyphenyl ring shows van der Waals interactions with Leu712. In the switched orientation, which is somewhat less favorably scored by DSX but found more frequently in the docking runs, the indole is placed above Leu712, whereas the hydroxy group of the ferulic acid-based moiety can reach Asp460 for a hydrogen-bond interaction. Based on the docking results for both compounds, binding of the capping groups to the L1 loop pocket can be assumed to be the likely reason for HDAC6 selectivity, in line with the elegant crystallographic analyses presented by Porter et al.²¹

To examine the cellular potency and selectivity of compounds **10b** and **8b**, acetylated tubulin and acetylated histone H3 and H4 were examined in HT-22 cells (Figure 3). As expected, **10b** strongly induced the increase of acetylated tubulin (AcTub), while a little-to-no increase was observed for acetylated histone H3 and H4 (AcHH3 and AcHH4). Compound **8b** also selectively increases the level of AcTub at 500 μ M. The Western blot data indicate that both **10b** and **8b** are selectively inhibiting HDAC6 activity but not the class I HDACs targeting histone acetylation.

Antioxidant Activities. By combination of antioxidants melatonin and ferulic acid, compounds were designed to maintain their antioxidant capacity. Their antioxidant capacities were evaluated using both 2,2-diphenyl-1-picrylhy-

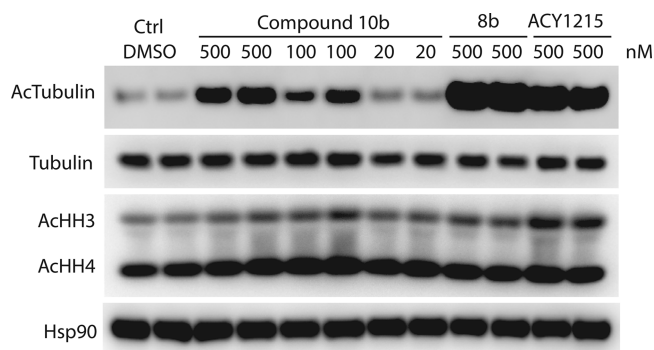


Figure 3. Western blot analysis of acetylated tubulin (AcTubulin), acetylated histone H3 (AcHH3), acetylated histone H4 (AcHH4), and Hsp90 in HT22 cell lines after 24 h treatment with compounds **10b** (500, 100, and 20 nM) and **8b** (500 nM) using ACY1215 (500 nM) as a positive control. Tubulin was used as a loading control.

drazyl radical (DPPH) and oxygen radical absorbance capacity (ORAC) assays. These assays are well-established techniques for determining the radical scavenging activity (RSA) of a test compound. Reactive oxygen species (ROS), such as the hydroxyl or superoxide radicals, cause lipid peroxidation, protein oxidation, and DNA damage, which can lead to organelles malfunction and further cellular disorders.⁵⁰

Melatonin is inactive regarding inactivation of the DPPH radical, and HDAC6 inhibitor ACY1215 shows only weak scavenging activities. Among all target compounds, tertiary amide-based compounds **10a**, **10c**, and **15a** show the highest radical scavenging ability, and compound **10b** is comparable to ferulic acid. Various linker groups also affect radical scavenging activities: the compounds bearing the cinnamate group (e.g. compounds **3a**, **5b** and **8a**) exhibit stronger scavenging activities than compounds bearing a phenylene (e.g. compounds **3b**, **5a** and **8b**) or an alkylene chain (e.g. compounds **5d** and **8c**), respectively. ACY1215 also shows higher radical scavenging activity than melatonin indicating that the hydroxamic acid group is supportive to scavenge the DPPH radical. The ORAC values shown in Table 1 are expressed as trolox (water-soluble analogue of vitamin E) equivalents (TE), in relation to radical scavenging properties of trolox. Ferulic acid and melatonin were used as positive controls showing ORAC values of 3.1 and 2.0, respectively. All evaluated compounds exhibit strong radical scavenging properties with TE values ranging from 1.0 (**10a**) to 3.2 (**15c**). HDAC6 selective compound **10b** possesses a TE value of 2.1, which is comparable to melatonin. Compounds **8a–8c** show lower TE values than melatonin and most other compounds tested, indicating the importance of unsubstituted indole-N to maintain the antioxidant capacity of melatonin. There is no obvious effect for amide linkage regarding DPPH scavenging or TE values in compounds **5a** and **3a**, **5b** and **3b**. Compounds **15a–15c** show no significant difference to compounds **10a–10c**, which means that the presence of an acetyl group is not necessary. Introduction of one alkylene chain is much more effective than aromatic linkers, as seen from the TE values of compounds **5d**, **10c**, and **15c**, respectively. Also, the presence of ferulic acid moiety is poorly correlated with the observed TE values unlike for the DPPH radical scavenging capacity.

Cerebral biometals (such as copper, zinc, and iron) play crucial roles in $A\beta$ aggregation and neurotoxicity, being a driving force for neurodegeneration in AD.⁵¹ As shown in Figure S1, compounds **8b**, **10b**, and ACY1215 exhibit

comparable chelating abilities to each other at all concentrations tested and also comparable abilities to EDTA when chelating copper ions. In contrast to nonselective chelation of EDTA, compounds **8b**, **10b**, and ACY1215, respectively, show higher selectivity to the copper ion over ferrous and zinc ions, which might render them superior regarding copper-ion dysregulation-related neurodegeneration diseases like AD.⁵²

In a summary, compounds **8b** and **10b** show the best selective HDAC6 inhibition and additional potent total antioxidant capacities, especially, compound **10b** exhibits comparable radical scavenging capacities to both ferulic acid and melatonin in DPPH assay and ORAC assay, respectively.

Neurotoxicity. HDAC inhibitors usually possess high cytotoxicity, which might counteract their application as CNS-targeting therapeutics. Hence, it was important to investigate their neurotoxicity profile. A survival assay was performed, treating murine hippocampal neuronal HT-22 cells with 10 μ M of each of the target compounds (Figure 4).

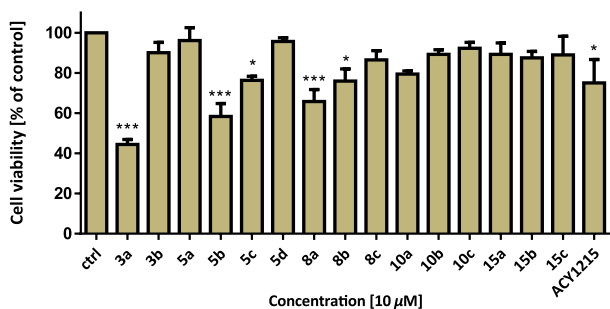


Figure 4. Neurotoxicity of target compounds in HT-22 cells at 10 μ M. Statistical analysis was performed applying One-way ANOVA followed by Dunnett's multiple comparison post-test. Levels of significance: *** $p < 0.001$, * $p < 0.05$ referring to control cells treated with DMSO.

Generally, the compounds proved to be safe and showed no neurotoxicity. Compound **10b** showed no significant neurotoxicity, and slight neurotoxic effects were observed for compound **8b** and reference compound ACY1215.

Interestingly, compounds **3a** and **5b** also showed some neurotoxic effects with 50 and 60% cell survival, respectively. This is not too surprising due to their potent inhibition of HDAC3 and might even be beneficial for further anticancer research. With 10 μ M, a relatively high concentration was tested and the viability rates should not counteract beneficial effects.

As shown in Figure S2 (cf. Supporting Information), the neuroprotection of target compounds against glutamate-induced oxytosis and iodoacetic acid-induced ATP depletion in HT-22 cells has been tested; only compound **10a** revealed significant neuroprotection at 50 μ M.

Immunomodulatory Effect. Activation of microglia cells, *i.e.*, CNS' macrophages, is a hallmark of neuroinflammation, a characteristic feature of neurodegenerative conditions. Depending on brain microenvironment, microglia acquire different phenotypes: the neurotoxic M1 phenotype, generally characterized by production of proinflammatory cytokines (TNF- α , IL-1 β) or reactive oxygen species (ROS), or the neuroprotective M2 phenotype distinguished by the expression of phagocytic protein TREM2 and of growth factors, such as TGF β 2.⁵³ To analyze the possible immunomodulatory activity, *i.e.*, the ability to shift the microglial phenotype from the

neurotoxic M1 to the neuroprotective M2, of HDACs inhibitors **8b**, **10b**, and control ACY1215, N9 microglial cells were treated with increasing concentration of compounds (0.1, 0.5, 1, 2.5, 5 μ M) in the presence or absence of 100 ng/mL LPS (lipopolysaccharide), which induces an M1 activation state. After 24 h of treatment, to investigate nitric oxide and IL1 β release, markers of M1 microglia, conditioned media were collected and evaluated by a colorimetric assay based on the Griess reaction and Western blot analysis, respectively. In parallel, cell lysates were analyzed by Western blot to measure the expression of the inducible nitric oxide synthase (iNOS, M1 marker), TREM2 and TGF β 2, both markers of M2 microglia. As shown in Figure 5, compound **10b** strongly reduces in dose-dependent manner nitrite accumulation (F) and IL1 β release (I) compared to compound **8b** and control ACY1215, as well as iNOS expression induced by LPS-mediated microglia activation (L). Additionally, compound **10b** leads to an increase in the phagocytic protein TREM2 (O) and TGF β 2 (R) expression, suggesting an immunomodulatory effect, *i.e.*, a switch from neurotoxic M1 to neuroprotective M2 microglia when cells are treated with high concentration of the compound (2.5, 5 μ M). Differently, no change in TREM2 and TGF β 2 expression was observed in the presence of increasing concentration of compound **8b** (E, H, K, N, Q).

In Vivo Studies. Due to its promising *in vitro* properties, compound **10b** was chosen to evaluate its neuroprotective properties in an *in vivo* model of AD in mice. The HDAC6 inhibitor ACY1215 was also tested as a comparator. Mice received an intracerebroventricular (icv) injection of the oligomerized A β _{25–35} peptide into the brain on day 1. Compounds were then injected intraperitoneally (ip) once daily (o.d.) from days 1 to 7. Spatial working memory was evaluated using the spontaneous alternation behavior when mice explored a Y maze, on day 8. Nonspatial long-term memory was analyzed using the step-through passive avoidance response, with training on day 9 and retention on day 10. In this administration scheme, not symptomatic effects, but neuroprotectivity can be assessed *in vivo*.^{54–57}

As shown in Figure S3 (cf. Supporting Information), none of the treatment (DMSO containing a vehicle or each compound) significantly affected the mouse body weight gain during the week of administration showing good tolerability. A transient weight loss was observed on day 2, related to the icv injection of the peptide under light gaseous anesthesia, but animals recovered during the following days.

As shown in Figure 6A,C, compound **10b** significantly attenuated the A β _{25–35}-induced spontaneous alternation deficits at a lower dose, 0.3 mg/kg, compared to ACY1215, active at 1 mg/kg. The compound **10b** was active in the 0.3–1 mg/kg dose-range, reflecting a more potent neuroprotective effect on working memory deficits. The hybrid molecule **10b** was compared to an equimolar (0.7 μ M) mixture of the three entities ACY-1215, melatonin, and ferulic acid (Figure 6E). Melatonin did not prevent A β _{25–35}-induced alternation deficits at this low, 0.16 mg/kg dose, and neither did the mixture. None of the treatment affected the exploratory response, measured in terms of number of arms entered during the session (Figure 6B,D,F).

In the passive avoidance test, compound ACY1215 attenuated the A β _{25–35}-induced deficit at all doses tested, but not significantly vs the A β _{25–35}-injected group (Figure 7A). Compound **10b** attenuated the deficit at both 0.1 and 0.3 mg/kg, significantly at the lowest dose tested, but was not active at

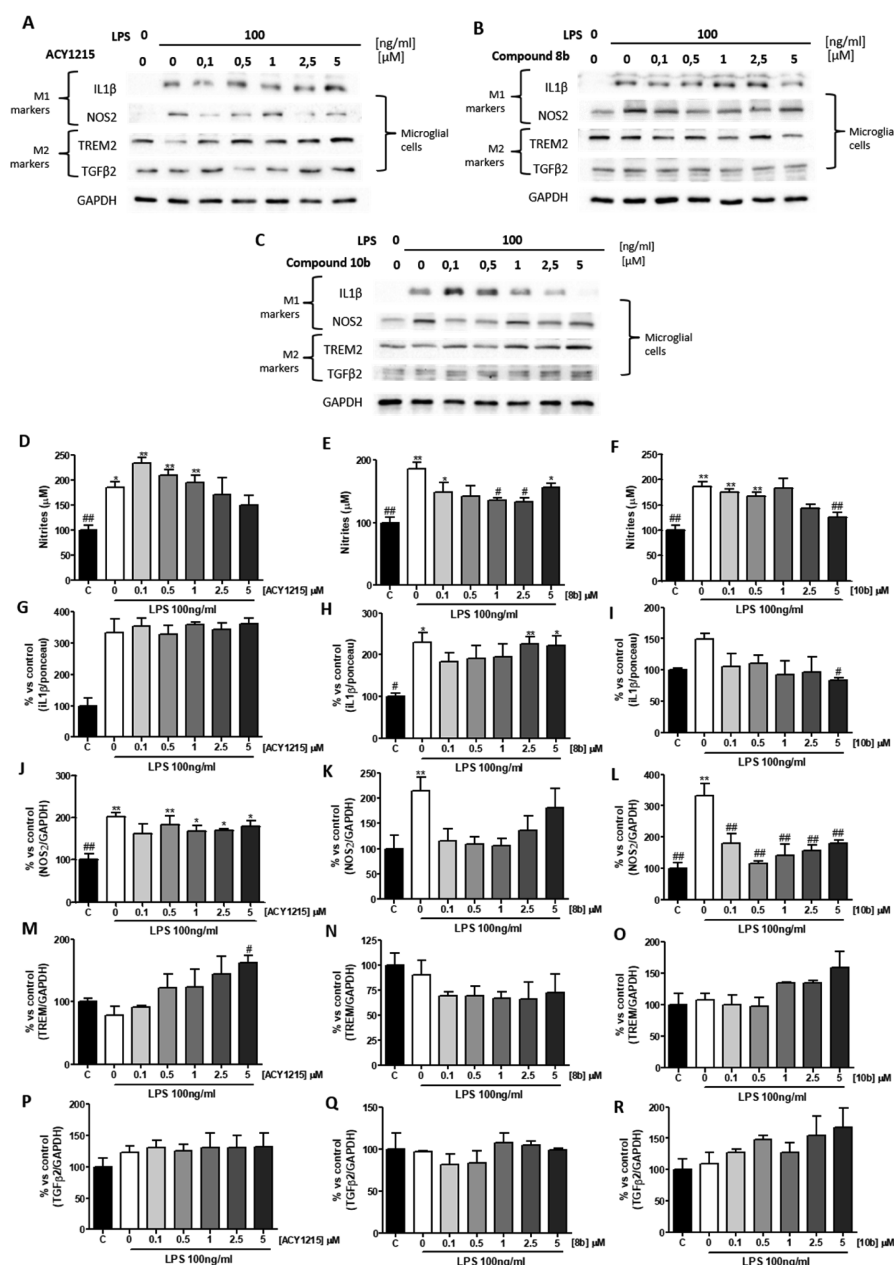


Figure 5. Effect of compounds **8b**, **10b** and control ACY1215 on murine N9 cells induced in a M1 activation state by LPS (100ng/mL) treatment. IL1 β release in N9-conditioned medium and expression of iNOS, TREM2 and TGF β 2 were analyzed by western blot after 24h treatment with LPS in presence of increasing concentrations (0.1, 0.5, 1, 2.5 and 5 μ M) of compounds ACY1215 (A), **8a** (B) and **10b** (C). Nitric Oxide release was evaluated through Griess reaction in media conditioned for 24h by microglial cells treated with LPS in presence of compounds ACY1215 (D), **8a** (E) and **10b** (F); as shown in figure F, only compound **10b** induced a significant reduction of NO release, with the strongest effect at 5 μ M. Additionally, IL1 β release and iNOS expression, both markers of M1 neurotoxic microglia, strongly decreased in the presence of increasing concentrations of compound **10b** compared to LPS-treated control (I, L); conversely, no significant effects were observed on N9 cells following ACY1215 (G, J), and **8a** (H, K) treatment. In parallel, expression of M2 microglial marker TREM2 increased in cells co-treated by LPS-**10b** (O) and LPS-ACY1215 (M) compounds, whereas no significant effects in TREM2 expression were obtained following LPS-**8a** treatment (N). In addition, compared to ACY1215 (P) and **8a** (Q), in LPS-**10b** treated cells TGF β 2 expression turned out to increase (R) suggesting, together with TREM expression (O), a shift from neurotoxic M1 to neuroprotective M2 microglia. All quantitative data are presented as means \pm S.E. from at last 3 independent experiments. Statistical significance between different treatments was calculated with GRAPHPAD PRISM 6 (La Jolla, California, USA) by using one-way analysis of variance (ANOVA) followed by post-hoc comparison through Bonferroni's test. * p <0.05; ** p <0.01 compared to un-treated control; # p <0.05; ## p <0.01 compared to LPS-treated control.

1 mg/kg (Figure 7B). These bell-shaped dose–response effects are commonly observed in cognitive and neuroprotection responses *in vivo*, as shown recently with the NMDAR antagonist memantine in the same A β _{25–35} mouse model of AD.⁵⁷ They are here observed in our study for both ACY1215

and **10b** at the 1 mg/kg dose, suggesting that this biphasic effect relies on HDAC6 inhibition. Melatonin or the equimolar mixture of the three compounds failed to attenuate A β _{25–35}-induced passive avoidance deficit, again showing the pronounced effect of the hybrid molecule (Figure 7C).

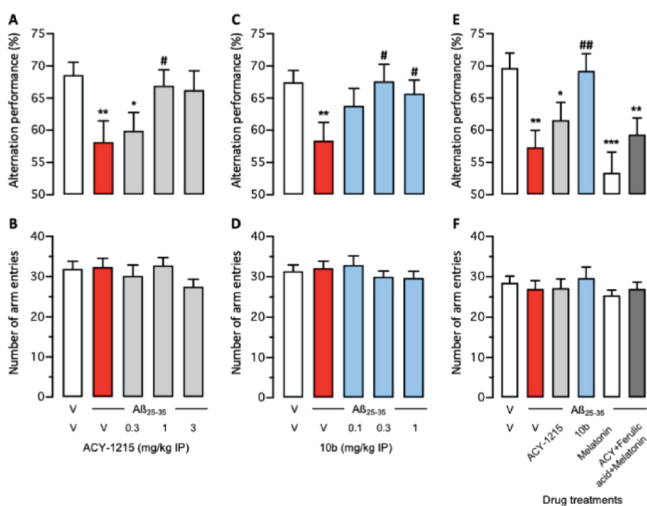


Figure 6. Effects of compound on the $A\beta_{25-35}$ -induced spontaneous alternation deficit in mice. Mice received $A\beta_{25-35}$ (9 nmol icv) or vehicle solution (3 μ L icv) on day 1 and compounds (A, B) ACY1215 or (C, D) 10b, in the 0.1–3 mg/kg ip dose range, o.d., from days 1 to 7. In (E, F), the effect of a drug combination with equimolar doses of ACY-1215 (0.3 mg/kg), melatonin (0.16 mg/kg), and ferulic acid (0.13 mg/kg) was compared to the efficacy of the hybrid molecule. Mice were then tested for spontaneous alternation performance in the YMT in day 8. Top panel (A, C, and E): spontaneous alternation performance; lower panel (B, D, and F): number of arm entries. Data show mean \pm SEM with $n = 12$ –22 per group. ANOVA: $F_{(4,76)} = 2.81$, $p < 0.05$ in (A); $F_{(4,86)} = 2.68$, $p < 0.05$ in (B); $F_{(4,76)} = 1.16$, $p > 0.05$ in (C); $F_{(4,86)} = 0.581$, $p > 0.05$ in (D); $F_{(5,76)} = 6.20$, $p < 0.0001$ in (E); $F_{(5,76)} = 0.554$, $p > 0.05$ in (F). * $p < 0.05$, ** $p < 0.01$, *** $p < 0.001$ vs (V + V)-treated group. # $p < 0.05$, ## $p < 0.01$ vs ($A\beta_{25-35}$ + V)-treated group; Dunnett's test.

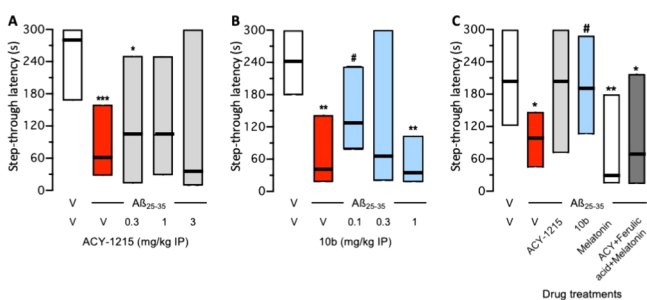


Figure 7. Effects of compounds on $A\beta_{25-35}$ -induced passive avoidance deficits in mice. Mice received $A\beta_{25-35}$ (9 nmol icv) or vehicle solution (3 μ L icv) on day 1 and compounds (A) ACY1215 and (B) 10b, in the 0.1–3 mg/kg ip dose range, o.d., from days 1 to 7. Animals were trained in the passive avoidance test on day 9, and retention (step-through latency) was analyzed on day 10. Data show the median and interquartile range with $n = 10$ –21 per group. Kruskal–Wallis ANOVA: $H = 10.76$, $p < 0.05$ in (A); $H = 16.59$, $p < 0.01$ in (B); $H = 14.25$, $p < 0.05$ in (C). * $p < 0.05$, ** $p < 0.01$, *** $p < 0.001$ vs (V + V)-treated group. # $p < 0.05$ vs ($A\beta_{25-35}$ + V)-treated group; Dunn's test.

Compound 10b therefore exhibited a remarkably effective neuroprotective properties *in vivo* at sub-mg/kg active dose-range against $A\beta_{25-35}$ -induced memory dysfunction, suggesting that HDAC6 inhibition could be an effective neuroprotective strategy for the treatment of AD.

CONCLUSIONS

In this work, we designed hybrid HDAC inhibitors by chemically merging the structures of melatonin and ferulic acid into the HDAC6 inhibitor to develop novel multitarget-directed drug candidates for AD with the aim to combine effects in a synergistic manner without losing affinity and selectivity at HDAC6. Altogether, 15 target compounds have been designed, synthesized, and evaluated comprehensively in several *in vitro* and *in vivo* assays.

The newly synthesized compounds were firstly evaluated for inhibition of HDACs. Melatonin-based compound 8b and melatonin-ferulic acid-based compound 10b show the highest HDAC6 inhibition with more than 20-fold selectivity over other subtypes and maintaining two-digit nanomolar IC_{50} s. Compound 8b and 10b also maintain the antioxidant capacities from melatonin and ferulic acid, especially compound 10b, which scavenges the DPPH radical comparable to ferulic acid and possesses the comparable ORAC value with regard to melatonin. Compound 10b does not exhibit neurotoxicity at 10 μ M and comparable Cu^{2+} chelating ability to the positive control and potent chelator EDTA, which indicates beneficial effects for reduction of metal-mediated oxidative stress, tau, and $A\beta$ aggregation.⁵²

Compound 10b shows an immunomodulatory effect, leading to a reduction in LPS-induced microglia inflammation and to a switch from neurotoxic M1 to the neuroprotective M2 microglial phenotype. Furthermore, it shows pronounced attenuation of spatial working memory and long-term memory alteration in an *in vivo* AD mouse model induced by icv $A\beta_{25-35}$ peptide injection, at very low doses, thereby proving neuroprotective properties. The superior *in vivo* efficacy of compound 10b may indicate a synergistic effect between HDAC6 inhibition and its antioxidant activities. In addition or alternatively, interaction with MT receptors is possible since expression levels of both MT receptor subtypes are altered in AD and melatonin was reported to rescue neurogenesis impairment by multiple modes of action,^{31–34} as well as beneficial pharmacokinetic properties. In any case, the tertiary amide-based HDAC6 selective inhibitor described herein shows that HDAC6 inhibitors cannot only be merged with melatonin and ferulic acid moieties and also maintain potent HDAC6 selective inhibition and the antioxidant properties but also represent a suitable scaffold to develop neuroprotective compounds *in vivo*, with potentially neurodegenerative disease-modifying properties.

EXPERIMENTAL SECTION

General Chemistry. Common reagents and solvents were purchased from commercial suppliers and used without further purification unless otherwise stated. Tetrahydrofuran (THF) was distilled from sodium-benzophenone under an argon atmosphere. Reaction progress was monitored using analytical thin-layer chromatography (TLC) on precoated silica gel GF254 plates (Macherey Nagel GmbH & Co. KG, Düren, Germany), and spots were detected under UV light (254 and 366 nm). Compounds were purified with flash column chromatography with a silica gel and particle size of 40–63 μ M (VWR chemicals, Leuven, Belgium) as the stationary phase and petroleum ether/ethyl acetate or dichloromethane/methanol mixtures as eluent systems. Nuclear magnetic resonance spectra were measured on a Bruker AV-400 NMR instrument (Bruker, Karlsruhe, Germany) in deuterated solvents ($DMSO-d_6$, $CDCl_3$, $MeOD-d_4$). Chemical shifts are expressed in ppm relative to $DMSO-d_6$, $CDCl_3$, or $MeOD-d_4$ (2.50/7.26/3.31 for 1H ; 39.52/77.16/49.00 for ^{13}C). 1H NMR signals marked with an asterisk

(*) correspond to peaks assigned to the minor rotamer conformation. Infrared spectra were measured using a Jasco FT/IR-4100, absorption values are expressed as wavenumbers (cm^{-1}). Uncorrected melting points were measured using a Stuart melting point apparatus SMP30.

Measurements for verification and purity of the compounds were performed by LC/MS (from Shimadzu), comprising a DGU-20A3R controller, pump LC-20AB, degasser DGU-20A, and SPD-20A UV/Vis detector. ESI ionization was accomplished by an LCMS-2020 single quadrupole mass spectrometer. As a stationary phase, for analytical purpose, a Synergi 4U fusion-RP 80 Å (150×4.6 mm) column and, for preparative purpose, a Synergi 4 U fusion-RP 80 Å (250×10.0 mm) were used. As a mobile phase, a gradient of MeOH/water (both containing 0.1% formic acid) (phase 1/phase 2) was used. The compounds were dissolved in MeOH and filtered through syringe filters. Method A: $V(1) / (V(1) + V(2)) =$ from 0 to 60% over 10 min, $V(1) / (V(1) + V(2)) = 60\%$ for 5 min, $V(1) / (V(1) + V(2)) =$ from 60 to 0% over 3 min. Method B: $V(1) / (V(1) + V(2)) =$ from 5 to 90% over 10 min, $V(1) / (V(1) + V(2)) = 90\%$ for 5 min, $V(1) / (V(1) + V(2)) =$ from 90 to 5% over 3 min. Methods were performed with a flow rate of 1.0 mL/min. Compounds were detected at $\lambda = 254$ nm, and target compounds were $\geq 95\%$ pure.

All designed target compounds did not show any promiscuous moieties in the pan-assay interference compound assay (PAINS) using two different in silico filters (<http://www.cbligand.org/PAINS/> and <http://fafdrugs4.mti.univ-paris-diderot.fr/>).

Methyl (E)-3-(4-(((2-(5-Methoxy-1H-indol-3-yl)ethyl)-amino)-methyl)phenyl)acrylate (2a). K_2CO_3 (0.25 g, 1.78 mmol) and methyl (E)-3-(4-(bromomethyl)phenyl)-acrylate (0.23 g, 0.89 mmol) were added in portions to a solution of 5-methoxytryptamine **1** (0.17 g, 0.89 mmol) in 5 mL of THF and 0.5 mL of H_2O at 70°C and stirred for 2 h. Excess MgSO_4 was added to the mixture and stirred for 30 min; the precipitation was filtered out and washed with THF twice. THF solution was combined and concentrated under vacuum and then purified with column chromatography to afford 0.16 g of red oil, yield 49%. ^1H NMR (400 MHz, $\text{DMSO}-d_6$): δ 10.60 (s, 1H), 7.71–7.62 (m, 3H), 7.40 (d, $J = 8.1$ Hz, 2H), 7.21 (d, $J = 8.7$ Hz, 1H), 7.08 (d, $J = 2.3$ Hz, 1H), 6.94 (d, $J = 2.4$ Hz, 1H), 6.70 (dd, $J = 8.7, 2.4$ Hz, 1H), 6.61 (d, $J = 16.1$ Hz, 1H), 3.80 (s, 2H), 3.73 (s, 6H), 2.86–2.75 (m, 4H) ppm (one exchangeable proton not observed). ^{13}C NMR (101 MHz, $\text{DMSO}-d_6$): δ 167.2, 153.4, 145.0, 132.9, 131.9, 128.9 (2C), 128.8, 128.7 (2C), 128.0, 123.7, 117.6, 112.7, 112.4, 111.5, 100.6, 55.8, 52.8, 51.9, 49.7, 25.8 ppm. LRMS (ESI+) m/z calcd for $[\text{C}_{22}\text{H}_{23}\text{N}_3\text{O}_3]^+$: 365.18, found: 365.20 $[\text{M} + \text{H}]^+$. HPLC (method B): $t_{\text{R}} = 8.71$ min.

Methyl 4-(((2-(5-Methoxy-1H-indol-3-yl)ethyl)-amino)methyl)-benzoate (2b). Intermediate **2b** was prepared from 5-methoxytryptamine **1** and methyl 4-(bromomethyl)benzoate in a similar manner as described for intermediate **2a**. Brown solid, yield 62%. ^1H NMR (400 MHz, $\text{DMSO}-d_6$): δ 10.59 (s, 1H), 7.90 (d, $J = 8.2$ Hz, 2H), 7.49 (d, $J = 8.2$ Hz, 2H), 7.21 (d, $J = 8.7$ Hz, 1H), 7.08 (d, $J = 2.3$ Hz, 1H), 6.94 (d, $J = 2.4$ Hz, 1H), 6.70 (dd, $J = 8.7, 2.4$ Hz, 1H), 3.85 (s, 3H), 3.84 (s, 2H), 3.73 (s, 3H), 2.87–2.74 (m, 4H) ppm (one exchangeable proton not observed). ^{13}C NMR (101 MHz, $\text{DMSO}-d_6$): δ 166.7, 153.3, 147.3, 131.9, 129.5, 128.6, 128.4, 128.0, 123.7, 112.7, 112.4, 111.4, 100.6, 55.8, 52.8, 52.5, 49.9, 25.9 ppm. LRMS (ESI+) m/z calcd for $[\text{C}_{20}\text{H}_{23}\text{N}_2\text{O}_3]^+$: 339.16, found: 339.15 $[\text{M} + \text{H}]^+$. HPLC (method B): $t_{\text{R}} = 8.05$ min.

Methyl 6-(((2-(5-Methoxy-1H-indol-3-yl)ethyl)-amino)hexanoate (2c). Intermediate **2c** was prepared from 5-methoxytryptamine **1** and methyl 6-bromo-hexanoate in a similar manner as described for intermediate **2a**. Brown solid, yield 35%. ^1H NMR (400 MHz, CDCl_3): δ 8.52 (s, 1H), 7.24 (d, $J = 8.8$ Hz, 1H), 7.08 (d, $J = 2.3$ Hz, 1H), 7.00 (d, $J = 1.3$ Hz, 1H), 6.87 (dd, $J = 8.8, 2.3$ Hz, 1H), 3.87 (s, 3H), 3.67 (s, 3H), 2.97 (s, 4H), 2.65 (t, $J = 7.3$ Hz, 2H), 2.30 (t, $J = 7.5$ Hz, 2H), 1.68–1.58 (m, 2H), 1.56–1.45 (m, 3H), 1.38–1.27 (m, 2H) ppm. ^{13}C NMR (101 MHz, CDCl_3): δ 174.2, 153.8, 131.5, 127.8, 122.8, 113.3, 112.1, 111.9, 100.7, 56.0, 51.5, 49.8, 49.5, 34.0, 29.6, 26.9, 25.6, 24.8 ppm. LRMS (ESI+) m/z calcd for $[\text{C}_{18}\text{H}_{27}\text{N}_2\text{O}_3]^+$: 319.19, found: 319.20 $[\text{M} + \text{H}]^+$. HPLC (method B): $t_{\text{R}} = 7.52$ min.

(E)-N-Hydroxy-3-(4-(((2-(5-methoxy-1H-indol-3-yl)-ethyl)-amino)-methyl)phenyl)acrylamide (3a). To a stirred solution of $\text{NH}_2\text{OH}\cdot\text{HCl}$ (23.35 g, 343 mmol) in 120 mL of MeOH was added KOH (28 g, 509 mmol) in 70 mL of MeOH at r.t. After 30 min, a white precipitate was filtered out to afford NH_2OK methanol solution. **2a** (80 mg, 0.22 mmol) was added to 5 mL of NH_2OK methanol solution, the mixture was stirred at room temperature for 5 min. The solvent was evaporated under vacuum; the residue was redissolved with 5 mL of water and then adjusted to pH 6–7 by hydrochloric acid. The precipitate was filtered and purified with column chromatography to afford light red solid 44 mg, yield 29%. ^1H NMR (400 MHz, $\text{DMSO}-d_6$): δ 10.88 (brs, 1H) 10.74 (s, 1H), 8.98 (brs, 1H), 7.58 (d, $J = 8.1$ Hz, 2H), 7.53 (d, $J = 8.1$ Hz, 2H), 7.45 (d, $J = 15.8$ Hz, 1H), 7.24 (d, $J = 8.7$ Hz, 1H), 7.14 (d, $J = 2.2$ Hz, 1H), 7.03 (d, $J = 2.3$ Hz, 1H), 6.73 (dd, $J = 8.7, 2.4$ Hz, 1H), 6.51 (d, $J = 15.8$ Hz, 1H), 4.07 (s, 2H), 3.75 (s, 3H), 3.01 (s, 4H) ppm (one exchangeable proton not observed). ^{13}C NMR (101 MHz, $\text{DMSO}-d_6$): δ 164.3, 153.5, 146.3, 137.9, 135.2, 131.9, 130.4 (2C), 127.9 (2C), 127.7, 124.1, 120.0, 112.6, 111.7, 110.6, 100.7, 55.9, 50.9, 48.1, 23.4 ppm. IR (film): ν 3174, 2918, 2823, 1651, 1613, 1579, 1481, 1450, 1435, 1418, 1338, 1288, 1208, 1162, 1064, 1038, 1017, 964, 818, 796, 745, 698 cm^{-1} . LRMS (ESI+) m/z calcd for $[\text{C}_{21}\text{H}_{24}\text{N}_3\text{O}_3]^+$: 366.17, found: 339.05 $[\text{M} + \text{H}]^+$. HPLC (method A): $t_{\text{R}} = 8.77$ min, purity = 96.1%. mp = 166–168 $^\circ\text{C}$.

N-Hydroxy-4-(((2-(5-methoxy-1H-indol-3-yl)ethyl)-amino)-methyl)benzamide (3b). Compound **3b** was prepared from **2b** in a similar manner as described for compound **3a**. Light red solid, yield 48%. ^1H NMR (400 MHz, $\text{DMSO}-d_6$): δ 11.30 (brs, 1H), 10.79 (s, 1H), 9.13 (brs, 1H), 7.80 (d, $J = 8.3$ Hz, 2H), 7.66 (d, $J = 8.3$ Hz, 2H), 7.25 (d, $J = 8.8$ Hz, 1H), 7.17 (d, $J = 2.4$ Hz, 1H), 7.09 (d, $J = 2.4$ Hz, 1H), 6.74 (dd, $J = 8.7, 2.4$ Hz, 1H), 4.21 (s, 2H), 3.76 (s, 3H), 3.10 (s, 4H) ppm (one exchangeable proton not observed). ^{13}C NMR (101 MHz, $\text{DMSO}-d_6$): δ 164.0, 153.6, 136.2, 133.4, 131.9, 130.3 (2C), 127.6, 127.5 (2C), 124.3, 112.7, 111.7, 109.8, 100.7, 56.0, 50.0, 47.5, 22.4 ppm. IR (film): ν 3197, 2928, 2861, 1623, 1579, 1553, 1487, 1460, 1442, 1384, 1317, 1232, 1210, 1182, 1165, 1111, 1036, 1017, 897, 836, 791, 699 cm^{-1} . LRMS (ESI+) m/z calcd for $[\text{C}_{19}\text{H}_{22}\text{N}_3\text{O}_3]^+$: 340.16, found: 340.10 $[\text{M} + \text{H}]^+$. HPLC (method A): $t_{\text{R}} = 7.50$ min, purity = 99.4%. mp = 190–192 $^\circ\text{C}$.

Methyl 4-(((2-(5-Methoxy-1H-indol-3-yl)ethyl)-carbamoyl)-benzoate (4a). TEA (0.48 g, 4.74 mmol) and TBTU (0.51 g, 1.58 mmol) were added to a solution of 4-(methoxycarbonyl)benzoic acid (0.28 g, 1.58 mmol) in 10 mL of THF and then stirred at r.t. for 1 h. 5-Methoxytryptamine **1** (0.3 g, 1.58 mmol) was added to the mixture and stirred for 2 h. By subsequently washing with water and brine, drying over MgSO_4 , and filtering, then, the solvent was removed under vacuum. The raw product was purified with column chromatography to afford red oil (0.37 g, yield 67%). ESI-MS m/z : 353.14 $[\text{M} + \text{H}]^+$. ^1H NMR (400 MHz, CDCl_3): δ 7.96 (d, $J = 8.2$ Hz, 2H), 7.64 (d, $J = 8.2$ Hz, 2H), 7.19 (s, 1H), 7.02–6.94 (m, 2H), 6.80 (dd, $J = 8.8, 2.3$ Hz, 1H), 6.23 (brs, 1H), 3.85 (s, 3H), 3.76–3.68 (m, 5H), 3.00 (t, $J = 6.5$ Hz, 2H) ppm (one exchangeable proton not observed). ^{13}C NMR (101 MHz, CDCl_3): δ 166.6, 166.3, 154.2, 138.6, 132.6, 131.6, 129.8 (2C), 127.7, 126.9 (2C), 122.9, 112.7 (2C), 112.1, 100.4, 55.9, 52.4, 40.5, 25.2 ppm. LRMS (ESI+) m/z calcd for $[\text{C}_{20}\text{H}_{21}\text{N}_2\text{O}_4]^+$: 353.14, found: 353.15 $[\text{M} + \text{H}]^+$. HPLC (method B): $t_{\text{R}} = 11.28$ min.

Methyl (E)-3-(4-(((2-(5-Methoxy-1H-indol-3-yl)ethyl)-carbamoyl)-phenyl)acrylate (4b). Intermediate **4b** was prepared from 5-methoxytryptamine **1** and (E)-4-(3-methoxy-3-oxoprop-1-en-1-yl)-benzoic acid in a similar manner as described for intermediate **4a**. Faint yellow solid, yield 71%. ^1H NMR (400 MHz, $\text{DMSO}-d_6$): δ 10.69 (s, 1H), 8.72 (t, $J = 5.6$ Hz, 1H), 7.94 (d, $J = 8.3$ Hz, 2H), 7.87 (d, $J = 8.3$ Hz, 2H), 7.75 (d, $J = 16.1$ Hz, 1H), 7.28 (d, $J = 8.7$ Hz, 1H), 7.19 (d, $J = 2.0$ Hz, 1H), 7.11 (d, $J = 2.2$ Hz, 1H), 6.83–6.74 (m, 2H), 3.80 (s, 3H), 3.77 (s, 3H), 3.60 (q, $J = 6.9$ Hz, 2H), 2.98 (t, $J = 7.4$ Hz, 2H) ppm. ^{13}C NMR (101 MHz, $\text{DMSO}-d_6$): δ 167.0, 165.9, 153.5, 144.0, 136.9, 136.5, 131.9, 128.7 (2C), 128.13 (2C), 128.09, 123.8, 119.8, 112.5, 112.2, 111.5, 100.6, 55.8, 52.1, 40.8, 25.6

ppm. LRMS (ESI+) m/z calcd for $[C_{22}H_{23}N_2O_4]^+$: 379.16, found: 379.20 $[M + H]^+$. HPLC (method B): $t_R = 11.69$ min.

Methyl (E)-4-(3-((2-(5-Methoxy-1H-indol-3-yl)ethyl)amino)-3-oxoprop-1-en-1-yl)benzoate (4c). Intermediate **4c** was prepared from 5-methoxytryptamine **1** and (E)-3-(4-(methoxycarbonyl)phenyl)acrylic acid in a similar manner as described for intermediate **4a**. Yellow solid, yield 79%. ESI-MS m/z : 379.15 $[M + H]^+$. 1H NMR (400 MHz, DMSO- d_6): δ 10.65 (s, 1H), 8.30 (t, $J = 5.7$ Hz, 1H), 7.99 (d, $J = 8.4$ Hz, 2H), 7.70 (d, $J = 8.4$ Hz, 2H), 7.50 (d, $J = 15.8$ Hz, 1H), 7.23 (d, $J = 8.7$ Hz, 1H), 7.14 (d, $J = 2.3$ Hz, 1H), 7.05 (d, $J = 2.4$ Hz, 1H), 6.78 (d, $J = 15.8$ Hz, 1H), 6.72 (dd, $J = 8.7, 2.4$ Hz, 1H), 3.87 (s, 3H), 3.76 (s, 3H), 3.49 (q, $J = 7.1$ Hz, 2H), 2.88 (t, $J = 7.2$ Hz, 2H), 2.70 (s, 4H) ppm. ^{13}C NMR (101 MHz, DMSO- d_6): δ 166.3, 165.0, 153.5, 140.1, 137.6, 131.9, 130.4, 130.2, 128.2, 128.0, 125.6, 123.9, 112.5, 112.1, 111.6, 100.6, 55.8, 52.7, 38.7, 25.6 ppm. LRMS (ESI+) m/z calcd for $[C_{22}H_{23}N_2O_4]^+$: 379.16, found: 379.20 $[M + H]^+$. HPLC (method B): $t_R = 11.81$ min.

Methyl 6-((2-(5-Methoxy-1H-indol-3-yl)ethyl)amino)-6-oxohexanoate (4d). Intermediate **4d** was prepared from 5-methoxytryptamine **1** and 6-methoxy-6-oxohexanoic acid in a similar manner as described for intermediate **4a**. Colorless oil, yield 60%. ESI-MS m/z : 319.15 $[M + H]^+$. 1H NMR (400 MHz, DMSO- d_6): δ 10.62 (s, 1H), 7.88 (t, $J = 5.6$ Hz, 1H), 7.22 (d, $J = 8.7$ Hz, 1H), 7.09 (d, $J = 2.2$ Hz, 1H), 7.02 (d, $J = 2.4$ Hz, 1H), 6.72 (dd, $J = 8.7, 2.4$ Hz, 1H), 3.76 (s, 3H), 3.59 (s, 3H), 3.35–3.27 (m, 2H), 2.77 (t, $J = 7.4$ Hz, 2H), 2.21 (t, $J = 6.9$ Hz, 2H), 2.07 (t, $J = 7.0$ Hz, 2H), 1.54–1.45 (m, 4H) ppm. ^{13}C NMR (101 MHz, DMSO- d_6): δ 173.7, 172.2, 153.4, 131.9, 128.0, 123.7, 112.4, 112.1, 111.5, 100.6, 55.8, 51.7, 35.6, 33.5, 25.8, 25.2, 24.6 ppm. LRMS (ESI+) m/z calcd for $[C_{18}H_{25}N_2O_4]^+$: 333.17, found: 333.20 $[M + H]^+$. HPLC (method B): $t_R = 10.31$ min.

N^1 -Hydroxy- N^6 -(2-(5-methoxy-1H-indol-3-yl)ethyl)-terephthalamide (5a). Compound **5a** was prepared from **4a** in a similar manner as described for compound **3a**. Gray solid, yield 19%. 1H NMR (400 MHz, DMSO- d_6): δ 11.32 (s, 1H), 10.65 (s, 1H), 9.11 (s, 1H), 8.70 (t, $J = 5.6$ Hz, 1H), 7.91 (d, $J = 8.4$ Hz, 2H), 7.82 (d, $J = 8.4$ Hz, 2H), 7.23 (d, $J = 8.7$ Hz, 1H), 7.15 (d, $J = 2.1$ Hz, 1H), 7.06 (d, $J = 2.3$ Hz, 1H), 6.72 (dd, $J = 8.7, 2.4$ Hz, 1H), 3.73 (s, 3H), 3.55 (q, $J = 7.3$ Hz, 2H), 2.93 (t, $J = 7.4$ Hz, 2H) ppm. ^{13}C NMR (101 MHz, DMSO- d_6): δ 165.9, 164.0, 153.5, 137.4, 135.4, 131.9, 128.1, 127.7 (2C), 127.3 (2C), 123.8, 112.5, 112.2, 111.5, 100.6, 55.8, 40.8, 25.6 ppm. IR (film): ν 3258, 2921, 2833, 1667, 1608, 1541, 1482, 1443, 1420, 1332, 1303, 1291, 1214, 1178, 1153, 1030, 1013, 838, 795, 723, 692, 677 cm^{-1} . LRMS (ESI+) m/z calcd for $[C_{19}H_{20}N_3O_4]^+$: 354.14, found: 354.00 $[M + H]^+$. HPLC (method A): $t_R = 11.36$ min, purity = 99.9%. mp = 179–181 °C.

(E)-4-(3-(Hydroxyamino)-3-oxoprop-1-en-1-yl)- N -(2-(5-methoxy-1H-indol-3-yl)ethyl)benzamide (5b). Compound **5b** was prepared from **4b** in a similar manner as described for compound **3a**. Red solid, yield 30%. 1H NMR (400 MHz, DMSO- d_6): δ 10.82 (brs, 1H), 10.65 (s, 1H), 8.65 (t, $J = 5.5$ Hz, 1H), 7.88 (d, $J = 8.3$ Hz, 2H), 7.64 (d, $J = 8.2$ Hz, 2H), 7.50 (d, $J = 15.8$ Hz, 1H), 7.23 (d, $J = 8.7$ Hz, 1H), 7.14 (d, $J = 2.0$ Hz, 1H), 7.06 (d, $J = 2.3$ Hz, 1H), 6.72 (dd, $J = 8.7, 2.4$ Hz, 1H), 6.56 (d, $J = 15.8$ Hz, 1H), 3.73 (s, 3H), 3.54 (q, $J = 6.8$ Hz, 2H), 2.93 (t, $J = 7.4$ Hz, 2H) ppm (one exchangeable proton not observed). ^{13}C NMR (101 MHz, DMSO- d_6): δ 166.0, 162.9, 153.5, 137.8, 137.8, 135.7, 131.9, 128.2 (2C), 128.1, 127.8 (2C), 123.8, 121.2, 112.5, 112.2, 111.5, 100.7, 55.8, 40.7, 25.6 ppm. IR (film): ν 3186, 2883, 2814, 1609, 1525, 1487, 1478, 1440, 1427, 1284, 1207, 1163, 1043, 1021, 974, 831, 792, 755, 704, 660 cm^{-1} . LRMS (ESI+) m/z calcd for $[C_{21}H_{22}N_3O_4]^+$: 380.15, found: 380.05 $[M + H]^+$. HPLC (method A): $t_R = 12.13$ min, purity = 99.1%. mp = 90–92 °C.

(E)- N -Hydroxy-4-(3-((2-(5-methoxy-1H-indol-3-yl)ethyl)amino)-3-oxoprop-1-en-1-yl)benzamide (5c). Compound **5c** was prepared from **4c** in a similar manner as described for compound **3a**. Yellow solid, yield 18%. 1H NMR (400 MHz, DMSO- d_6): δ 11.26 (brs, 1H), 10.65 (s, 1H), 9.07 (brs, 1H), 8.25 (t, $J = 5.7$ Hz, 1H), 7.78 (d, $J = 8.3$ Hz, 2H), 7.63 (d, $J = 8.3$ Hz, 2H), 7.47 (d, $J = 15.8$ Hz, 1H), 7.23 (d, $J = 8.7$ Hz, 1H), 7.14 (d, $J = 2.2$ Hz, 1H), 7.05 (d, $J = 2.3$ Hz, 1H), 6.77–6.65 (m, 2H), 3.76 (s, 3H), 3.48 (q, $J = 7.0$ Hz, 2H), 2.87 (t, $J = 7.2$ Hz, 2H) ppm. ^{13}C NMR (101 MHz, DMSO- d_6): δ 165.5, 165.1,

153.5, 138.1, 137.9, 133.7, 131.9, 128.0, 127.92 (2C), 127.87 (2C), 124.5, 123.8, 112.5, 112.1, 111.6, 100.6, 55.8, 49.1, 25.7 ppm. IR (film): ν 3198, 2894, 1659, 1565, 1536, 1491, 1459, 1356, 1317, 1224, 1204, 1174, 1029, 1013, 986, 895, 855, 801, 779, 713, 675 cm^{-1} . LRMS (ESI+) m/z calcd for $[C_{21}H_{22}N_3O_4]^+$: 380.15, found: 380.10 $[M + H]^+$. HPLC (method A): $t_R = 12.24$ min, purity = 97.1%. mp = 140–142 °C.

N^1 -Hydroxy- N^6 -(2-(5-methoxy-1H-indol-3-yl)ethyl)-adipamide (5d). Compound **5d** was prepared from **4d** in a similar manner as described for compound **3a**. White solid, yield 17%. 1H NMR (400 MHz, DMSO- d_6): δ 10.62 (s, 1H), 10.33 (s, 1H), 8.65 (s, 1H), 7.87 (t, $J = 5.4$ Hz, 1H), 7.22 (d, $J = 8.7$ Hz, 1H), 7.09 (d, $J = 2.1$ Hz, 1H), 7.02 (d, $J = 2.3$ Hz, 1H), 6.71 (dd, $J = 8.7, 2.4$ Hz, 1H), 3.76 (s, 3H), 3.31 (q, $J = 7.4$ Hz, 2H), 2.77 (t, $J = 7.4$ Hz, 2H), 2.06 (t, $J = 8.0$ Hz, 2H), 1.94 (t, $J = 8.0$ Hz, 2H), 1.51–1.43 (m, 4H) ppm. ^{13}C NMR (101 MHz, DMSO- d_6): δ 172.3, 169.5, 153.4, 131.9, 128.0, 123.7, 112.4, 112.1, 111.5, 100.6, 98.7, 55.8, 35.8, 32.6, 25.8, 25.5, 25.4 ppm. IR (film): ν 3386, 3318, 3189, 2972, 2871, 1637, 1616, 1586, 1549, 1485, 1466, 1452, 1434, 1416, 1288, 1213, 1170, 1036, 1020, 951, 923, 840, 812, 773, 702, 667 cm^{-1} . LRMS (ESI+) m/z calcd for $[C_{17}H_{24}N_3O_4]^+$: 334.17, found: 334.05 $[M + H]^+$. HPLC (method A): $t_R = 10.64$ min, purity = 96.5%. mp = 138–139 °C.

N -(2-(5-Methoxy-1H-indol-3-yl)ethyl)acetamide (Melatonin, 6). 5-Methoxytryptamine **1** (2.0 g, 10.5 mmol) was suspended in 25 mL of DCM, and acetic anhydride (4.4 g, 42.11 mmol) in 5 mL of DCM was added in drops to the solution at 0 °C and then stirred at r.t. for 2 h. The mixture was washed with sat. $NaHCO_3$ aq., water, and brine; dried with $MgSO_4$; filtered; and removed the solvent to afford brown solid 2.0 g, yield 82%. 1H NMR (400 MHz, $CDCl_3$): δ 8.00 (brs, 1H), 7.20 (d, $J = 8.7$ Hz, 1H), 6.97 (d, $J = 2.3$ Hz, 1H), 6.95 (s, 1H), 6.80 (dd, $J = 8.8, 2.2$ Hz, 1H), 5.53 (brs, 1H), 3.79 (s, 3H), 3.52 (q, $J = 6.4$ Hz, 2H), 2.86 (t, $J = 6.7$ Hz, 2H), 1.86 (s, 3H) ppm. LRMS (ESI+) m/z calcd for $[C_{13}H_{17}N_2O_2]^+$: 233.12, found: 233.15 $[M + H]^+$. HPLC (method B): $t_R = 8.98$ min, purity 98.7%.

Methyl (E)-3-(4-(3-(2-Acetamidoethyl)-5-methoxy-1H-indol-1-yl)methyl)phenyl)acrylate (7a). Melatonin (0.5 g, 2.2 mmol) and t -BuOK (0.49 g, 4.4 mmol) were stirred in 15 mL of THF at 70 °C for 40 min; then methyl (E)-3-(4-(bromomethyl)phenyl)acrylate (0.66 g, 2.6 mmol) was added and stirred for 12 h. The mixture was cooled to r.t. and concentrated under vacuum; the residue was redissolved in DCM and then washed with 0.1 M HCl, water, and brine. The organic phase was dried over $MgSO_4$ and filtered, the solvent was removed and then redissolved in MeOH, and $SOCl_2$ (0.79 g, 6.6 mmol) was added in drop with an ice bath and after that stirred at r.t. overnight. The solvent was removed under vacuum and redissolved with DCM, then washed with 0.1 M NaOH, water, and brine and finally purified with column chromatography to afford yellow solid 0.83 g, yield 66%. 1H NMR (400 MHz, DMSO- d_6): δ 7.94 (t, $J = 5.5$ Hz, 1H), 7.64 (d, $J = 8.3$ Hz, 2H), 7.61 (d, $J = 16.4$ Hz, 1H), 7.27 (d, $J = 8.8$ Hz, 1H), 7.27 (s, 1H), 7.18 (d, $J = 8.1$ Hz, 2H), 7.06 (d, $J = 2.3$ Hz, 1H), 6.73 (dd, $J = 8.8, 2.3$ Hz, 1H), 6.58 (d, $J = 16.0$ Hz, 1H), 5.34 (s, 2H), 3.76 (s, 3H), 3.71 (s, 3H), 3.32 (q, $J = 7.4$ Hz, 2H), 2.79 (t, $J = 7.4$ Hz, 2H), 1.81 (s, 3H) ppm. ^{13}C NMR (101 MHz, DMSO- d_6): δ 169.5, 167.1, 153.8, 144.6, 141.6, 133.5, 131.8, 129.0 (2C), 128.7, 127.9 (2C), 127.6, 118.1, 112.2, 111.7, 111.2, 101.2, 55.9, 51.9, 49.3, 25.6, 23.2 ppm. LRMS (ESI+) m/z calcd for $[C_{24}H_{27}N_2O_4]^+$: 407.19, found: 407.20 $[M + H]^+$. HPLC (method B): $t_R = 12.48$ min.

Methyl 4-((3-(2-Acetamidoethyl)-5-methoxy-1H-indol-1-yl)methyl)benzoate (7b). Intermediate **7b** was prepared from melatonin and methyl 4-(bromomethyl)benzoate in a similar manner as described for intermediate **7a**. Off-white solid, yield 63%. 1H NMR (400 MHz, DMSO- d_6): δ 7.93 (t, $J = 5.0$ Hz, 1H), 7.88 (d, $J = 8.3$ Hz, 2H), 7.27 (s, 1H), 7.25 (d, $J = 8.3$ Hz, 2H), 7.24 (d, $J = 8.8$ Hz, 1H), 7.06 (d, $J = 2.4$ Hz, 1H), 6.73 (dd, $J = 8.8, 2.4$ Hz, 1H), 5.42 (s, 2H), 3.82 (s, 3H), 3.76 (s, 3H), 3.32 (q, $J = 7.4$ Hz, 2H), 2.80 (t, $J = 7.4$ Hz, 2H), 1.80 (s, 3H) ppm. ^{13}C NMR (101 MHz, DMSO- d_6): δ 169.5, 166.4, 153.8, 144.6, 131.8, 129.9, 129.0, 128.7, 127.7, 127.5, 112.3, 111.8, 111.2, 101.2, 55.9, 52.6, 49.2, 25.6, 23.2 ppm. LRMS (ESI+) m/z calcd for $[C_{22}H_{25}N_2O_4]^+$: 381.17, found: 381.20 $[M + H]^+$. HPLC (method B): $t_R = 12.08$ min.

Methyl 6-(3-(2-Acetamidoethyl)-5-methoxy-1H-indol-1-yl)-hexanoate (7c). Intermediate 7c was prepared from melatonin and methyl 6-bromohexanoate in a similar manner as described for intermediate 7a. Yellow oil, yield 57%. ¹H NMR (400 MHz, CDCl₃): δ 7.13 (d, J = 8.9 Hz, 1H), 6.94 (d, J = 2.1 Hz, 1H), 6.84 (s, 1H), 6.81 (dd, J = 8.9, 2.1 Hz, 1H), 6.05 (brs, 1H), 3.97 (t, J = 6.9 Hz, 2H), 3.79 (s, 3H), 3.60 (s, 3H), 3.56 (s, 3H), 3.54–3.47 (m, 2H), 2.87 (t, J = 6.0 Hz, 2H), 2.21 (t, J = 7.3 Hz, 2H), 1.78–1.70 (m, 2H), 1.57–1.51 (m, 2H), 1.30–1.20 (m, 2H) ppm. ¹³C NMR (101 MHz, CDCl₃): δ 169.2, 165.4, 149.1, 127.0, 123.4, 121.6, 107.2, 106.2, 105.5, 95.9, 51.2, 46.8, 41.4, 35.3, 29.0, 25.2, 21.7, 20.5, 19.7, 18.6 ppm. LRMS (ESI+) *m/z* calcd for [C₂₀H₂₉N₂O₄]⁺: 361.20, found: 361.20 [M + H]⁺. HPLC (method B): *t_R* = 11.83 min.

(E)-3-(4-((3-(2-Acetamidoethyl)-5-methoxy-1H-indol-1-yl)-methyl)phenyl)-N-hydroxyacrylamide (8a). Compound 8a was prepared from 7a in a similar manner as described for compound 3a. Red solid, yield 34%. ¹H NMR (400 MHz, DMSO-*d*₆): δ 8.21 (s, 2H), 7.94 (t, J = 5.3 Hz, 1H), 7.48 (d, J = 8.0 Hz, 2H), 7.40 (d, J = 15.8 Hz, 1H), 7.27 (d, J = 7.6 Hz, 1H), 7.26 (s, 1H), 7.18 (d, J = 8.1 Hz, 2H), 7.05 (d, J = 2.3 Hz, 1H), 6.73 (dd, J = 8.8, 2.4 Hz, 1H), 6.40 (d, J = 15.8 Hz, 1H), 5.33 (s, 2H), 3.76 (s, 3H), 3.31 (q, J = 7.4 Hz, 2H), 2.79 (t, J = 7.4 Hz, 2H), 1.80 (s, 3H) ppm. ¹³C NMR (101 MHz, DMSO-*d*₆): δ 169.5, 165.5, 153.8, 140.4, 138.3, 134.3, 131.8, 128.7, 128.1 (2C), 127.9 (2C), 127.6, 119.4, 112.1, 111.7, 111.2, 101.2, 55.9, 49.3, 39.9, 25.6, 23.2 ppm. IR (film): ν 3276, 2919, 2839, 1662, 1631, 1562, 1492, 1455, 1440, 1358, 1303, 1222, 1178, 1040, 975, 831, 795, 738, 669 cm⁻¹. LRMS (ESI+) *m/z* calcd for [C₂₃H₂₆N₃O₄]⁺: 408.18, found: 408.10 [M + H]⁺. HPLC (method A): *t_R* = 13.31 min, purity = 95.2%. mp = 187–189 °C.

4-((3-(2-Acetamidoethyl)-5-methoxy-1H-indol-1-yl)-methyl)-N-hydroxybenzamide (8b). Compound 8b was prepared from 7b in a similar manner as described for compound 3a. Off-white solid, yield 14%. ¹H NMR (400 MHz, DMSO-*d*₆): δ 11.13 (s, 1H), 8.99 (s, 1H), 7.94 (t, J = 5.6 Hz, 1H), 7.66 (d, J = 8.2 Hz, 2H), 7.27 (s, 1H), 7.26 (d, J = 8.3 Hz, 1H), 7.20 (d, J = 8.2 Hz, 2H), 7.05 (d, J = 2.4 Hz, 1H), 6.73 (dd, J = 8.8, 2.4 Hz, 1H), 5.36 (s, 2H), 3.76 (s, 3H), 3.31 (q, J = 7.3 Hz, 2H), 2.79 (t, J = 7.4 Hz, 2H), 1.80 (s, 3H). ¹³C NMR (101 MHz, DMSO-*d*₆): δ 169.5, 164.4, 153.8, 142.2, 132.3, 131.7, 128.7, 127.6, 127.5 (2C), 127.3 (2C), 112.1, 111.7, 111.2, 101.2, 55.9, 49.2, 39.9, 25.6, 23.2. IR (film): ν 3204, 3012, 2812, 2633, 2531, 1646, 1627, 1585, 1574, 1495, 1453, 1411, 1356, 1224, 1040, 1030, 844, 837, 807, 773, 715 cm⁻¹. LRMS (ESI+) *m/z* calcd for [C₂₁H₂₄N₃O₄]⁺: 382.17, found: 382.05 [M + H]⁺. HPLC (method A): *t_R* = 12.14 min, purity = 98.0%. mp = 90–92 °C.

6-(3-(2-Acetamidoethyl)-5-methoxy-1H-indol-1-yl)-N-hydroxyhexanamide (8c). Compound 8c was prepared from 7c in a similar manner as described for compound 3a. Pale yellow solid, yield 26%. ¹H NMR (400 MHz, DMSO-*d*₆): δ 10.31 (s, 1H), 8.64 (s, 1H), 7.93 (t, J = 5.4 Hz, 1H), 7.30 (d, J = 8.8 Hz, 1H), 7.12 (s, 1H), 7.02 (d, J = 2.3 Hz, 1H), 6.76 (dd, J = 8.8, 2.4 Hz, 1H), 4.04 (t, J = 7.0 Hz, 2H), 3.77 (s, 3H), 3.31 (q, J = 7.4 Hz, 2H), 2.76 (t, J = 7.4 Hz, 2H), 1.92 (t, J = 7.4 Hz, 2H), 1.81 (s, 3H), 1.74–1.65 (m, 2H), 1.56–1.44 (m, 2H), 1.26–1.15 (m, 2H) ppm. ¹³C NMR (101 MHz, DMSO-*d*₆): δ 169.5, 169.4, 153.5, 131.7, 128.4, 127.0, 111.5, 111.3, 110.8, 101.0, 55.9, 45.7, 39.9, 32.6, 30.1, 26.4, 25.6, 25.2, 23.2 ppm. IR (film): ν 3298, 3265, 2933, 2879, 1667, 1659, 1596, 1504, 1461, 1398, 1332, 1231, 1185, 1094, 1040, 966, 849, 791, 769, 676 cm⁻¹. LRMS (ESI+) *m/z* calcd for [C₁₉H₂₈N₃O₄]⁺: 362.20, found: 362.10 [M + H]⁺. HPLC (method A): *t_R* = 12.28 min, purity = 99.5%. mp = 130–131 °C.

Methyl (E)-3-(4-(((E)-3-(4-((Ethoxycarbonyloxy)-3-methoxyphenyl)-N-(2-(5-methoxy-1H-indol-3-yl)ethyl)acrylamido)methyl)phenyl)acrylate (9a). TEA (0.33 g, 3.3 mmol) and ethyl chloroformate (0.28 g, 2.6 mmol) were added to a solution of ferulic acid (0.26 g, 1.3 mmol) in 15 mL of THF and then stirred at room temperature for 5 min. 2a (0.40 g, 1.1 mmol) was added to the mixture in portions and then stirred at r.t. for 30 min. The solvent was removed under vacuum, and the residue was purified with column chromatography to afford pale-yellow solid 0.40 g, yield 60%. ¹H NMR (400 MHz, DMSO-*d*₆): δ 10.66/10.64* (d, J = 1.6 Hz, 1H),

7.72*/7.71 (d, J = 8.1 Hz, 2H), 7.66/7.64* (d, J = 15.9 Hz, 1H), 7.62*/7.40 (d, J = 15.4 Hz, 1H), 7.46*/7.28 (d, J = 1.9 Hz, 1H), 7.35/7.31* (d, J = 8.1 Hz, 2H), 7.22*/7.18 (d, J = 8.8 Hz, 1H), 7.20*/7.11 (d, J = 8.8 Hz, 1H), 7.09 (d, J = 2.2 Hz, 1H), 7.04*/6.99 (d, J = 2.2 Hz, 1H), 6.85 (dd, J = 8.8, 1.6 Hz, 1H), 6.82 (d, J = 15.7 Hz, 1H), 6.71 (dd, J = 8.7, 2.3 Hz, 1H), 6.63/6.62* (d, J = 16.0 Hz, 1H), 4.87*/4.72 (s, 2H), 4.30–4.19 (m, 2H), 3.83*/3.80 (s, 3H), 3.75*/3.73 (s, 3H), 3.71 (s, 3H), 3.71–3.58 (m, 2H), 3.02–2.84 (m, 2H), 1.29/1.27* (t, J = 7.1 Hz, 3H) ppm (the minor rotamer: 35%). ¹³C NMR (101 MHz, DMSO-*d*₆): δ 167.2, 167.1, 166.3, 153.6, 153.5, 152.8, 151.4, 144.7, 141.6, 140.8, 140.6, 134.8, 133.3, 131.9, 129.2, 129.0, 128.7, 128.0, 127.8, 124.7, 120.4, 119.5, 118.0, 112.9, 112.6, 111.6, 110.9, 100.4, 100.0, 65.2, 56.6, 56.4, 55.79, 55.75, 51.9, 48.5, 48.0, 25.1, 14.5 ppm. LRMS (ESI+) *m/z* calcd for [C₃₅H₃₇N₂O₈]⁺: 613.25, found: 613.30 [M + H]⁺. HPLC (method B): *t_R* = 13.33 min.

Methyl (E)-4-((3-(4-((Ethoxycarbonyloxy)-3-methoxyphenyl)-N-(2-(5-methoxy-1H-indol-3-yl)ethyl)acrylamido)methyl)benzoate (9b). Intermediate 9b was prepared from 2b and ferulic acid in a similar manner as described for intermediate 9a. Yellow solid, yield 90%. ¹H NMR (400 MHz, DMSO-*d*₆): δ 10.66/10.64* (d, J = 1.5 Hz, 1H), 7.95 (d, J = 8.2 Hz, 2H), 7.62*/7.40 (d, J = 15.2 Hz, 1H), 7.44 (d, J = 8.2 Hz, 2H), 7.41 (d, J = 8.4 Hz, 1H), 7.28/7.26* (d, J = 1.7 Hz, 1H), 7.24*/6.82 (d, J = 15.6 Hz, 1H), 7.22*/7.17 (d, J = 8.8 Hz, 1H), 7.20*/7.11 (d, J = 8.8 Hz, 1H), 7.08 (d, J = 2.4 Hz, 1H), 7.03*/6.99 (d, J = 2.2 Hz, 1H), 6.85 (dd, J = 8.8, 1.6 Hz, 1H), 6.71 (dd, J = 8.7, 2.3 Hz, 1H), 4.93*/4.78 (s, 2H), 4.29–4.20 (m, 2H), 3.85/3.83* (s, 3H), 3.83*/3.80 (s, 3H), 3.74*/3.71 (s, 3H), 3.70–3.58 (m, 2H), 3.00–2.84 (m, 2H), 1.29/1.28* (t, J = 7.0 Hz, 3H) ppm (the minor rotamer: 32%). ¹³C NMR (101 MHz, DMSO-*d*₆): δ 166.8, 166.7, 166.6, 166.5, 153.7, 153.5, 149.0, 148.8, 148.3, 148.2, 144.9, 144.8, 143.1, 142.5, 131.9, 130.0, 129.8, 129.1, 128.8, 128.3, 128.0, 127.9, 127.6, 127.12, 127.05, 124.6, 123.9, 122.8, 121.9, 116.1, 115.3, 112.6, 112.5, 112.3, 111.9, 111.8, 111.6, 111.0, 100.6, 100.4, 56.2, 56.1, 55.8, 55.4, 52.5, 51.1, 48.7, 48.1, 47.7, 25.2, 23.9, 14.3 ppm. LRMS (ESI+) *m/z* calcd for [C₃₃H₃₅N₂O₈]⁺: 587.23, found: 587.25 [M + H]⁺. HPLC (method B): *t_R* = 13.13 min.

Methyl (E)-6-(3-(4-((Ethoxycarbonyloxy)-3-methoxyphenyl)-N-(2-(5-methoxy-1H-indol-3-yl)ethyl)acrylamido)hexanoate (9c). Intermediate 9c was prepared from 2c and ferulic acid in a similar manner as described for intermediate 9a. Yellow oil, yield 49%. ¹H NMR (400 MHz, DMSO-*d*₆): δ 10.66/10.64* (d, J = 1.5 Hz, 1H), 7.55*/7.30 (d, J = 15.6 Hz, 1H), 7.48*/7.03 (d, J = 2.2 Hz, 1H), 7.33*/6.82 (dd, J = 8.3, 1.5 Hz, 1H), 7.25–7.22 (m, 1H), 7.18 (d, J = 8.7 Hz, 1H), 7.16–7.11 (m, 2H), 7.09 (d, J = 8.2 Hz, 1H), 6.76–6.69 (m, 1H), 4.25*/4.24 (q, J = 7.1 Hz, 2H), 3.87*/3.79 (s, 3H), 3.77*/3.72 (s, 3H), 3.72*/3.62 (t, J = 7.3 Hz, 2H), 3.59/3.54* (s, 3H), 3.48*/3.39 (t, J = 7.3 Hz, 2H), 2.94/2.92* (t, J = 7.0 Hz, 2H), 2.32/2.27* (t, J = 7.4 Hz, 2H), 1.65–1.48 (m, 4H), 1.36–1.23 (m, 5H) ppm (the minor rotamer: 42%). ¹³C NMR (101 MHz, DMSO-*d*₆): δ 173.8, 173.7, 165.7, 165.6, 153.6, 152.9, 151.5, 151.4, 140.8, 140.5, 139.9, 135.0, 131.8, 127.9, 124.7, 123.8, 122.9, 121.0120.3, 120.1, 119.9, 112.8, 112.6, 112.5, 112.0, 111.54, 111.50, 111.0, 100.8, 100.4, 65.2, 56.5, 56.4, 55.8, 55.7, 51.6, 51.6, 48.2, 45.8, 33.7, 33.6, 29.6, 27.6, 26.5, 26.0, 25.4, 24.7, 24.6, 24.1, 14.5 ppm. LRMS (ESI+) *m/z* calcd for [C₃₁H₃₉N₂O₈]⁺: 567.26, found: 567.30 [M + H]⁺. HPLC (method B): *t_R* = 12.90 min.

(E)-3-(4-Hydroxy-3-methoxyphenyl)-N-(4-(((E)-3-(hydroxyamino)-3-oxoprop-1-en-1-yl)benzyl)-N-(2-(5-methoxy-1H-indol-3-yl)ethyl)acrylamide (10a). Compound 10a was prepared from 9a in a similar manner as described for compound 3a. Gray solid 0.16 g, yield 60%. ¹H NMR (400 MHz, DMSO-*d*₆): δ 10.75 (s, 1H), 10.67/10.64* (s, 1H), 9.40 (s, 1H), 9.03 (s, 1H), 7.54 (d, J = 7.5 Hz, 2H), 7.45/7.44* (d, J = 15.8 Hz, 1H), 7.38 (d, J = 15.3 Hz, 1H), 7.33/7.29* (d, J = 8.1 Hz, 2H), 7.24 (d, J = 3.5 Hz, 1H), 7.21 (d, J = 8.6 Hz, 1H), 7.12–7.06 (m, 2H), 7.03*/7.00 (d, J = 1.9 Hz, 1H), 6.81–6.64 (m, 3H), 6.45/6.44* (d, J = 15.8 Hz, 1H), 4.83*/4.70 (s, 2H), 3.80*/3.77 (s, 3H), 3.74*/3.73 (s, 3H), 3.68/3.61* (t, J = 6.8 Hz, 2H), 3.01–2.85 (m, 2H) ppm (the minor rotamer: 38%). ¹³C NMR (101 MHz, DMSO-*d*₆): δ 166.7, 166.6, 163.3, 153.6, 153.5, 149.0, 148.8, 148.3, 148.1, 142.9, 142.3, 140.6, 138.5, 134.1, 131.9, 128.7 (2C), 128.3,

128.1 (2C), 128.0, 127.8, 127.13, 127.07, 124.6, 123.8, 122.8, 121.9, 119.4, 119.2, 116.04, 115.98, 115.5, 112.6, 112.3, 111.9, 111.8, 111.6, 111.0, 100.6, 100.4, 56.24, 56.15, 55.8, 48.4, 47.9, 47.5, 25.1, 23.9 ppm. IR (film): ν 3229, 2952, 2885, 1626, 1572, 1505, 1472, 1450, 1434, 1412, 1352, 1259, 1230, 1204, 1171, 1148, 1120, 1022, 976, 835, 816, 792, 748, 701, 656 cm^{-1} . LRMS (ESI+) m/z calcd for $[\text{C}_{31}\text{H}_{32}\text{N}_3\text{O}_6]^+$: 542.22, found: 542.30 $[\text{M} + \text{H}]^+$. HPLC (method B): $t_{\text{R}} = 11.20$ min, purity = 99.8%. mp = 135–137 °C.

(E)-N-Hydroxy-4-((3-(4-hydroxy-3-methoxyphenyl)-N-(2-(5-methoxy-1H-indol-3-yl)ethyl)acrylamido)-methyl)benzamide (10b). Compound **10b** was prepared from **9b** in a similar manner as described for compound **3a**. Orange oil, yield 46%. ^1H NMR (400 MHz, DMSO- d_6): δ 11.18 (s, 1H), 10.68/10.64* (s, 1H), 9.42*/9.40 (s, 1H), 9.01 (brs, 1H), 7.77–7.69 (m, 2H), 7.58–7.16 (m, 5H), 7.12–6.98 (m, 3H), 6.82–6.64 (m, 3H), 4.85*/4.71 (s, 2H), 3.79*/3.77 (s, 3H), 3.74*/3.73 (s, 3H), 3.69/3.61* (t, $J = 6.6$ Hz, 2H), 3.00–2.85 (m, 2H) ppm (the minor rotamer: 38%). ^{13}C NMR (101 MHz, DMSO- d_6): δ 169.2, 166.8, 153.6, 153.49, 153.46, 148.8, 148.1, 147.8, 147.6, 142.4, 142.3, 132.8, 131.9, 128.4, 128.0, 127.6, 127.5, 127.3, 127.3, 127.0, 124.6, 124.1, 123.8, 122.4, 121.9, 116.0, 115.8, 115.4, 113.0, 112.6, 112.3, 111.6, 111.0, 110.9, 100.4, 100.2, 56.2, 56.1, 56.0, 55.9, 55.8, 55.8, 55.4, 49.1, 25.1, 21.0 ppm. IR (film): ν 3201, 2930, 2856, 1639, 1574, 1513, 1482, 1452, 1366, 1268, 1211, 1155, 1124, 1070, 1025, 1013, 973, 894, 815, 796, 747 cm^{-1} . LRMS (ESI+) m/z calcd for $[\text{C}_{29}\text{H}_{30}\text{N}_3\text{O}_6]^+$: 516.21, found: 516.25 $[\text{M} + \text{H}]^+$. HPLC (method B): $t_{\text{R}} = 10.77$ min, purity = 95.7%. mp = 86–88 °C.

(E)-N-Hydroxy-6-(3-(4-hydroxy-3-methoxyphenyl)-N-(2-(5-methoxy-1H-indol-3-yl)ethyl)acrylamido)-hexanamide (10c). Compound **10c** was prepared from **9c** in a similar manner as described for compound **3a**. White solid, yield 33%. ^1H NMR (400 MHz, DMSO- d_6): δ 10.67/10.63* (s, 1H), 10.34/10.32* (s, 1H), 9.35 (brs, 1H), 8.66 (s, 1H), 7.48*/7.27 (d, $J = 15.2$ Hz, 1H), 7.26–7.09 (m, 1H), 7.16–7.10 (s, 1H), 7.03 (s, 1H), 6.91*/6.58 (d, $J = 15.3$ Hz, 1H), 6.81*/6.73 (d, $J = 8.1$ Hz, 1H), 6.76–6.67 (m, 2H), 6.18–6.14 (m, 1H), 3.83*/3.77 (s, 3H), 3.75*/3.74 (s, 3H), 3.70/3.60* (t, $J = 7.2$ Hz, 2H), 3.45*/3.36 (t, $J = 7.2$ Hz, 2H), 2.94/2.90* (t, $J = 6.80$ Hz, 2H), 2.02–1.90 (m, 2H), 1.62–1.46 (m, 4H), 1.34–1.18 (m, 2H) ppm (the minor rotamer: 40%). ^{13}C NMR (101 MHz, DMSO- d_6): δ 169.6, 169.5, 166.1, 166.0, 163.0, 153.6, 153.5, 148.8, 148.6, 148.3, 148.1, 142.1, 141.4, 131.9, 127.9, 127.3, 124.6, 123.8, 122.4, 121.7, 116.1, 115.8, 112.6, 112.2, 112.0, 111.5, 111.5, 111.1, 100.8, 100.4, 56.3, 56.1, 55.79, 55.75, 48.2, 47.5, 45.9, 32.7, 29.7, 27.8, 26.7, 26.2, 25.5, 25.3 ppm. IR (film): ν 3304, 3199, 2922, 2851, 1637, 1582, 1513, 1481, 1454, 1427, 1372, 1268, 1214, 1161, 1124, 1101, 1064, 1028, 972, 917, 816, 795 cm^{-1} . LRMS (ESI+) m/z calcd for $[\text{C}_{27}\text{H}_{34}\text{N}_3\text{O}_6]^+$: 496.24, found: 496.25 $[\text{M} + \text{H}]^+$. HPLC (method B): $t_{\text{R}} = 10.77$ min, purity = 97.6%. mp = 85–87 °C.

tert-Butyl (2-((2-(5-Methoxy-1H-indol-3-yl)ethyl)-amino)-2-oxoethyl)carbamate (11). TEA (1.07 g, 10.50 mmol), EDCI (2.40 g, 12.60 mmol), and DMAP (1.28 g, 10.5 mmol) were added to a solution of Boc-Glu-OH (2.20 g, 12.60 mmol) in 40 mL of THF; then 5-methoxytryptamine **1** (2.00 g, 10.50 mmol) was added to the mixture and, after that, stirred overnight at r.t. THF was removed, and the residue was redissolved in DCM, washed with 0.1 M HCl, water, and brine, dried over MgSO_4 , and purified with column chromatography to afford a 3.20 g white solid, yield 88%. ^1H NMR (400 MHz, CDCl_3): δ 7.99 (brs, 1H), 7.18 (d, $J = 7.9$ Hz, 1H), 6.95 (d, $J = 2.3$ Hz, 1H), 6.93 (s, 1H), 6.79 (dd, $J = 8.8, 2.4$ Hz, 1H), 6.13 (brs, 1H), 5.03 (brs, 1H), 3.79 (s, 3H), 3.66 (s, 2H), 3.53 (q, $J = 6.1$ Hz, 2H), 2.87 (t, $J = 6.7$ Hz, 2H), 1.35 (s, 9H) ppm. ^{13}C NMR (101 MHz, CDCl_3): δ 172.2, 169.3, 154.1, 131.6, 127.7, 122.9, 112.4 (2C), 112.0, 100.5, 56.0, 44.5, 39.5, 28.3 (3C), 25.3 ppm. LRMS (ESI+) m/z calcd for $[\text{C}_{18}\text{H}_{26}\text{N}_3\text{O}_4]^+$: 348.18, found: 348.20 $[\text{M} + \text{H}]^+$. HPLC (method B): $t_{\text{R}} = 10.74$ min.

2-Amino-N-(2-(5-methoxy-1H-indol-3-yl)ethyl)acet-amide (12). **11** (2.5 g, 7.20 mmol) was dissolved in 30 mL of DCM; then 8 mL of TFA was added and stirred at r.t. for 30 min. After that, the solvent was removed under vacuum and purified with column chromatography to afford light red oil 1.6 g, yield 90%. ^1H NMR (400

MHz, DMSO- d_6): δ 10.65 (s, 1H), 8.01 (s, 1H), 7.23 (d, $J = 8.7$ Hz, 1H), 7.12 (d, $J = 2.3$ Hz, 1H), 7.05 (d, $J = 2.4$ Hz, 1H), 6.72 (dd, $J = 8.7, 2.4$ Hz, 1H), 3.77 (s, 3H), 3.38 (q, $J = 7.1$ Hz, 2H), 3.11 (s, 2H), 2.81 (t, $J = 7.4$ Hz, 2H), 2.29 (brs, 2H) ppm. ^{13}C NMR (101 MHz, DMSO- d_6): δ 173.0, 153.5, 131.9, 128.0, 123.8, 112.5, 111.9, 111.5, 100.7, 55.8, 55.4, 44.7, 25.7 ppm. LRMS (ESI+) m/z calcd for $[\text{C}_{13}\text{H}_{18}\text{N}_3\text{O}_2]^+$: 248.13, found: 248.20 $[\text{M} + \text{H}]^+$. HPLC (method B): $t_{\text{R}} = 6.15$ min.

Methyl (E)-3-(4-(((2-(5-Methoxy-1H-indol-3-yl)-ethyl)amino)-2-oxoethyl)amino)methyl)phenylacrylate (13a). Intermediate **13a** was prepared from intermediate **12** and methyl (E)-3-(4-(bromomethyl)-phenyl)acrylate in a similar manner as described for intermediate **2a**. Yellow oil, yield 30%. ^1H NMR (400 MHz, DMSO- d_6): δ 10.66 (s, 1H), 7.90 (t, $J = 5.7$ Hz, 1H), 7.65 (d, $J = 15.7$ Hz, 1H), 7.64 (d, $J = 8.4$ Hz, 2H), 7.32 (d, $J = 8.1$ Hz, 2H), 7.24 (d, $J = 8.7$ Hz, 1H), 7.12 (d, $J = 2.3$ Hz, 1H), 7.05 (d, $J = 2.4$ Hz, 1H), 6.73 (dd, $J = 8.7, 2.4$ Hz, 1H), 6.62 (d, $J = 16.1$ Hz, 1H), 3.76 (s, 3H), 3.73 (s, 3H), 3.66 (s, 2H), 3.40 (q, $J = 7.0$ Hz, 2H), 3.07 (s, 2H), 2.81 (t, $J = 7.2$ Hz, 2H) ppm (one exchangeable proton not observed). ^{13}C NMR (101 MHz, DMSO- d_6): δ 171.0, 167.2, 153.5, 144.9, 143.3, 133.0, 131.9, 129.0 (2C), 128.7 (2C), 128.0, 123.8, 117.7, 112.5, 111.9, 111.5, 100.7, 55.8, 55.4, 52.7, 51.9, 51.8, 25.7 ppm. LRMS (ESI+) m/z calcd for $[\text{C}_{24}\text{H}_{28}\text{N}_3\text{O}_4]^+$: 422.20, found: 422.20 $[\text{M} + \text{H}]^+$. HPLC (method B): $t_{\text{R}} = 8.69$ min.

Methyl 4-(((2-(5-Methoxy-1H-indol-3-yl)ethyl)-amino)-2-oxoethyl)amino)methyl)benzoate (13b). Intermediate **13b** was prepared from intermediate **12** and methyl 4-(bromomethyl)benzoate in a similar manner as described for intermediate **2a**. Pale yellow oil, yield 16%. ^1H NMR (400 MHz, DMSO- d_6): δ 10.66 (s, 1H), 7.93–7.84 (m, 3H), 7.41 (d, $J = 8.2$ Hz, 2H), 7.23 (d, $J = 8.7$ Hz, 1H), 7.12 (d, $J = 2.2$ Hz, 1H), 7.05 (d, $J = 2.3$ Hz, 1H), 6.73 (dd, $J = 8.7, 2.4$ Hz, 1H), 3.85 (s, 3H), 3.76 (s, 3H), 3.69 (s, 2H), 3.40 (q, 7.0 Hz, 2H), 3.07 (s, 2H), 2.81 (t, $J = 7.2$ Hz, 2H) ppm (one exchangeable proton not observed). ^{13}C NMR (101 MHz, DMSO- d_6): δ 171.1, 166.7, 153.5, 146.6, 131.9, 129.5 (2C), 128.6 (2C), 128.5, 128.0, 123.8, 112.5, 112.0, 111.5, 100.7, 55.8, 52.7, 52.5, 52.0, 25.7 ppm. LRMS (ESI+) m/z calcd for $[\text{C}_{22}\text{H}_{26}\text{N}_3\text{O}_4]^+$: 396.18, found: 396.20 $[\text{M} + \text{H}]^+$. HPLC (method B): $t_{\text{R}} = 8.30$ min.

Methyl 6-(((2-(5-Methoxy-1H-indol-3-yl)ethyl)-amino)-2-oxoethyl)amino)hexanoate (13c). Intermediate **13c** was prepared from intermediate **12** and methyl 6-bromohexanoate in a similar manner as described for intermediate **2a**. Yellow oil, yield 42%. ^1H NMR (400 MHz, MeOD- d_4): δ 7.24 (d, $J = 8.8$ Hz, 1H), 7.07 (s, 1H), 7.07 (d, $J = 2.4$ Hz, 1H), 6.77 (dd, $J = 8.8, 2.4$ Hz, 1H), 3.84 (s, 3H), 3.74 (s, 2H), 3.67 (s, 3H), 3.61–3.54 (m, 2H), 2.95 (t, $J = 7.0$ Hz, 2H), 2.77 (t, $J = 7.6$ Hz, 2H), 2.34 (t, $J = 7.3$ Hz, 2H), 1.93–1.83 (m, 2H), 1.74–1.52 (m, 2H), 1.43–1.23 (m, 2H) ppm (exchangeable protons not observed). ^{13}C NMR (101 MHz, MeOD- d_4): δ 174.2, 167.6153.6, 131.0, 127.3, 122.9, 112.2, 111.7, 111.4, 99.8, 54.6, 52.5, 50.7, 49.8, 48.6, 33.2, 28.2, 26.3, 24.9, 24.6 ppm. LRMS (ESI+) m/z calcd for $[\text{C}_{20}\text{H}_{30}\text{N}_3\text{O}_4]^+$: 376.22, found: 376.20 $[\text{M} + \text{H}]^+$. HPLC (method B): $t_{\text{R}} = 7.96$ min.

Methyl (E)-3-(4-(((E)-3-(4-((Ethoxycarbonyl)oxy)-3-methoxyphenyl)-N-(2-((2-(5-methoxy-1H-indol-3-yl)-ethyl)amino)-2-oxoethyl)acrylamido)methyl)phenyl)-acrylate (14a). Intermediate **14a** was prepared from intermediate **13a** and ferulic acid in a similar manner as described for intermediate **9a**. White solid, yield 44%. ^1H NMR (400 MHz, CDCl_3): δ 8.22/8.20* (s, 1H), 7.73*/7.67 (d, $J = 15.2$ Hz, 1H), 7.65/7.60* (d, $J = 16.0$ Hz, 1H), 7.45/7.31* (d, $J = 8.0$ Hz, 2H), 7.22/7.15* (d, $J = 8.8$ Hz, 2H), 7.19–7.01 (m, 5H), 6.99/6.95* (s, 1H), 6.88–6.76 (m, 1H), 6.65/6.62* (d, $J = 15.2$ Hz, 1H), 6.55/6.01* (t, $J = 5.4$ Hz, 1H), 6.42/6.37* (d, $J = 16.1$ Hz, 1H), 4.60/4.58* (s, 2H), 4.40–4.28 (m, 2H), 4.03/4.02* (s, 2H), 3.85 (s, 3H), 3.84 (s, 3H), 3.82 (s, 3H), 3.58/3.52* (q, $J = 6.4$ Hz, 2H), 2.95/2.86* (t, $J = 6.6$ Hz, 2H), 1.46–1.35 (m, 3H) ppm (the minor rotamer: 31%). ^{13}C NMR (101 MHz, CDCl_3): δ 168.9, 167.7, 167.3, 167.3, 154.1, 153.0, 151.6, 151.5, 143.9, 143.8, 141.5, 138.3, 134.2, 133.8, 128.9, 128.7, 128.5, 127.9, 127.1, 123.2, 122.8, 120.9, 120.6, 118.3, 116.5, 112.3, 112.3, 112.0, 112.0, 100.5, 100.4, 65.2, 65.2, 56.1, 56.0, 55.9, 52.2, 51.8, 51.0, 46.9, 39.7, 39.2, 24.9, 14.2, 8.6 ppm. LRMS

(ESI+) m/z calcd for $[C_{37}H_{40}N_3O_9]^+$: 670.27, found: 670.30 $[M + H]^+$. HPLC (method B): $t_R = 12.72$ min.

Methyl (E)-4-((3-(4-((Ethoxycarbonyloxy)-3-methoxyphenyl)-N-(2-((2-(5-methoxy-1H-indol-3-yl)ethyl)amino)-2-oxoethyl)acrylamido)methyl)benzoate (14b). Intermediate **14b** was prepared from intermediate **13b** and ferulic acid in a similar manner as described for intermediate **9a**. White solid, yield 71%. 1H NMR (400 MHz, $CDCl_3$): δ 8.05/8.02* (s, 1H), 7.91/7.81* (d, $J = 8.1$ Hz, 2H), 7.67–7.49 (m, 1H), 7.17–7.08 (m, 3H), 7.08–6.98 (m, 2H), 6.98–6.91 (m, 2H), 6.88 (s, 1H), 6.81–6.69 (m, 1H), 6.52*/6.50 (d, $J = 15.3$ Hz, 1H), 6.44/5.94* (t, $J = 5.1$ Hz, 1H), 4.54/4.52* (s, 2H), 4.32–4.15 (m, 2H), 3.95/3.91* (s, 2H), 3.84 (s, 3H), 3.80*/3.76 (s, 3H), 3.77*/3.75 (s, 3H), 3.59–3.39 (m, 2H), 2.87/2.79* (t, $J = 6.7$ Hz, 2H), 1.36–1.26 (m, 3H) ppm (the minor rotamer: 33%). ^{13}C NMR (101 MHz, $CDCl_3$): δ 169.3, 168.8, 167.7, 166.5, 154.1, 153.0, 151.5, 143.9, 141.5, 141.3, 133.8, 131.5, 130.3, 130.1, 129.9, 128.2, 126.5, 123.1, 122.9, 122.8, 121.4, 120.6, 118.0, 116.4, 116.2, 112.4, 112.3, 112.0, 111.9, 100.5, 65.2, 65.2, 56.0, 55.9, 52.2, 52.2, 51.2, 46.7, 39.7, 39.3, 24.9, 24.9, 14.2, 8.6 ppm. LRMS (ESI+) m/z calcd for $[C_{35}H_{38}N_3O_9]^+$: 644.25, found: 644.30 $[M + H]^+$. HPLC (method B): $t_R = 12.40$ min.

Methyl (E)-6-(3-(4-((Ethoxycarbonyloxy)-3-methoxyphenyl)-N-(2-((2-(5-methoxy-1H-indol-3-yl)ethyl)amino)-2-oxoethyl)acrylamido)hexanoate (14c). Intermediate **14c** was prepared from intermediate **13c** and ferulic acid in a similar manner as described for intermediate **9a**. Colorless oil, yield 35%. 1H NMR (400 MHz, $CDCl_3$): δ 8.18/8.16* (brs, 1H), 7.91–7.78 (m, 2H), 7.53–7.40 (m, 1H), 7.20–7.10 (m, 2H), 7.02–6.90 (m, 2H), 6.88–6.78 (m, 1H), 6.75*/6.71 (d, $J = 15.2$ Hz, 1H), 6.45/6.00* (t, $J = 5.2$ Hz, 1H), 4.30–4.15 (m, 2H), 3.89/3.86* (s, 2H), 3.82–3.58 (m, 9H), 3.55–3.47 (m, 2H), 2.83–2.67 (m, 4H), 2.52–2.23 (m, 2H), 1.66–1.45 (m, 4H), 1.35–1.20 (m, 5H) ppm (the minor rotamer: 34%). ^{13}C NMR (101 MHz, $CDCl_3$): δ 173.1, 173.0, 171.2, 168.7, 167.1, 165.2, 153.7, 148.5, 148.1, 143.5, 134.3, 128.2, 127.9, 127.3, 123.12, 123.08, 122.6, 120.4, 116.7, 115.1, 113.4, 112.0, 110.9, 99.3, 63.02, 62.96, 56.2, 55.9, 55.4, 55.2, 41.2, 31.9, 28.2, 27.4, 26.9, 25.9, 25.7, 25.6, 24.9, 24.8, 24.7, 24.6, 14.3, 8.6 ppm. LRMS (ESI+) m/z calcd for $[C_{33}H_{42}N_3O_9]^+$: 624.28, found: 624.30 $[M + H]^+$. HPLC (method B): $t_R = 12.19$ min.

(E)-3-(4-Hydroxy-3-methoxyphenyl)-N-(4-((E)-3-(hydroxyamino)-3-oxoprop-1-en-1-yl)benzyl)-N-(2-((2-(5-methoxy-1H-indol-3-yl)ethyl)amino)-2-oxoethyl)acrylamide (15a). Compound **15a** was prepared from **14a** in a similar manner as described for compound **3a**. Off-white solid, yield 44%. 1H NMR (400 MHz, $MeOD-d_4$): δ 7.67–7.30 (m, 4H), 7.27–7.12 (m, 3H), 7.12–6.93 (m, 4H), 6.90–6.60 (m, 3H), 6.54–6.36 (m, 1H), 4.75–4.50 (m, 2H), 4.17–3.91 (m, 2H), 3.89–3.73 (m, 6H), 3.51/3.47* (t, $J = 7.3$ Hz, 1H), 3.00–2.82 (m, 2H) ppm (exchangeable protons not observed) (the minor rotamer: 22%). ^{13}C NMR (101 MHz, $MeOD-d_4$): δ 171.2, 169.5, 169.3, 168.9, 164.9, 153.6, 148.9, 147.9, 144.3, 144.2, 139.7, 138.8, 134.3, 132.0, 128.7, 128.3, 127.9, 127.8, 127.7, 127.3, 126.9, 123.1, 122.9, 122.4, 117.3, 115.1, 113.5, 113.3, 111.8, 111.6, 111.5, 111.2, 110.5, 110.5, 100.0, 55.1, 54.98, 54.95, 51.9, 50.0, 49.6, 39.9, 39.8, 24.7, 24.6 ppm. IR (film): ν 3222, 2934, 2831, 1644, 1591, 1516, 1489, 1459, 1444, 1423, 1279, 1208, 1174, 1126, 1029, 972, 792, 743, 706, 662 cm^{-1} . LRMS (ESI+) m/z calcd for $[C_{33}H_{35}N_4O_7]^+$: 599.24, found: 599.30 $[M + H]^+$. HPLC (method B): $t_R = 10.38$ min, purity = 98.9%. mp = 140–142 °C.

(E)-N-Hydroxy-4-((3-(4-hydroxy-3-methoxyphenyl)-N-(2-((2-(5-methoxy-1H-indol-3-yl)ethyl)amino)-2-oxoethyl)acrylamido)methyl)benzamide (15b). Compound **15b** was prepared from **14b** in a similar manner as described for compound **3a**. Golden yellow solid, yield 22%. 1H NMR (400 MHz, $MeOD-d_4$): δ 8.15–7.54 (m, 3H), 7.50–7.19 (m, 3H), 7.19–6.92 (m, 4H), 6.88–6.48 (m, 3H), 4.80–4.54 (m, 2H), 4.23–3.92 (m, 2H), 3.91–3.68 (m, 6H), 3.52/3.47* (t, $J = 6.8$ Hz, 2H), 2.99–2.82 (m, 2H) ppm (exchangeable protons not observed) (the minor rotamer: 19%). ^{13}C NMR (101 MHz, $MeOD-d_4$): δ 171.5, 171.3, 169.6, 169.1, 168.5, 166.7, 153.6, 149.0, 148.9, 147.9, 147.4, 144.7, 144.4, 141.3, 134.8, 132.0, 130.9, 129.3, 128.3, 128.0, 127.82, 127.75, 127.5, 127.4, 127.23, 127.15, 126.8, 123.1, 123.0, 122.9, 122.5, 122.0, 119.3, 115.1, 114.8, 113.0, 111.9, 111.62,

111.60, 111.4, 111.1, 110.5, 100.0, 55.2, 55.1, 55.03, 54.99, 52.6, 51.9, 50.5, 50.1, 40.1, 39.9, 24.8, 24.6 ppm. IR (film): ν 3229, 2933, 2830, 1641, 1595, 1581, 1521, 1491, 1462, 1447, 1283, 1253, 1211, 1173, 1127, 1024, 1013, 894, 793, 708 cm^{-1} . LRMS (ESI+) m/z calcd for $[C_{31}H_{33}N_4O_7]^+$: 573.23, found: 573.30 $[M + H]^+$. HPLC (method B): $t_R = 9.91$ min, purity = 97.0%. mp = 98–100 °C.

(E)-N-Hydroxy-6-(3-(4-hydroxy-3-methoxyphenyl)-N-(2-((2-(5-methoxy-1H-indol-3-yl)ethyl)amino)-2-oxoethyl)acrylamido)hexanamide (15c). Compound **15c** was prepared from **14c** in a similar manner as described for compound **3a**. Red solid, yield 60%. 1H NMR (400 MHz, $MeOD-d_4$): δ 7.57–7.18 (m, 2H), 7.17–7.03 (m, 3H), 7.01–6.41 (m, 4H), 4.24–3.75 (m, 8H), 3.60–3.50 (m, 2H), 2.95/2.90* (t, $J = 6.6$ Hz, 2H), 2.12/2.00* (t, $J = 7.0$ Hz, 2H), 1.74–1.43 (m, 4H), 1.41–1.04 (m, 4H) ppm (exchangeable protons not observed) (the minor rotamer: 17%). ^{13}C NMR (101 MHz, $MeOD-d_4$): δ 171.0, 170.1, 170.0, 167.7, 167.0, 164.7, 153.6, 148.8, 147.9, 143.8, 132.0, 127.81, 127.77, 127.0, 123.1, 122.2, 119.1, 115.1, 114.0, 111.6, 111.2, 110.7, 99.9, 63.0, 62.9, 55.2, 55.1, 55.01, 54.97, 40.0, 32.1, 28.3, 27.4, 26.6, 25.9, 25.72, 25.66, 24.91, 24.85, 24.7, 24.6 ppm. IR (film): ν 3174, 3074, 3020, 2936, 2881, 1632, 1575, 1511, 1480, 1450, 1433, 1370, 1273, 1209, 1195, 1162, 1123, 1070, 1024, 996, 974, 815, 792, 663 cm^{-1} . LRMS (ESI+) m/z calcd for $[C_{29}H_{37}N_4O_7]^+$: 553.26, found: 553.25 $[M + H]^+$. HPLC (method B): $t_R = 9.97$ min, purity = 97.7%. mp = 55–58 °C.

In Vitro HDAC Inhibition Fluorescence Assay. All the HDAC enzymes were bought from BPS Bioscience. *In vitro* HDAC inhibition assays were conducted as previously described with minor modifications.⁵⁸ In brief, 20 μ L of recombinant HDAC enzyme solution (HDAC1–4, 6–9) was mixed with various concentrations of tested compound (20 μ L). The mixture was incubated at 30 °C for 1 h; then 10 μ L of fluorogenic substrate (Boc-Lys (acetyl)-AMC for HDAC1, 2, 3, and 6, Boc-Lys (trifluoroacetyl)-AMC for HDAC 4, 7, 8 and 9) was added. After incubation at 30 °C for 2 h, the catalysis was stopped by the addition of 10 μ L of developer containing trypsin. Thirty minutes later, fluorescence intensity was measured using a microplate reader at excitation and emission wavelengths of 360 and 460 nm, respectively. All samples were prepared in duplicate, and the minimum of two independent assays was performed for each compound. The inhibition ratios were calculated from the fluorescence intensity readings of tested wells relative to those of control wells, and the IC₅₀ curves and values were determined by GraphPad Prism 7.0, using the “log(inhibitor) versus normalized response - variable slope” function.

Western Blot Analysis of Cellular HDAC Inhibition. HT22 cells (1,500,000 per well) were plated in flat-bottom six-well plates and allowed to grow for 12 h and then treated with different concentrations of compounds. Twenty-four hours later, cells were harvested, washed by PBS, and lysed with RIPA buffer, which comprised 50 mM Tris base, 150 mM NaCl, 5 mM EDTA, 0.1% (v/v) SDS, 0.5% (v/v) sodium deoxycholate, and 1% (v/v) Triton-x-100. After lysing, the suspension was ultrasonicated and centrifuged at 14,000 rpm for 15 min at 4 °C. The mixture of 75 μ L of the supernatant and 25 μ L of β -mercaptoethanol/LDS solution (15:85) was heated at 90 °C for 15 min and normalization according to BCA test carried out before loading. Lysates were run on Invitrogen NuPAGE 4–12% Bis-Tris 15 well gels at 170 V for approximately 60 min in MES buffer. Gels were transferred to methylcellulose and run at 30 V for 3 h. Membranes were incubated at 4 °C overnight with 1/1000 primary antibodies, which were diluted in 2.5% (w/v) milk or 5% (w/v) bovine serum albumin. The membrane was washed twice with TBST buffer before being incubated with secondary antibodies. Images were acquired using a GE ImageQuant LAS 4000.

Computational Docking. Docking studies for compounds **8b** and **10b** were conducted based on the crystal structure of HDAC6 complexed with compound **A** (PDB: 6DVM).²¹ The preparation of the structures and the setup of the docking calculations with GOLD^{59,60} are described in detail in the Supporting Information. Figures were prepared with the PyMOL molecular graphics system (Schrödinger-LLC, version 2.4.1).

DPPH Assay. For determination of antioxidative properties, a 2,2-diphenyl-1-picrylhydrazyl (DPPH) radical assay was used as previously described.⁶¹ A stock solution (200 μM) of DPPH was freshly prepared in MeOH. Compounds were dissolved in MeOH (5 mM) as stock solution. To start the reaction, 50 μL of the DPPH stock solution was added to a 100 μL diluted compound or pure methanol as a negative control. The 96-well plate was incubated at room temperature in the dark for 30 min, and absorbance was then determined with a microplate reader at 517 nm. The experiments were performed in triplicates. A dilution series of compound served as a blank to the particular compound and was subtracted from each measurement point. The scavenging potency is expressed as the concentration that scavenged 50% of the DPPH free radicals (EC_{50}) determined via a nonlinear regression curve. Ferulic acid was used as references under the same assay conditions.

ORAC Assay. To study the antioxidant capacities of target compounds and the SAR of melatonin, we used the ORAC-fluorescein method of Ou *et al.*⁶² partially modified by Dávalos *et al.*⁶³ that uses fluorescein (FL) as a fluorescent probe, (\pm)-6-hydroxy-2,5,7,8-tetramethyl-chromane-2-carboxylic acid (Trolox) as a reference, and compound 2,2'-azobis(amidinopropane) dihydrochloride (AAPH) as a free-radical generator. When the free-radical generator is added, production of free radicals starts, and those oxidize fluorescein decreasing its fluorescence. When an antioxidant is present, the scavenger traps free radicals and the fluorescence remains unchanged. Reactions were performed in 75 mM PBS (pH 7.4), and the final reaction mixture volume was 200 μL at 37 $^{\circ}\text{C}$. Derivatives at the desired concentrations (20 μL) and FL (120 μL , 70 nM, final concentration) solutions were mixed in a black 96-well microplate (SARSTEDT) and preincubated for 15 min at 37 $^{\circ}\text{C}$. Subsequently, AAPH solution (60 μL , 12 mM, final concentration) was added rapidly and the plate was placed in a TECAN microplate reader to measure the fluorescence (485 nm excitation and 510 nm emission filters) intensity every 2 min for 90 min. Samples were measured at two different concentrations (2 and 4 μM). A blank (FL + AAPH in PBS) and a calibration curve of Trolox (1, 2, 4, 6, 8, 10, 12, and 15 μM) were included in each experiment. All samples were prepared in duplicate, and three independent assays were performed for each compound. The area under the fluorescence decay curve (fluorescence vs time) (AUC) was calculated as

$$\text{AUC} = 1 + \sum_{i=1}^{i=45} f_i/f_0$$

where f_0 is the initial fluorescence reading at 0 min and f_i is the fluorescence reading at time $2i$. The net AUC corresponding to a sample was calculated by subtracting the AUC corresponding to the blank (Net AUC = $\text{AUC}_{\text{antioxidant}} - \text{AUC}_{\text{blank}}$). Linear regression equations were calculated by plotting the net AUC against the trolox antioxidant standard concentration ($R^2 > 0.99$). ORAC-FL values were expressed as trolox equivalents by using the standard curve calculated for each assay, where the ORAC-FL value of Trolox was taken as 1, plot the Trolox standard curve, and interpolate it to determine sample ORAC values.

Metal Chelating Assays. The chelating ability to the ferrous ion was carried out as Santos *et al.*⁶⁴ described and partially modified. The ferrous ion in ferrous sulfate readily reacts with ferrozine (3-(2-Pyridyl)-5,6-diphenyl-1,2,4-triazine-*p,p'*-disulfonic acid monosodium salt hydrate) to form a Fe^{2+} -ferrozine complex, a purple-colored chromogen whose intensity is measured at 562 nm. The presence of antioxidant chelators reduces the formation of Fe^{2+} -ferrozine complex. Lower absorbance indicates higher metal-chelating activity. NaAc buffer was prepared (50 mM, pH 6.0). To start the reaction, 50 μL of Fe^{2+} aq. (80 μM in buffer) was added to 100 μL diluted compounds-MeOH solution or pure methanol as a negative control. The 96-well plate was incubated at room temperature for 2 min, 50 μL of ferrozine aq. (250 μM in buffer) was added to each well and then incubated at room temperature for 10 min, and absorbance was then determined with a microplate reader at 562 nm. The experiments were performed in duplicates. The mixture of a dilution series of

compound and Fe^{2+} aq. served as a blank to the particular compound and was subtracted from each measurement point. EDTA-2Na in water was diluted with MeOH, which was served as a reference under the same assay conditions.

The ability of compounds to chelate Cu^{2+} was assessed using the method as Santos *et al.*⁶⁴ described and partially modified that employs pyrocatechol violet (PV) as the chromogen agent. In aqueous medium buffered at slightly acidic medium (pH 6.0). There is usually a leftover of Cu^{2+} in the reactional medium because not all the copper is bound by chemical compounds present in a test sample. Thereafter, the remaining Cu^{2+} reacts with pyrocatechol violet at a proportion of 2:1, forming a blue-colored complex that can be monitored at 632 nm. However, the dark color turns into yellow in the presence of chelating agents that dissociate the complex, and the chelating activity can thus be estimated by the measurement of the rate of color reduction. Briefly, in each well, 50 μL of Cu^{2+} aq. (400 μM in buffer) was added to 100 μL diluted compounds-MeOH solution or pure methanol as negative control. The 96-well-plate was incubated at room temperature for 2 min, 50 μL of PV aq. (400 μM in buffer) was added to each well (avoid the light) and then incubated at room temperature for 10 min, and absorbance was then determined with a microplate reader at 632 nm. The experiments were performed in duplicates. EDTA-2Na in water was diluted with MeOH, which was served as a reference under the same assay conditions.

The chelating ability to zinc ions was carried out as Catapano *et al.*⁶⁵ described and partially modified. Stock solutions of target compounds (10 mM) were prepared in DMSO, whereas that of zinc chloride (10 mM) and EDTA (10 mM) were prepared in ultrapure water. Dithizone (10 mM) as the chromogen agent was prepared in DMSO. NaAc buffer was prepared (50 mM, pH 6.0). Firstly, zinc-ion solutions (50 μL , 60 μM) or water was added to the buffers (150 μL). Thereafter, 50 μL of diluted compounds-DMSO solution or pure DMSO was added. After 2 min of mixing, 50 μL of dithizone-DMSO solution (250 μM) was added, and the absorbance was measured immediately at 540 nm.

The chelation ratios were calculated from the absorbance intensity readings of tested wells relative to those of control wells, data are expressed as means \pm SEM of two different independent experiments.

Neurotoxicity Assay. HT-22 cells were grown in Dulbecco's modified Eagle medium (DMEM, Sigma-Aldrich, Munich Germany) supplemented with 10% (v/v) heat-inactivated fetal calf serum (FCS) and 1% (v/v) penicillin-streptomycin. Cells were subcultured every 2 days and incubated at 37 $^{\circ}\text{C}$ with 5% CO_2 in a humidified incubator. Compounds were dissolved in DMSO (Sigma-Aldrich, Munich, Germany) and diluted with a medium. Generally, 80% confluent cells were seeded with 5000 cells per well into sterile 96-well plates and were incubated for 24 h. For the neurotoxicity assay, the previous medium was removed and 10 μM of the compound was added to the wells, DMSO (0.05%) in DMEM served as a control. Cells were incubated for 24 h. MTT solution (4 mg/mL in PBS) was diluted 1:10 with medium and added to the wells after the removal of the previous medium. Cells were incubated for 3 h when the supernatant was removed, and lysis buffer (10% SDS) was applied. The next day, absorbance at 560 nm was determined with a multiwell plate photometer (Tecan-SpectraMax 250). Experiments were performed in triplicates. Results are presented as percentage to untreated control cells. Data are expressed as means \pm SD of three different independent experiments. Analysis was accomplished using GraphPad Prism 7 Software applying oneway ANOVA followed by Dunnett's multiple comparison posttest. Levels of significance: * $p < 0.05$; ** $p < 0.01$; *** $p < 0.001$.

For the oxytosis assay, 5 mM glutamate (monosodium-L-glutamate, Sigma-Aldrich, Munich, Germany) together with respective compounds was added to the cells and incubated for 24 h. Quercetin (25 μM) (Sigma-Aldrich, Munich, Germany) together with 5 mM glutamate served as a positive control. After 24 h incubation, cell viability was determined using a colorimetric MTT assay as described above. Results are presented as percentage of untreated control cells. Data is expressed as means \pm SEM of two independent experiments. Analysis was accomplished using GraphPad Prism 7 Software applying

Oneway ANOVA followed by Dunnett's multiple comparison posttest. Levels of significance: *** $p < 0.001$.

For the ATP depletion assay, 3×10^3 cells per well were seeded into sterile 96-well plates and incubated overnight. The next day medium was exchanged with fresh medium. Iodoacetic acid (20 μ M) (IAA) was added with a vehicle (DMSO) as a negative control, or together with respective compounds for protection. After 2 h incubation at 37 °C in the incubator, the medium was aspirated, the fresh medium was applied, and only the compounds at the same respective concentrations were added without IAA. After 24 h, cell viability was determined using a colorimetric MTT assay. Results are presented as percentage of untreated control cells.

Immunomodulation Analysis. Mouse N9-microglial cells were cultured in Dulbecco modified eagle medium (DMEM) supplemented with 10% heat inactivated Fetal Bovine Serum (FBS), 1% penicillin/streptomycin, and 2 mM glutamine (all from Aurogene Srl, Rome, Italy). To evaluate the immunomodulatory effect, 2.5×10^5 microglial cells were plated in a 35 mm dish in the presence or absence of 100 ng/mL LPS (lipopolysaccharide) with increasing concentrations of compounds. After 24 h of treatment, the microglial conditioned medium was collected and used for nitrite measurement, or concentrated using Microcon YM-3 (Millipore, Billerica, MA), and resuspended in 4 \times loading buffer (0.2 M Tris-HCL pH 6.8; sodium dodecyl sulfate; 40% glycerol; 0.4% bromophenol blue and 0.4 M dithiothreitol; Sigma-Aldrich) for Western blot analysis. In parallel, microglial cells were collected in lysis buffer (1% SDS, 50 Mm Tris pH 7.4, 1 mM EDTA, 10 μ L/mL protease inhibitors and 10 μ L/mL phosphatase inhibitors), and protein content was determined by using the Lowry protein assay.

For Western blot analysis, media and cell samples were briefly sonicated and loaded into 12% sodium-dodecyl sulfate-polyacrylamide gels (SDS-PAGE; Bio-Rad). After electrophoresis and transfer onto nitrocellulose membranes (GE Healthcare, Milano, Italy), membranes were blocked 1 h in blocking solution PBS-0.1% Tween-20 (Sigma-Aldrich), 4% non-fat dry milk (Bio-Rad), and incubated overnight at 4 °C with primary antibodies in PBS-0.1% Tween-20: rabbit anti-iNOS (1:1000, Cell Signaling Technology, Danvers, Massachusetts, USA), rabbit anti-TREM2 (1:1000, Cell Signaling Technology), mouse anti-TGF β 2 (1:1000 Abcam, Cambridge, UK), and mouse anti-GAPDH (1:20,000, Dako North America, Agilent Technologies, USA). The next day, membranes were then incubated with specific antibodies conjugated to horseradish peroxidase (goat anti-rabbit and goat-anti mouse, 1:5000, Jackson ImmunoResearch, Cambridge, UK) for 90 min at RT in PBS-0.1% Tween-20. Proteins were visualized by using the Clarity Western ECL Substrate (Bio-Rad) and detected using Bio-Rad Image Lab Software with a ChemiDoc imaging system (Bio-Rad).

For nitrite measurement, accumulation of NO in microglial conditioned media was quantified by a colorimetric assay based on Greiss reaction in a 96-well-plate. A nitrate standard curve was performed with NaNO₂ at known concentrations. To start the reaction, 5 mM sulfanilamide (Sigma-Aldrich) was added to the culture medium and standard curve; it reacts with nitrite under acidic conditions to form a diazonium cation, which subsequently couples to *N*-1-naphthylethylenediamine dihydrochloride 40 mM (NEDA; Sigma-Aldrich) to produce a colored azo dye. After 15 min of incubation at RT in the dark, absorbance was read at 540 nm with a multiplate spectrophotometric reader (Bio-rad Laboratories Srl, Milano, Italy).

All quantitative data are presented as means \pm S.E. from at least three independent experiments. Statistical significance between different treatments was calculated with GRAPHPAD PRISM6 (L Jolla, California, USA) using one-way analysis of variance (ANOVA) followed by post-hoc comparison Bonferroni's test. A value of $p < 0.05$ was considered statistically significant.

In Vivo Studies. Protocols for the behavioral experiments were established previously.^{54–57} Compound **10b** and the control ACY1215 were tested for their neuroprotective properties in the *in vivo* pharmacological model of Alzheimer's disease induced by intracerebroventricular (icv) injection of the oligomerized A β _{25–35}

peptide in the mouse. Compounds were injected intraperitoneally (ip) o.d. between days 1 and 7, the oligomerized A β _{25–35} peptide was injected icv on the first day of the study, and behavioral evaluation was performed between days 8 and 10 followed by sacrifice on day 11. Brain samples were collected and stored at –80 °C awaiting further biochemical analyses.

Animals. Male Swiss mice, 6 weeks old, weighing 31–36 g, from JANVIER (Saint Berthevin, France), were kept for housing, and experiments took place within the animal facility building of the University of Montpellier (CECEMA, Office of Veterinary Services agreement # B-34-172-23). Upon arrival, animals were divided into groups and housed with access to food and water *ad libitum*, except during behavioral experiments. Mice were kept in a temperature- and humidity-controlled animal facility on a 12 h/12 h light/dark cycle (lights off at 07:00 PM). All animal procedures were conducted in strict adherence to the European Union directive of September 22, 2010 (2010/63/UE) and the ARRIVE guidelines. The project was authorized by the French National Ethic Committee (APAFIS #1485-15034).

Preparation of Compound Injection. Compounds were weighed, dissolved in pure DMSO at a concentration of 1 mg/mL, and diluted into final test concentrations with saline. The final percentage of DMSO in saline was 60% for all compounds. Vehicle solution used for control groups was 60% DMSO in saline. General behavior of the mice in the home cage was checked visually after injections. In particular, weight gain was checked every day. As shown in Figure S2, the icv injection affected animals on day 1, but then weight gain was regular and not significantly different from control. All treatments showed good compound and vehicle solution tolerability. Moreover, animals were tested in behavioral tests 24 h after the last compound/vehicle administration.

Amyloid Peptide Preparation and icv Injection. Mice were anesthetized with isoflurane (2.5%) and icv injected with the A β _{25–35} peptide (9 nmol/mouse), and homogeneous oligomeric preparation of the A β _{25–35} peptide was performed as described by Maurice *et al.*⁵⁴ The control group received bidistilled water icv as we previously reported that injection of a control peptide does not result in memory deficits or toxicity.

Spontaneous Alternation Performances in the Y Maze. On day 8, all animals were tested for spontaneous alternation performance in the Y maze to evaluate their spatial working memory. The Y maze is made of gray poly(vinyl chloride). Each arm is 40 cm long, 13 cm high, 3 cm wide at the bottom, 10 cm wide at the top, and converging at an equal angle. Each mouse is placed at the end of one arm and allowed to explore the maze freely for 8 min. The sequence of arm entries (including possible returns into the same arm) was checked visually and noted down. If the mouse enters all three arms on consecutive occasion, this is defined as an alternation. Therefore, the total number of arm entries minus two is also the maximum number of alternations. The percentage of alternation was calculated as (actual alternations/maximum alternations) \times 100. Parameters for the evaluation of behavior are given as the percentage of alternation (memory index) and the total number of arm entries (exploration index). When an extreme behavior (alternation percentage $< 20\%$ or $> 90\%$ or a number of arm entries of < 10) was observed, animals were excluded from the calculations, which corresponded to a 4.7% attrition in this study.

Passive Avoidance Test. On days 9 and 10 of the study, a passive avoidance test was performed to measure nonspatial long-term memory, as described previously.^{54–57} The setup for the experiment consists of a two-compartment (15 \times 20 \times 15 cm high) poly(vinyl chloride) box, whereas one compartment is white and illuminated with a bulb (60 W, 40 cm above the apparatus), and the other is black with a cover and grid floor. A guillotine door separates the two compartments. On day 9, during the training session, each animal was placed in the white compartment with the door closed. After 5 s, the door was opened, and the mouse was allowed to enter the dark compartment. When it had placed all its paws on the grid floor, the door was closed, and a foot shock was delivered (0.3 mA) for 3 s using a scrambled shock generator (Lafayette Instruments, Lafayette,

USA). The time spent to enter the dark compartment (step-through latency) and the level of sensitivity to the shock were evaluated (no sign = 0, flinching reactions = 1, vocalizations = 2). None of the treatments affected the step-through latency or shock sensitivity in the present study (data not shown). The retention test was carried out on day 10. Five seconds after the mouse was placed in the white compartment, the door was opened, and the mouse was allowed to explore the box. The time spent to enter the dark compartment (step-through latency) was measured up to 300 s. Animals showing latencies during the training and retention session lower than 10 s and shock sensitivity = 0 were considered as failing to learn the task and discarded from calculations. In this study, it corresponded to 0.6% attrition.

Statistical Analyses. All values, except passive avoidance latencies, are expressed as mean \pm SEM. Statistical analyses were performed on the different conditions using one-way ANOVA (F value), followed by Dunnett's post hoc multiple comparison test. Passive avoidance latencies do not follow a Gaussian distribution since upper cutoff times (300 s) are defined. Therefore, they were analyzed using a Kruskal–Wallis nonparametric ANOVA (H value) followed by Dunn's multiple comparison test. $p < 0.05$ was considered as statistically significant.

■ ASSOCIATED CONTENT

Supporting Information

The Supporting Information is available free of charge at <https://pubs.acs.org/doi/10.1021/acs.jmedchem.0c01940>.

HPLC-chromatograms of target compounds, details of computational docking, metal chelation, neuroprotection against oxytosis and ATP depletion, and weight of animals during *in vivo* studies (PDF)

Molecular formula strings (CVS)

■ AUTHOR INFORMATION

Corresponding Authors

Tangui Maurice – MMDN, Univ Montpellier, EPHE, INSERM, Montpellier 34095, France;
Email: tangui.maurice@umontpellier.fr

Michael Decker – Pharmaceutical and Medicinal Chemistry, Institute of Pharmacy and Food Chemistry, Julius Maximilian University of Würzburg, Würzburg 97074, Germany; orcid.org/0000-0002-6773-6245;
Phone: +49-93131-89676; Email: michael.decker@uni-wuerzburg.de; Fax: +49-931 31-85494

Authors

Feng He – Pharmaceutical and Medicinal Chemistry, Institute of Pharmacy and Food Chemistry, Julius Maximilian University of Würzburg, Würzburg 97074, Germany

C. James Chou – Department of Drug Discovery and Biomedical Sciences, South Carolina College of Pharmacy, Medical University of South Carolina, Charleston, South Carolina 29425, United States; orcid.org/0000-0001-6808-9089

Matthias Scheiner – Pharmaceutical and Medicinal Chemistry, Institute of Pharmacy and Food Chemistry, Julius Maximilian University of Würzburg, Würzburg 97074, Germany

Eleonora Poeta – Department of Pharmacy and Biotechnologies, University of Bologna, Bologna 40126, Italy

Natalia Yuan Chen – Pharmaceutical and Medicinal Chemistry, Institute of Pharmacy and Food Chemistry, Julius Maximilian University of Würzburg, Würzburg 97074, Germany

Sandra Gunesch – Pharmaceutical and Medicinal Chemistry, Institute of Pharmacy and Food Chemistry, Julius Maximilian University of Würzburg, Würzburg 97074, Germany

Matthias Hoffmann – Pharmaceutical and Medicinal Chemistry, Institute of Pharmacy and Food Chemistry, Julius Maximilian University of Würzburg, Würzburg 97074, Germany

Christoph Sotriffer – Pharmaceutical and Medicinal Chemistry, Institute of Pharmacy and Food Chemistry, Julius Maximilian University of Würzburg, Würzburg 97074, Germany

Barbara Monti – Department of Pharmacy and Biotechnologies, University of Bologna, Bologna 40126, Italy;
orcid.org/0000-0003-0330-482X

Complete contact information is available at:
<https://pubs.acs.org/doi/10.1021/acs.jmedchem.0c01940>

Author Contributions

The manuscript was written through the contributions of all authors. Synthesis of the target compounds, DPPH assay, ORAC assay, and metal chelation assay were performed by F.H. HDAC inhibition assay was performed by C.J.C. The docking study was conducted by N.Y.C. and C.S. The neurotoxicity experiment was performed by S.G. The immunomodulation study was performed by E.P. and B.M. *In vivo* experiments were performed by M.S., M.H., and T.M. M.D. was responsible for the oversight and development of the whole project.

Funding

M.D. acknowledges the German Research Council (Deutsche Forschungsgemeinschaft) under DFG DE 1546/6-3. M.D. and T.M. acknowledge support from Campus France (PHC Procope) and the German Academic Exchange Service (DAAD) with funds of the Federal Ministry of Education and Research (BMBF) under Grant # 57387204, as well as support from BayFrance (Franco-Bavarian University cooperation center) under Grant # FK03-2020. F.H. acknowledges the Ph.D. scholarship from the China Scholarship Council (CSC). N.Y.C. acknowledges support from the German Academic Exchange Service (DAAD). M.H. acknowledges the German Academic Scholarship Foundation (“Studienstiftung des deutschen Volkes”) for a Ph.D. fellowship and the Elite Network of Bavaria (International Doctoral Program “Receptor Dynamics”) for support.

Notes

The authors declare no competing financial interest.

■ ABBREVIATIONS

AAPH, 2,2'-azobis(amidinopropane) dihydrochloride; A β , amyloid-beta; AChE, acetylcholinesterase; AD, Alzheimer's disease; ANOVA, analysis of variance; APP, amyloid precursor protein; ChEs, cholinesterases; DCM, dichloromethane; DMSO, dimethylsulfoxide; EDTA, ethylenediaminetetraacetic acid; FL, fluorescein; HDAC, histone deacetylase; HSP-90, heat shock protein 90; Il-1 β , interleukin 1 beta; iNOS, inducible nitric oxide synthase; LPS, lipopolysaccharides; MIF, macrophage migration inhibitory factor; MTT, 3-(4,5-dimethylthiazol-2-yl)-2,5-diphenyltetrazolium bromide; M.P., melting point; NFTs, neurofibrillary tangles; NMDAR, N-methyl-D-aspartate receptor; PBS, phosphate buffered saline; PDE5, phosphodiesterase 5 (PDE5); ROS, reactive oxygen species;

TBTU, *O*-(benzotriazol-1-yl)-*N,N,N,N'*-tetra-methyluronium tetrafluoroborate; TEA, trimethylamine; TFA, trifluoroacetic acid; TGF β 2, transforming growth factor beta-2; THF, tetrahydrofuran; TREM2, triggering receptor expressed on myeloid cells 2; Trolox, (\pm)-6-hydroxy-2,5,7,8-tetramethylchromane-2-carboxylic acid; TSA, trichostatin A; YMT, Y-maze test; ZBG, zinc binding group;

REFERENCES

- (1) Ho, T. C. S.; Chan, A. H. Y.; Ganesan, A. Thirty years of HDAC inhibitors: 2020 insight and hindsight. *J. Med. Chem.* **2020**, *63*, 12460–12484.
- (2) Penney, J.; Tsai, L.-H. Histone deacetylases in memory and cognition. *Sci. Signaling* **2014**, *7*, re12.
- (3) Ding, H.; Dolan, P. J.; Johnson, G. V. W. Histone deacetylase 6 interacts with the microtubule-associated protein tau. *J. Neurochem.* **2008**, *106*, 2119–2130.
- (4) Shen, S.; Kozikowski, A. P. A patent review of histone deacetylase 6 inhibitors in neurodegenerative diseases (2014–2019). *Expert Opin. Ther. Pat.* **2020**, *30*, 121–136.
- (5) Brindisi, M.; Saraswati, A. P.; Brogi, S.; Gemma, S.; Butini, S.; Campiani, G. Old but gold: tracking the new guise of histone deacetylase 6 (HDAC6) enzyme as a biomarker and therapeutic target in rare diseases. *J. Med. Chem.* **2020**, *63*, 23–39.
- (6) Thomas, E. A.; D'Mello, S. R. Complex neuroprotective and neurotoxic effects of histone deacetylases. *J. Neurochem.* **2018**, *145*, 96–110.
- (7) Fan, S. J.; Huang, F. I.; Liou, J. P.; Yang, C. R. The novel histone deacetylase 6 inhibitor, MPTOG211, ameliorates tau phosphorylation and cognitive deficits in an Alzheimer's disease model. *Cell Death Dis.* **2018**, *9*, 655.
- (8) Gaisina, I. N.; Lee, S. H.; Kaidery, N. A.; Ben Aissa, M.; Ahuja, M.; Smirnova, N. N.; Wakade, S.; Gaisin, A.; Bourassa, M. W.; Ratan, R. R.; Nikulin, S. V.; Poloznikov, A. A.; Thomas, B.; Thatcher, G. R. J.; Gazaryan, I. G. Activation of Nrf2 and hypoxic adaptive response contribute to neuroprotection elicited by phenylhydroxamic acid selective HDAC6 inhibitors. *ACS Chem. Neurosci.* **2018**, *9*, 894–900.
- (9) Lee, H.-Y.; Fan, S.-J.; Huang, F.-I.; Chao, H.-Y.; Hsu, K.-C.; Lin, T. E.; Yeh, T.-K.; Lai, M.-J.; Li, Y.-H.; Huang, H.-L.; Yang, C.-R.; Liou, J.-P. 5-Aroylindoles act as selective histone deacetylase 6 inhibitors ameliorating Alzheimer's disease phenotypes. *J. Med. Chem.* **2018**, *61*, 7087–7102.
- (10) Kinney, J. W.; Bemiller, S. M.; Murtishaw, A. S.; Leisgang, A. M.; Salazar, A. M.; Lamb, B. T. Inflammation as a central mechanism in Alzheimer's disease. *Alzheimer's Dementia* **2018**, *4*, 575–590.
- (11) Schotterl, S.; Brennenstuhl, H.; Naumann, U. Modulation of immune responses by histone deacetylase inhibitors. *Crit. Rev. Oncog.* **2015**, *20*, 139–154.
- (12) Song, Y.; Qin, L.; Yang, R.; Yang, F.; Kenechukwu, N. A.; Zhao, X.; Zhou, X.; Wen, X.; Li, L. Inhibition of HDAC6 alleviating lipopolysaccharide-induced p38MAPK phosphorylation and neuroinflammation in mice. *Pharm. Biol.* **2019**, *57*, 263–268.
- (13) Proschak, E.; Stark, H.; Merk, D. Polypharmacology by design: a medicinal chemist's perspective on multitargeting compounds. *J. Med. Chem.* **2019**, *62*, 420–444.
- (14) Zhou, J.; Jiang, X.; He, S.; Jiang, H.; Feng, F.; Liu, W.; Qu, W.; Sun, H. Rational design of multitarget-directed ligands: strategies and emerging paradigms. *J. Med. Chem.* **2019**, *62*, 8881–8914.
- (15) Bolognesi, M. L. Harnessing polypharmacology with medicinal chemistry. *ACS Med. Chem. Lett.* **2019**, *10*, 273–275.
- (16) Albertini, C.; Salerno, A.; de Sena Murteira Pinheiro, P.; Bolognesi, M. L. From combinations to multitarget-directed ligands: A continuum in Alzheimer's disease polypharmacology. *Med. Res. Rev.* **2020**, *1*.
- (17) De Simone, A.; Milelli, A. Histone deacetylase inhibitors as multitarget ligands: new players in Alzheimer's disease drug discovery? *ChemMedChem* **2019**, *14*, 1067–1073.
- (18) de Lera, A. R.; Ganesan, A. Two-hit wonders: the expanding universe of multitargeting epigenetic agents. *Curr. Opin. Chem. Biol.* **2020**, *57*, 135–154.
- (19) Smalley, J. P.; Cowley, S. M.; Hodgkinson, J. T. Bifunctional HDAC therapeutics: one drug to rule them all? *Molecules* **2020**, *25*, 4394.
- (20) Tomaselli, D.; Lucidi, A.; Rotili, D.; Mai, A. Epigenetic polypharmacology: a new frontier for epi-drug discovery. *Med. Res. Rev.* **2019**, *40*, 190–244.
- (21) Porter, N. J.; Osko, J. D.; Diedrich, D.; Kurz, T.; Hooker, J. M.; Hansen, F. K.; Christianson, D. W. Histone deacetylase 6-selective inhibitors and the influence of capping groups on hydroxamate-zinc denticity. *J. Med. Chem.* **2018**, *61*, 8054–8060.
- (22) Rabal, O.; Sánchez-Arias, J. A.; Cuadrado-Tejedor, M.; de Miguel, I.; Pérez-González, M.; García-Barroso, C.; Ugarte, A.; de Mendoza, A. E.-H.; Sáez, E.; Espeloso, M.; Ursua, S.; Haizhong, T.; Wei, W.; Musheng, X.; Garcia-Osta, A.; Oyarzabal, J. Design, synthesis, and biological evaluation of first-in-class dual acting histone deacetylases (HDACs) and phosphodiesterase 5 (PDE5) inhibitors for the treatment of Alzheimer's disease. *J. Med. Chem.* **2016**, *59*, 8967–9004.
- (23) Cuadrado-Tejedor, M.; Garcia-Barroso, C.; Sánchez-Arias, J. A.; Rabal, O.; Pérez-González, M.; Mederos, S.; Ugarte, A.; Franco, R.; Segura, V.; Perea, G.; Oyarzabal, J.; Garcia-Osta, A. A first-in-class small-molecule that acts as a dual inhibitor of HDAC and PDE5 and that rescues hippocampal synaptic impairment in Alzheimer's disease mice. *Neuropsychopharmacology* **2017**, *42*, 524–539.
- (24) Rabal, O.; Sánchez-Arias, J. A.; Cuadrado-Tejedor, M.; de Miguel, I.; Pérez-González, M.; García-Barroso, C.; Ugarte, A.; de Mendoza, A. E.-H.; Sáez, E.; Espeloso, M.; Ursua, S.; Tan, H.; Wu, W.; Xu, M.; Pineda-Lucena, A.; Garcia-Osta, A.; Oyarzabal, J. Multitarget approach for the treatment of Alzheimer's disease: inhibition of phosphodiesterase 9 (PDE9) and histone deacetylases (HDACs) covering diverse selectivity profiles. *ACS Chem. Neurosci.* **2019**, *10*, 4076–4101.
- (25) De Simone, A.; La Pietra, V.; Betari, N.; Petragiani, N.; Conte, M.; Daniele, S.; Pietrobono, D.; Martini, C.; Petralla, S.; Casadei, R.; Davani, L.; Frabetti, F.; Russomanno, P.; Novellino, E.; Montanari, S.; Tumiatti, V.; Ballerini, P.; Sarno, F.; Nebbioso, A.; Altucci, L.; Monti, B.; Andrisano, V.; Milelli, A. Discovery of the first-in-class GSK-3 β /HDAC dual inhibitor as disease-modifying agent to combat Alzheimer's disease. *ACS Med. Chem. Lett.* **2019**, *10*, 469–474.
- (26) He, F.; Ran, Y.; Li, X.; Wang, D.; Zhang, Q.; Lv, J.; Yu, C.; Qu, Y.; Zhang, X.; Xu, A.; Wei, C.; Chou, C. J.; Wu, J. Design, synthesis and biological evaluation of dual-function inhibitors targeting NMDAR and HDAC for Alzheimer's disease. *Bioorg. Chem.* **2020**, *103*, 104109.
- (27) Xu, A.; He, F.; Zhang, X.; Li, X.; Ran, Y.; Wei, C.; Chou, C. J.; Zhang, R.; Wu, J. Tacrine-hydroxamate derivatives as multitarget-directed ligands for the treatment of Alzheimer's disease: Design, synthesis, and biological evaluation. *Bioorg. Chem.* **2020**, *98*, 103721.
- (28) Tseng, H.-J.; Lin, M.-H.; Shiao, Y.-J.; Yang, Y.-C.; Chu, J.-C.; Chen, C.-Y.; Chen, Y.-Y.; Lin, T. E.; Su, C.-J.; Pan, S.-L.; Chen, L.-C.; Wang, C.-Y.; Hsu, K.-C.; Huang, W.-J. Synthesis and biological evaluation of acridine-based histone deacetylase inhibitors as multitarget agents against Alzheimer's disease. *Eur. J. Med. Chem.* **2020**, *192*, 112193.
- (29) Rosales-Corral, S. A.; Reiter, R. J.; Tan, D.-X.; Manchester, L. C.; Liu, X. Antioxidant and Anti-Inflammatory Role of Melatonin in Alzheimer's Neurodegeneration. In *Aging*; Preedy, V. R., Ed. Academic Press: San Diego, 2014; pp. 177–193.
- (30) Nabavi, S. F.; Devi, K. P.; Malar, D. S.; Sureda, A.; Daglia, M.; Nabavi, S. M. Ferulic acid and Alzheimer's disease: promises and pitfalls. *Mini-Rev. Med. Chem.* **2015**, *15*, 776–788.
- (31) Mihardja, M.; Roy, J.; Wong, K. Y.; Aquili, L.; Heng, B. C.; Chan, Y.-S.; Fung, M. L.; Lim, L. W. Therapeutic potential of neurogenesis and melatonin regulation in Alzheimer's disease. *Ann. N. Y. Acad. Sci.* **2020**, *1478*, 43–62.

- (32) Gu, L.; Cui, X.; Wei, W.; Yang, J.; Li, X. Ferulic acid promotes survival and differentiation of neural stem cells to prevent gentamicin-induced neuronal hearing loss. *Exp. Cell Res.* **2017**, *360*, 257–263.
- (33) Savaskan, E.; Olivieri, G.; Meier, F.; Brydon, L.; Jockers, R.; Ravid, R.; Wirz-Justice, A.; Müller-Spahn, F. Increased melatonin 1a-receptor immunoreactivity in the hippocampus of Alzheimer's disease patients. *J. Pineal Res.* **2002**, *32*, 59–62.
- (34) Savaskan, E.; Ayoub, M. A.; Ravid, R.; Angeloni, D.; Fraschini, F.; Meier, F.; Eckert, A.; Müller-Spahn, F.; Jockers, R. Reduced hippocampal MT₂ melatonin receptor expression in Alzheimer's disease. *J. Pineal Res.* **2005**, *38*, 10–16.
- (35) Smil, D. V.; Manku, S.; Chantigny, Y. A.; Leit, S.; Wahhab, A.; Yan, T. P.; Fournel, M.; Maroun, C.; Li, Z.; Lemieux, A.-M.; Nicolescu, A.; Rahil, J.; Lefebvre, S.; Panetta, A.; Besterman, J. M.; Déziel, R. Novel HDAC6 isoform selective chiral small molecule histone deacetylase inhibitors. *Bioorg. Med. Chem. Lett.* **2009**, *19*, 688–692.
- (36) Bergman, J. A.; Woan, K.; Perez-Villaruel, P.; Villagra, A.; Sotomayor, E. M.; Kozikowski, A. P. Selective histone deacetylase 6 inhibitors bearing substituted urea linkers inhibit melanoma cell growth. *J. Med. Chem.* **2012**, *55*, 9891–9899.
- (37) Wang, F.; Lu, W.; Zhang, T.; Dong, J.; Gao, H.; Li, P.; Wang, S.; Zhang, J. Development of novel ferulic acid derivatives as potent histone deacetylase inhibitors. *Bioorg. Med. Chem.* **2013**, *21*, 6973–6980.
- (38) Wang, X.; Li, X.; Li, J.; Hou, J.; Qu, Y.; Yu, C.; He, F.; Xu, W.; Wu, J. Design, synthesis, and preliminary bioactivity evaluation of N¹-hydroxyterephthalamide derivatives with indole cap as novel histone deacetylase inhibitors. *Chem. Biol. Drug Des.* **2017**, *89*, 38–46.
- (39) Cheng, T.; Grasse, L.; Shah, J.; Chandra, J. Panobinostat, a pan-histone deacetylase inhibitor: rationale for and application to treatment of multiple myeloma. *Drugs Today* **2015**, *51*, 491–504.
- (40) Gunesch, S.; Hoffmann, M.; Kiermeier, C.; Fischer, W.; Pinto, A. F. M.; Maurice, T.; Maher, P.; Decker, M. 7-O-Esters of taxifolin with pronounced and overadditive effects in neuroprotection, anti-neuroinflammation, and amelioration of short-term memory impairment in vivo. *Redox Biol.* **2020**, *29*, 101378.
- (41) Gunesch, S.; Soriano-Castell, D.; Lamer, S.; Schlosser, A.; Maher, P.; Decker, M. Development and application of a chemical probe based on a neuroprotective flavonoid hybrid for target identification using activity-based protein profiling. *ACS Chem. Neurosci.* **2020**, *11*, 3823–3837.
- (42) Diedrich, D.; Hamacher, A.; Gertzen, C. G. W.; Alves Avelar, L. A.; Reiss, G. J.; Kurz, T.; Gohlke, H.; Kassack, M. U.; Hansen, F. K. Rational design and diversity-oriented synthesis of peptoid-based selective HDAC6 inhibitors. *Chem. Commun.* **2016**, *52*, 3219–3222.
- (43) Krieger, V.; Hamacher, A.; Gertzen, C. G. W.; Senger, J.; Zwinderman, M. R. H.; Marek, M.; Romier, C.; Dekker, F. J.; Kurz, T.; Jung, M.; Gohlke, H.; Kassack, M. U.; Hansen, F. K. Design, multicomponent synthesis, and anticancer activity of a focused histone deacetylase (HDAC) inhibitor library with peptoid-based cap groups. *J. Med. Chem.* **2017**, *60*, 5493–5506.
- (44) Yoo, B.; Kirshenbaum, K. Peptoid architectures: elaboration, actuation, and application. *Curr. Opin. Chem. Biol.* **2008**, *12*, 714–721.
- (45) Li, X.; Peterson, Y. K.; Inks, E. S.; Himes, R. A.; Li, J.; Zhang, Y.; Kong, X.; Chou, C. J. Class I HDAC inhibitors display different antitumor mechanism in leukemia and prostatic cancer cells depending on their p53 status. *J. Med. Chem.* **2018**, *61*, 2589–2603.
- (46) Osko, J. D.; Porter, N. J.; Narayana Reddy, P. A.; Xiao, Y.-C.; Rokka, J.; Jung, M.; Hooker, J. M.; Salvino, J. M.; Christianson, D. W. Exploring structural determinants of inhibitor affinity and selectivity in complexes with histone deacetylase 6. *J. Med. Chem.* **2020**, *63*, 295–308.
- (47) Porter, N. J.; Mahendran, A.; Breslow, R.; Christianson, D. W. Unusual zinc-binding mode of HDAC6-selective hydroxamate inhibitors. *Proc. Natl. Acad. Sci. U. S. A.* **2017**, *114*, 13459–13464.
- (48) Santo, L.; Hideshima, T.; Kung, A. L.; Tseng, J. C.; Tamang, D.; Yang, M.; Jarpe, M.; van Duzer, J. H.; Mazitschek, R.; Ogier, W. C.; Cirstea, D.; Rodig, S.; Eda, H.; Scullen, T.; Canavese, M.; Bradner, J.; Anderson, K. C.; Jones, S. S.; Raje, N. Preclinical activity, pharmacodynamic, and pharmacokinetic properties of a selective HDAC6 inhibitor, ACY-1215, in combination with bortezomib in multiple myeloma. *Blood* **2012**, *119*, 2579–2589.
- (49) Neudert, G.; Klebe, G. DSX: a knowledge-based scoring function for the assessment of protein-ligand complexes. *J. Chem. Inf. Model.* **2011**, *51*, 2731–2745.
- (50) Conrad, M.; Schick, J.; Angeli, J. P. F. Glutathione and thioredoxin dependent systems in neurodegenerative disease: what can be learned from reverse genetics in mice. *Neurochem. Int.* **2013**, *62*, 738–749.
- (51) Duce, J. A.; Bush, A. I. Biological metals and Alzheimer's disease: implications for therapeutics and diagnostics. *Prog. Neurobiol.* **2010**, *92*, 1–18.
- (52) Liu, Y.; Nguyen, M.; Robert, A.; Meunier, B. Metal ions in Alzheimer's disease: a key role or not? *Acc. Chem. Res.* **2019**, *52*, 2026–2035.
- (53) Wang, W.-Y.; Tan, M.-S.; Yu, J.-T.; Tan, L. Role of pro-inflammatory cytokines released from microglia in Alzheimer's disease. *Ann. Transl. Med.* **2015**, *3*, 136.
- (54) Maurice, T.; Lockhart, B. P.; Privat, A. Amnesia induced in mice by centrally administered β -amyloid peptides involves cholinergic dysfunction. *Brain Res.* **1996**, *706*, 181–193.
- (55) Scheiner, M.; Dolles, D.; Gunesch, S.; Hoffmann, M.; Nabissi, M.; Marinelli, O.; Naldi, M.; Bartolini, M.; Petralia, S.; Poeta, E.; Monti, B.; Falkeis, C.; Vieth, M.; Hübner, H.; Gmeiner, P.; Maitra, R.; Maurice, T.; Decker, M. Dual-acting cholinesterase-human cannabinoid receptor 2 ligands show pronounced neuroprotection in vitro and overadditive and disease-modifying neuroprotective effects in vivo. *J. Med. Chem.* **2019**, *62*, 9078–9102.
- (56) Hoffmann, M.; Stiller, C.; Endres, E.; Scheiner, M.; Gunesch, S.; Sotriffer, C.; Maurice, T.; Decker, M. Highly selective butyrylcholinesterase inhibitors with tunable duration of action by chemical modification of transferable carbamate units exhibit pronounced neuroprotective effect in an Alzheimer's disease mouse model. *J. Med. Chem.* **2019**, *62*, 9116–9140.
- (57) Couly, S.; Denus, M.; Bouchet, M.; Rubinstenn, G.; Maurice, T. Anti-amnesic and neuroprotective effects of fluoroethylnormemantine in a pharmacological mouse model of Alzheimer's disease. *Int. J. Neuropsychopharmacol.* **2021**, *24*, 142–157.
- (58) Heltweg, B.; Trapp, J.; Jung, M. In vitro assays for the determination of histone deacetylase activity. *Methods* **2005**, *36*, 332–337.
- (59) Jones, G.; Willett, P.; Glen, R. C.; Leach, A. R.; Taylor, R. Development and validation of a genetic algorithm for flexible docking. *J. Mol. Biol.* **1997**, *267*, 727–748.
- (60) Verdonk, M. L.; Cole, J. C.; Hartshorn, M. J.; Murray, C. W.; Taylor, R. D. Improved protein–ligand docking using GOLD. *Proteins: Struct., Funct., Bioinf.* **2003**, *52*, 609–623.
- (61) Sharma, O. P.; Bhat, T. K. DPPH antioxidant assay revisited. *Food Chem.* **2009**, *113*, 1202–1205.
- (62) Ou, B.; Hampsch-Woodill, M.; Prior, R. L. Development and validation of an improved oxygen radical absorbance capacity assay using fluorescein as the fluorescent probe. *J. Agric. Food Chem.* **2001**, *49*, 4619–4626.
- (63) Dávalos, A.; Gómez-Cordovés, C.; Bartolomé, B. Extending applicability of the oxygen radical absorbance capacity (ORAC–fluorescein) assay. *J. Agric. Food Chem.* **2004**, *52*, 48–54.
- (64) Santos, J. S.; Alvarenga Brizola, V. R.; Granato, D. High-throughput assay comparison and standardization for metal chelating capacity screening: A proposal and application. *Food Chem.* **2017**, *214*, 515–522.
- (65) Catapano, M. C.; Tvrdý, V.; Karličková, J.; Mercolini, L.; Mladěnka, P. A simple, cheap but reliable method for evaluation of zinc chelating properties. *Bioorg. Chem.* **2018**, *77*, 287–292.

Melatonin- and Ferulic Acid-Based HDAC6 Selective Inhibitors Exhibit Pronounced Immunomodulatory Effects in Vitro and Neuroprotective Effects in a Pharmacological Alzheimer's Disease Mouse Model

Feng He[†], C. James Chou[‡], Matthias Scheiner[†], Eleonora Poeta[§], Natalia Yuan Chen[†], Sandra Gunesch[†], Matthias Hoffmann[†], Christoph Sotriffer[†], Barbara Monti[§], Tangui Maurice^{||*}, Michael Decker^{†*}

[†]Pharmaceutical and Medicinal Chemistry, Institute of Pharmacy and Food Chemistry, Julius Maximilian University of Würzburg, Am Hubland, 97074 Würzburg, Germany

[‡]Department of Drug Discovery and Biomedical Sciences, South Carolina College of Pharmacy, Medical University of South Carolina, Charleston, South Carolina 29425, United States

[§]Department of Pharmacy and Biotechnologies, University of Bologna, Via Selmi 3, 40126, Bologna, Italy

^{||}MMDN, Univ. Montpellier, EPHE, INSERM, Montpellier, France

Content

HPLC-Chromatograms of target compounds	S3
Metal chelation	S10
Neuroprotection regarding oxytosis and ATP depletion	S11
Weight of animals during <i>in vivo</i> studies	S12
Computational docking	S13

HPLC CHROMATOGRAMS OF TARGET COMPOUNDS

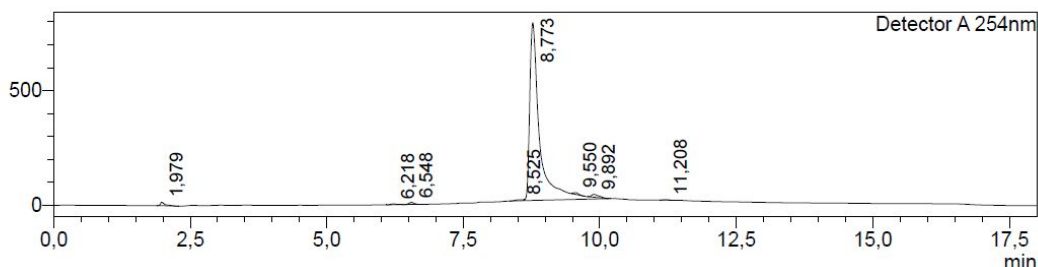
Measurements for verification and purity of the compounds were performed by LC/MS (from Shimadzu), comprising a DGU-20A3R controller, pump LC-20AB, degasser DGU-20A, and SPD-20A UV/Vis detector. ESI ionization was accomplished by an LCMS-2020 single quadrupol mass spectrometer. As a stationary phase, for analytical purpose, a Synergi 4U fusion-RP 80 Å (150 × 4.6 mm) column and for preparative purpose, a Synergi 4U fusion-RP 80 Å (250 × 10.0 mm) were used. As a mobile phase, a gradient of MeOH/water (both containing 0.1% formic acid) (phase 1/phase 2) was used. The compounds were dissolved in MeOH and filtered through syringe filters. Methods were performed with a flow rate of 1.0 mL/min.

Method A: $V(1)/(V(1) + V(2)) =$ from 0 to 60% over 10 min, $V(1)/(V(1) + V(2)) = 60\%$ for 5 min, $V(1)/(V(1) + V(2)) =$ from 60 to 0% over 3 min, used by compounds **3a-3b**, **5a-5d** and **8a-8c**.

Method B: $V(1)/(V(1) + V(2)) =$ from 5 to 90% over 10 min, $V(1)/(V(1) + V(2)) = 90\%$ for 5 min, $V(1)/(V(1) + V(2)) =$ from 90 to 5% over 3 min, used by compound **10a-10c** and **15a-15c**.

3a

mV

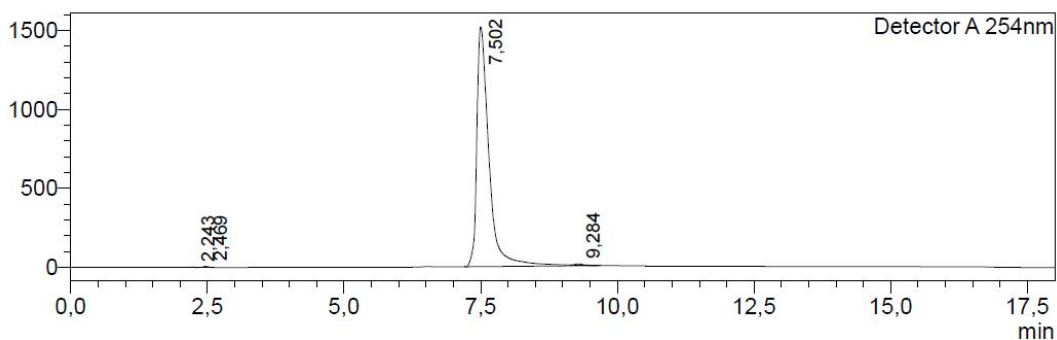


Peak Table

Peak#	Ret. Time	Area	Height	Area%
1	1.979	91134	14946	0.888
2	6.218	28119	3525	0.274
3	6.548	61863	8950	0.603
4	8.525	46530	4830	0.454
5	8.773	9852949	773899	96.057
6	9.550	44756	7343	0.436
7	9.892	116358	12659	1.134
8	11.208	15685	2438	0.153
Total		10257395	828590	100.000

3b

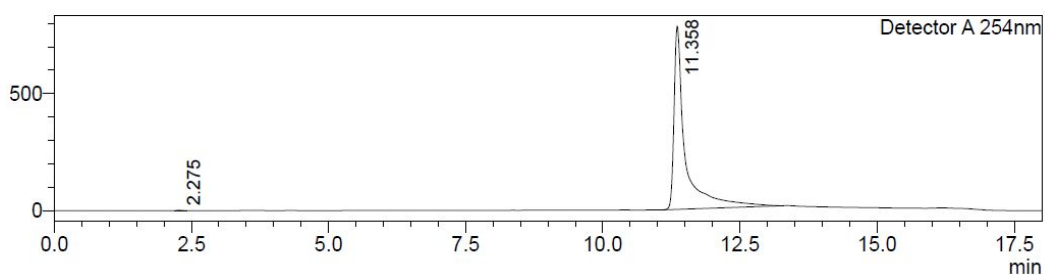
mV



Peak#	Ret. Time	Area	Area%
1	2.243	12994	0.055
2	2.469	45937	0.194
3	7.502	23532488	99.420
4	9.284	78266	0.331
Total		23669684	100.000

5a

mV

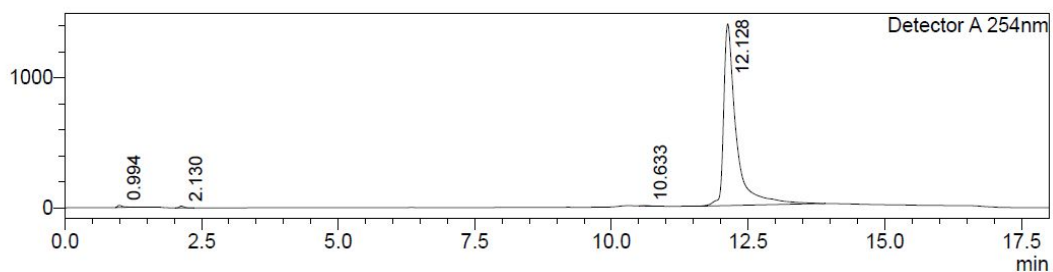


Peak Table

Peak#	Ret. Time	Area	Height	Area%
1	2.275	10116	1783	0.090
2	11.358	11274614	782669	99.910
Total		11284729	784453	100.000

5b

mV

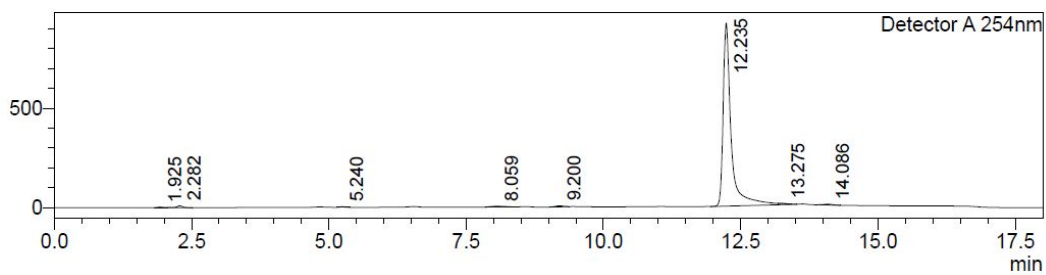


Peak Table

Peak#	Ret. Time	Area	Height	Area%
1	0.994	97056	16898	0.429
2	2.130	76672	13324	0.339
3	10.633	28457	3515	0.126
4	12.128	22415393	1395632	99.106
Total		22617578	1429369	100.000

5c

mV

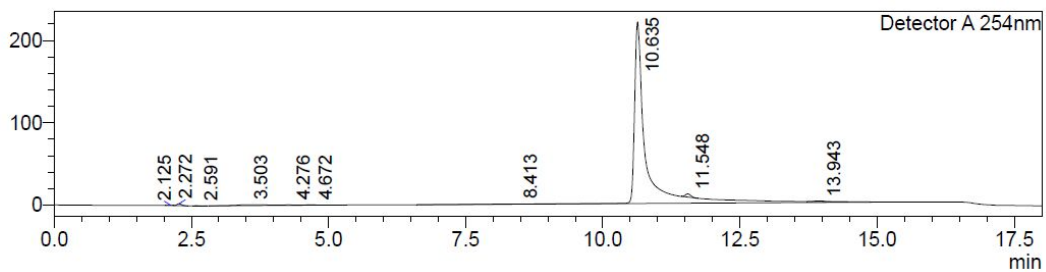


Peak Table

Peak#	Ret. Time	Area	Height	Area%
1	1.925	22672	3033	0.234
2	2.282	75209	9588	0.776
3	5.240	16072	2616	0.166
4	8.059	69634	4216	0.718
5	9.200	47565	5050	0.491
6	12.235	9414587	917808	97.124
7	13.275	9640	1420	0.099
8	14.086	38007	4087	0.392
Total		9693386	947818	100.000

5d

mV

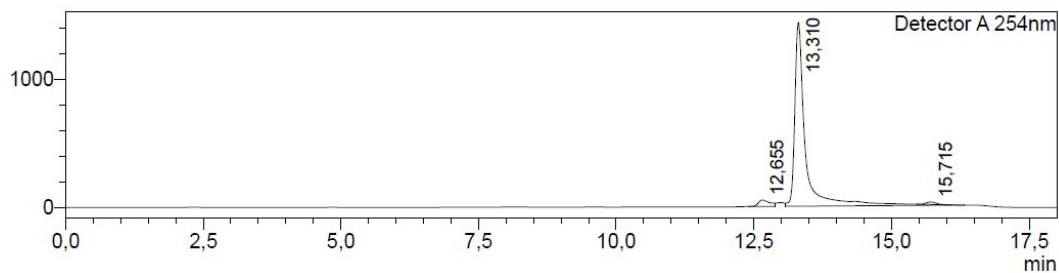


Peak Table

Peak#	Ret. Time	Area	Height	Area%
1	2.125	1715	232	0.051
2	2.272	14915	2312	0.446
3	2.591	2205	293	0.066
4	3.503	36581	845	1.094
5	4.276	9332	387	0.279
6	4.672	4052	309	0.121
7	8.413	11529	315	0.345
8	10.635	3226640	220110	96.460
9	11.548	28002	3936	0.837
10	13.943	10067	648	0.301
Total		3345039	229385	100.000

8a

mV



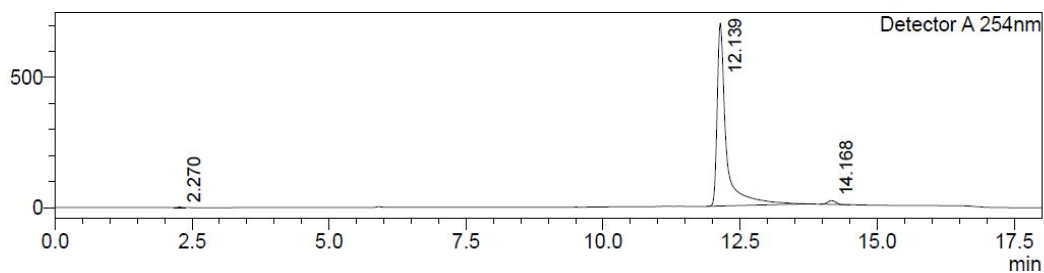
Peak Table

Detector A 254nm

Peak#	Ret. Time	Area	Height	Area%
1	12.655	726858	50478	3.570
2	13.310	19383459	1431528	95.193
3	15.715	251988	19495	1.238
Total		20362306	1501501	100.000

8b

mV



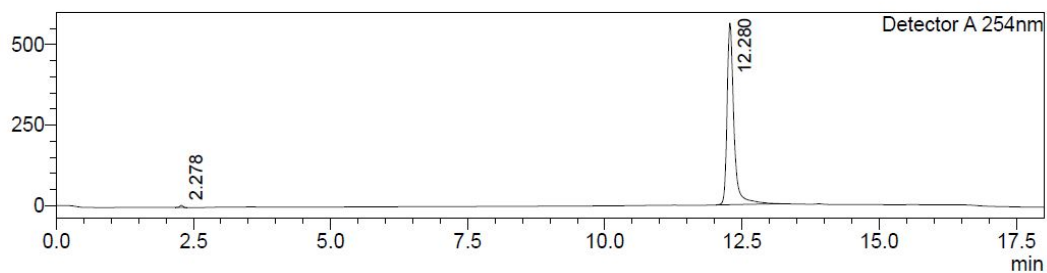
Peak Table

Detector A 254nm

Peak#	Ret. Time	Area	Height	Area%
1	2.270	10318	2069	0.123
2	12.139	8193589	702362	98.020
3	14.168	155172	14230	1.856
Total		8359078	718661	100.000

8c

mV



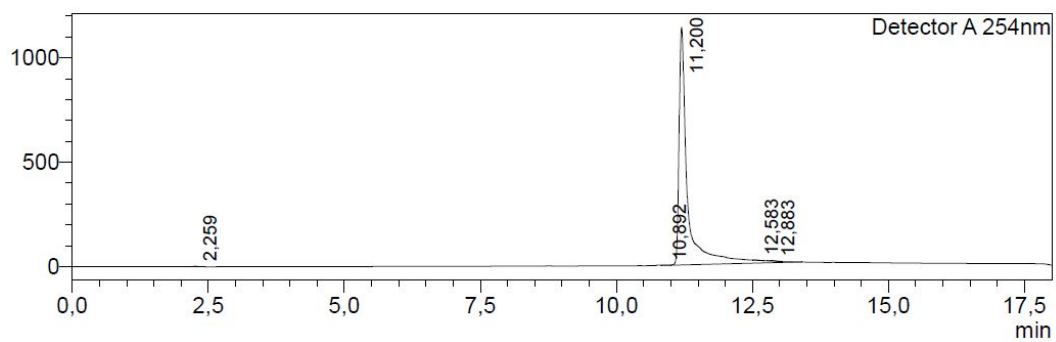
Peak Table

Detector A 254nm

Peak#	Ret. Time	Area	Height	Area%
1	2.278	26933	6711	0.544
2	12.280	4924022	563738	99.456
Total		4950955	570450	100.000

10a

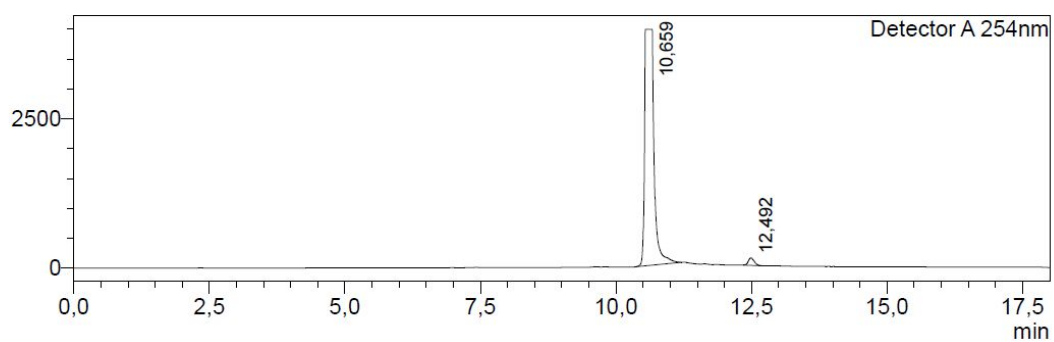
mV



Peak#	Ret. Time	Area	Area%
1	2,259	7992	0,064
2	10,892	3397	0,027
3	11,200	12455737	99,770
4	12,583	5127	0,041
5	12,883	12159	0,097
Total		12484411	100,000

10b

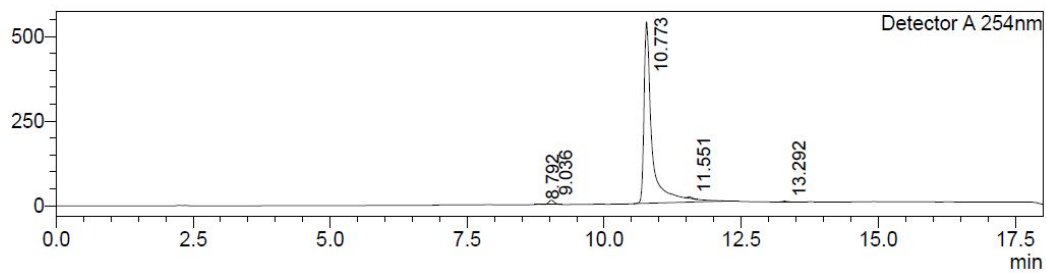
mV



Peak#	Ret. Time	Area	Area%
1	10,659	47010198	98,056
2	12,492	932079	1,944
Total		47942277	100,000

10c

mV



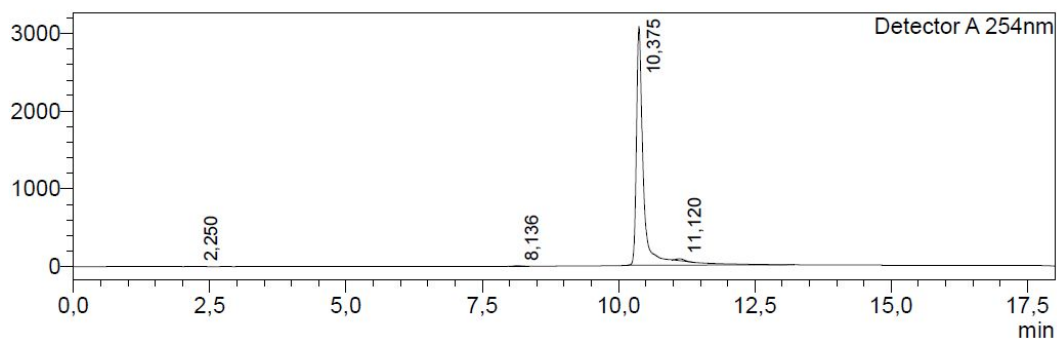
Peak Table

Detector A 254nm

Peak#	Ret. Time	Area	Height	Area%
1	8.792	9253	1196	0.164
2	9.036	91536	12838	1.620
3	10.773	5514062	535257	97.611
4	11.551	19917	3457	0.353
5	13.292	14226	2283	0.252
Total		5648993	555031	100.000

15a

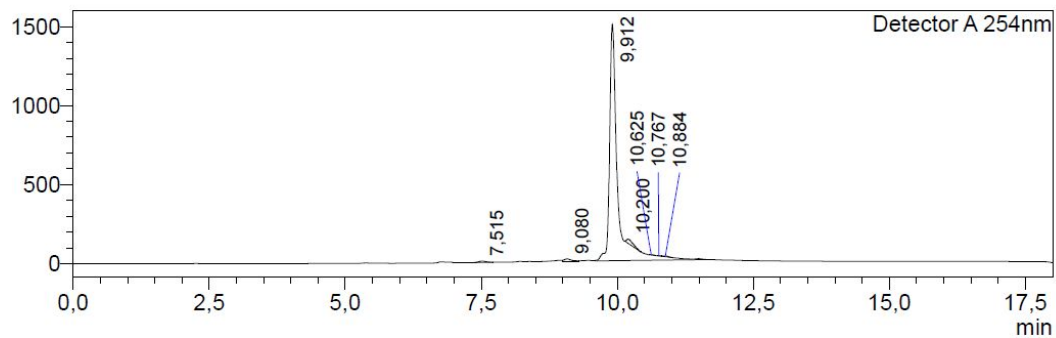
mV



Peak#	Ret. Time	Area	Area%
1	2.250	10021	0.035
2	8.136	76717	0.265
3	10.375	28652014	98.917
4	11.120	226937	0.783
Total		28965689	100.000

15b

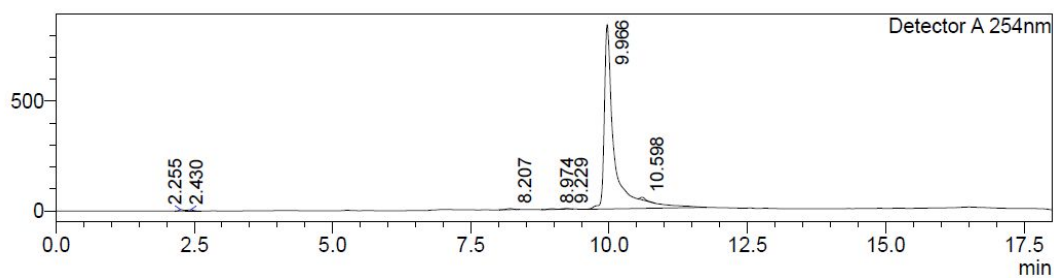
mV



Peak#	Ret. Time	Area	Area%
1	7,515	67420	0,420
2	9,080	137694	0,859
3	9,912	15547020	96,964
4	10,200	234969	1,465
5	10,625	8189	0,051
6	10,767	6089	0,038
7	10,884	32488	0,203
Total		16033869	100,000

15c

mV



Detector A 254nm

Peak Table

Peak#	Ret. Time	Area	Height	Area%
1	2,255	34513	5969	0,321
2	2,430	43826	5142	0,408
3	8,207	44663	5198	0,416
4	8,974	27860	3231	0,259
5	9,229	25788	2934	0,240
6	9,966	10498712	836579	97,698
7	10,598	70716	11830	0,658
Total		10746078	870883	100,000

METAL CHELATION

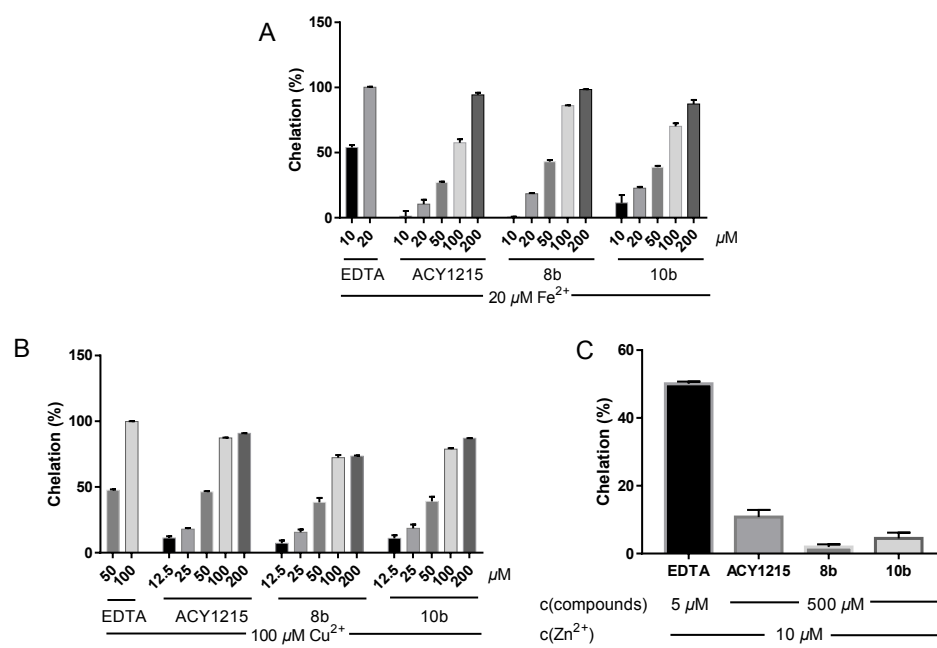


Figure S1. The chelating ratio (Mean \pm SEM) of target compounds at different concentration to Fe²⁺, Cu²⁺ and Zn²⁺. A) Target compounds (10, 20, 50, 100 and 200 μ M) and EDTA (10 and 20 μ M), with Fe²⁺ (20 μ M) and indicator ferrozine (62.5 μ M); B) Target compounds (12.5, 25, 50, 100 and 200 μ M) and EDTA (50 and 100 μ M), with Cu²⁺ (100 μ M) and indicator pyrocatechol violet (PV, 37.5 μ M); C) Target compounds (500 μ M) and EDTA (50 μ M), with Zn²⁺ (10 μ M) and indicator dithizone (41.7 μ M).

NEUROPROTECTION AGAINST OXYTOSIS AND ATP

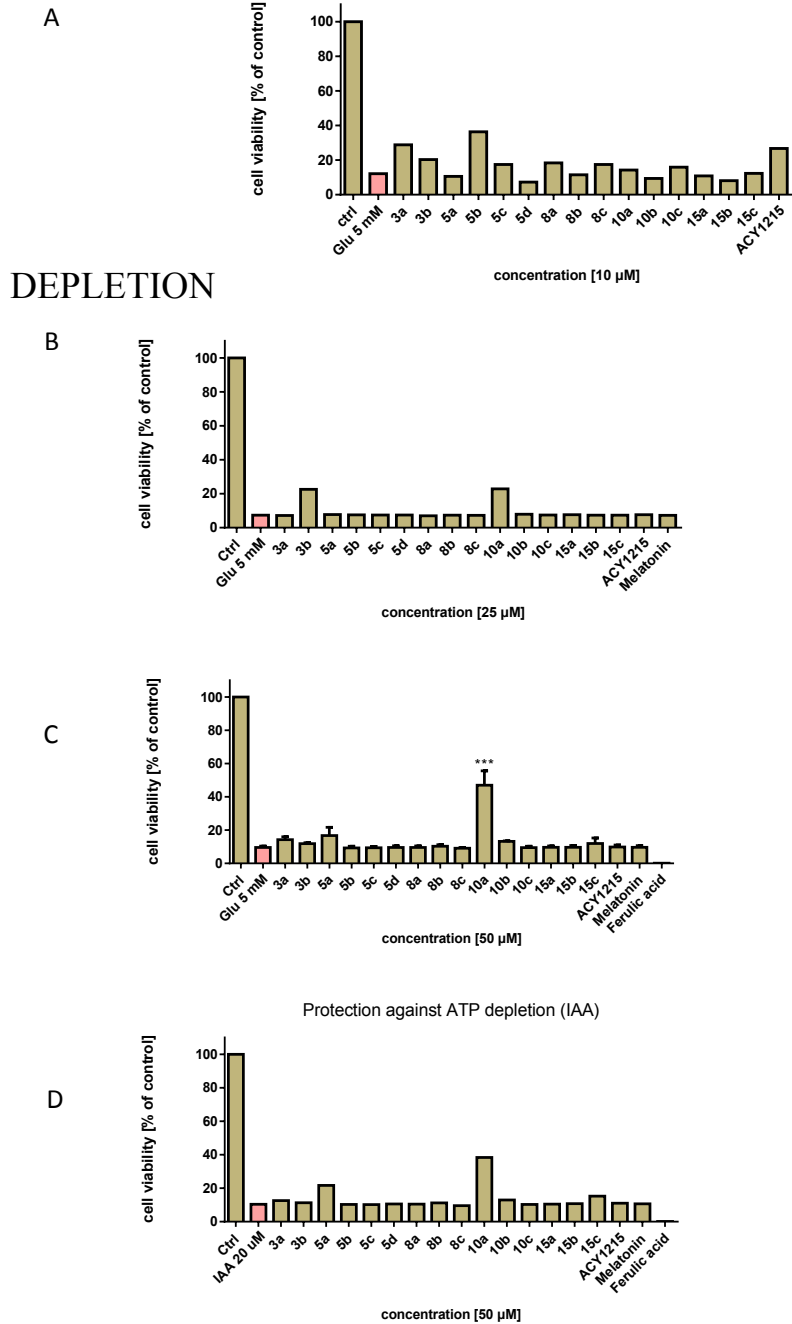


Figure S2. Neuroprotection in HT-22 cells against glutamate (5 mM) induced oxytosis (A, B and C) and iodoacetic acid (IAA, 20 µM) induced ATP depletion (D) in HT22 cells. Target compounds at 10 µM (A), 25 µM (B) and 50 µM (C and D). Statistical analysis was performed applying One-way ANOVA followed by Dunnett's multiple comparison post-test. Levels of significance: *** $p < 0.001$ referring to cells treated with glutamate.

WEIGHT OF ANIMALS DURING *IN VIVO* STUDIES

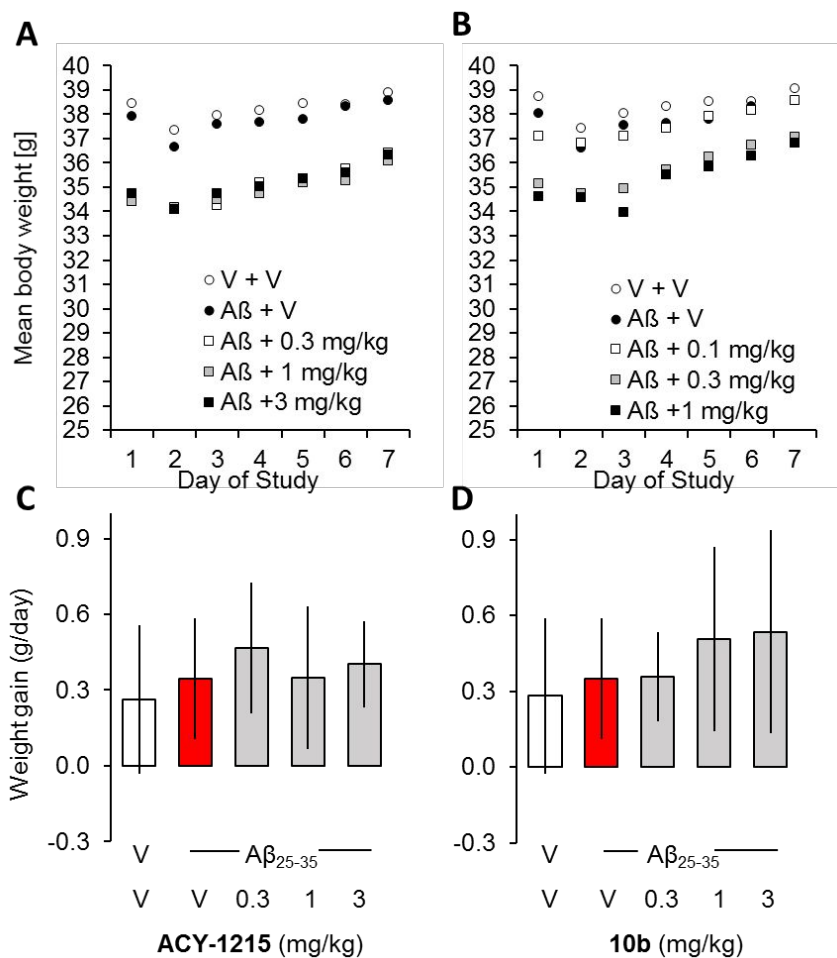


Figure S3. Development of body weight. Top panel: stress-induced weight loss is observed on day 2. Animals recovered during the following days. Data show mean. Bottom panel: average weight gain from day 2-7. Data show mean \pm SEM. ANOVA: $F_{(4,95)} = 2.26$, $p = 0.07$, $n = 12-25$ in B, $F_{(4,97)} = 2.47$, $p = 0.05$, $n = 12-25$ in D. Data are not significantly different from A β +V-treated group, Dunnett's test.

COMPUTATIONAL DOCKING

Methods

Protein and ligand preparations were carried out with the Molecular Operating Environment (MOE) 2020.09.¹ The protein structure was prepared from the well-resolved crystal structure of *Danio rerio* (zebrafish) HDAC6 complexed with compound A (PDB 6DVM, 1.47 Å).² As discussed by Porter et al.², the zebrafish HDAC6 is an excellent and more readily studied surrogate of human HDAC6. Protonation states were set according to the expected ionization at pH 7.4. Further assessment of the ligand protonation states was achieved with Epik.³ The hydroxamic acid as zinc binding group was deprotonated to the negatively charged hydroxamate. The Zn²⁺ ion as well as three conserved water molecules were retained for the docking calculations. Each ligand was built in MOE and energy minimized with the MMFF94x force field in tether mode to an rms-gradient of 0.001 kcal/(mol·Å).

Docking studies were carried out with the Genetic Optimization for Ligand Docking (GOLD) program v.5.8.1.^{4,5} Selection of suitable genetic algorithm (GA) parameters as well as the fitness function were done after comprehensive redocking calculations. The latter were performed with a set of HDAC6 complexes cocrystallized with phenylhydroxamate ligands (6DVM, 6DVO, 6PZS, and 6PZO).^{2,6} Improved convergence towards reasonable binding modes was achieved with the following GA search parameters: population size 500, number of operations 500,000, crossover frequency 90, and migration frequency 20. For compounds **8b** and **10b**, 100 independent GA runs were performed, using ASP and ChemPLP as scoring functions. The water molecule coordinated to the Zn²⁺ ion was handled in toggle mode, whereas the two water molecules next to His614 and Phe643 were kept “on”. For optimal placement and orientation of water molecules during docking, a translation distance of 1 Å and a “Trans spin” state were set. Constrained docking calculations were performed for compound **10b**, using the phenylhydroxamate substructure as scaffold. The obtained docking poses for each ligand were clustered based on a root-mean-square-deviation

(RMSD) of 2 Å as cut-off and rescored with the scoring function DSX.⁷ The PyMOL Molecular Graphics System v.2.4.1.⁸ was used for visual inspection and figure preparation.

Redocking studies of HDAC6 protein-ligand complexes

The binding modes of the cocrystallized ligands could be reproduced with good convergence and reasonable accuracy by the top-ranked docking pose after rescoring with DSX. The obtained RMSD values with respect to the experimental reference structure were 1.03 Å for 6DVO, 1.91 Å for 6PZS, and 2.83 Å for 6PZO.

Special attention was paid to 6DVM as it contains ligand **A** (according to **Figure 1** of the main manuscript) and is, hence, the reference structure most closely related to compounds **8b** and **10b**. This protein-ligand complex is influenced by crystal packing, because the ligand forms extensive interactions with a symmetry-related ligand molecule, including a staggered π -stacking interaction of the dimethylaniline moieties.² In the absence of the crystal environment, the tolyl moiety of the ligand is entirely exposed and oriented away from the protein surface (cf. binding mode shown in green in **Figure S4**), a situation which is unlikely to represent the binding mode in solution. This is reflected by the docking calculations: performing the redocking in the presence of the symmetry-related molecule leads to virtually perfect reproduction of the crystallographic binding mode with an RMSD of 0.89 Å. In contrast, in the absence of the symmetry-related molecule, a different binding mode is obtained (shown in orange in **Figure S4**), in which the tolyl group is oriented toward Leu712. Although this different orientation leads to an overall RMSD of 4.31 Å with respect to the crystal structure, it appears as the more reasonable binding mode in solution where the crystal environment is not present. Furthermore, a similar orientation is found for the capping groups of the investigated compounds **8b** and, in particular, **10b**, as can be seen by comparison of **Figure S4** with **Figure 2** of the main manuscript.

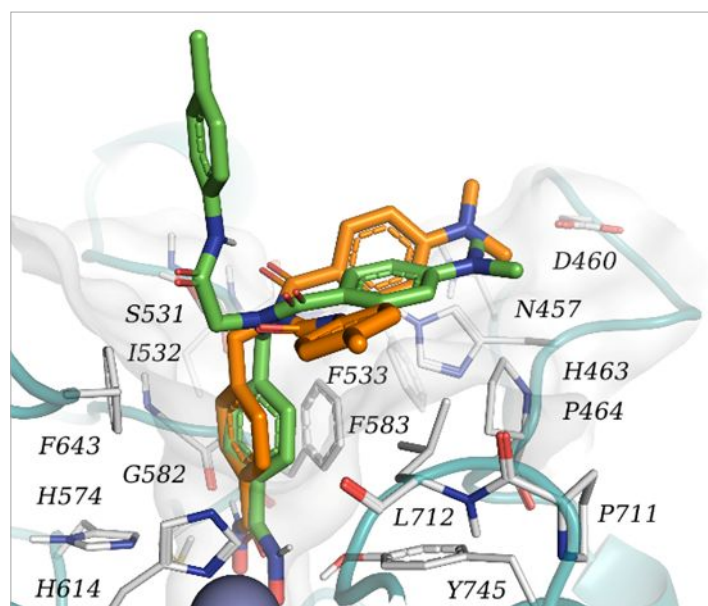


Figure S4. Docking solution (shown in orange) obtained for 6DVM without considering the symmetry-related molecule from the crystal structure in comparison to the binding mode observed in the crystal structure (shown in green).

References

1. ULC, C. C. G. *Molecular Operating Environment (MOE)*, 2020.09, 1010 Sherbooke St. West, Suite No.910, Montreal, QC, Canada, H3A 2R7, 2021.
2. Porter, N. J.; Osko, J. D.; Diedrich, D.; Kurz, T.; Hooker, J. M.; Hansen, F. K.; Christianson, D. W., Histone Deacetylase 6-Selective Inhibitors and the Influence of Capping Groups on Hydroxamate-Zinc Denticity. *Journal of Medicinal Chemistry* **2018**, *61*, 8054-8060.
3. *Epik*, Schrödinger, LLC, New York, NY, 2021.
4. Jones, G.; Willett, P.; Glen, R. C.; Leach, A. R.; Taylor, R. Development and validation of a genetic algorithm for flexible docking. *Journal of Molecular Biology* **1997**, *267*, 727-748.
5. Verdonk, M. L.; Cole, J. C.; Hartshorn, M. J.; Murray, C. W.; Taylor, R. D., Improved protein-ligand docking using GOLD. *Proteins-Structure Function and Genetics* **2003**, *52*, 609-623.
6. Reßing, N.; Sönnichsen, M.; Osko, J. D.; Schöler, A.; Schliehe-Diecks, J.; Skerhut, A.; Borkhardt, A.; Hauer, J.; Kassack, M. U.; Christianson, D. W.; Bhatia, S.; Hansen, F. K., Multicomponent Synthesis, Binding Mode, and Structure-Activity Relationship of Selective Histone Deacetylase 6 (HDAC6) Inhibitors with Bifurcated Capping Groups. *Journal of Medicinal Chemistry* **2020**, *63*, 10339-10351.
7. Neudert, G.; Klebe, G., DSX: A Knowledge-Based Scoring Function for the Assessment of Protein-Ligand Complexes. *Journal of Chemical Information and Modeling* **2011**, *51*, 2731-2745.
8. Schrödinger-LLC *The PyMOL Molecular Graphics System*, version 2.4.1; 2021.

Appendix II

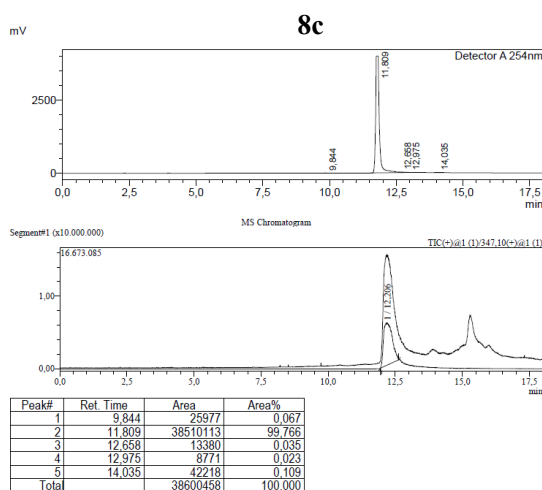
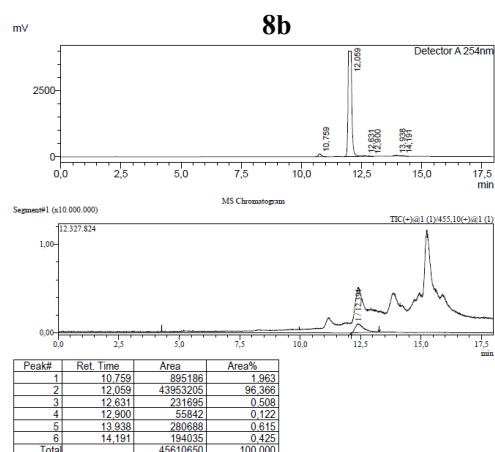
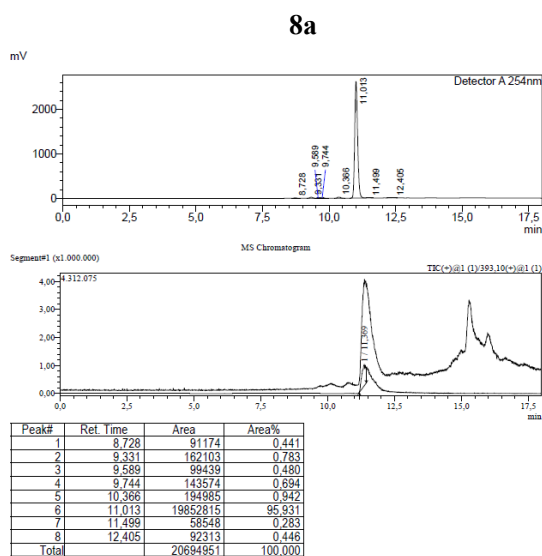
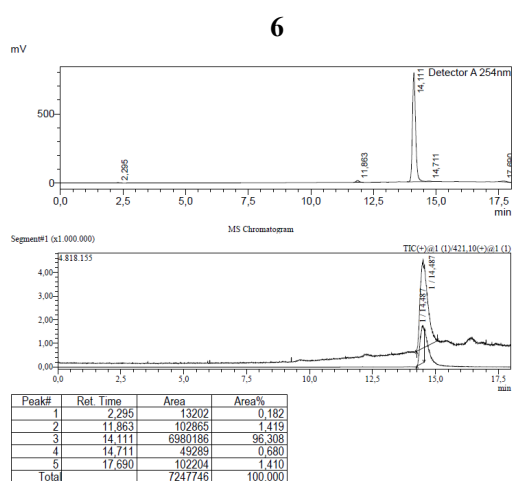
4.1. Design, Synthesis and Bio-Evaluation of Hybrid Neuroprotectants based on Vitamin K Derivatives for Treatment of Neurodegenerative Disorders

Supporting Information

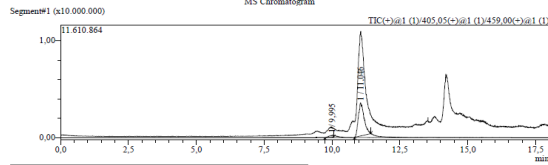
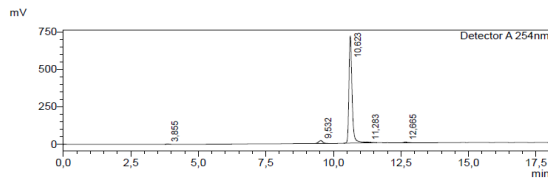
LCMS Data of Target Compounds

Measurements for verification and purity of the compounds were performed by LC/MS (from Shimadzu), comprising a DGU-20A3R controller, pump LC-20AB, degasser DGU-20A, and SPD-20A UV/Vis detector. ESI ionization was accomplished by an LCMS-2020 single quadrupol mass spectrometer. As a stationary phase, for analytical purpose, a Synergi 4U fusion-RP 80 Å (150 × 4.6 mm) column and for preparative purpose, a Synergi 4U fusion-RP 80 Å (250 × 10.0 mm) were used. As a mobile phase, a gradient of MeOH/water (both containing 0.1% formic acid) (phase 1/phase 2) was used. The compounds were dissolved in MeOH and filtered through syringe filters. Methods were performed with a flow rate of 1.0 mL/min.

Method: $V(1)/(V(1) + V(2)) = \text{from } 5 \text{ to } 90\% \text{ over } 10 \text{ min}$, $V(1)/(V(1) + V(2)) = 90\%$ for 5 min, $V(1)/(V(1) + V(2)) = \text{from } 90 \text{ to } 5\% \text{ over } 3 \text{ min}$.

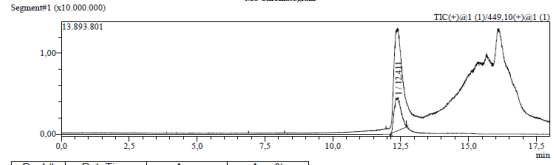
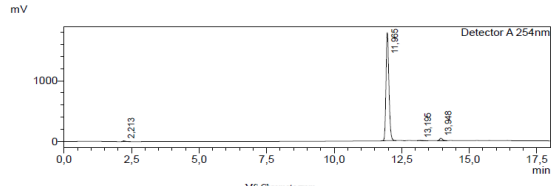


8d



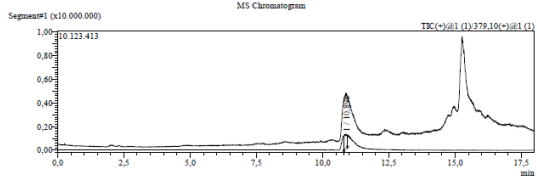
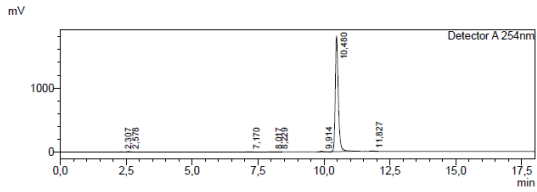
Peak#	Ret. Time	Area	Area%
1	3.855	10274	0.171
2	9.632	199069	3.305
3	10.623	5761240	95.639
4	11.283	6534	0.108
5	12.665	48811	0.777
Total		6023929	100.000

8e



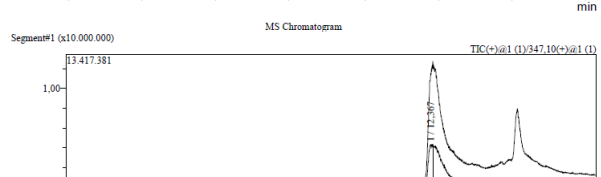
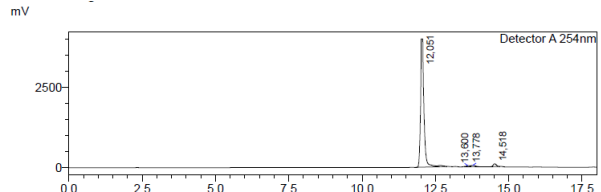
Peak#	Ret. Time	Area	Area%
1	2.213	91323	0.859
2	11.965	13432153	96.880
3	13.195	51931	0.375
4	13.948	289267	2.086
Total		13864673	100.000

13



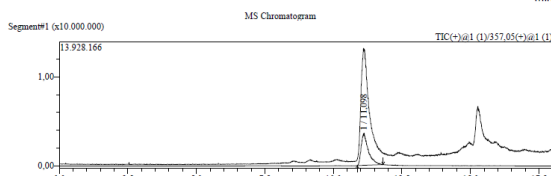
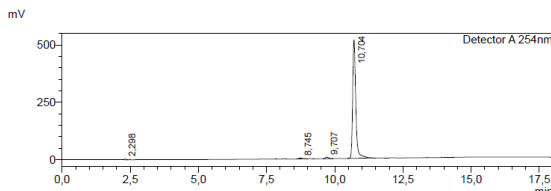
Peak#	Ret. Time	Area	Area%
1	2.307	18168	0.124
2	2.578	80888	0.553
3	7.170	36473	0.249
4	8.017	22141	0.151
5	8.229	30862	0.211
6	9.914	77829	0.532
7	10.480	14321300	97.889
8	11.827	42527	0.291
Total		14630188	100.000

14



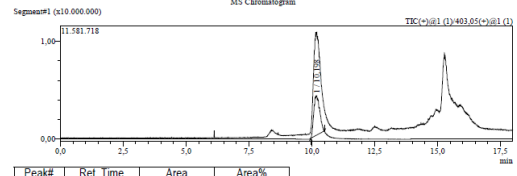
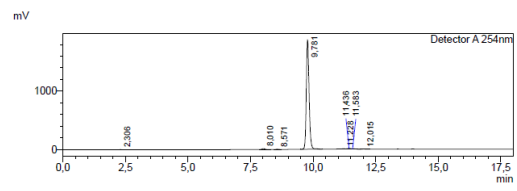
Peak#	Ret. Time	Area	Area%
1	12.051	32186129	95.906
2	13.600	289212	0.862
3	13.778	425828	1.269
4	14.518	659039	1.964
Total		33560208	100.000

16



Peak#	Ret. Time	Area	Area%
1	2.298	14295	0.336
2	8.745	34494	0.812
3	9.707	52700	1.240
4	10.704	4147078	97.611
Total		4248566	100.000

17



Peak#	Ret. Time	Area	Area%
1	2.306	14132	0.096
2	8.010	107412	0.727
3	8.571	26319	0.178
4	9.781	14469055	97.877
5	11.228	934	0.007
6	11.436	85730	0.580
7	11.583	43841	0.297
8	12.015	26298	0.178
Total		14782822	100.000

Pan-Assay Interference Compounds (PAIS) Exclusion Assay

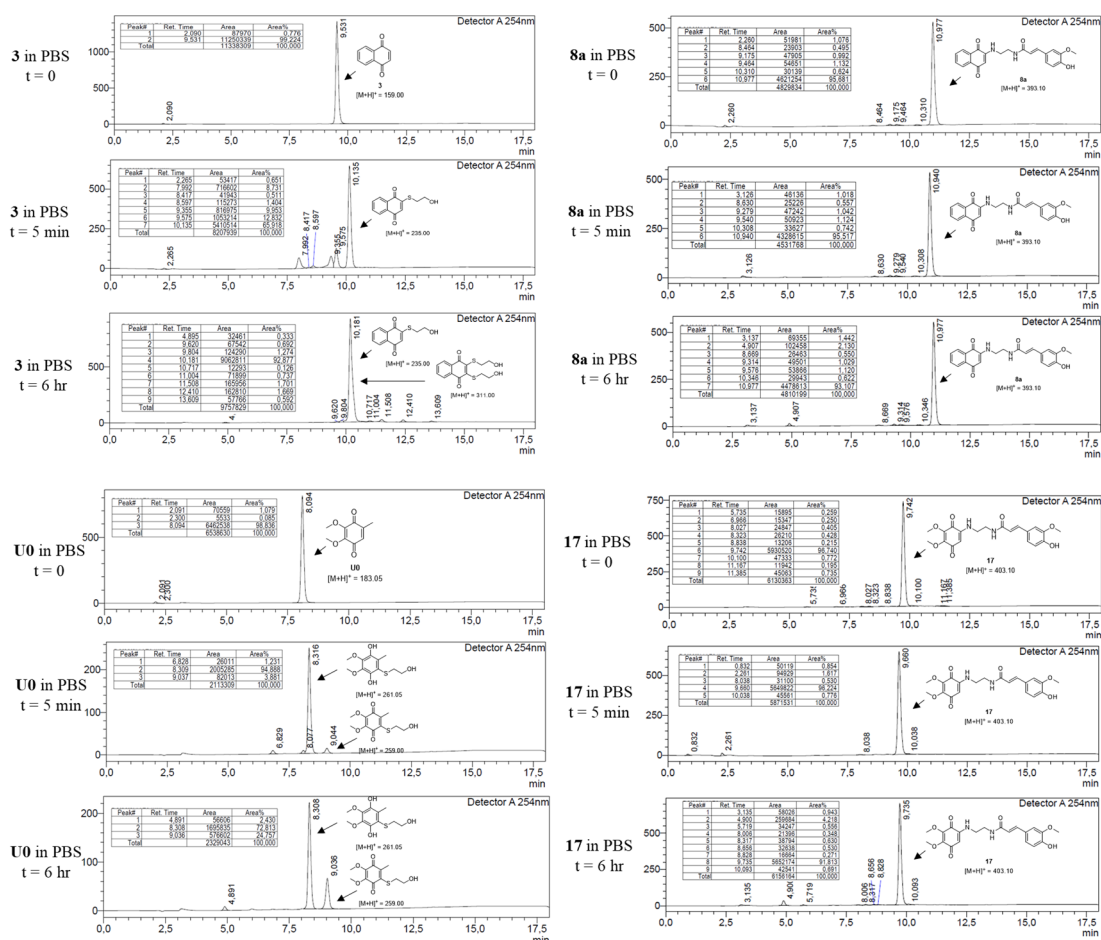


Figure II-1. LCMS records reactions of compounds 1,4-naphthoquinone (**3**), **8a**, 2,3-dimethoxy-5-methylcyclohexa-2,5-diene-1,4-dione (**U0**), and **17** with two equivalent of 2-mercaptoethanol (BME) in PBS (pH 7.4).

Appendix III

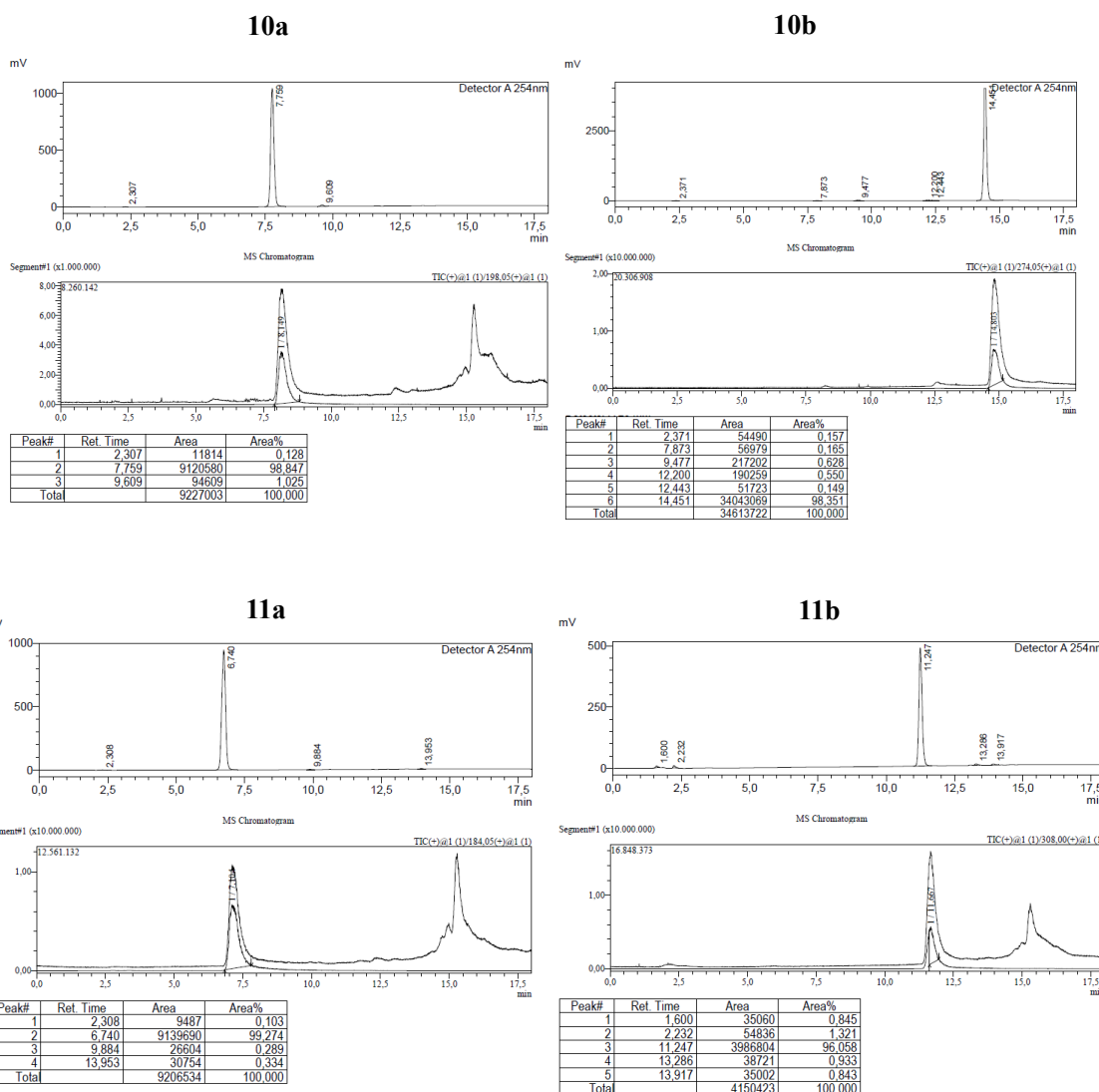
4.2. Structure-Activity Relationship (SAR) study of quinones as free radical scavengers and neuroprotectants

Supporting Information

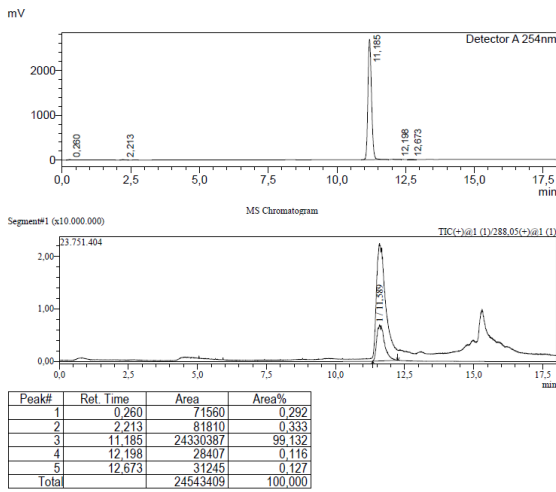
LCMS DATA OF TARGET COMPOUNDS

Measurements for verification and purity of the compounds were performed by LC/MS (from Shimadzu), comprising a DGU-20A3R controller, pump LC-20AB, degasser DGU-20A, and SPD-20A UV/Vis detector. ESI ionization was accomplished by an LCMS-2020 single quadrupole mass spectrometer. As a stationary phase, for analytical purpose, a Synergi 4U fusion-RP 80 Å (150 × 4.6 mm) column and for preparative purpose, a Synergi 4U fusion-RP 80 Å (250 × 10.0 mm) were used. As a mobile phase, a gradient of MeOH/water (both containing 0.1% formic acid) (phase 1/phase 2) was used. The compounds were dissolved in MeOH and filtered through syringe filters. Methods were performed with a flow rate of 1.0 mL/min.

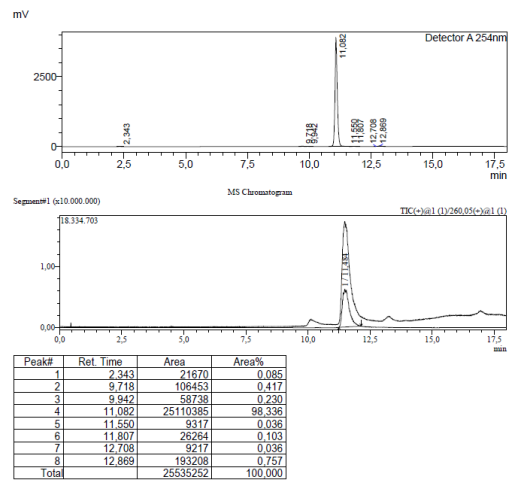
Method: $V(1)/(V(1) + V(2)) = \text{from } 5 \text{ to } 90\% \text{ over } 10 \text{ min}$, $V(1)/(V(1) + V(2)) = 90\%$ for 5 min, $V(1)/(V(1) + V(2)) = \text{from } 90 \text{ to } 5\% \text{ over } 3 \text{ min}$.



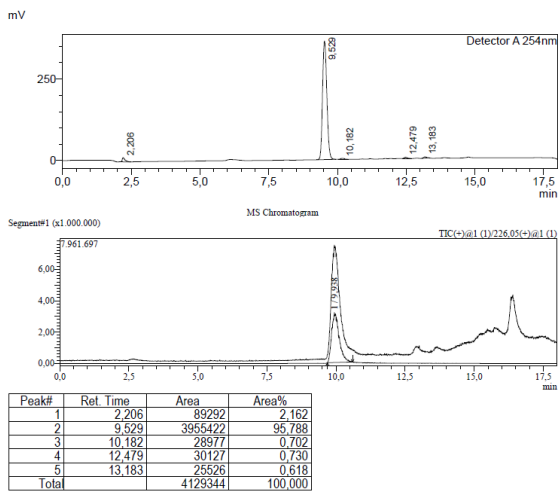
11c



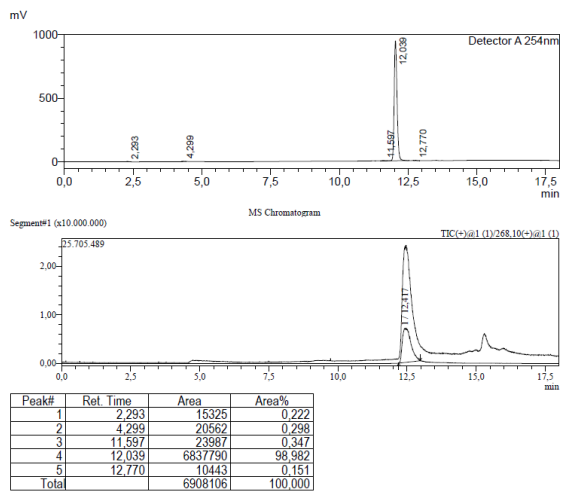
11d



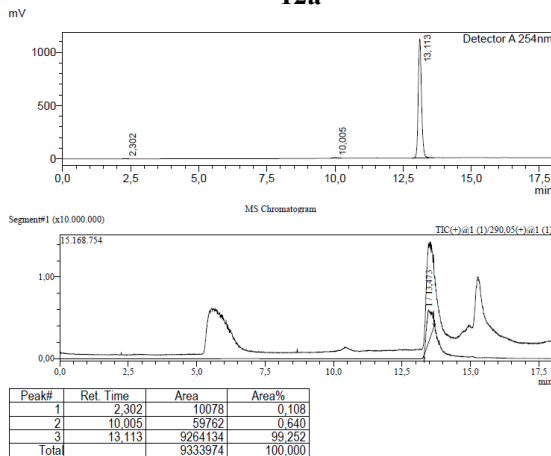
11e



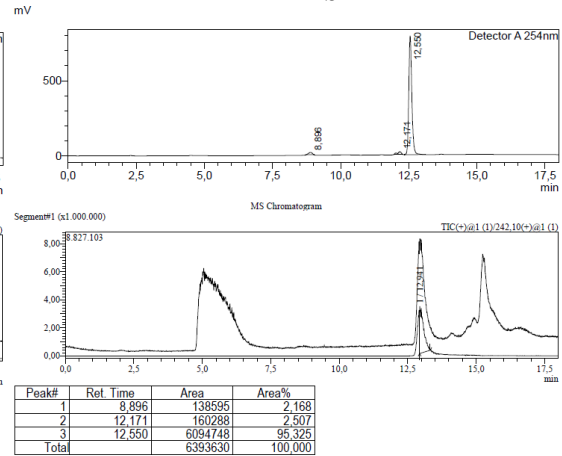
11f



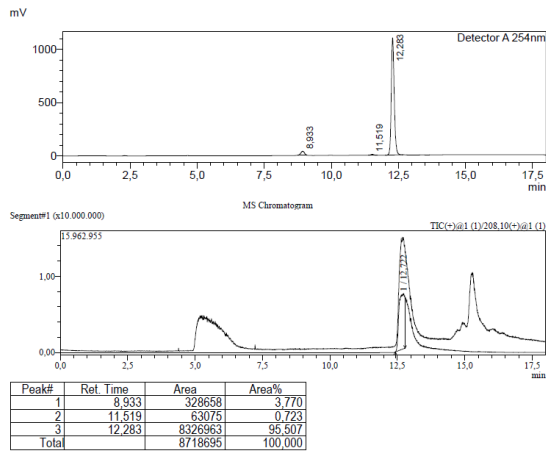
12a



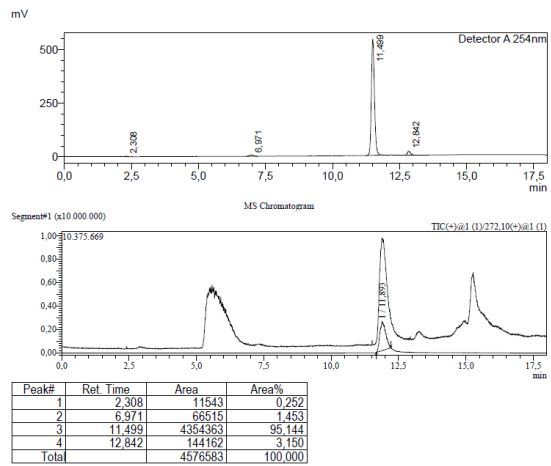
12b



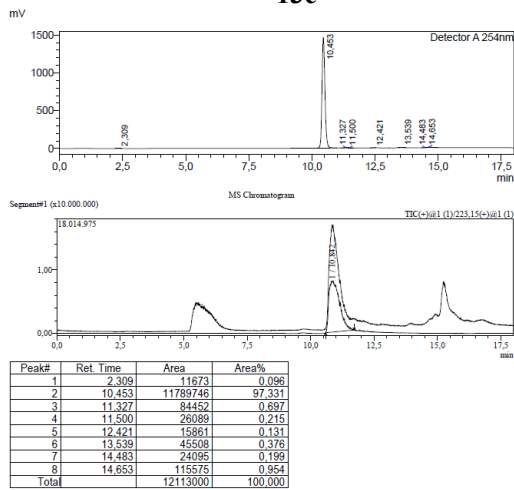
12c



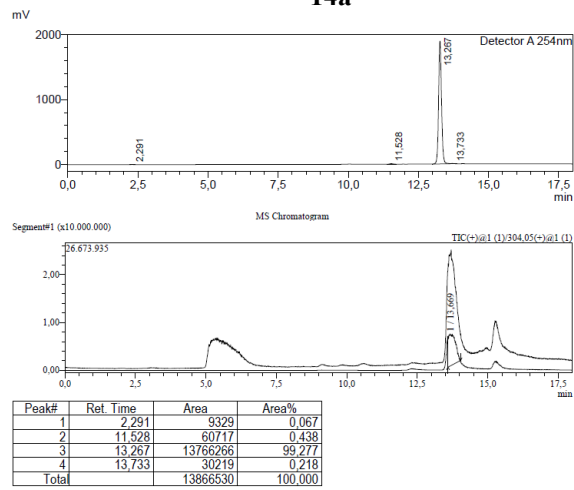
12d



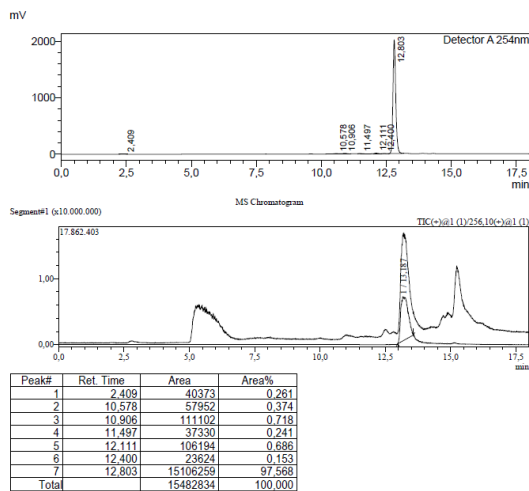
13c



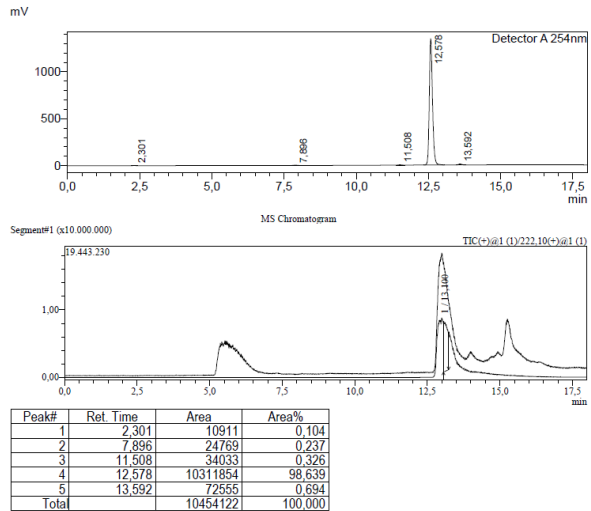
14a

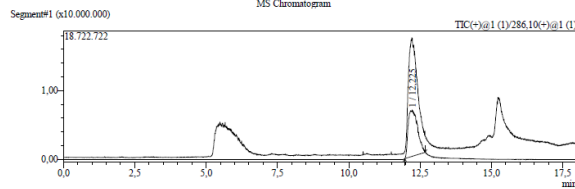
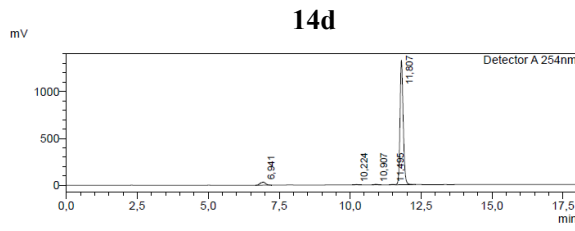


14b

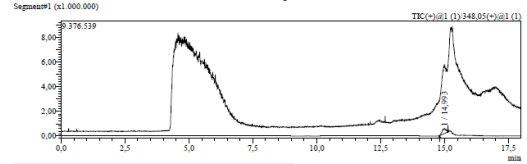
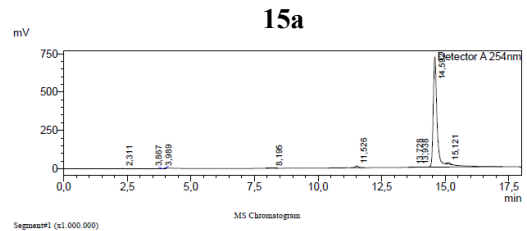


14c

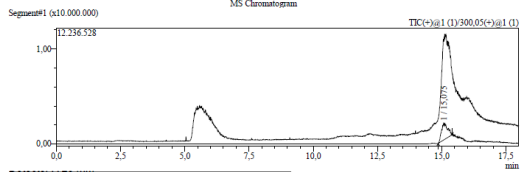
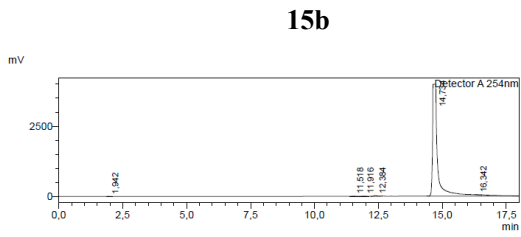




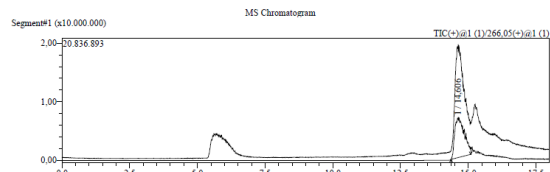
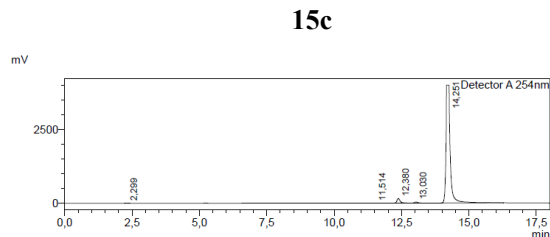
Peak#	Ret. Time	Area	Area%
1	6.941	417682	3.833
2	10.224	29960	0.275
3	10.907	48561	0.427
4	11.495	29359	0.269
5	11.807	10374672	95.196
Total		10898234	100.000



Peak#	Ret. Time	Area	Area%
1	2.311	7178	0.086
2	3.867	1391	0.017
3	3.989	19864	0.236
4	8.195	7623	0.091
5	11.526	96271	1.155
6	13.728	14247	0.171
7	13.938	4941	0.059
8	14.592	8105417	97.252
9	15.121	77484	0.930
Total		8334417	100.000

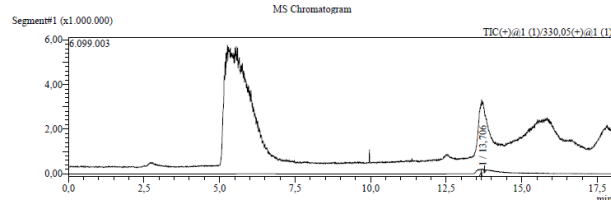
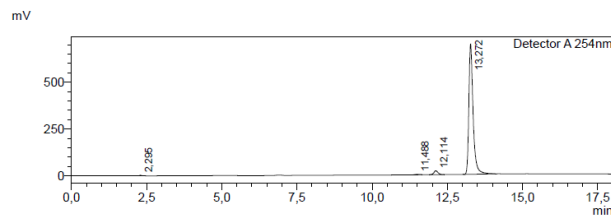


Peak#	Ret. Time	Area	Area%
1	1.942	33991	0.059
2	11.518	54070	0.093
3	11.916	61744	0.107
4	12.384	194292	0.335
5	14.734	57551062	99.376
6	16.342	17167	0.030
Total		57912325	100.000



Peak#	Ret. Time	Area	Area%
1	2.299	11656	0.026
2	11.514	29676	0.065
3	12.380	1251776	2.761
4	13.030	286035	0.631
5	14.251	43753441	96.517
Total		45332584	100.000

15d



Peak#	Ret. Time	Area	Area%
1	2.295	13199	0.186
2	11.488	20585	0.290
3	12.114	199460	2.805
4	13.272	6876994	96.720
Total		7110238	100.000

Pan-Assay Interference Compounds (PAINS) Exclusion Assay

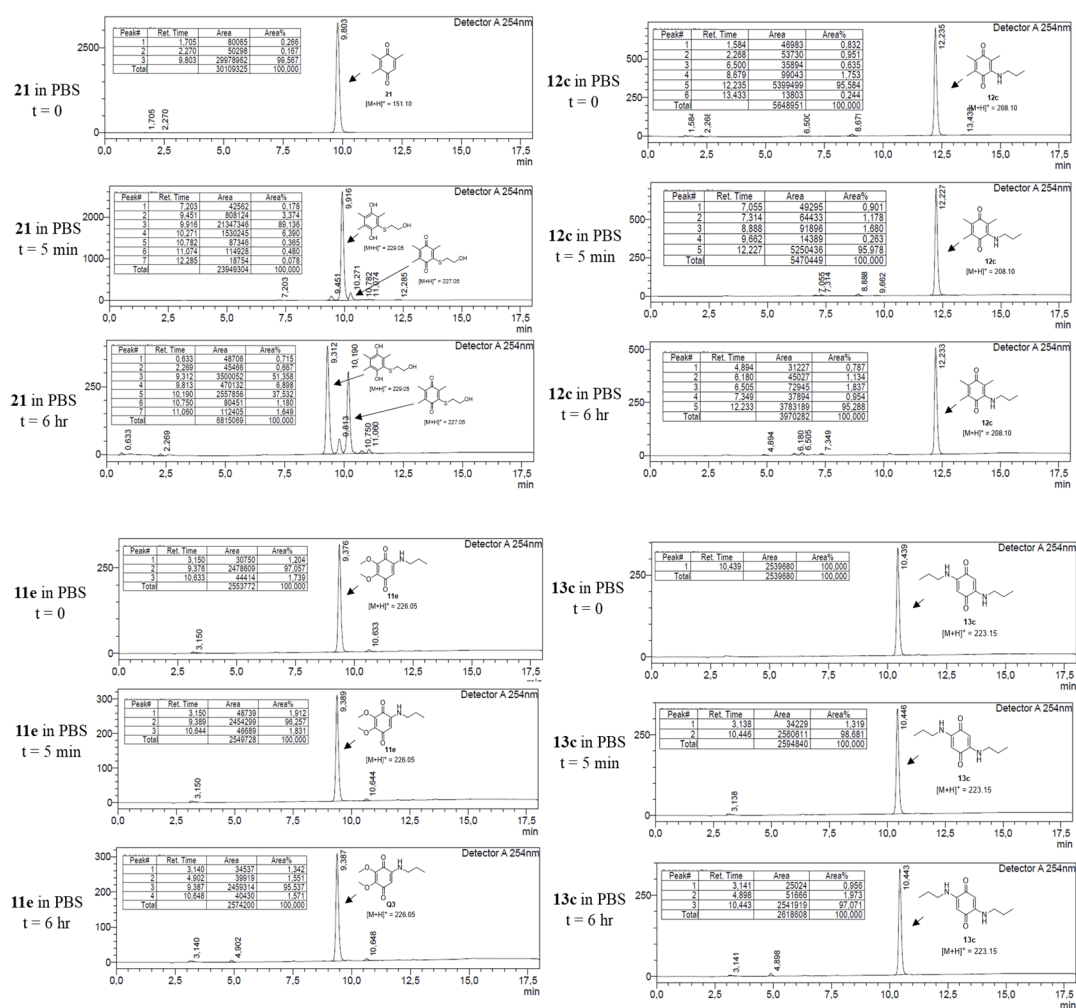


Figure III-1. LCMS records reactions of quinone derivatives 21, 12c, 11e and 13c with two equivalent of 2-mercaptoethanol (BME) in PBS (pH 7.4).

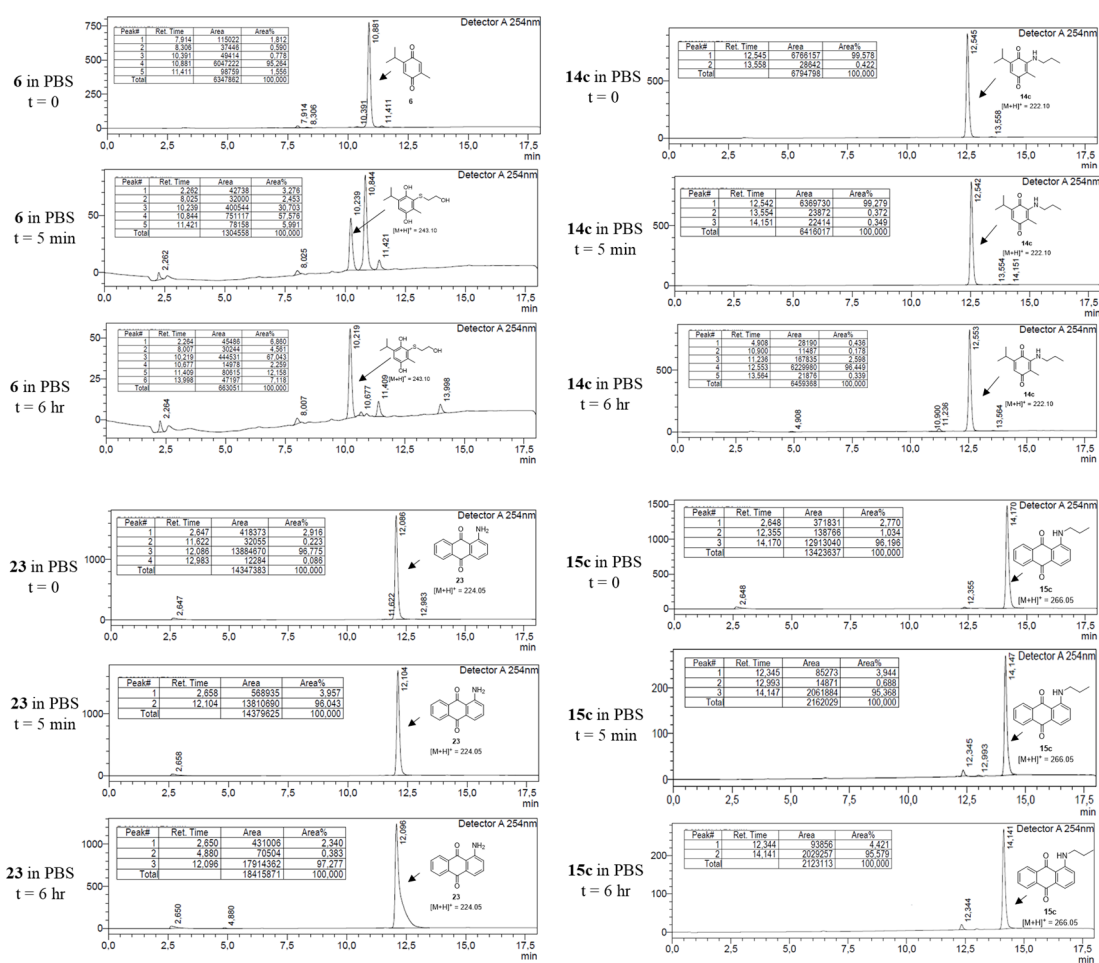


Figure III-2. LCMS records reactions of quinone derivatives **6**, **14c**, **23**, and **15c** with two equivalent of 2-mercaptoethanol (BME) in PBS (pH 7.4).

Appendix IV

4.3. Design, Synthesis, Photophysical Characterization and Bio-Evaluation Photoswitchable HDAC6 Inhibitors

Supporting Information

Photophysical Properties

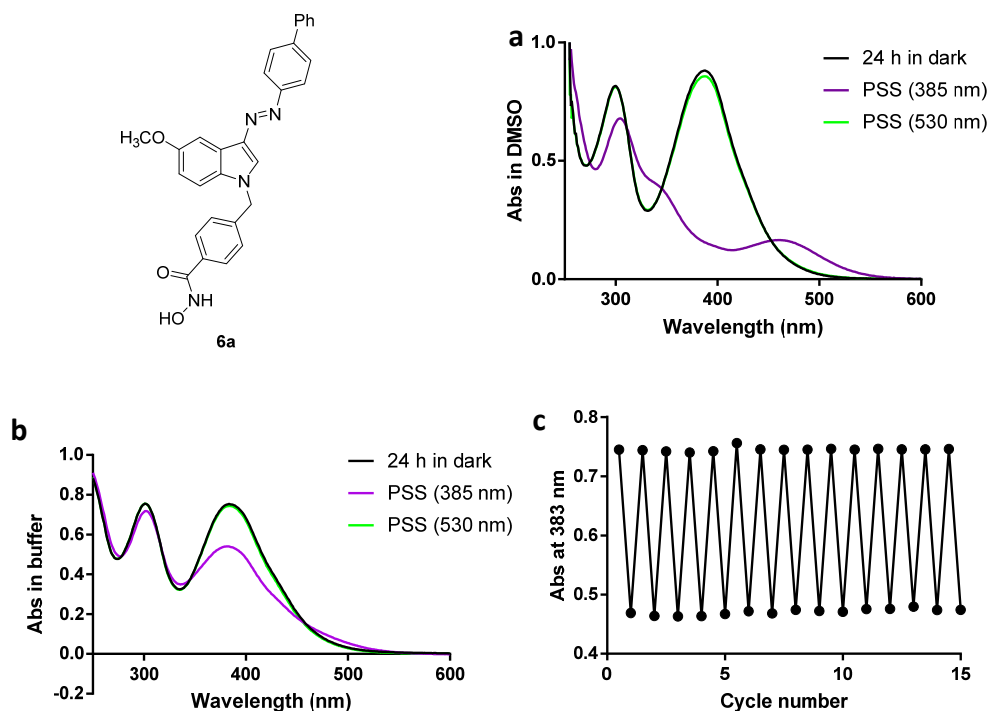


Figure IV-1. Photochemical properties of compound **6a** (50 μ M). Absorption spectra of photostationary state (PSS) at the dark-adapted state and after irradiation with 385 nm (to *cis*) and 530 nm (to *trans*) for 1 min in DMSO (a) and HDAC assay buffer (pH7.4) (b). 15 cycles of 385 nm/530 nm light irradiation performed without significant photodecomposition (c).

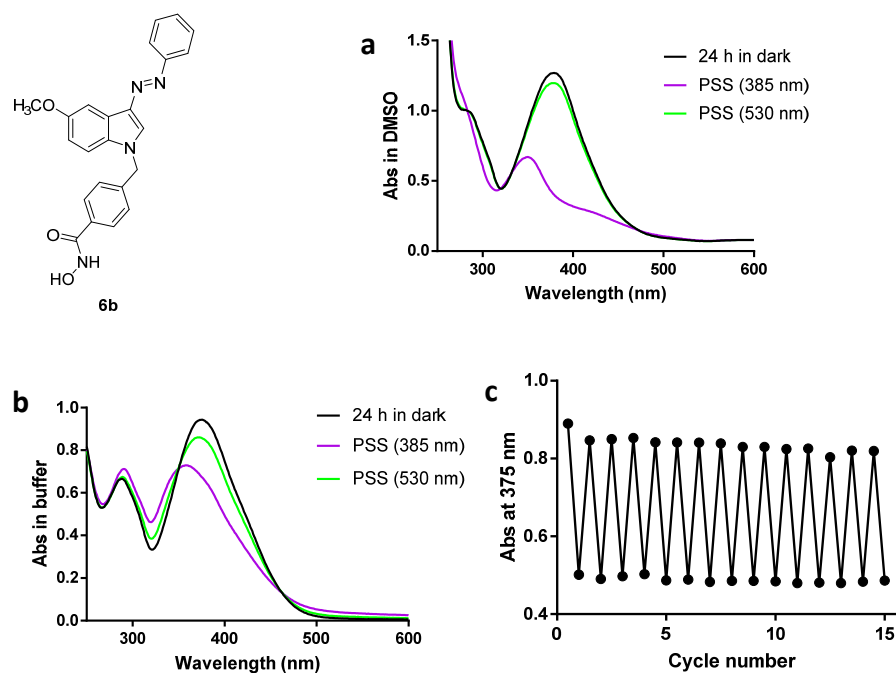


Figure IV-2. Photochemical properties of compound **6b** (50 μ M). Absorption spectra of PSS at the dark-adapted state and after irradiation with 385 nm (to *cis*) and 530 nm (to *trans*) for 1 min in

DMSO (a) and HDAC assay buffer (pH7.4) (b). 15 cycles of 385 nm/530 nm light irradiation performed without significant photodecomposition in buffer (c).

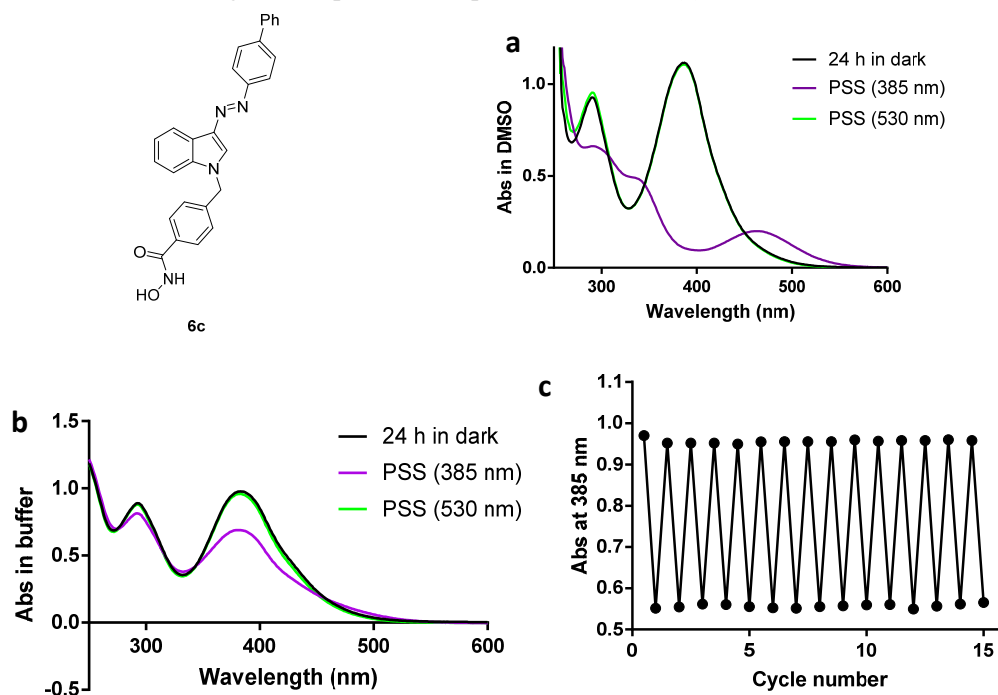


Figure IV-3. Photochemical properties of compound **6c** (50 μ M). Absorption spectra of PSS at the dark-adapted state and after irradiation with 385 nm (to *cis*) and 530 nm (to *trans*) for 1 min in DMSO (a) and HDAC assay buffer (pH7.4) (b). 15 cycles of 385 nm/530 nm light irradiation performed without significant photodecomposition in buffer (c).

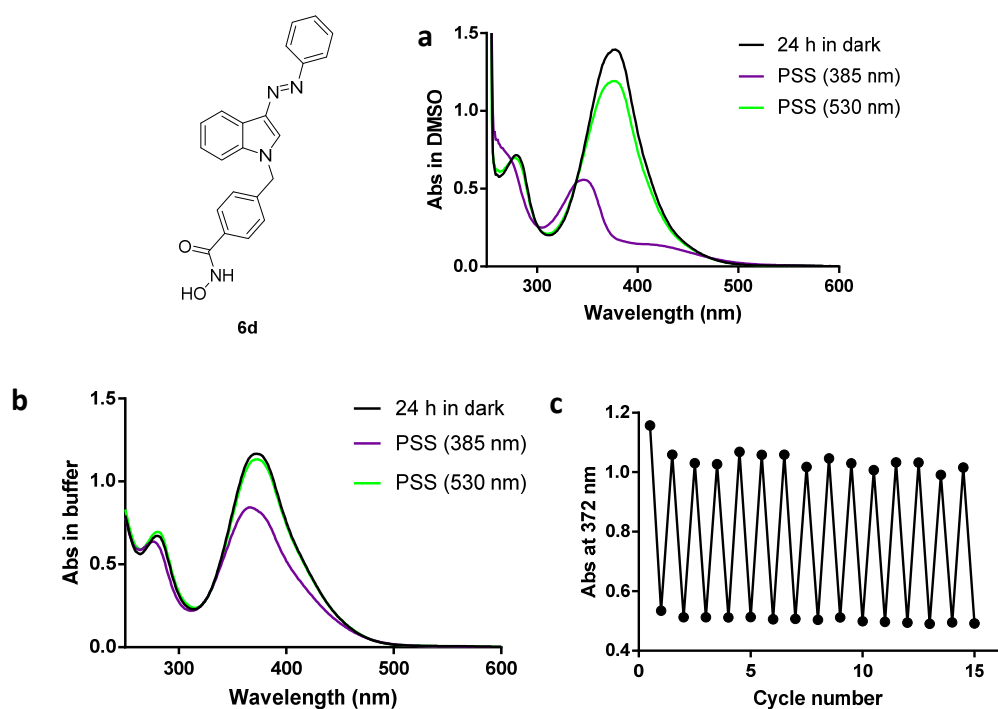


Figure IV-4. Photochemical properties of compound **6d** (50 μ M). Absorption spectra of PSS at the dark-adapted state and after irradiation with 385 nm (to *cis*) and 530 nm (to *trans*) for 1 min in

DMSO (a) and HDAC assay buffer (pH7.4) (b). 15 cycles of 385 nm/530 nm light irradiation performed without significant photodecomposition in buffer (c).

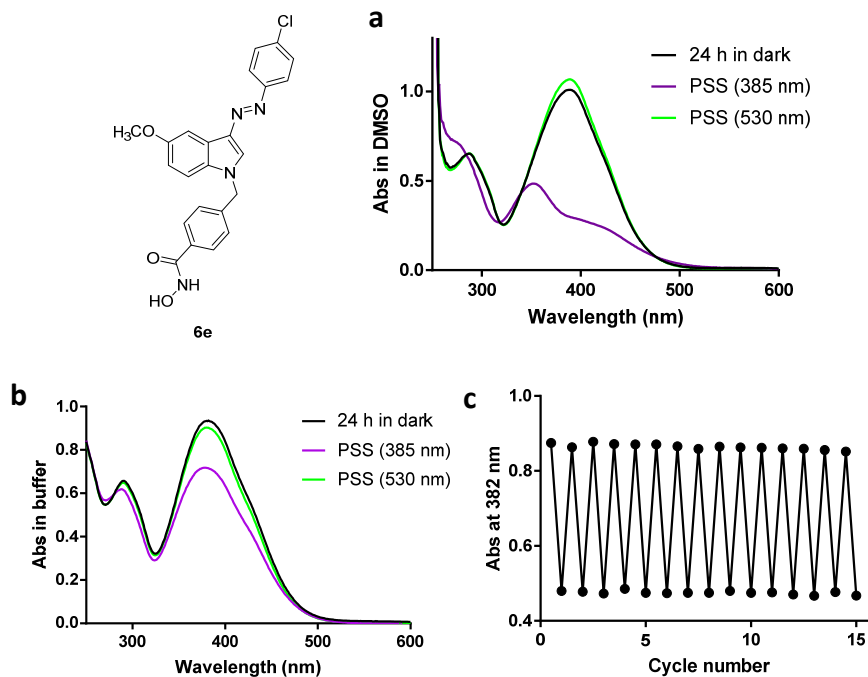


Figure IV-5. Photochemical properties of compound **6e** (50 μ M). Absorption spectra of PSS at the dark-adapted state and after irradiation with 385 nm (to *cis*) and 530 nm (to *trans*) for 1 min in DMSO (a) and HDAC assay buffer (pH7.4) (b). 15 cycles of 385 nm/530 nm light irradiation performed without significant photodecomposition in buffer (c).

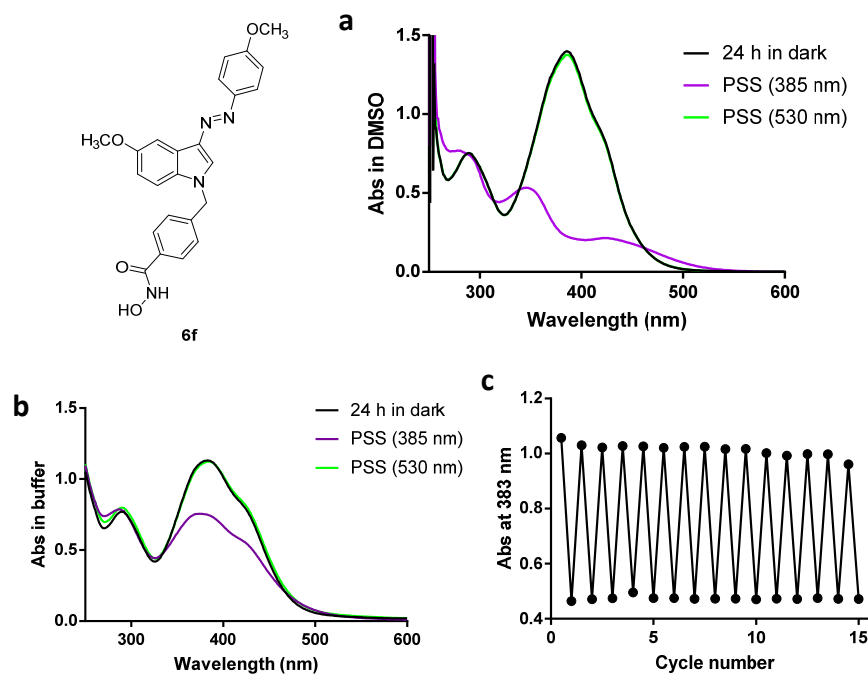


Figure IV-6. Photochemical properties of compound **6f** (50 μ M). Absorption spectra of PSS at the dark-adapted state and after irradiation with 385 nm (to *cis*) and 530 nm (to *trans*) for 1 min in DMSO (a) and HDAC assay buffer (pH7.4) (b). 15 cycles of 385 nm/530 nm light irradiation

performed without significant photodecomposition in buffer (c).

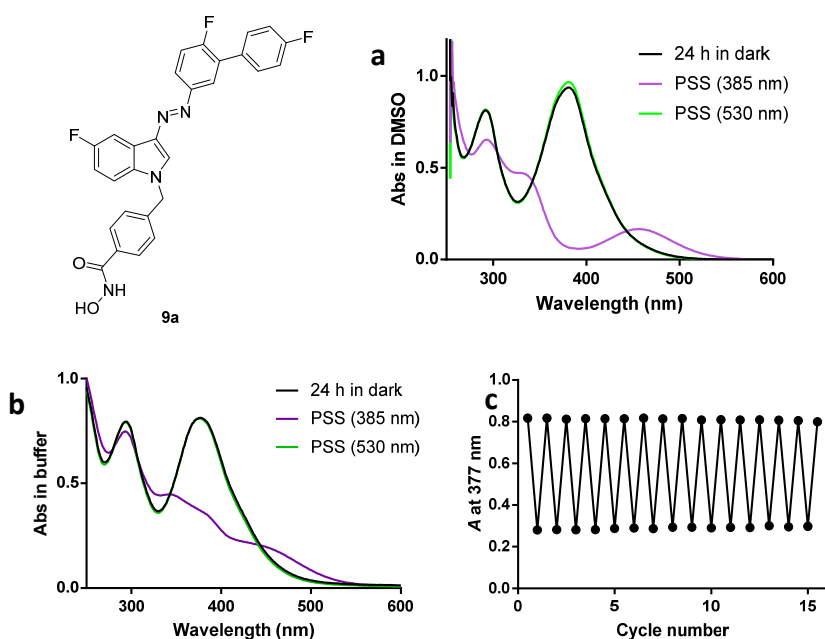


Figure IV-7. Photochemical properties of compound **9a** (40.6 μM). Absorption spectra of PSS at the dark-adapted state and after irradiation with 385 nm (to *cis*) and 530 nm (to *trans*) for 1 min in DMSO (a) and HDAC assay buffer (pH7.4) (b). 15 cycles of 385 nm/530 nm light irradiation performed without significant photodecomposition in buffer (c).

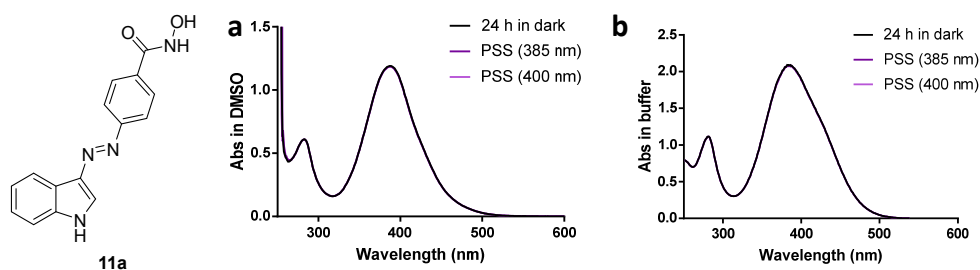


Figure IV-8. Photochemical properties of compound **11a** (50 μM). Absorption spectra of PSS at the dark-adapted state and after irradiation with 385 and 400 nm for 1 min in DMSO (a) and HDAC assay buffer (pH7.4) (b).

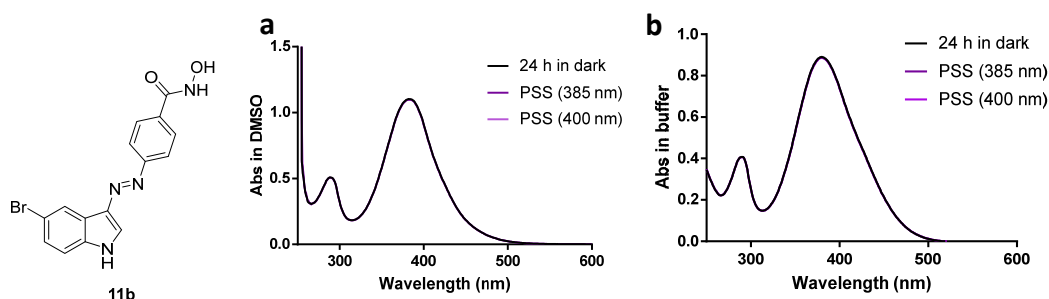


Figure IV-9. Photochemical properties of compound **11b** (50 μM). Absorption spectra of PSS at the dark-adapted state and after irradiation with 385 and 400 nm for 1 min in DMSO (a) and HDAC assay buffer (pH7.4) (b).

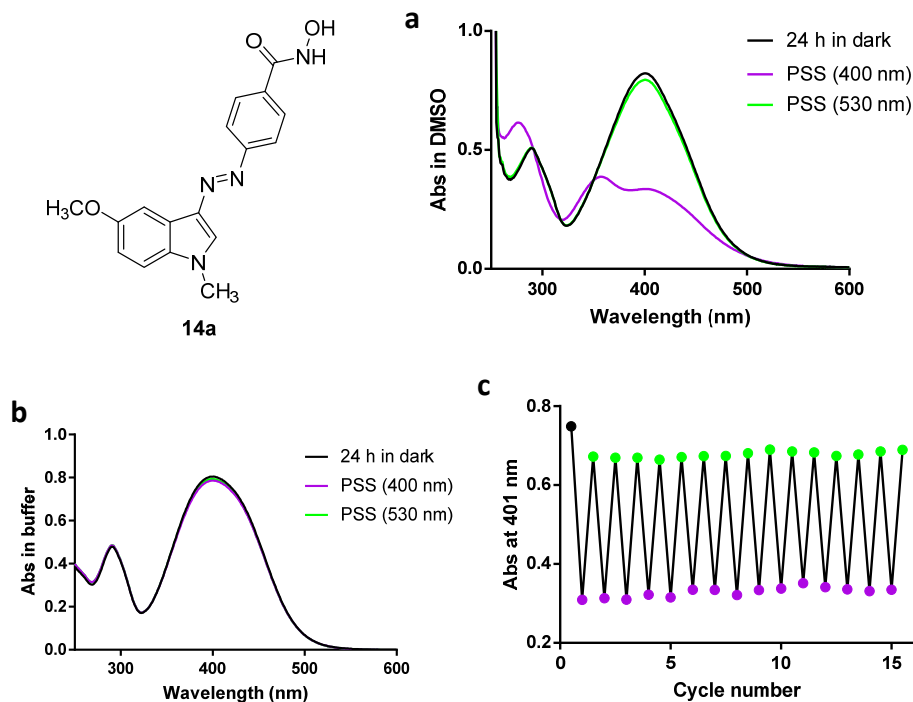


Figure IV-10. Photochemical properties of compound **14a** (50 μ M). Absorption spectra of PSS at the dark-adapted state and after irradiation with 400 nm (to *cis*) and 530 nm (to *trans*) for 1 min in DMSO (a) and HDAC assay buffer (pH7.4) (b). 15 cycles of 400 nm/530 nm light irradiation performed without significant photodecomposition in DMSO (c).

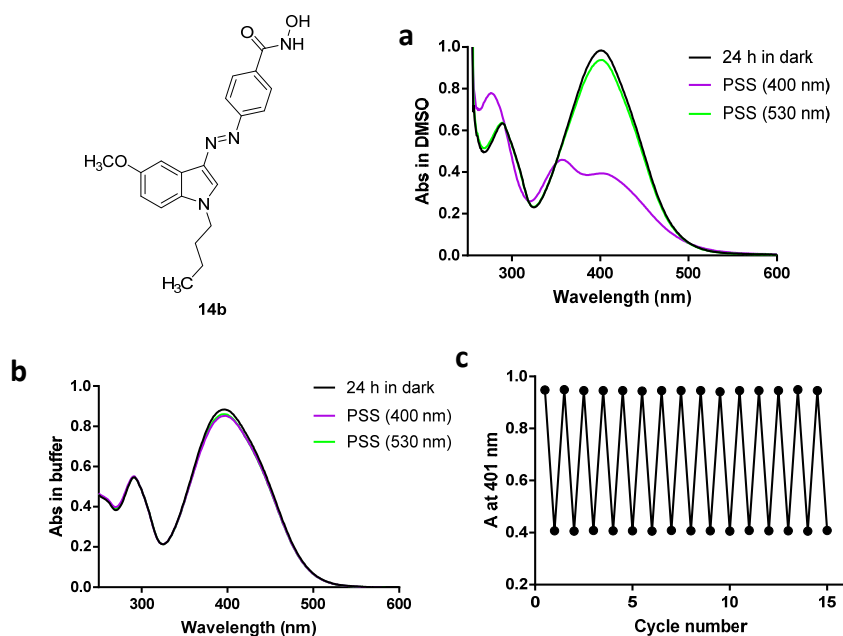


Figure IV-11. Photochemical properties of compound **14b** (50 μ M). Absorption spectra of PSS at the dark-adapted state and after irradiation with 400 nm (to *cis*) and 530 nm (to *trans*) for 1 min in DMSO (a) and HDAC assay buffer (pH7.4) (b). 15 cycles of 400 nm/530 nm light irradiation performed without significant photodecomposition in DMSO (c).

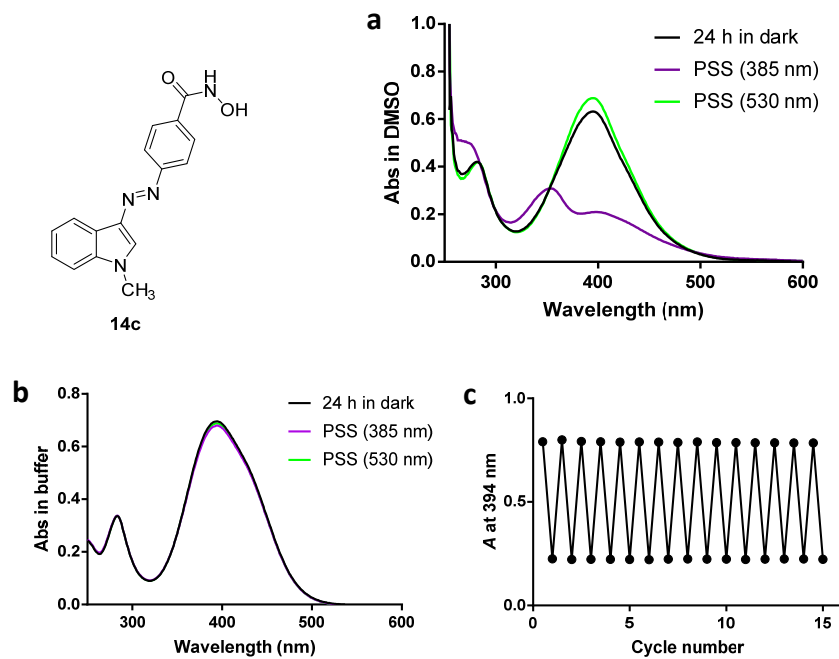


Figure IV-12. Photochemical properties of compound **14c** (50 μM). Absorption spectra of PSS at the dark-adapted state and after irradiation with 385 nm (to *cis*) and 530 nm (to *trans*) for 1 min in DMSO (a) and HDAC assay buffer (pH7.4) (b). 15 cycles of 385 nm/530 nm light irradiation performed without significant photodecomposition in DMSO (c).

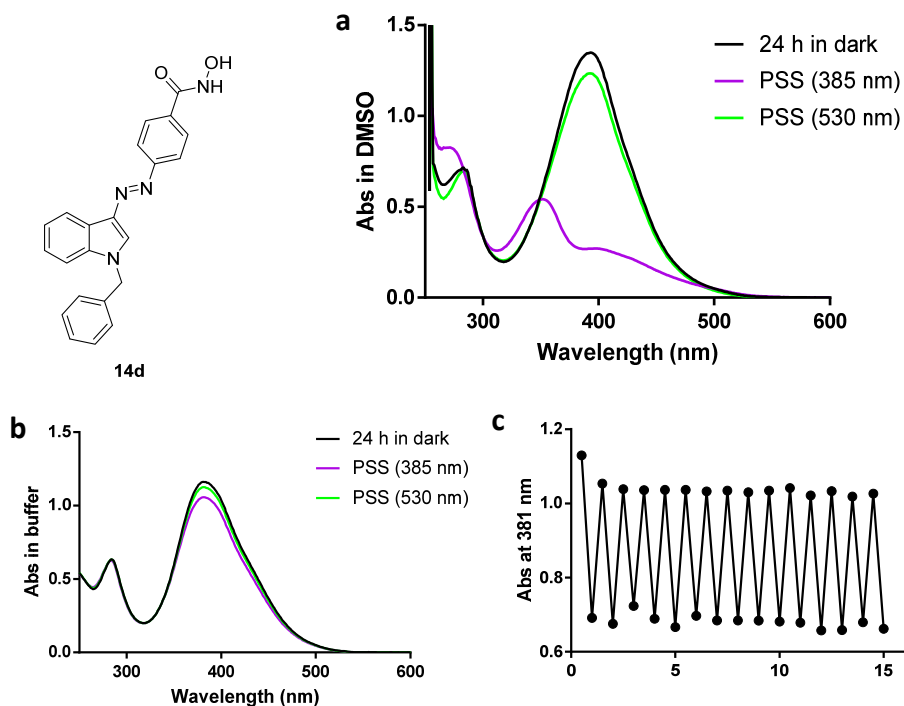


Figure IV-13. Photochemical properties of compound **14d** (50 μM). Absorption spectra of PSS at the dark-adapted state and after irradiation with 385 nm (to *cis*) and 530 nm (to *trans*) for 1 min in DMSO (a) and HDAC assay buffer (pH7.4) (b). 15 cycles of 385 nm/530 nm light irradiation performed without significant photodecomposition in buffer (c).

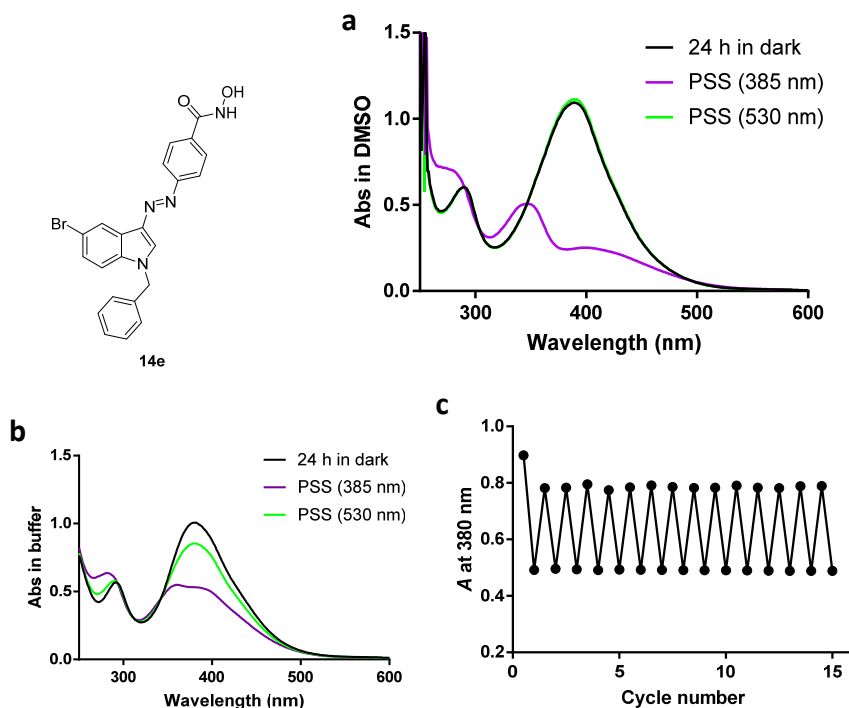


Figure IV-14. Photochemical properties of compound **14e** (50 μM). Absorption spectra of PSS at the dark-adapted state and after irradiation with 385 nm (to *cis*) and 530 nm (to *trans*) for 1 min in DMSO (a) and HDAC assay buffer (pH7.4) (b). 15 cycles of 385 nm/530 nm light irradiation performed without significant photodecomposition in buffer (c).

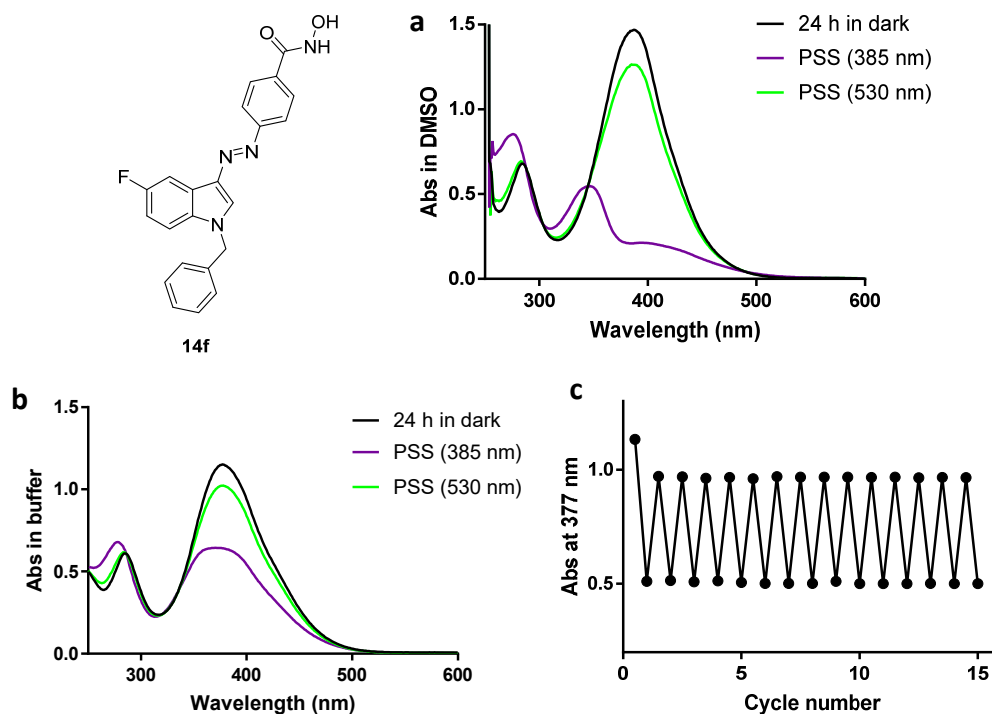


Figure IV-15. Photochemical properties of compound **14f** (50 μM). Absorption spectra of PSS at the dark-adapted state and after irradiation with 385 nm (to *cis*) and 530 nm (to *trans*) for 1 min in DMSO (a) and HDAC assay buffer (pH7.4) (b). 15 cycles of 385 nm/530 nm light irradiation

performed without significant photodecomposition in buffer (c).

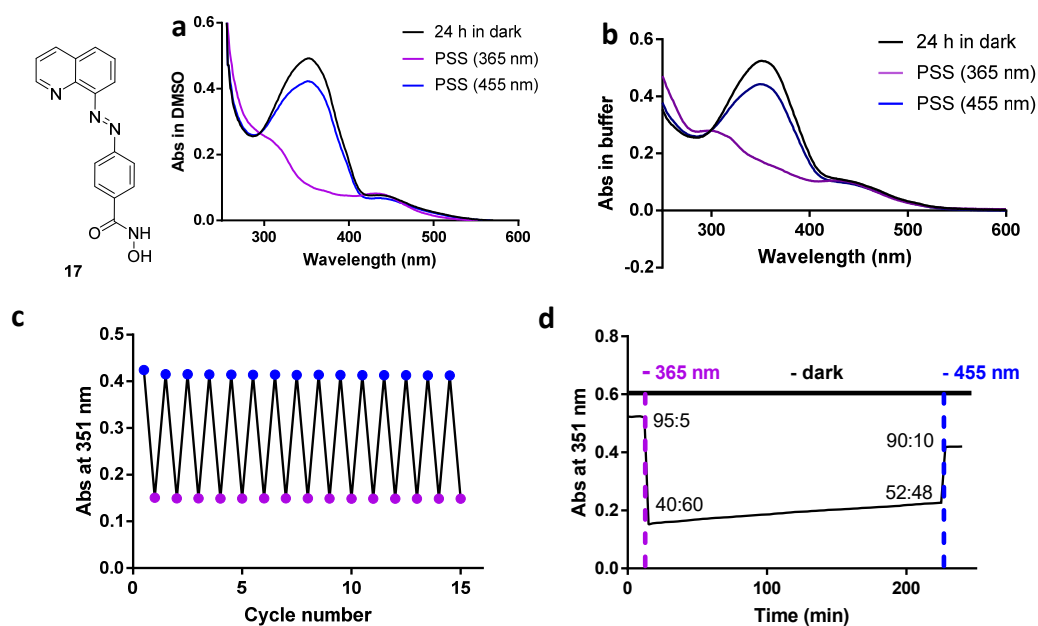


Figure IV-16. Photochemical properties of compound **17** (50 μ M). Absorption spectra of PSS at the dark-adapted state and after irradiation with 365 nm (to *cis*) and 455 nm (to *trans*) for 1 min in DMSO (a) and HDAC assay buffer (pH7.4) (b). 15 cycles of 365 nm/455 nm light irradiation performed without significant photodecomposition in buffer (c). Stability measurement of *cis*-isomer during 210 min in darkness at 30 °C, HPLC ratios of *trans* vs *cis*-isomer show in corresponding time point (d).

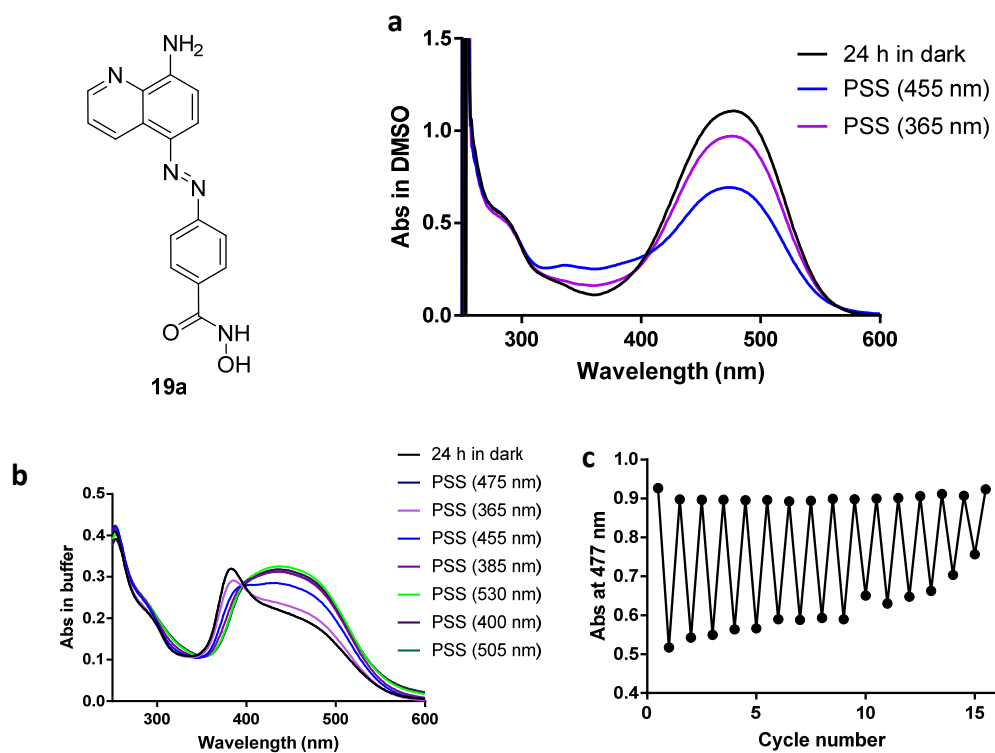


Figure IV-17. Photochemical properties of compound **19a**. Absorption spectra of PSS at the dark-

adapted state and after irradiation with 455 nm (to *cis*) and 365 nm (to *trans*) for 1 min, 50 μM in DMSO (a) and 25 μM in HDAC assay buffer (pH7.4) (b). The abnormal spectra red-shift at the irradiation of various lights, which may induced by chelation with remaining metal ions. 15 cycles of 455 nm/365 nm light irradiation performed with significant photodecomposition in DMSO (c).

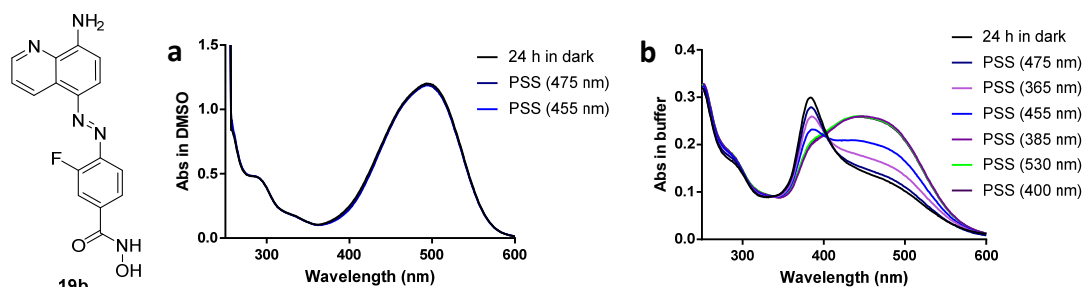


Figure IV-18. Photochemical properties of compound **19b**. Absorption spectra of PSS at the dark-adapted state and after irradiation with 455 nm and 475 nm for 1 min, 50 μM in DMSO (a) and 25 μM in HDAC assay buffer (pH7.4) (b). The abnormal spectra red-shift at the irradiation of various lights, which may induced by chelation with remaining metal ions.

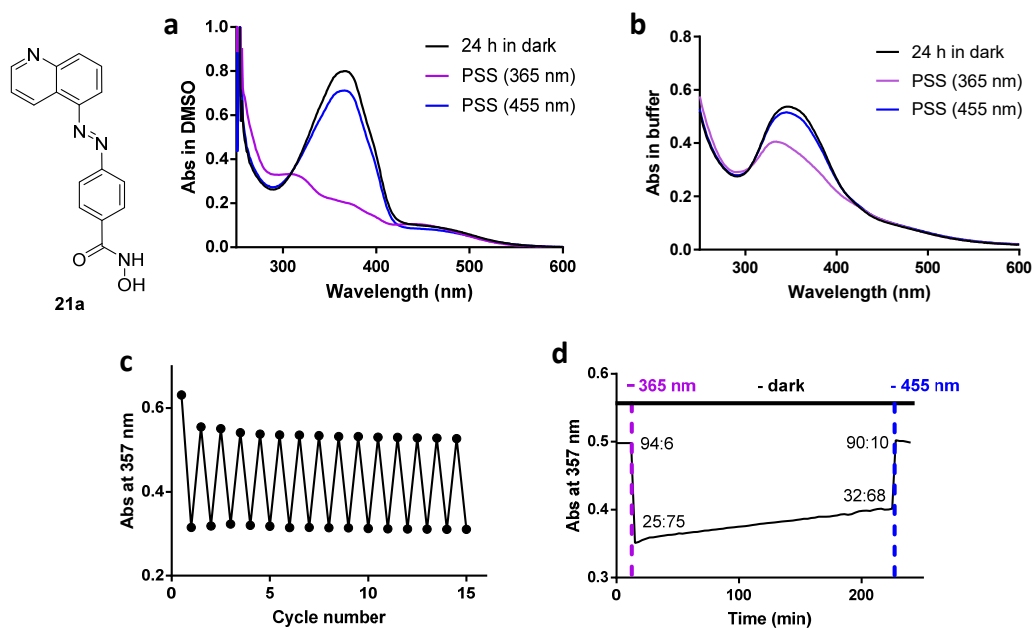


Figure IV-19. Photochemical properties of compound **21a** (50 μM). Absorption spectra of PSS at the dark-adapted state and after irradiation with 365 nm (to *cis*) and 455 nm (to *trans*) for 1 min in DMSO (a) and HDAC assay buffer (pH7.4) (b). 15 cycles of 365 nm/455 nm light irradiation performed without significant photodecomposition in buffer (c). Stability measurement of *cis*-isomer during 210 min in darkness at 30 $^{\circ}\text{C}$, HPLC ratios of *trans* vs *cis*-isomer show in corresponding time point (d).

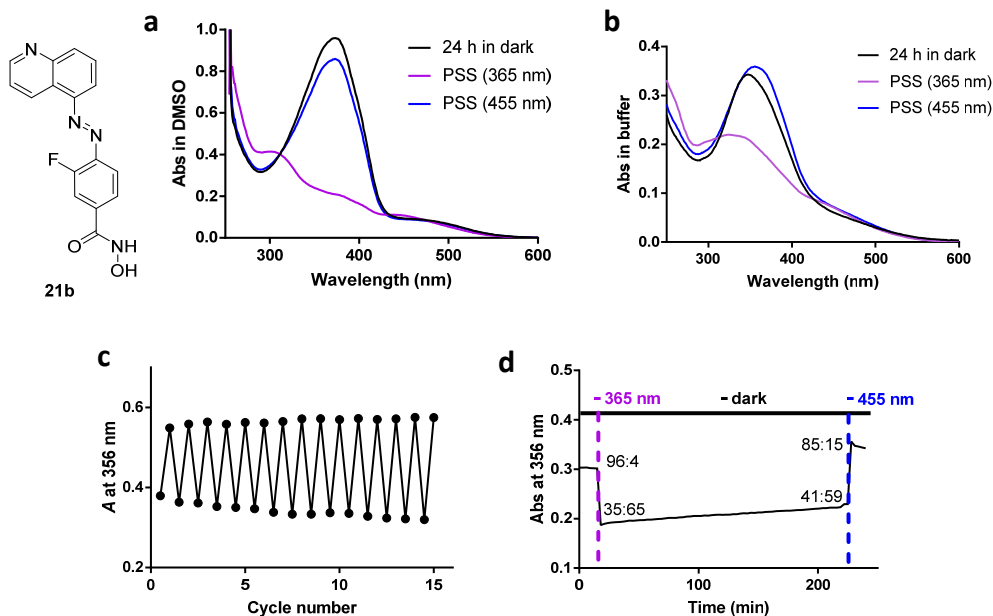


Figure IV-20. Photochemical properties of compound **21b**. Absorption spectra of PSS at the dark-adapted state and after irradiation with 365 nm (to *cis*) and 455 nm (to *trans*) for 1 min, 50 μ M in DMSO (a) and 25 μ M HDAC assay buffer (pH7.4) (b). 15 cycles of 365 nm/455 nm light irradiation performed without significant photodecomposition in buffer at 50 μ M (c). Stability measurement of *cis*-isomer during 210 min in darkness at 50 μ M, 30 $^{\circ}$ C, HPLC ratios of *trans* vs *cis*-isomer show in corresponding time point (d).

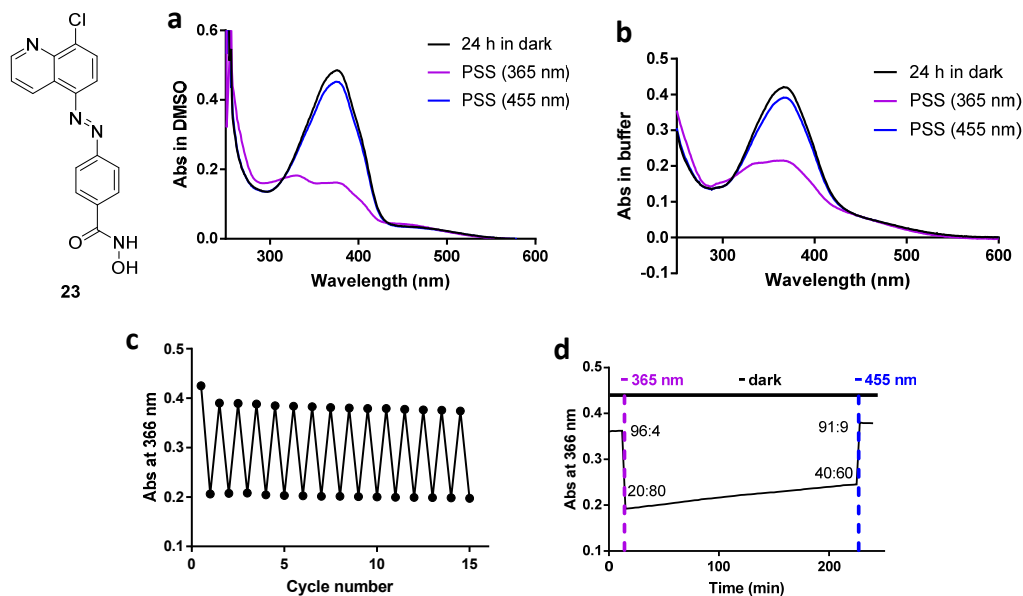


Figure IV-21. Photochemical properties of compound **23** (50 μ M). Absorption spectra of PSS at the dark-adapted state and after irradiation with 365 nm (to *cis*) and 455 nm (to *trans*) for 1 min in DMSO (a) and HDAC assay buffer (pH7.4) (b). 15 cycles of 365 nm/455 nm light irradiation performed without significant photodecomposition in buffer (c). Stability measurement of *cis*-isomer during 210 min in darkness at 30 $^{\circ}$ C, HPLC ratios of *trans* vs *cis*-isomer show in corresponding time point (d).

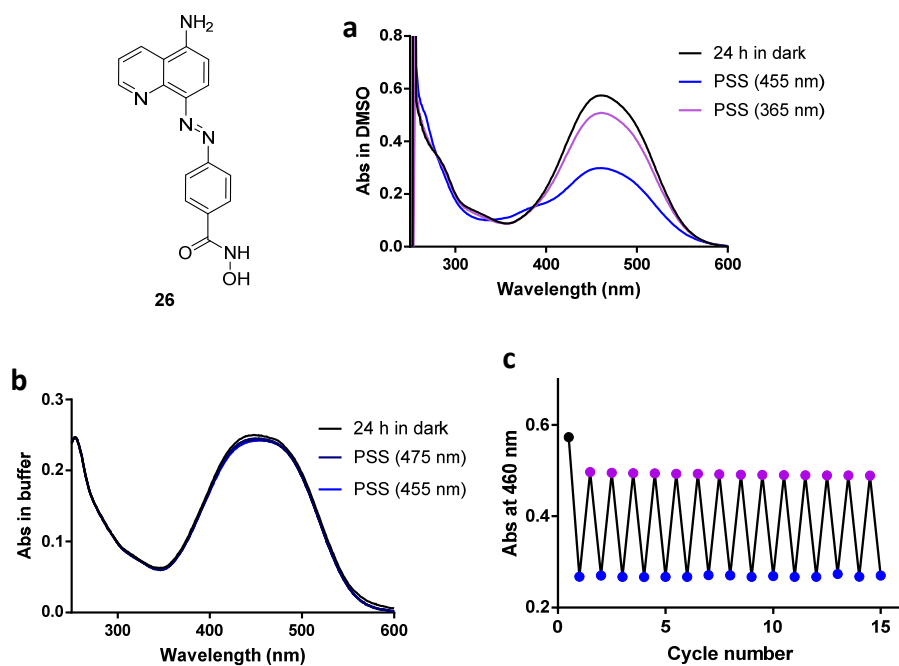
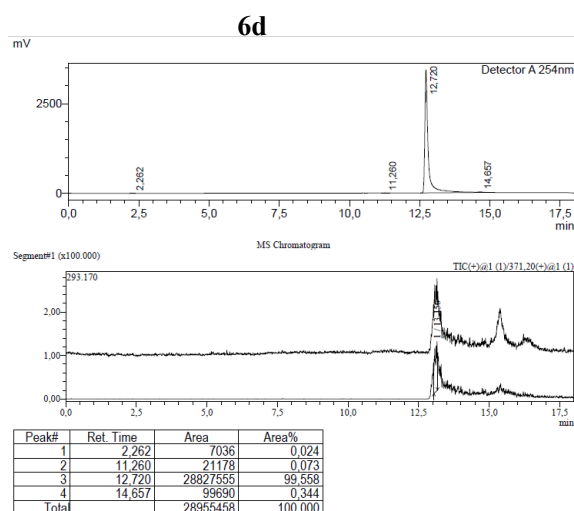
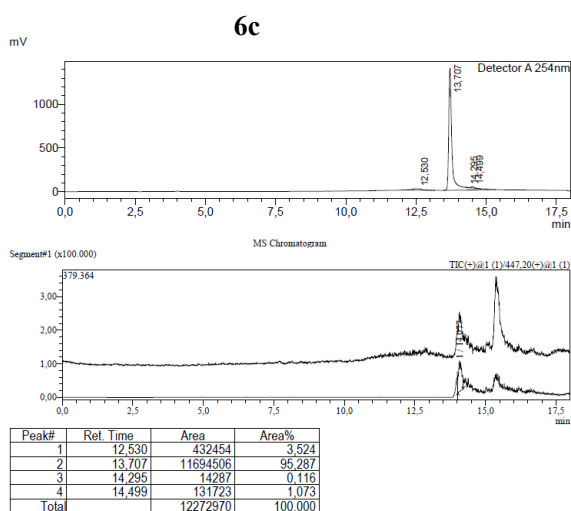
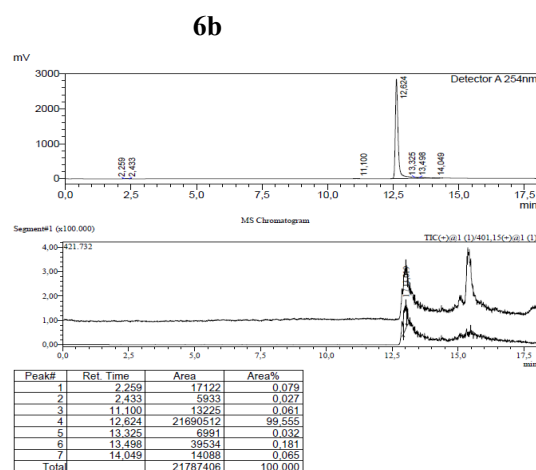
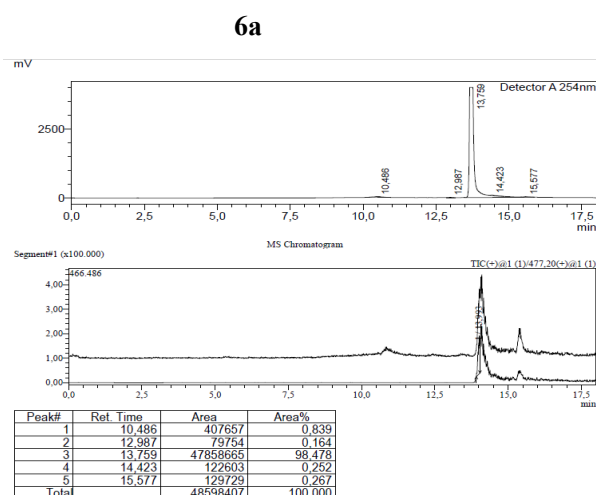


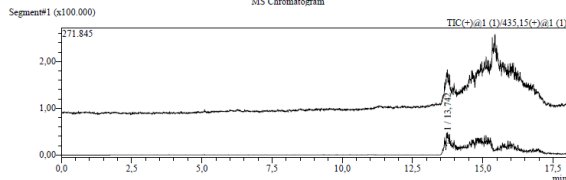
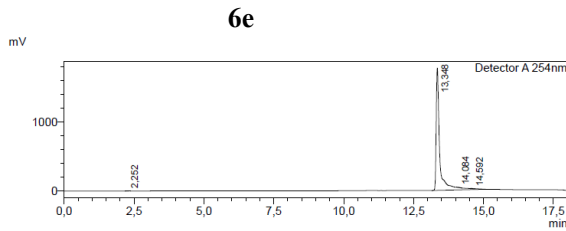
Figure IV-22. Photochemical properties of compound **26**. Absorption spectra of PSS at the dark-adapted state and after irradiation with 455 nm (to *cis*) and 365 nm (to *trans*) for 1 min, 50 μ M in DMSO (a) and 25 μ M HDAC assay buffer (pH7.4) (b). 15 cycles of 455 nm/365 nm light irradiation performed without significant photodecomposition in DMSO (c).

LCMS DATA OF TARGET COMPOUNDS

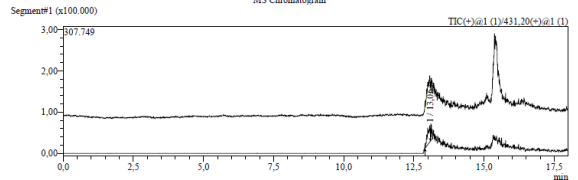
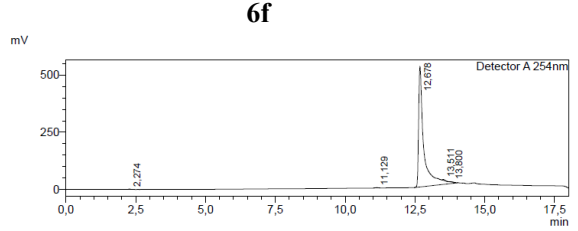
Measurements for verification and purity of the compounds were performed by LC/MS (from Shimadzu), comprising a DGU-20A3R controller, pump LC-20AB, degasser DGU-20A, and SPD-20A UV/Vis detector. ESI ionization was accomplished by an LCMS-2020 single quadrupol mass spectrometer. As a stationary phase, for analytical purpose, a Synergi 4U fusion-RP 80 Å (150 × 4.6 mm) column and for preparative purpose, a Synergi 4U fusion-RP 80 Å (250 × 10.0 mm) were used. As a mobile phase, a gradient of MeOH/water (both containing 0.1% formic acid) (phase 1/phase 2) was used. The compounds were dissolved in MeOH and filtered through syringe filters. Methods were performed with a flow rate of 1.0 mL/min.

Method: V(1)/(V(1) + V(2)) = from 5 to 90% over 10 min, V(1)/(V(1) + V(2)) = 90% for 5 min, V(1)/(V(1) + V(2)) = from 90 to 5% over 3 min.

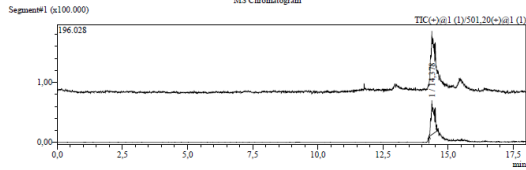
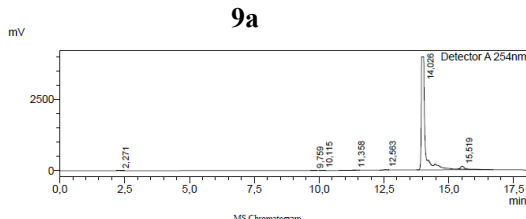




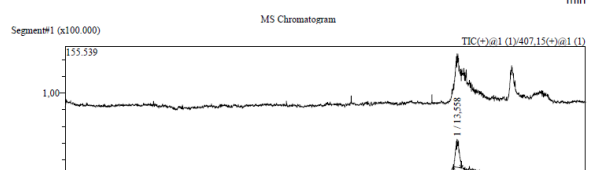
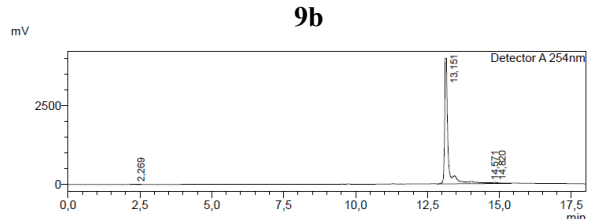
Peak#	Ret. Time	Area	Area%
1	2.252	9412	0.060
2	13.348	15719891	99.764
3	14.084	17330	0.110
4	14.592	10484	0.067
Total		15757118	100.000



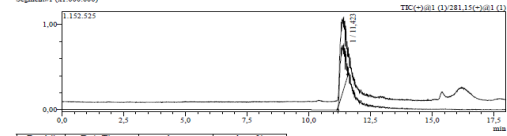
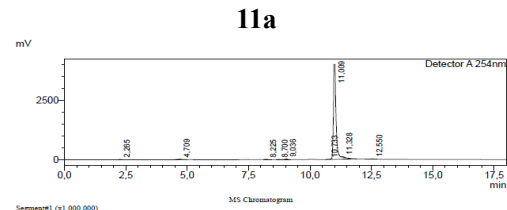
Peak#	Ret. Time	Area	Area%
1	2.274	8138	0.119
2	11.129	12657	0.185
3	12.678	6781032	99.293
4	13.511	17959	0.263
5	13.800	9542	0.140
Total		6829329	100.000



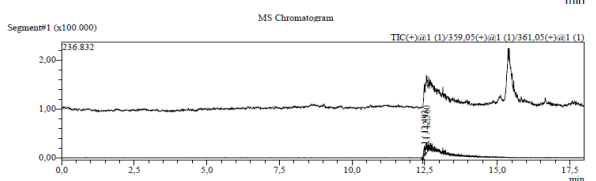
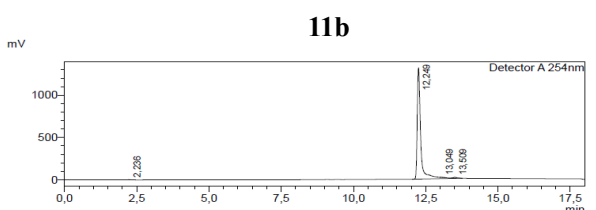
Peak#	Ret. Time	Area	Area%
1	2.271	17896	0.040
2	9.759	12990	0.030
3	10.115	19436	0.044
4	11.358	95802	0.219
5	12.563	108657	0.249
6	14.028	4244350	97.087
7	15.519	1018711	2.330
Total		43716442	100.000



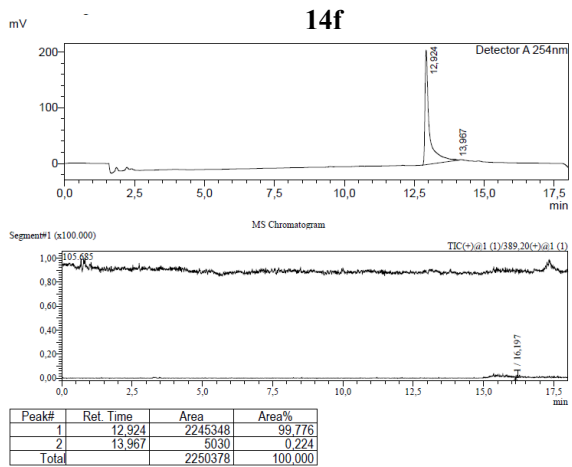
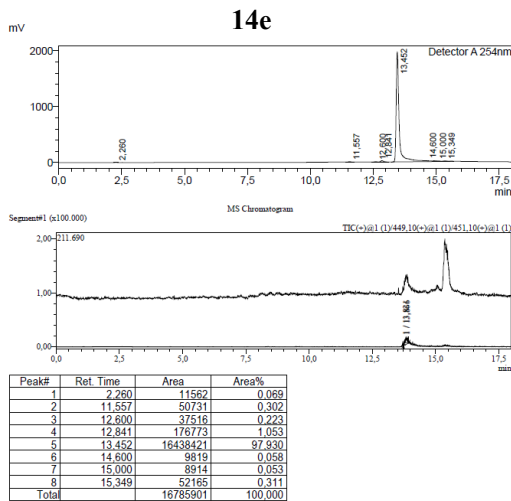
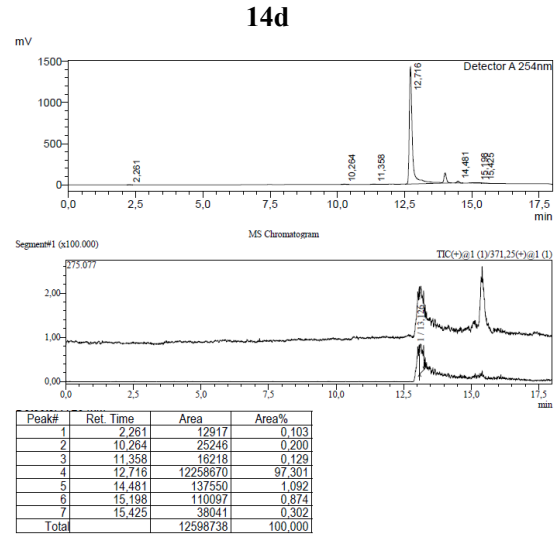
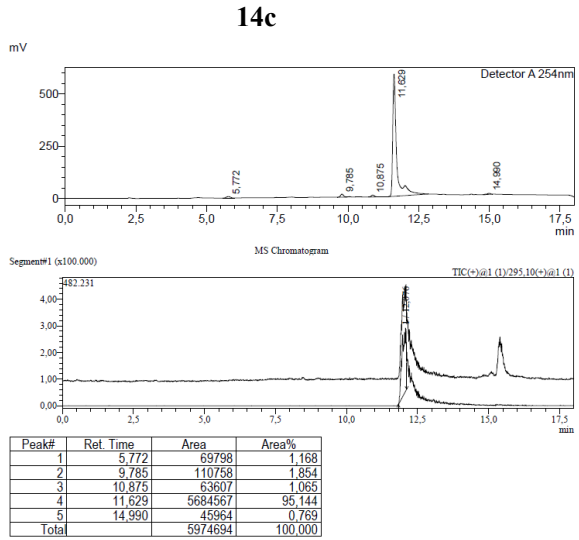
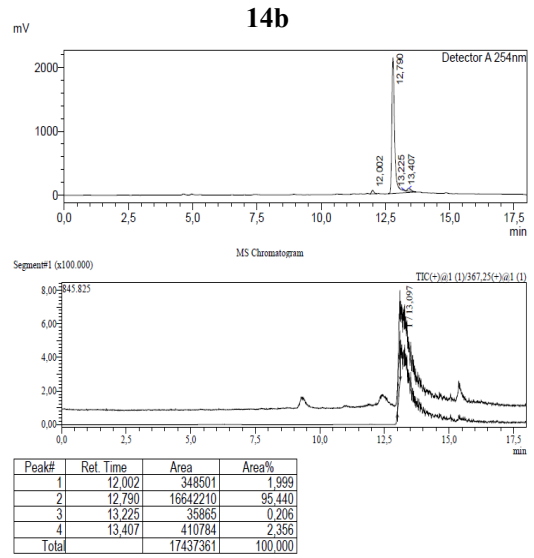
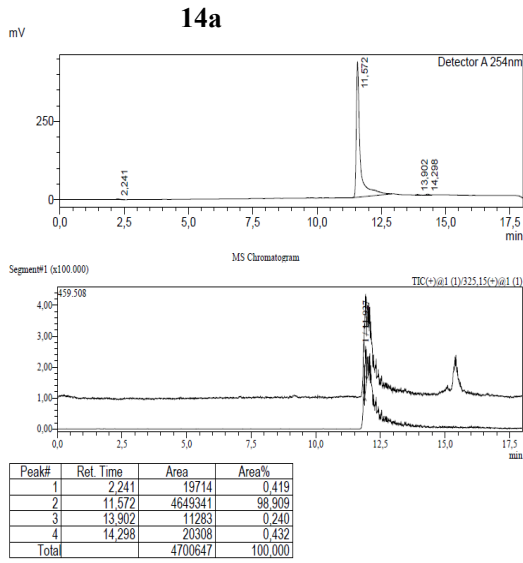
Peak#	Ret. Time	Area	Area%
1	2.269	20104	0.059
2	13.151	33150662	96.612
3	14.571	315242	0.919
4	14.820	827330	2.411
Total		34313338	100.000



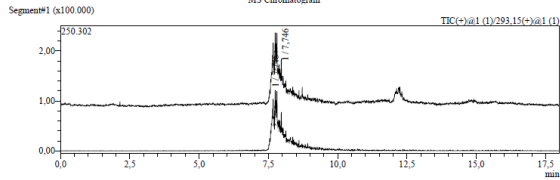
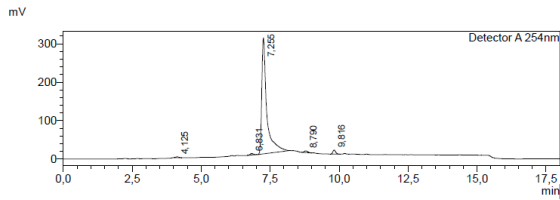
Peak#	Ret. Time	Area	Area%
1	2.265	98280	0.312
2	4.709	350265	1.113
3	8.225	110545	0.351
4	8.700	67715	0.215
5	10.036	196053	0.623
6	10.733	37511	0.119
7	11.009	30420014	96.667
8	11.328	132132	0.420
9	12.550	56470	0.179
Total		31468384	100.000



Peak#	Ret. Time	Area	Area%
1	2.236	16668	0.149
2	12.249	11099771	99.207
3	13.049	13998	0.125
4	13.509	58062	0.519
Total		11188499	100.000

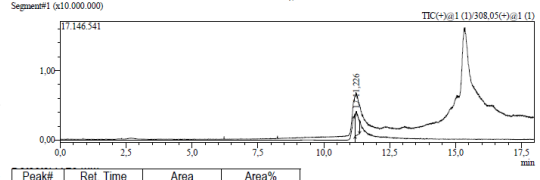
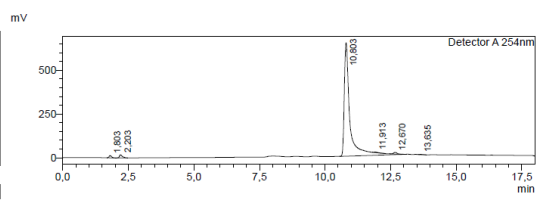


17



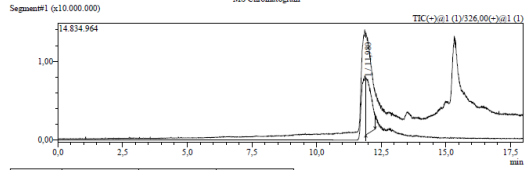
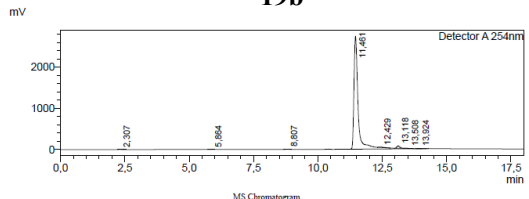
Peak#	Ret. Time	Area	Area%
1	4.125	16682	0.418
2	6.831	33226	0.832
3	7.255	3832516	95.916
4	8.790	39618	0.992
5	9.816	73670	1.844
Total		3995713	100.000

19a



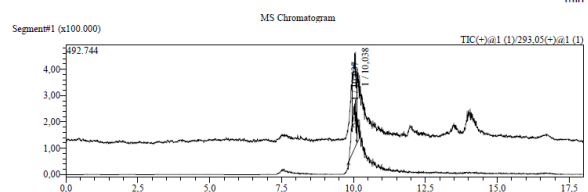
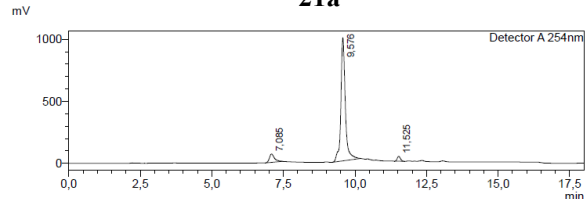
Peak#	Ret. Time	Area	Area%
1	1.803	80459	0.801
2	2.203	142472	1.419
3	10.803	9892314	96.514
4	11.913	31088	0.308
5	12.670	83364	0.830
6	13.635	12757	0.127
Total		10042434	100.000

19b



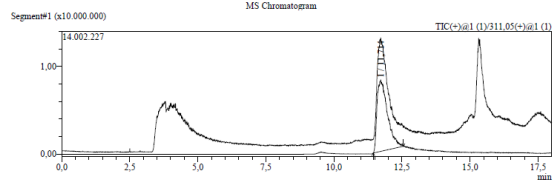
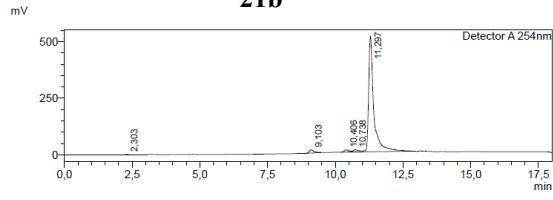
Peak#	Ret. Time	Area	Area%
1	2.307	15924	0.050
2	5.864	18669	0.058
3	8.807	28410	0.088
4	11.461	31494502	97.906
5	12.429	131917	0.410
6	13.118	438356	1.356
7	13.508	8842	0.027
8	13.924	33636	0.105
Total		32168356	100.000

21a



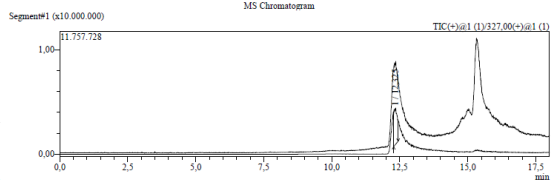
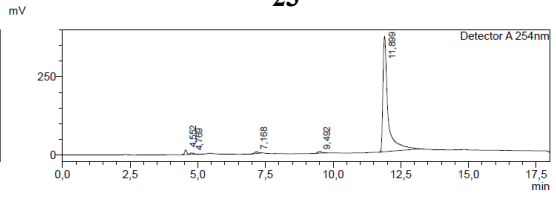
Peak#	Ret. Time	Area	Area%
1	7.085	840666	7.076
2	8.576	10730493	90.324
3	11.525	308851	2.600
Total		11880009	100.000

21b

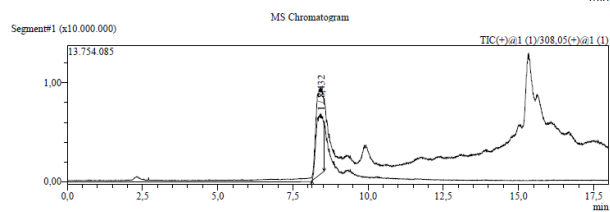
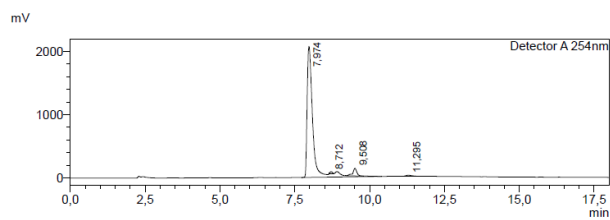


Peak#	Ret. Time	Area	Area%
1	2.303	14646	0.204
2	9.103	169523	2.366
3	10.406	111923	1.562
4	10.738	150573	2.101
5	11.297	6718571	93.766
Total		7165236	100.000

23



Peak#	Ret. Time	Area	Area%
1	4.552	85239	1.675
2	4.769	42504	0.835
3	7.168	54858	1.078
4	9.492	55688	1.094
5	11.899	4849794	95.317
Total		5088061	100.000



Peak#	Ret. Time	Area	Area%
1	7.974	27677026	95,031
2	8.712	135393	0,465
3	9.608	1108561	3,806
4	11.295	203231	0,698
Total		29124210	100,000